Performance of Stone Columns in Cohesive Soil

Mahmoud Adel Mahmoud Khalifa

A Thesis

In the Department

of

Building, Civil, and Environmental Engineering

Presented in Partial Fulfillment of the Requirements

For the Degree of

Doctor of Philosophy (Civil Engineering) at

Concordia University

Montreal, Quebec, Canada

October 2019

CONCORDIA UNIVERSITY

SCHOOL OF GRADUATE STUDIES

This is to certify that the thesis prepared

By: Mahmoud Adel Mahmoud Khalifa

Entitled: Performance of Stone Columns in Cohesive Soil

and submitted in partial fulfillment of the requirements for the degree of

Doctor Of Philosophy (Civil Engineering)

complies with the regulations of the University and meets the accepted standards with respect to originality and quality.

Signed by the final examining committee:

_____ Chair
Dr. Anjali Awasthi

_____ External Examiner
Dr. Richard J. Bathurst

_____ External to Program
Dr. Gerard J. Gouw

_____ Examiner
Dr. Attila Michael Zsaki

_____ Examiner
Dr. Biao Li

_____ Examiner
Dr. Anjan Bhowmick

_____ Thesis Supervisor
Dr. Adel M. Hanna

Approved by _____
Dr. Michelle Nokken, Graduate Program Director

November 25, 2019

_____
Dr. Amir Asif, Dean
Gina Cody School of Engineering & Computer Science

ABSTRACT

Performance of stone columns in cohesive soil

Mahmoud Adel Mahmoud Khalifa, Ph.D.
Concordia University, 2019

Stone columns are widely used and generally considered to be one of the most cost-effective and environmental-friendly soil improvement technique for highways and embankments. They are also used as drainage to reduce the consolidation period, which accordingly increases the bearing capacity, reduces settlement, and reduces the liquefaction potential.

Current design theories used to estimate the bearing capacity of a group of stone columns are based on the unit cell or homogenized material concepts, which neglect the effect of the column interactions and installation technique. This thesis therefore presents an experimental investigation, together with numerical modelling, to examine the performance of a single stone column and group of stone columns subjected to vertical loading. An analytical model is developed to capture the effect of an arrangement of stone columns and the mode of failure within a column and the surrounding soft clay material.

A single stone column and a group of stone columns were investigated in a large-scale experimental set-up. The testing program was divided into four steps: (a) filling the testing tank with the clay, (b) installing the stone columns in the clay bed, (c) extracting samples of the reinforced soil (a block of stone columns surrounded by the soft clay loading), and (d) testing the samples in a triaxial apparatus. The results showed that the mode of failure of the reinforced soil depends on the column spacing and the strength of the column materials and the surrounding soil.

Numerically, a 3-D finite element model was developed to examine the influence of the governing parameters on the bearing capacity of the group. The model was validated against experimental results from this study and results available in the literature. The numerical model was used to simulate the actual driving process during installation of the columns. The model was then used to predict the actual failure plane under a rigid footing reinforced by stone columns for a given geometry/soil condition.

An analytical model was developed utilizing the actual failure plane deduced from the numerical model to develop a theory to predict the bearing capacity of the reinforced soil. The theory developed was validated against the results obtained from the numerical model and results reported in the literature.

ACKNOWLEDGEMENT

First and foremost, I would like to express my sincere appreciation and gratitude to my advisor, Prof. Adel Hanna, for his guidance, support, and advice. His knowledge and experience have greatly contributed to my academic pursuits and my understanding of the dynamics of soil field.

Also. I would like to express my appreciation for the technical staff at Concordia University for their help and support during my time at the foundation laboratory. I am especially grateful for the physical and technical help provided by Eng. Riccardo Gioia and Mr. Joseph Hrib. Their professionalism and experience helped in the construction of the experimental setup.

I would like to thank all my colleagues and friends within our research group at Concordia University. The group has been a source of friendship, good advice and collaboration. I would like to thank my colleagues and best friends Yasir Alharthi and Ahmed Elkady for their input and help for solving many engineering problems that I faced during my research.

I gratefully acknowledge the financial support provided by Concordia University and Natural Sciences and Engineering Research Council of Canada (NSERC) that made my Ph.D. study possible.

I would like to express my sincere gratitude to all my family members and friends for their love, encouragement, and support. I would like to thank my late father Adel who made me love Civil Engineering from my early childhood, my mother Aida for her prayers and continuous support even though we are thousand of Kilometers apart. Lastly but most importantly, I would like to thank my wife Sara for her support, patience, and unconditional love.

Table of Contents

List of Figures

List of Tables

List of symbols

A	Cross section area of stone columns
α	Cam clay transition surface factor
A_{avg}	Average cross-section area of triaxial sample
A_s	Replacement ratio
B	Footing width
b	Stone column trench width in 2-D analysis
c_c	Drained cohesion of clay soil
C_c	Compression index
c_{comp}'	Cohesion of homogenized soil
c_s	Undrained cohesion of stone
C_s	Swelling index
c_u	Undrained cohesion of clay
c_{um}	Undrained cohesion after stone column installation
c_{uo}	Undrained cohesion before stone column installation
C_v	Consolidation coefficient
D	Stone column diameter
d	Particle size diameter
d_c	Cohesion parameter in Drucker-Prager constitutive model
d_e	Average diameter of stone column effective zone
Dr	Relative density
ΔV	Volumetric change
e	Voids ratio
ε_s	Axial strain
ϕ_c'	Drained angle of shear resistance of clay
F_c', F_q'	Cavity expansion factors
ϕ_{comp}	Angle of shear resistance of homogenized soil
ϕ_s'	Drained angle of shear resistance of stone
γ_χ	Unit weight of clay

$\gamma_{\chi o \mu \pi}$	Unit weight of homogenized soil
γ_{σ}	Unit weight of stone
G_s	Specific gravity
I_F	Bearing capacity improvement factor
IR	Bearing capacity improvement ratio
k	Coefficient of lateral earth pressure
κ	Volumetric parameter
K	Permeability coefficient
$K\phi_c$	Drained friction angle coefficient for clay soil
$K\phi_s$	Drained friction angle coefficient for stone columns
K_g	Group coefficient
k_o	At rest earth pressure coefficient
K_p	Passive earth pressure coefficient
L	Stone column length
λ	Plastic compressibility
LL	Liquid limit
n	Stress concentration ratio
N	Number of stone columns
ν	Poisson's ratio
N_c, N_q, N_γ	Bearing capacity factors
N_m	SPT no. after stone column installation
N_o	SPT no. before stone column installation
OCR	Over consolidation ratio
p_f'	Effective mean stress at failure
θ_l	Angle of failure plane
q_f'	Effective shear stress at failure
q_u	Ultimate bearing capacity
R	Cam clay cap eccentricity
S	Spacing between stone columns
σ_3	Confinement pressure
σ_c	Pre-consolidation pressure

σ_{ro}	Effective lateral stress
TV	Time factor
u	Pore water pressure
U	Degree of consolidation
ω	Dilatancy angle

Chapter 1: Introduction

1.1 Stone column technique

Buildings, infrastructures, and earth dams on soft cohesive soil may suffer from excessive settlement and low bearing capacity. In case of low to moderate loads, improving the weak subsoil to support conventional shallow foundations is one solution. There are various techniques available for soil improvement, such as preloading, vertical sand drains, dynamic consolidation, and stone columns.

The stone column technique was first introduced in France in 1830, and has been widely used around the world since 1950 (Hu, 1995; Hanna et al., 2013). Stone columns are currently recognized as one of the most cost-effective, environmental-friendly, sustainable, and practical ground improvement techniques (Hanna et al., 2013; Wood et al., 2000).

Adding compacted granular material to soft cohesive soil improves the overall stiffness of the soil, increases the soil bearing capacity and reduces the corresponding settlement (Mitchell et al., 1985; Priebe, 1995; Wood et al., 2000; Kelly, 2014; Etezad et al., 2015). Stone columns also reduce the drainage path of the water during consolidation, since they have a higher permeability coefficient compared with clay soil; this reduces the time required for consolidation settlement (Sivakumar et al., 2004). Moreover, when used in loose cohesionless soil, stone columns increase the stability of natural slopes and reduce liquefaction potential (Etezad et al., 2015).

The construction of stone columns requires forming a hole in the soil, for which there are two main methods: replacement method, and displacement method. The replacement method typically involves filling a pre-bored hole with compacted sand. This approach reduces the influence of the stone column construction process on the surrounding clay, which makes it applicable for sensitive clay. The displacement method is widely used for stone column construction and is also known as the vibro-replacement method (Baumann et al., 1974). In the vibro-replacement method, a vibrator sinks into the clay soil under its own weight, assisted by an air jet for the case of partially saturated soil or water jet in saturated soil, to the required depth. Compacted granular materials gradually fill the hole; usually well-graded gravel of average diameter between 25 mm and 50 mm is used

(Wood et al., 2000), creating stone column as shown in Figure 1.1. Stone column usually extends to stiff stratum, but occasionally floating columns are used. The diameter of stone column after installation ranges from 30 cm to 100 cm (Poorooshasb et al., 1997). Usually, stone columns are used in groups with a triangular, hexagonal, or square arrangement in plane view, which replaces about 10 % to 35 % of the surface area of the cohesive soil (Hu, 1995; Black et al., 2007; Hanna et al., 2013).

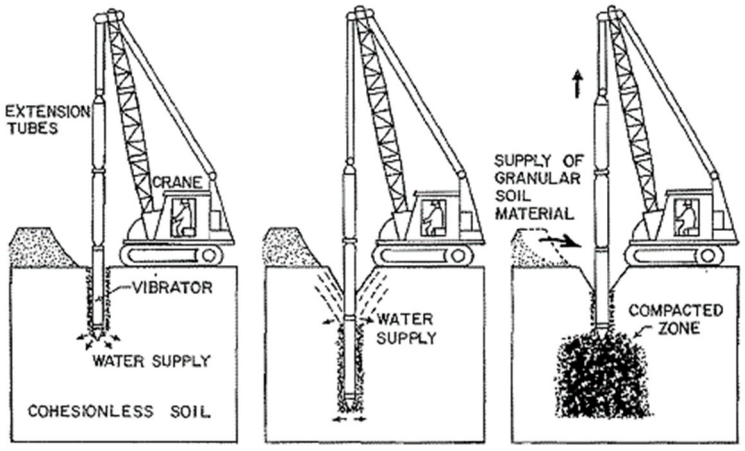

Figure 1.1 Vibro replacement method (Baumann et al., 1974)

1.2 Problem statement

The main parameters governing the capacity of a clay soil reinforced by stone columns can be divided into two groups. The first group is the geometric properties of the stone columns, which are: the replacement ratio - the area of stone columns to the total area of clay, spacing between columns, length of stone columns, and the installation method. The second group is the shear strength properties of the stone columns and the surrounding soil.

The unit cell concept was one of the first methods used to estimate the bearing capacity of the ground reinforced with stone columns (Hughes et al., 1974b; Gibson et al., 1961). The bulging mode of failure was only observed in this method, as seen in Figure 1.2. The effect of all the geometry properties are neglected, and the capacity of a single stone column was predicted by estimating the horizontal capacity of the clay soil around the stone column (Balaam et al., 1981).

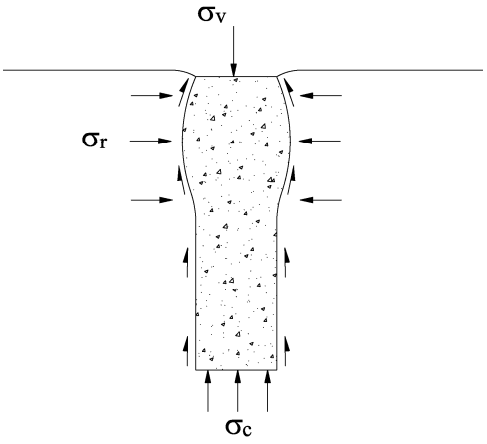

Figure 1.2 Bulging failure and stresses acting on a single stone column under vertical load (Hughes et al., 1974)

Based on the unit cell technique, the bearing capacity of a group of stone columns is the sum of the capacity of the individual columns, neglecting the interaction between the stone columns. Hu (1995) performed laboratory tests on a group of end bearing and floating stone columns and reported shear, punching, and bulging modes of failure, as shown in Figure 1.3. He concluded that the collapse pattern for soil mass reinforced by stone columns changes from general shear failure mechanism to punching shear based on the length of the stone columns. The reported group interaction was confirmed by the numerical analysis carried out by Lee et al. (1998) and Wood et al. (2000). Hanna et al. (2013) developed charts to predict the mode of failure based on the diameter of the stone columns and the shear resistance of the column material and the adjacent clay soil.

Regarding the bearing capacity calculations, Bouassida et al. (2009) presented design charts to determine the ultimate bearing capacity of a group of floating stone columns. In their study, the friction between the footing and the soil was neglected, as well as the arrangement of the stone columns. An analytical model was developed by Etezad et al. (2015) using the limit equilibrium method and equivalent soil properties under the footing to calculate the bearing capacity of a rigid footing placed on the ground reinforced with stone columns. However, this analytical model was not valid for punching and bulging shear failure; also spacing and length of the stone columns was neglected.

In order to simplify the problem, all previous studies have focused exclusively on stone columns installed by the replacement method, which has an insignificant influence on the surrounding soil. However, the conventional method of installation is the displacement method, which has a

significant effect on the clay soil around the columns (Baumann et al., 1974; Kirsch, 2006; Babu et al., 2013).

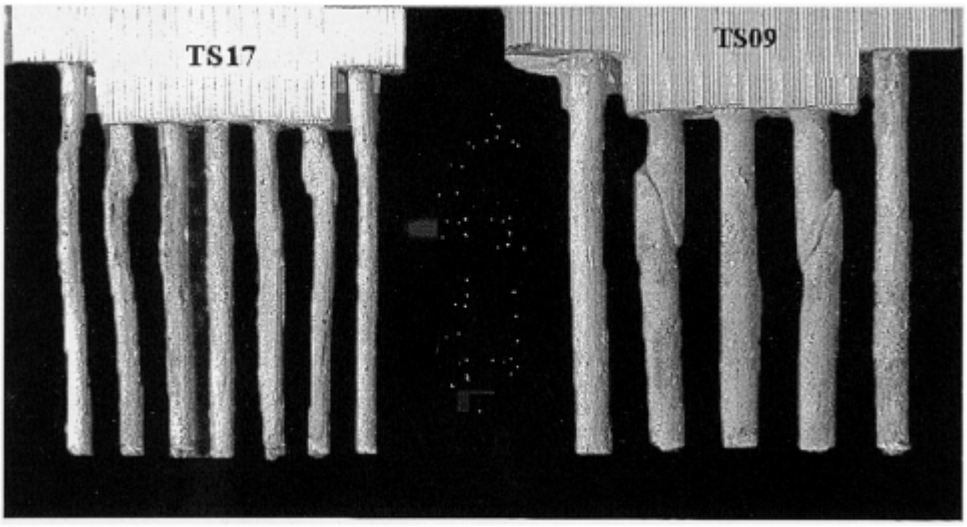

Figure 1.3 Shear failure mechanism in a group of floating stone columns (Hu, 1995)

It can therefore be concluded that the influence of the replacement ratio, spacing between columns, length of stone columns, and the installation method of stone columns on the bearing capacity of reinforced soil have been investigated separately. Moreover, all current bearing capacity equations are based on the homogenization method of the reinforced soil by combining elastic-plastic behaviour of the stone columns and surrounding soil. The actual plane of failure, which takes place under a footing on stone columns, has not yet been defined. Furthermore, the effect of the stone column installation method, stone column spacing, and the over consolidation ratio (OCR) of the surrounding clay on the reinforced soil bearing capacity have not been adequately investigated. Therefore, an in-depth study needs to be carried out to determine the actual failure mechanisms and investigate the synergistic effect of all the parameters that are expected to influence the behaviour of stone columns.

1.3 Research objectives

This research introduces a new experimental approach to simulate the displacement method of installing stone columns. This approach is utilized to investigate the full behaviour of vibro-replacement (displacement) stone columns. Also, a detailed 3-D finite element (FE) numerical

model is presented and is used to develop a parametric study on the capacity of reinforced soil incorporating the effect of installation and spacing between stone columns. For practical use, design charts are developed using a novel analytical model based on the method of slices. The main objectives of the research were to:

1- Investigate the influence of the installation method on the cohesive soils reinforced by a single column and a group of displacement stone columns.

2- Optimize the bearing capacity of reinforced soil supporting a rigid footing based on the stone columns geometry by developing a 3-D finite element numerical model simulating the experiment.

3- Develop a high-fidelity full-scale 3-D FE model to capture the actual failure mechanisms for a group of displacement stone columns.

4- Conduct a parametric study to develop design charts for practical use, using a new limit equilibrium approach based on the method of slices to predict the bearing capacity of a clay soil reinforced by end bearing displacement stone columns.

1.4 Thesis outline

Chapter 2 provides a comprehensive review of previous studies of soft clay soil reinforced by stone columns. The studies are categorized into three groups: experimental, numerical, and analytical. A summary of the current bearing capacity equations for clay soil reinforced by a single stone column and group of stone columns is also presented.

Chapter 3 describes the experimental program. Extensive information related to the preparation of the clay samples in the laboratory, the simulation of the displacement stone columns installation method, and the loading criteria is provided. The mechanical and chemical properties of the clay and sand used in the experiments are also presented.

Chapter 4 summarizes the results obtained from the experimental program. The main observations from the tests are presented first. A comparison between the results is then summarized to investigate the effect of changing some testing parameters on the performance of the reinforced

soil. In particular, the effect of the spacing between stone columns, the diameter of the stone columns, and the compaction energy used during installation of the columns are assessed. Finally, a comparison between the behaviour of soft clay soil reinforced by a single stone column and group of stone columns is presented.

Chapter 5 presents a comprehensive parametric study that investigates the bearing capacity of a rigid footing supported by a soft clay soil reinforced by stone columns. The parametric study was conducted using a 3-D finite element analysis, which was divided into three stages. First, the finite element approach is validated against the experimental data obtained in Chapter 4. Second, a finite element model simulating the installation method used in the experimental work was developed. This model was used to evaluate the effect of the installation of stone columns on the reinforced clay soil. The last stage presents a full-scale finite element model that simulates a rigid footing supported by a clay soil reinforced by stone columns. The results of this model are then used to evaluate the effect of the arrangement of stone columns under the footing, on the bearing capacity of the reinforced soil. This allows the detailed failure plane under the footing to be obtained.

Chapter 6 summarizes an analytical model to estimate the bearing capacity of a clay soil reinforced by stone columns with a specified geometry. The analytical model is developed based on the obtained failure plane from the finite element analysis. This analytical model was validated against the results obtained in Chapter 5 and other experimental work found in the literature. Finally, design charts are presented for practical use to estimate the bearing capacity of the reinforced soil considering the arrangement of stone columns under the footing.

Chapter 7 presents the conclusions of this thesis and provides recommendations for future studies.

Chapter 2: Literature Review

2.1 General

The stone column technique was used for the first time by the French military in 1830 (Hughes et al., 1974a). Groups of stone columns of 2 m height and 0.2 m diameter were used to improve a soft deposit of cohesive soil under the foundation in Bayonne, France. The process of vibro flotation was proposed by Steuerman (1939), whereby water jets and vibration are used to assist the vibrator to sink in soft soil, which has a significant effect on increasing the bearing capacity of the soil.

To derive a bearing capacity equation for soil, the plastic flow after the failure of the soil support foundation must be estimated (Terzaghi, 1947; Madhav et al., 1978). During the last 40 years, many techniques have been used to estimate the modes of failure of stone columns, and the factors affecting the failure type such as spacing between columns (S), replacement area (A_s) (total surface area of stone columns to the total area), the column length to diameter ratio (L/D), and group arrangement (Kelly, 2014). Based on a two-dimensional numerical model, Hanna et al. (2013) divided modes of failure into three types: general shear failure, local shear failure, and punching failure. Due to the analytical complexity of modelling the failure plane in soil reinforced by stone columns, simplified assumptions were used to develop a bearing capacity equation. However, these assumptions lead to an inaccurate modelling of the composite system and accordingly inaccurate bearing capacity predictions.

2.1 Laboratory modelling

2.1.1 Unit cell technique

The unit cell technique was the first method to study the behaviour of soil-stone column interaction. Hughes et al. (1974a) were one of the first researchers to analyze the complex behaviour of stone columns in cohesive soil. They studied the behaviour of a 150 mm-long sand column, with a diameter ranging from 12.5 mm to 38 mm, in kaolin clay considering bulging failure only (Figure 2.1). The bulging of the stone column took place to a depth of four-times the column diameter from the top of the column (Figure 2.2). They reported that the ultimate bearing

capacity of the soil strongly depends on the lateral reaction from the soil around the column in the bulging area. The interaction between columns in groups was neglected as spacing of two and a half times the column diameter between the centers of stone columns is suggested to allow them to act independently.

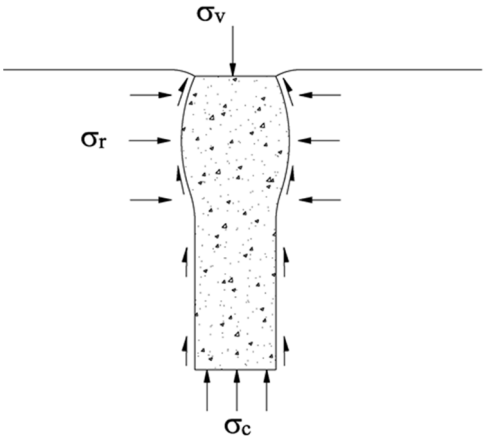

Figure 2.1 The bulging failure and stresses on a single stone column under vertical load (Hughes et al., 1974a)

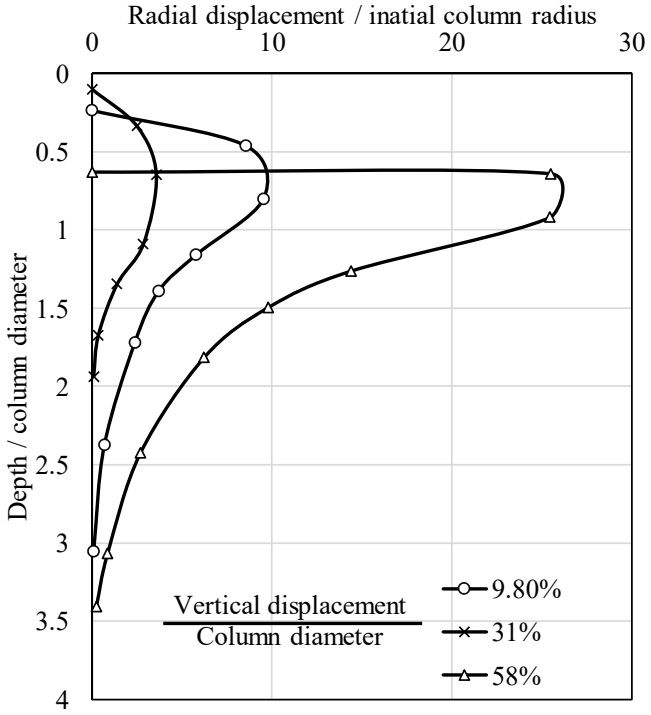

Figure 2.2 Change in the redial displacement/initial column radius with depth (Hughes et al., 1974a)

Many studies have been conducted to estimate the capacity of stone columns using the unit cell concept (Madhav et al., 1978; Goughnour et al., 1979; Balaam et al., 1981; Priebe, 1995; Poorooshasb et al., 1997), which assumes that each column has individual domain of the surrounding soil (Figure 2.3). Accordingly, the overall capacity of the stone columns was predicted based on bulging failure by summation of the individual column capacity in the group.

This concept makes some assumption, which may lead to questionable results. The unit cell concept ignores the interaction between columns and the lateral deformation of the outer sides of the cell. Since general shear and punching failure mechanisms cannot be simulated using this concept, only bulging failure is considered.

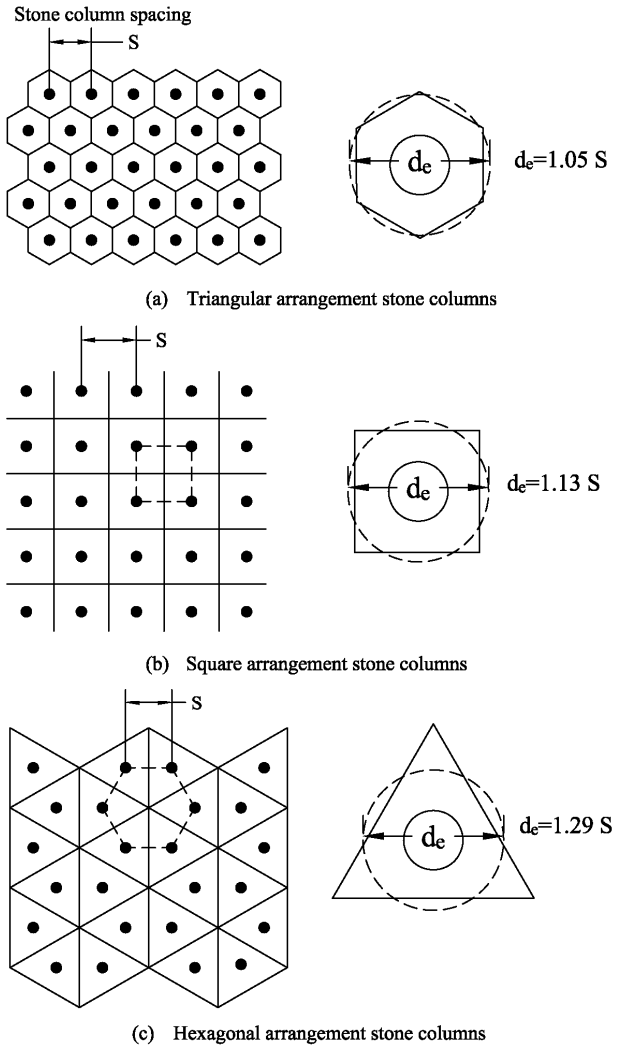

Figure 2.3 Domain of influence of each stone column for different column arrangements (Balaam et al., 1981)

2.1.2 Grouping techniques for stone columns

The column group technique is used to investigate the effect of the interaction between stone columns. Barksdale et al. (1983a) conducted a small-scale test on a small group of stone columns to study the behaviour mechanism and design of stone columns. They reported that stress carried by the columns is more than the stress carried by the adjacent soil, since stone columns are stiffer than the soil and settlement is approximately the same in both materials. The ratio between stresses in the soil to stresses in stone columns is defined as the stress concentration factor (*n*). They reported that this factor varies from 1.5 to 5.0 based on a single model test. They also formulated the following equation for estimating the bearing capacity for a single pile:

$$q_u = c_u N_c^{\sim} \tag{2-1}$$

Where c_u is the undrained cohesion of the surrounding soil and $N_c^{\sim}$ is the bearing capacity factor that varies between 18 and 22, or 25 according to Mitchell (1981).

Terashi et al. (1991) conducted a centrifuge test to investigate the bearing capacity of cohesive soil reinforced by sand columns with a low replacement ratio. They reported that the bearing capacity of reinforced cohesive soil must be calculated from the yield load of the ground (the intersection between the tangent drawn from the start of the load-displacement and another tangent from the end of the curve). They reported a shear failure mechanism, which is different from those created in a unit cell concept (Figure 2.4). Full-scale tests carried out in Kyoto, Japan were reported by Terashi et al. (1991) whereby different replacement ratios were used beneath the superstructure. The replacement ratios used in this study were 25 % and 70 % on the left and right side of the superstructure, respectively. From slip surface failure analysis of the superstructure (Figure 2.5), a value for the stress concentration ratio (*n)* of 3.0 was recommended.

Hu (1995) performed a large-scale test on groups of floating and end bearing stone columns (Figure 2.6). He concluded from the study that the bulging failure takes place at a distance of *L/D* = 6, which was the same finding as Sivakumar et al. (2007). Also, it is concluded that the value of *n* (stress concentration ratio) ranged from 1.5 to 5, and it was not constant with depth of column but depended on the stress level.

.

Figure 2.4 Failure mechanism reported by Terashi et al. (1991)

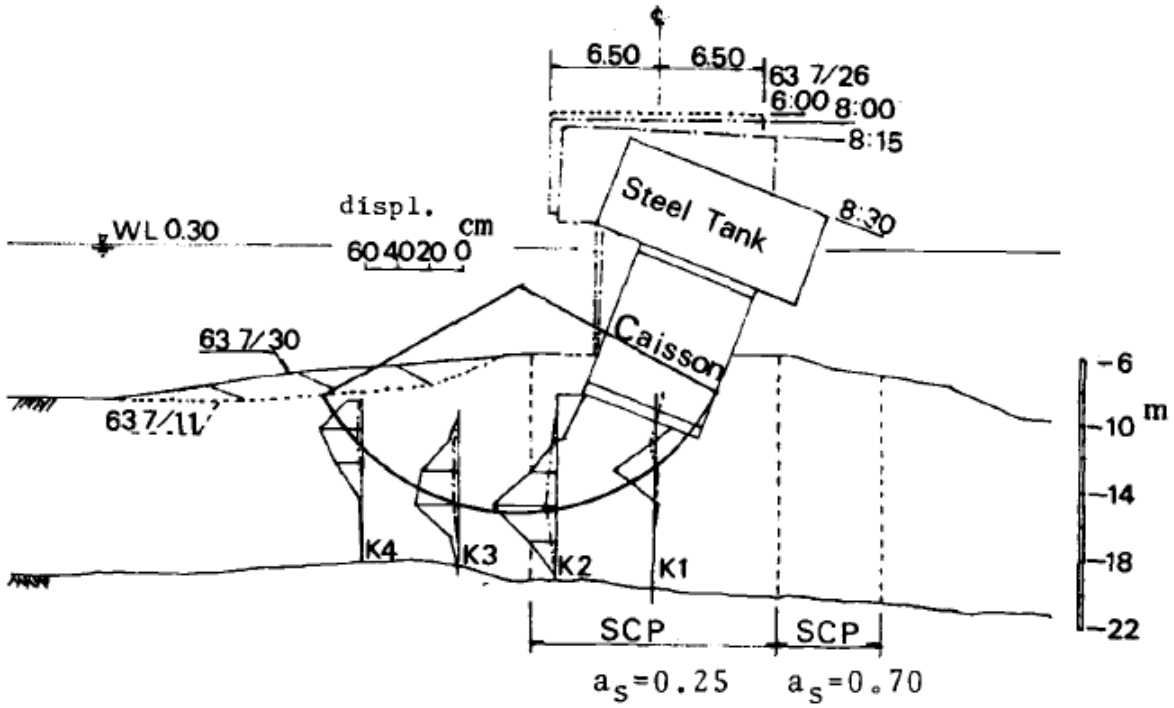

Figure 2.5 Displacement ground deformation under the super structure (Terashi et al., 1991)

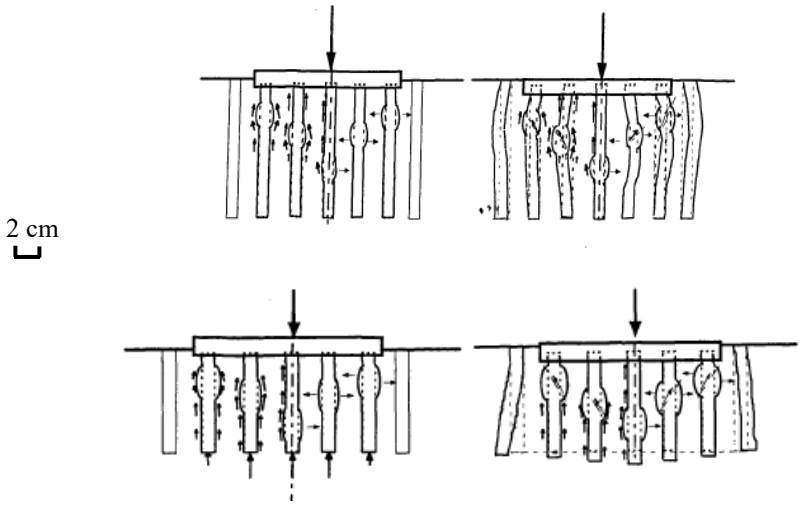

(a) Failure mechanism in long columns (b) Failure mechanism in short columns

Figure 2.6 Modes of failure for (a) long columns and (b) short columns (Hu, 1995)

Rao et al. (1997) conducted laboratory tests on a single stone column and groups of stone columns. They reported that the water content of cohesive soil around stone columns influences the bearing capacity of those columns. Furthermore, they suggested spacing of three times the stone column diameter. They found that the spacing between columns had a significant effect on the group bearing capacity. They also found that the length of the bulging zone ranges from 5 to 10 times the column diameter, which is in close agreement with the values reported by Hu (1995), McKelvey (2002), and Sivakumar et al. (2007).

Christoulas et al. (2000) performed a laboratory test on a large-scale model. In order to measure the pore water pressure and the horizontal stresses, electric piezometers and pressure cells were used. They reported that the bulging failure took place in the upper part of the column with a length of 2.5 to 3 times the column diameter. Although the observations from the test concurred with the results of Hughes et al. (1974a), a boundary effect is suspected since their columns were close to the boundary (Figure 2.7).

Ambily et al. (2007) experimentally examined the effect of some parameters, such as spacing between columns and cohesion of the surrounding soil, on a single stone column and groups of stone columns. They reported that the effect from the spacing between columns and the shear resistance of the surrounding soil had an insignificant effect on the capacity of a single column. They also concluded that there is a slight change in the axial capacity of the column for spacing

larger than three times *D*, which does not agree with the findings of Rao et al. (1997) who recommended three times *D* spacing for design.

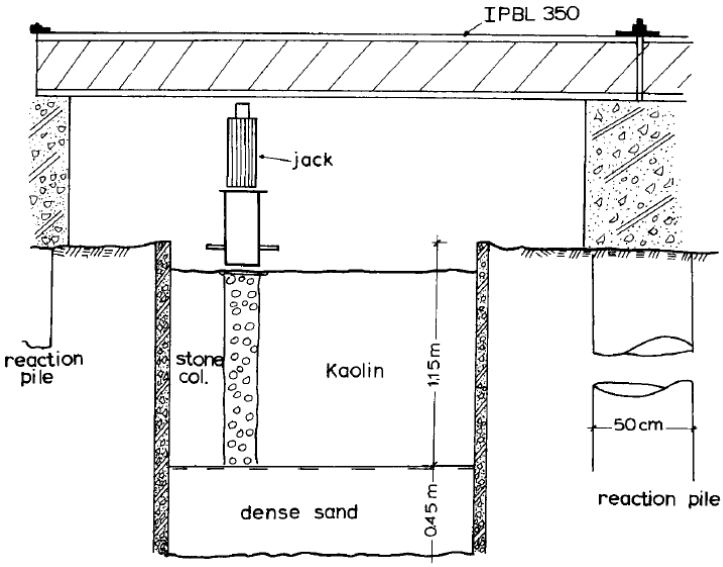

Figure 2.7 Cross-section of the test setup (Christoulas et al., 2000)

Black et al. (2007) investigated the performance of stone columns in peat. They studied the effect of adding reinforcement to the stone columns. Stone columns were reinforced with tubular wire, metal bridging rods, and a concrete plug. They observed that adding this reinforcement to the stone column caused a significant increase in the axial capacity of the columns.

Drained tests were conducted by Shahu et al. (2011) in the laboratory on floating stone columns. They found that there is a critical vertical load after which excessive settlement occurs without any stress change. This critical stress could be assumed as the bearing capacity of stone columns. They also concluded, based on a finite element model, that the footing thickness, the dilation angle, and the friction angle of stone columns have a minor effect on the behaviour of stone columns. This finding does not agree with many other studies such as Madhav et al. (1978), Priebe (1991), and Etezad et al. (2015).

2.1.3 Stone column simulation using triaxial apparatus

Triaxial apparatus was used to simulate the interaction between the stone columns and the surrounding soil. In these tests, horizontal deformation was allowed while the horizontal stress was controlled to remain constant. Sivakumar et al. (2004) used an assumption first made by Hughes

et al. (1974a) that the stone column in the ground could be modeled as an individual unit cell. A stone column of 32 mm diameter with different heights (60 mm, 120 mm, 160 mm, and 200 mm) were installed in Kaolin clay samples of 100 mm diameter and 200 mm height. A single stone column was installed in each clay sample by one of three methods: wet sand compacted in a predrilled hole, frozen sand column inserted in a drilled hole, or frozen sand columns surrounded by a geosynthetic sheet. Also, two loading techniques were used, the first was by applying the load on the sample and the second was by applying the load by a 40 mm diameter footing as shown in Figure 2.8.

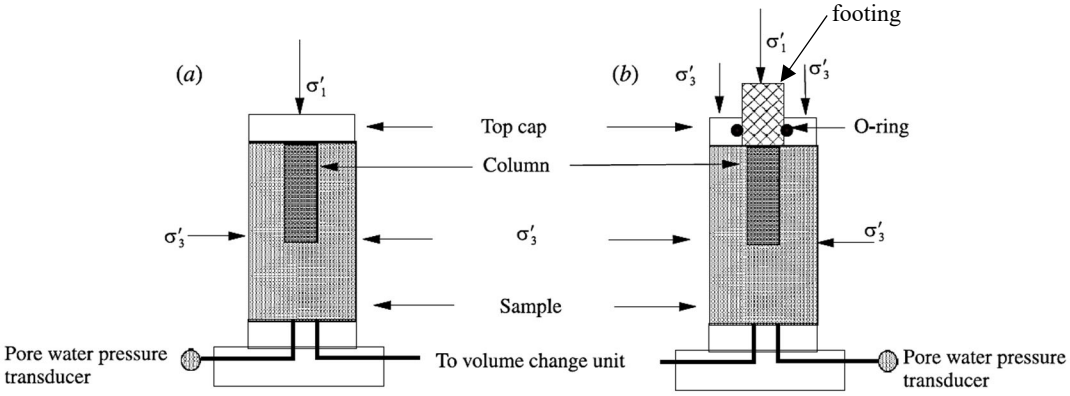

Figure 2.8 Loading methods: (a) uniform loading, (b) footing loading (Sivakumar et al., 2004)

The results from the wet compacted sand method were disturbed. However, the results from the frozen technique were clear. Thus, it is concluded that the method of installation has a significant effect on the behaviour of stone columns. Only bulging failure mechanisms were reported in this study. It was also reported that there is a significant increase (40%) in the vertical capacity of the column even when the area ratio A_s was 10%, which conflicts with the findings from other researchers, such as Hu (1995) and Hanna et al. (2013), who reported that there is a minor change in the vertical capacity of stone columns when A_s is less than 20%.

Black et al. (2007) built on the work by Sivakumar et al. (2004). In additional to examining the behaviour of stone columns in drained and undrained conditions, they studied the effect of using three stone columns of 20 mm diameter each and one column of 32 mm diameter inside a clay sample in a triaxial test. The frozen sand column technique was used in the study, which is different from the installation method in the field. They concluded that resistance of a group of stone

columns is the same as a single column with the same cross-sectional area. However, they recommended that this conclusion be confirmed by other researchers.

2.1.4 Monitoring soil and stone column movements

The first method used to track the soil movement around stone columns during loading was the radiographic technique (Hughes et al., 1974a). Shot markers were inserted in the soil, and by turning on the X-ray source during the loading process to track the markers, the soil movement could be defined. This technique has not been used since because it is very expensive, and the use of x-ray poses a potential health hazard.

Hu (1995) explored the failure mechanism of a group of stone columns by removing the wet sand in the stone column area by a vacuum then using a liquid plaster to fill the holes; after 24 hours, the clay around the solid plaster was excavated. However, since the failure mechanism during loading cannot be simulated, this method presents the final shape of the failed columns.

McKelvey et al. (2004) and Kelly (2014) replaced the clay around the stone column by a transparent material. Although this method detected the process of deformation during loading, the performance of the transparent material did not consider all characteristics of the clay soil.

2.2 Numerical modelling

Numerical models can be powerful and useful tool that is widely used to simulate many complicated soil structure problems, such as the interaction between stone columns and cohesive soil. The unit cell technique can be used to simplify this problem (Balaam, 1978; Balaam et al., 1983; Barksdale et al., 1983a). Other studies used homogenous composite domains to simulate stone column problems (Mitchell et al., 1985; Schweiger et al., 1986; Hu, 1995). Currently, two and three-dimensional numerical models are used to investigate the interaction between stone columns and the surrounding soil (Muir Wood et al., 2000; Wehr, 2004; Egan et al., 2008; Hanna et al., 2013).

Balaam (1978) presented a numerical model for a single stone column utilizing the finite element loading path method. An elastic perfectly plastic material behaviour obeying the Mohr-column yield criteria were used to simulate both clay and stone columns. The clay was treated as cohesive while the stone columns were treated as frictional material with a dilatancy angle to govern the

volumetric change. Interface element used with reduced properties simulate column-soil interaction. This model was validated against the results from a field test by Hughes et al. (1975) as shown in Figure 2.9. Balaam et al. (1983) utilized the same model to anticipate the settlement of rigid raft on soil reinforced by stone columns, considering the unit cell concept. However, the results had a good agreement for stone columns with larger spacing more than stone columns with smaller spacing.

Barksdale et al. (1983a) used a finite element model developed in Georgia Tech to create design charts based on a single column technique. Due to boundary conditions, horizontal displacement was not allowed. However, field observations showed that under vertical pressure, horizontal deformations would occur in the columns as well as the soil (Goughnour et al., 1984). Thus, the authors modified the Georgia Tech model by adding another layer of elastic material around the soil to allow horizontal deformations (Figure 2.10). The stiffness of this layer had a significant effect on the result, as shown in (Figure 2.11).

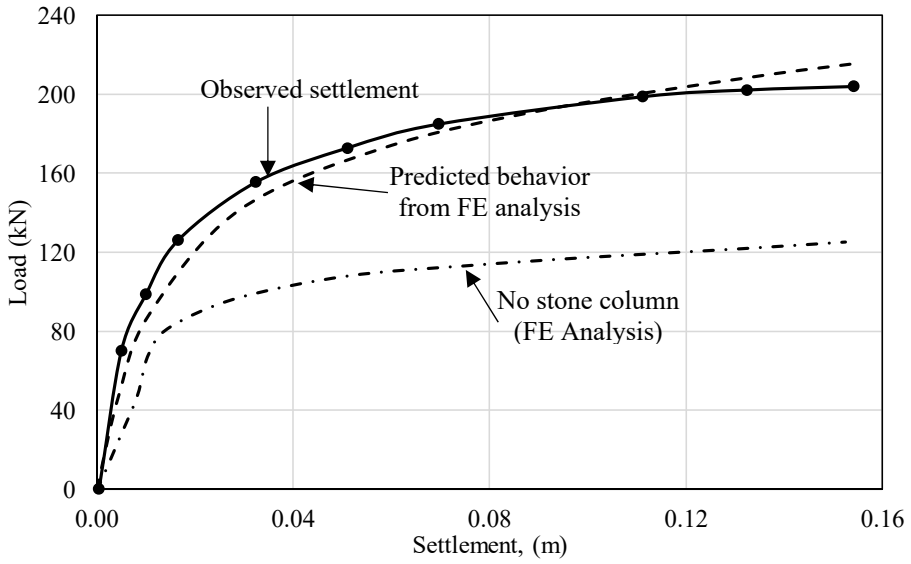

Figure 2.9 validation of numerical model results with Hughes and Withers field test results (Balaam, 1978)

The homogenization method is based on combining the elastic-plastic behaviour of stone columns and the surrounding soil. Gerrard et al. (1984) utilized this method to simulate a group of stone columns under a flexible strip footing. Tresca yield criteria were used for clay, and Mohr-Coulomb yield was used for the stone material. A constant vertical strain was assumed in the clay and the

stone columns, and the maximum vertical stress was located at a depth of 0.25 to 1 times the footing width.

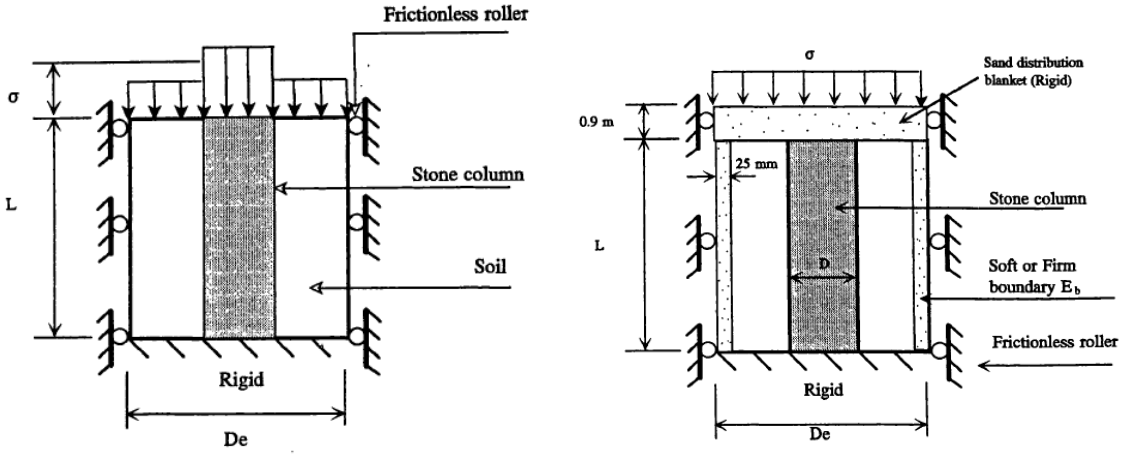

(a) Unit cell model (b) Modified unit cell model

Figure 2.10 Unit cell model (Barksdale et al., 1983a)

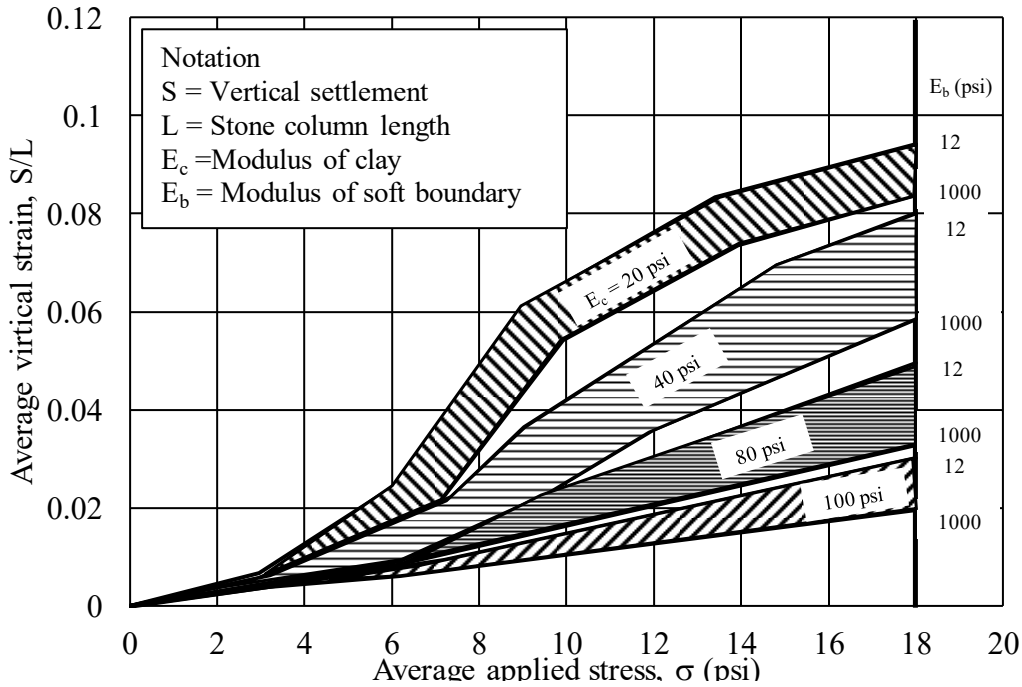

Figure 2.11 Effect of the stiffness of boundary layer on the capacity of a single stone column (Barksdale et al., 1983a)

The same concept was used by Schweiger et al. (1986) to estimate the settlement and the failure load under a raft resting on a clay soil reinforced by stone columns. The behaviour of the center

and edge column was studied under rigid and flexible footings. Their model is validated against the results obtained by Balaam et al. (1985). According to this study, they concluded that the plastic zone extended to a depth of 65% to 85% of the footing diameter. In 1988 they used the homogenization technique to model the settlement of a road embankment constructed on clay soil stabilized by stone columns.

A large scale physical model by Hu (1995) was compared to the numerical model that was developed at Swansea University by Lee et al. (1998). Figure 2.12 shows that the numerical prediction over-estimated the ultimate virtical capacity of stone columns by approximate 20%. Furthermore, the replacement area (A_s) recommended according to this numerical analysis was between 10% and 24%. However, Hu reported that the minimum replacement area required for bearing capacity improvement is 25%. Lee et al. (1998) improved their numerical model by considering the volume fraction of stone columns and used modified cam clay and Mohr-Coulomb failure criteria to model clay and stone columns, respectively. As shown in Figure 2.13, the new model showed a good agreement with the experimental test results of Hu (1995).

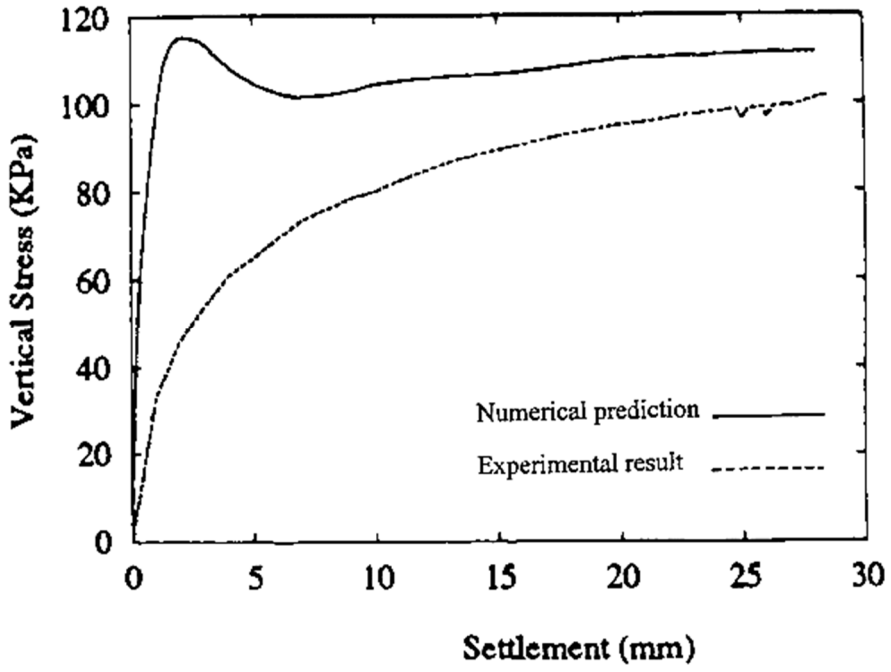

Figure 2.12 Comparison of the experimental results and numerical predictions (Hu, 1995)

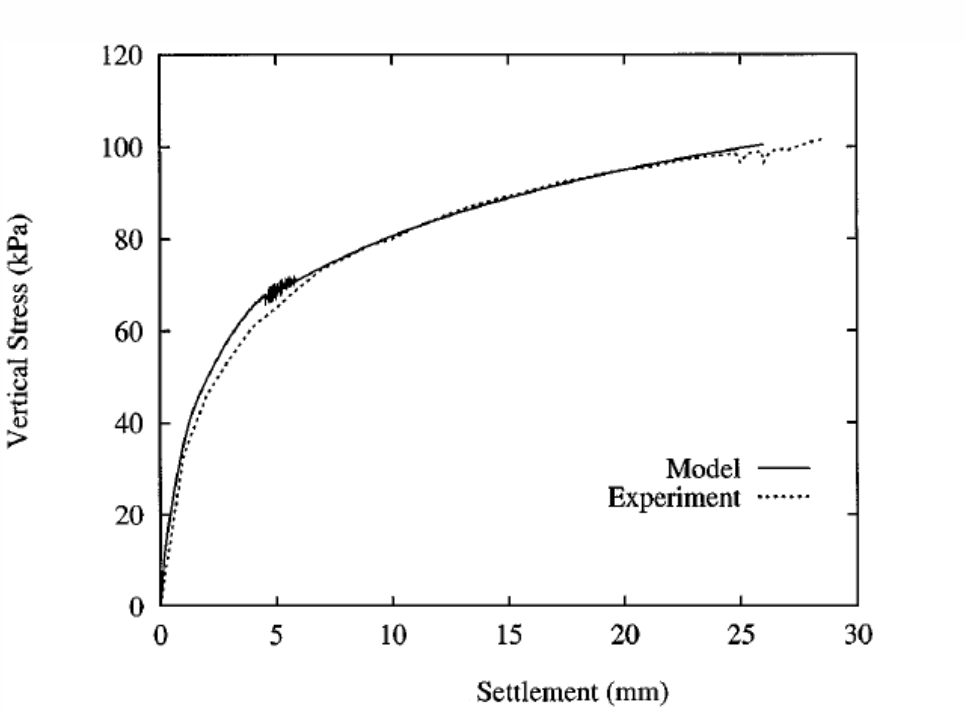

Figure 2.13 Experimental and numerical settlement and stress relationship (Lee et al., 1998)

Muir Wood et al. (2000) preformed a fully drained two-dimensional numerical analysis using Fast Lagrangian Analysis of Continua (*FLAC*) numerical modeling software. A rectangular rigid footing was utilized to apply a vertical load on a clay soil improved by a vertical sand trench. The clay and sand were modelled as strain hardening frictional material and strain-softening material, respectively. The model was validated with small scale experimental data and it was concluded that the critical depth is not constant, and that it increases as the replacement area increases (Figure 2.14). They argued that a clear understanding of the behaviour of stone columns and adjacent soil can only come from three-dimensional numerical modelling.

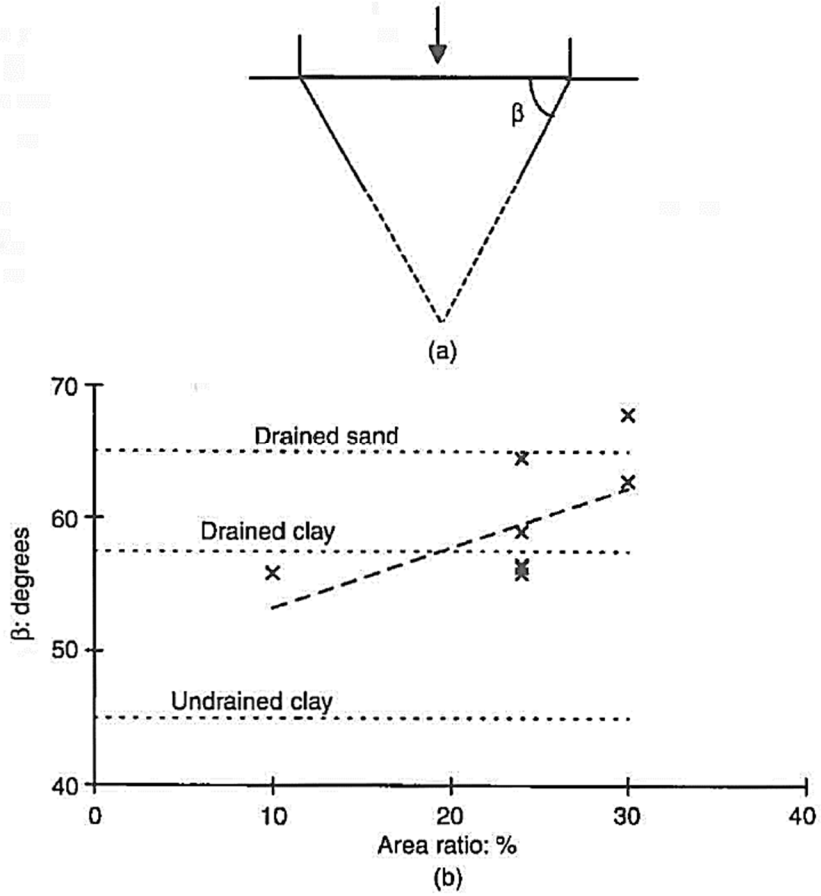

Figure 2.14 (a) Rigid zone below footing; (b) The effect of replacement ratio on the rigid zone (Muir Wood et al., 2000)

A qualitative two-dimensional finite element analysis study by Bae et al. (2002) showed that the critical depth of the stone columns ranged from 2.3*D* to 3.8*D*. Furthermore, they concluded that the bearing capacity of the stone columns is affected by the replacement area and the undrained shear strength of the adjacent clay. Wehr (2004) used the same concept to illustrate the difference between the failure mechanism of a single stone column and a group of columns. He reported that a group of stone columns failed in a cone shape, not in a bulging like a single column. This finding had an agreement with the observations made by Hu (1995) and Bae et al. (2002). They also confirmed that the undrained shear strength of the surrounding clay has a significant effect on the bearing capacity of stone columns.

Based on two-dimensional numerical analysis, Ambily et al. (2007) reported that the stress concentration ratio (n) increases as the cohesive strength of the adjacent clay decreases. They also found that the concentration ratio (n) for the group of columns with spacing between 1.5 D and 4 D is the same as a single column. In contrast with Bae et al. (2002) and Wehr (2004), they found that the cohesive strength of the adjacent clay has an insignificant effect on the overall stiffness of the soil reinforced by stone columns, but that it mainly depends on the internal friction angle of the stone.

Guetif et al. (2007) and Egan et al. (2008) utilized numerical analysis to study the effect of the stone column installation method on the properties of the surrounding clay. They reported that the lateral coefficient of earth pressure, as well as the Young's modulus of the adjacent clay, significantly increased due to the installation of vibro displacement columns. Based on a numerical model validated against field data, Castro et al. (2010) found that the lateral earth pressure coefficient was approximately 1.4 times the lateral coefficient for unreinforced soil. Moreover, they recommended a reduction of 15% to 20% in the undrained cohesion of the soil around the column. However, this reduction is limited to the soil extended to eight to ten times the column radius (Figure 2.15).

Hanna et al. (2013) developed a two-dimensional model to investigate the failure mechanism of a single and group failure. A Mohr-Coulomb constitutive model was used to represent the columns and the surrounding soil. The model was validated against experimental results reported by Hu (1995). A parametric study has been done to investigate the effect of the parameters shown in Table 2.1 on the bearing capacity of reinforced clay as well as the failure mechanism. A replacement ratio ranging from 10% to 35% was used in the study to represent group interaction. They reported design charts which categorized the failure mechanism of a group of stone columns in three groups, general, local, and punching shear failure (Figure 2.16) according to the replacement area and the column and soil friction angles.

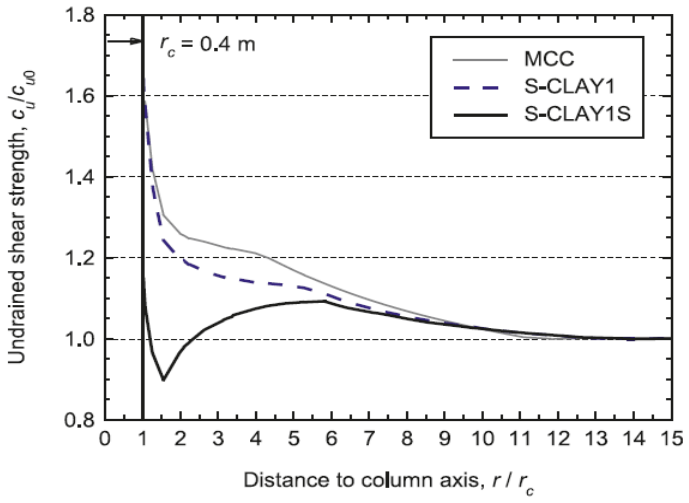

Figure 2.15 Effect of stone column installation on the shear strength of adjacent clay (Castro et al., 2010)

Table 2.1 Parameters used in the parametric study (Hanna et al., 2013)

Site conditions	Range of values
Clay module of elasticity (kN/m^2)	1,500–14,000
Sand module of elasticity (kN/m^2)	35,000–175,000
Clay Poisson's ratio	0.15–0.45
Sand Poisson's ratio	0.2–0.45
Sand friction angle	38–45°
Angle of dilatancy	$\Psi = \varphi - 30°$ (Bolton 1986)
Area ratio	10, 20, 30, and 35%
Stone column diameter	0.6, 0.8, 1, and 1.2 m
Stone column length	14–20 m
Type of loading	Uniform rigid loading

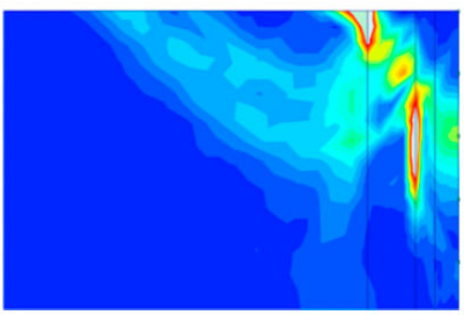

a) General shear failure

b) local shear failure

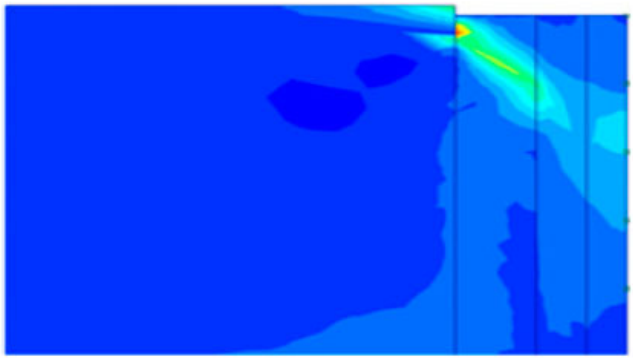

c) Punching shear failure

Figure 2.16 Failure types on a group of stone columns (Hanna et al., 2013)

Castro (2014) examined the behaviour of a single stone column and group of stone columns in drained condition using two and three-dimensional numerical modelling techniques. He found that the arrangement of the columns below a small rigid footing had an insignificant effect on the load-displacement curve. The interaction between columns and the surrounding soil was neglected as well as the installation effect on the horizontal earth pressure coefficient of the soil, which had a significant effect on the results (Guetif et al., 2007; Egan et al., 2008; Castro et al., 2010). An elastic perfectly plastic behaviour was utilized to simulate the granular column and the adjacent soil by using Mohr-Coulomb failure criteria. It was stated that the effect of columns spacing, as well as the number of columns, was small for a replacement area of 10% (Figure 2.17) since the group interaction is negligible at a replacement ratio less than 10% (Hanna et al., 2013). Although a small replacement ratio was used in the study, general shear failure occurred in the columns with large spacing, and bulging happened in columns near to the center of the footing (Figure 2.18). Also, it was recommended that the critical length of the columns must be related to the footing width, not the diameter of the column.

As a conclusion, the unit cell concept or the homogenization technique is applicable for small replacement ratios around 10%. Nevertheless, the optimum replacement ratio is between 30% to 40% (Black et al., 2011). Consequently, the unit cell concept does not represent the actual behaviour of the stone columns, and the group interaction must be considered as a principal factor.

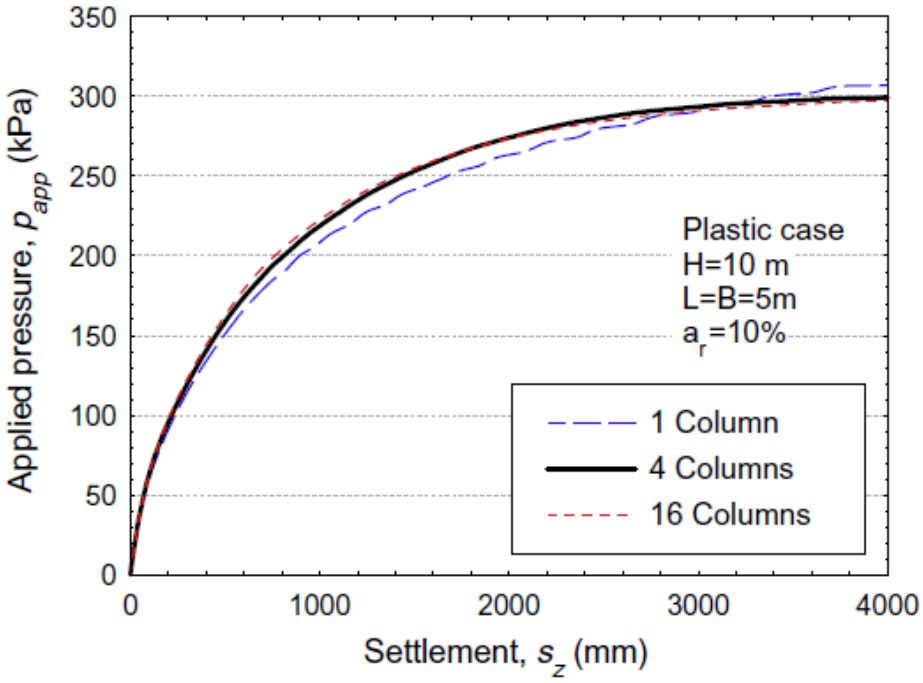

Figure 2.17 Load settlement curve for different column numbers (Castro, 2014)

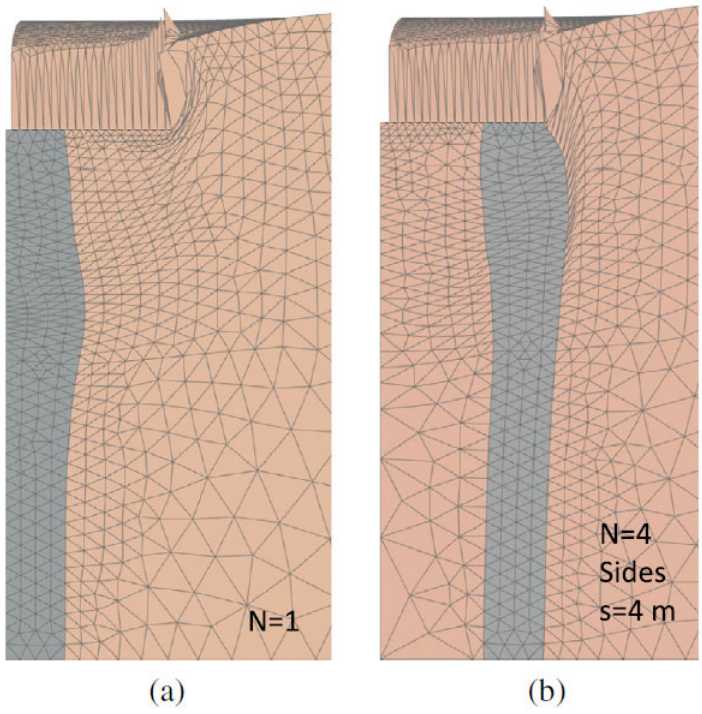

Figure 2.18 Effect of column spacing on the failure mechanism (Castro, 2014)

2.3 Bearing capacity of soil reinforced by stone columns

The unit cell concept was the first method used to estimate the bearing capacity of stone columns. By predicting the bearing capacity of a single stone column, the capacity of the group is equal to the capacity of the single pile multiplied by the number of columns. The bulging failure is only considered in this method. Thus, the bearing capacity of a single stone column could be calculated by estimating the horizontal capacity of the clay soil around the pile. Hughes et al. (1974a) used elastic-plastic theory developed by Gibson et al. (1961) to calculate the maximum vertical stress that can be carried by a single stone column due to bulging failure. Therefore, the ultimate capacity of a single stone column could be calculated using the following equation:

$$q_u = k_p(\sigma_{ro} + 4c_u - u) \times \mathrm{A} \qquad (2\text{-}2)$$

Where k_p , is the passive earth pressure coefficient for the column material, σ_{ro} is the effective lateral stress, c_u and u are the cohesion and the pore water pressure in the surrounding soil.

Brauns (1978) assumed a shear failure, as shown in Figure 2.19 with an angle of $45 + \frac{\phi_s}{2}$. Therefore, a theory of bearing capacity was developed supposing that the behaviour of the stone column is like the behaviour of a cylindrical sample of cohesionless soil. Barksdale et al. (1983a) utilized the cylindrical cavity expansion theory developed by Vesic (1972) to estimate the bearing capacity of a single stone column using the following equation:

$$q_{ult} = \left[c_u \times F_c^{'} + q \times F_q^{'} \right] K_p \qquad (2\text{-}3)$$

Where c_u and q are the cohesion and the mean stress at the equivalent failure depth. $F_c^{'}$, and $F_q^{'}$ are the cavity expansion factors which are a function of soil properties around the column and the foundation rigidity. K_p, is the passive earth pressure of the surrounding clay. They also developed equation (2-4) to estimate the ultimate bearing capacity of a footing resting on a cohesive layer reinforced by stone columns depending on the assumed shear failure plane shown in Figure 2.20.

$$q_{ult} = \left(\frac{\gamma_c \times B \times \tan(45 + \frac{\phi_{avg}}{2})}{2} + 2c \right) \times \tan^2(45 + \frac{\phi_{avg}}{2}) + 2\,c_{avg} \tan(45 + \frac{\phi_{avg}}{2}) \qquad (2\text{-}4)$$

Where B is the footing width, γ_c and c_u are the unit weight and the cohesion of the clay respectively, ϕ_{comp} and c_{comp} are calculated using the following equations:

$$\phi_{comp} = \tan^{-1}(nA_s \tan\phi_s) \qquad (2\text{-}5)$$

$$c_{comp} = (1 - A_s)c_u \qquad (2\text{-}6)$$

Where μ_s and A_s are the stress concentration factor for the stone and the replacement ratio, respectively. ϕ_s, and $c$are the undrained friction angle of the granular material in stone columns and the undrained cohesion of the adjacent clay soil, respectively.

Madhav et al. (1978) reported that general shear failure, bulging, or punching could occur in the stone columns system (Figure 2.21). Two general failure planes were used to represent the failure in cases where the footing width is bigger or smaller than the trench width (Figure 2.22). Accordingly, they developed an equation to estimate the bearing capacity of a strip footing lies on a trench of granular material using the upper bound theorem and considering Mohr Coulomb's failure criteria. This equation is presented in a form similar to the general bearing capacity equation for a shallow foundation.

$$q_u = c_u N_c + D_f \gamma_c N_q + \frac{1}{2} B \gamma_c N_\gamma \qquad (2\text{-}7)$$

Where

$$N_c = \frac{c_s}{c_u} N_{c1} + N_{c2} \qquad (2\text{-}7)$$

and

$$N_\gamma = \frac{\gamma_s}{\gamma_c} N_{\gamma 1} + N_{\gamma 2} \qquad (2\text{-}8)$$

N_{c1}, N_{g1}, N_{c2}, N_{g2}, and N_q are factors depend on the properties of the granular material and the soft soil and the A/B Ratio. A and B are the width of the granular trench and the strip footing, respectively. c_u, γ_c and c_s, γ_s are the cohesion and the unit weight of the soil and granular trench, respectively.

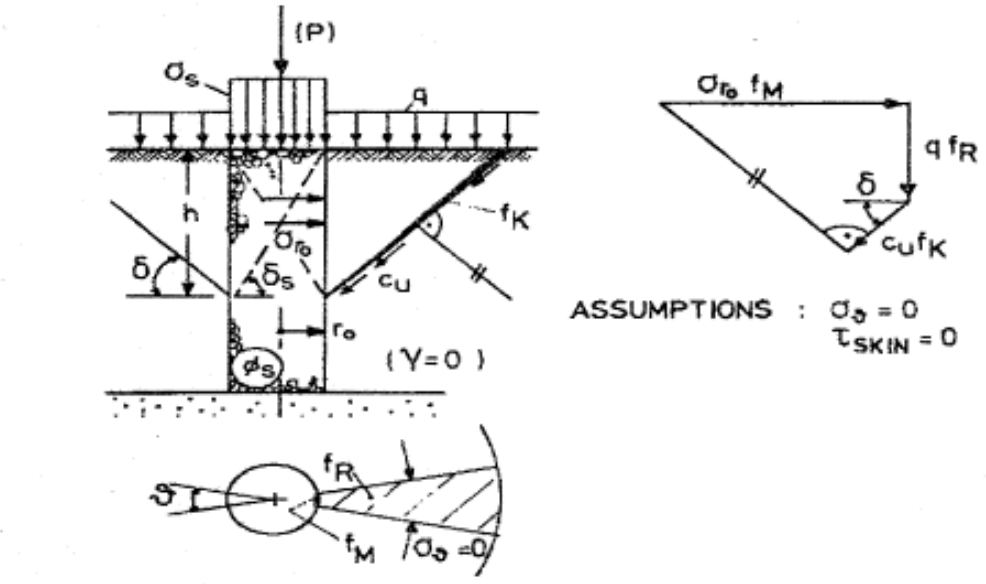

Figure 2.19 Analysis of bearing capacity of stone columns (Brauns, 1978)

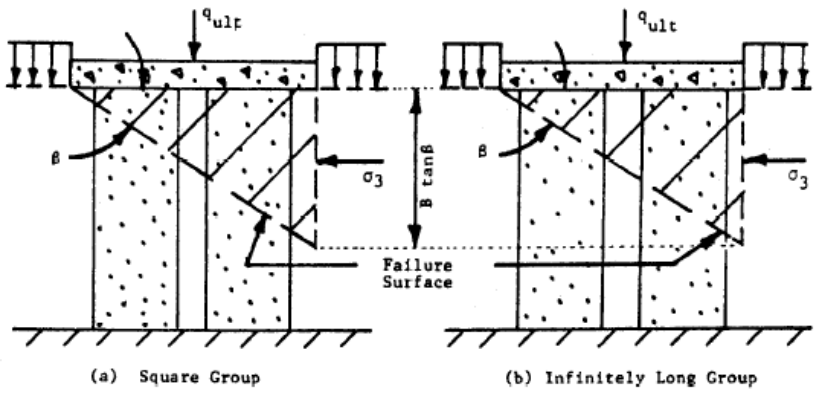

Figure 2.20 Failure plane for strip and square stone column group (Barksdale et al., 1983a)

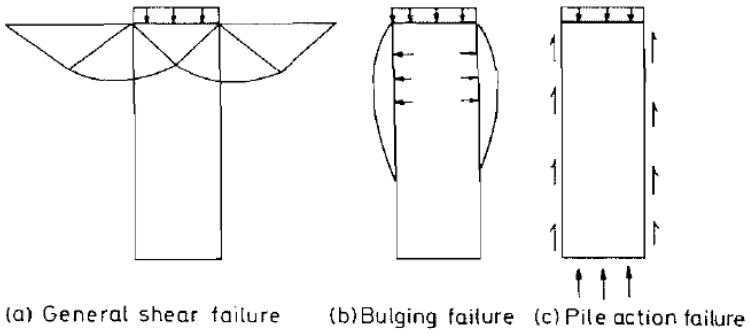

Figure 2.21 Types of failure (Madhav et al., 1978)

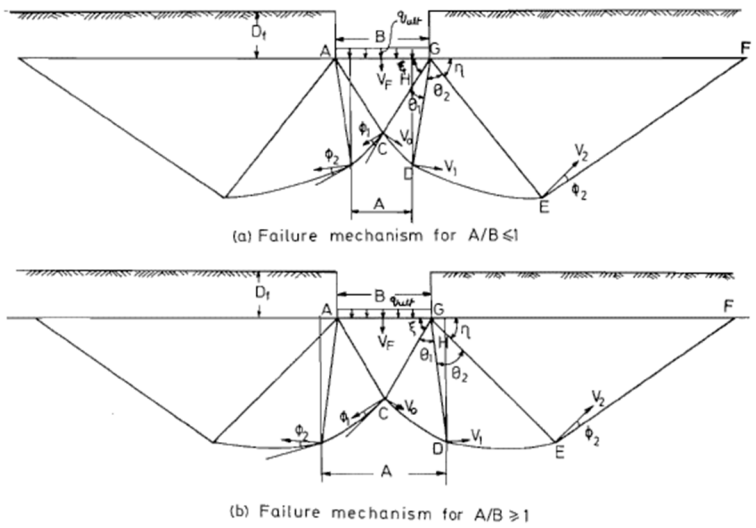

Figure 2.22 Failure mechanism of a trench of granular material under strip footing (Madhav et al., 1978)

Based on general shear failure (Figure 2.23) and equivalent soil assumption, Priebe (1991) reported two methods to estimate the bearing capacity of a footing on a group of stone columns. In the first method, the average values of friction angle, and average values of the cohesion along the failure plane were considered, and the bearing capacity was calculated using the same method for unreinforced soil. In the second method, an equivalent footing width was assumed, which is larger than the actual footing width, as shown in Figure 2.23, and the bearing capacity calculated as normal using the equivalent width and the shear properties of the unreinforced soil.

Bouassida et al. (2009) developed a limit analysis approach for a rigid footing rest on floating piles. In their study, the friction between the footing and the soil was neglected as well as the distribution of stone columns. A maximum column length was calculated from the properties of reinforced soil using the chart shown in Figure 2.24. This maximum length was required to achieve the maximum value of the lower bound bearing capacity regardless of the type of soil at the column tip. Based on this maximum length, they developed a design chart to estimate the ultimate bearing capacity of a group of stone columns.

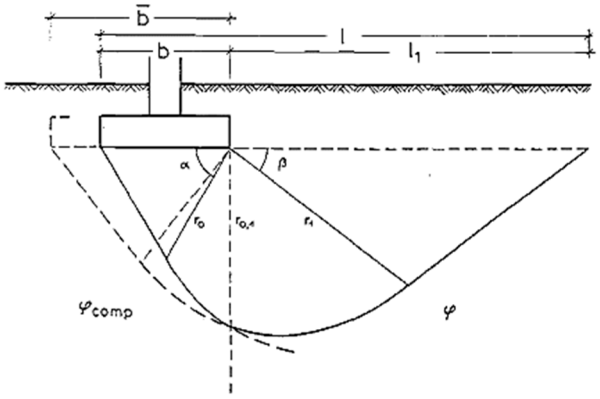

Figure 2.23 General shear failure (Priebe, 1991)

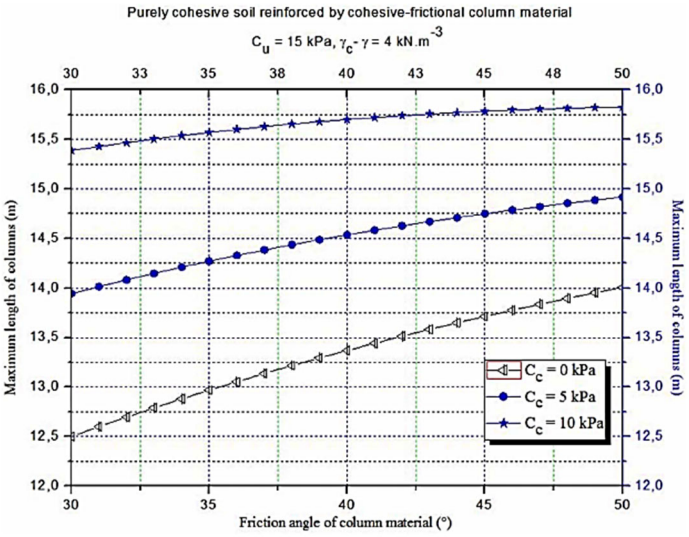

Figure 2.24 Estimation of maximum column length with respect to its friction angle (Bouassida et al., 2009)

An analytical model was developed by Etezad et al. (2015) using the limit equilibrium method and equivalent soil properties under the footing to calculate the bearing capacity of raft footing supported by stone columns. Based on a two-dimensional numerical analysis by Hanna et al. (2013), a general shear failure mechanism was utilized and divided into three zones (Figure 2.25). Under the footing, a triangular shape was assumed following the classic bearing capacity theory. The second zone consisted of a log spiral curve separated into two parts, one within the equivalent soil and the other part in the original clay. The last part connected the second part with the ground. The form of a general bearing capacity equation for shallow foundation was used to present the devised equation.

$$q_{ult} = c_{comp} N_c + qN_q + \frac{1}{2} B\gamma_{comp} N_\gamma \tag{2-9}$$

Where N_c, N_q, N_γ are the bearing capacity factors, and c_{comp}, γ_{comp} and ϕ_{comp} are the equivalent properties of the soil under the footing, calculated using the following equations:

$$c_{comp} = A_s c_s + (1 - A_s) c_u \tag{2-10}$$

$$\gamma_{comp} = A_s \gamma_s + (1 - A_s) \gamma_c \tag{2-11}$$

$$\phi_{comp} = \tan^{-1}\left[A_s \mu_s \tan\phi_s' + (1 + A_s) \mu_c \tan\phi_c' \right]$$

$$\mu_s = \frac{n}{1 + (n-1)} A_s \tag{2-12}$$

$$\mu_c = \frac{n}{1 + (n-1)} A_s$$

Where A_s is the replacement area, c_s, γ_s and ϕ_s' are the cohesion, unit weight and friction angle of the stone column material, c_u, γ_c and ϕ_c' are the cohesion, unit weight, friction angle of the soil, and n is the stress concentration ratio.

This equation was validated against classic bearing capacity factors. However, the value N_γ was slightly higher than the values calculated by Soubra (1999) and lower than Bouassida et al. (2002) and Chen et al. (2012). Also, the bearing capacity calculations using this equation was validated against a numerical study by Hanna et al. (2013) and an experimental study by Hu (1995) and McKelvey et al. (2004), both of which showed a good agreement.

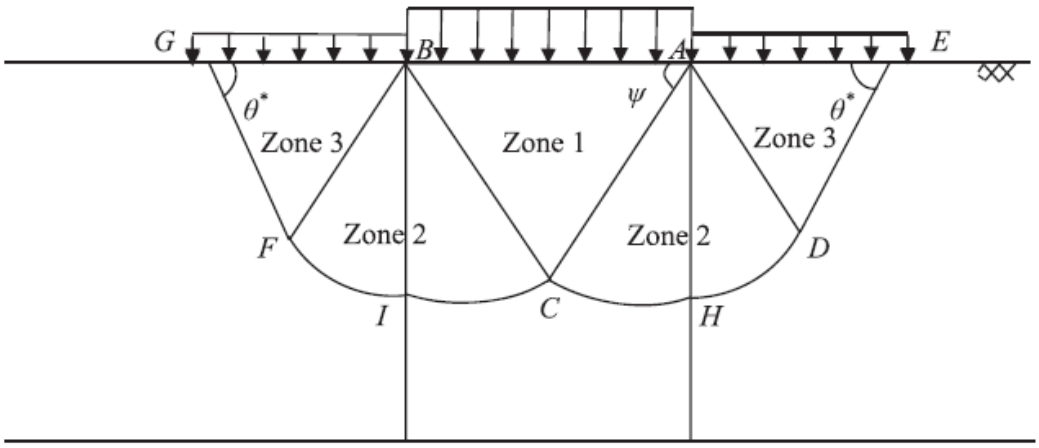

Figure 2.25 Failure Plane (Etezad et al., 2015)

2.4 Effect of displacement method

The installation of stone columns using the displacement method (vibro-replacement) requires a large horizontal deformation in the soil adjacent to the stone columns. Therefore, the properties of the surrounding soil significantly change (Indraratna et al., 1998; Guetif et al., 2007; Egan et al., 2008; Castro et al., 2014).

Vautrain (1980), Al-Khafaji et al. (2000), Almeida et al. (2000), and Alamgir et al. (2001) introduced the influence of displacement method on the surrounding soil as an increase in the undrained shear resistant of the soil (c_u). The change in the ratio between the shear resistance of soil before (C_{uo}) and after (C_{um}) stone columns installation with depth is shown in Figure 2.26. It could be concluded from the figure that the improvement in the cohesion ranges from 1 to 4.5 times the cohesion of the clay soil before stone column installation.

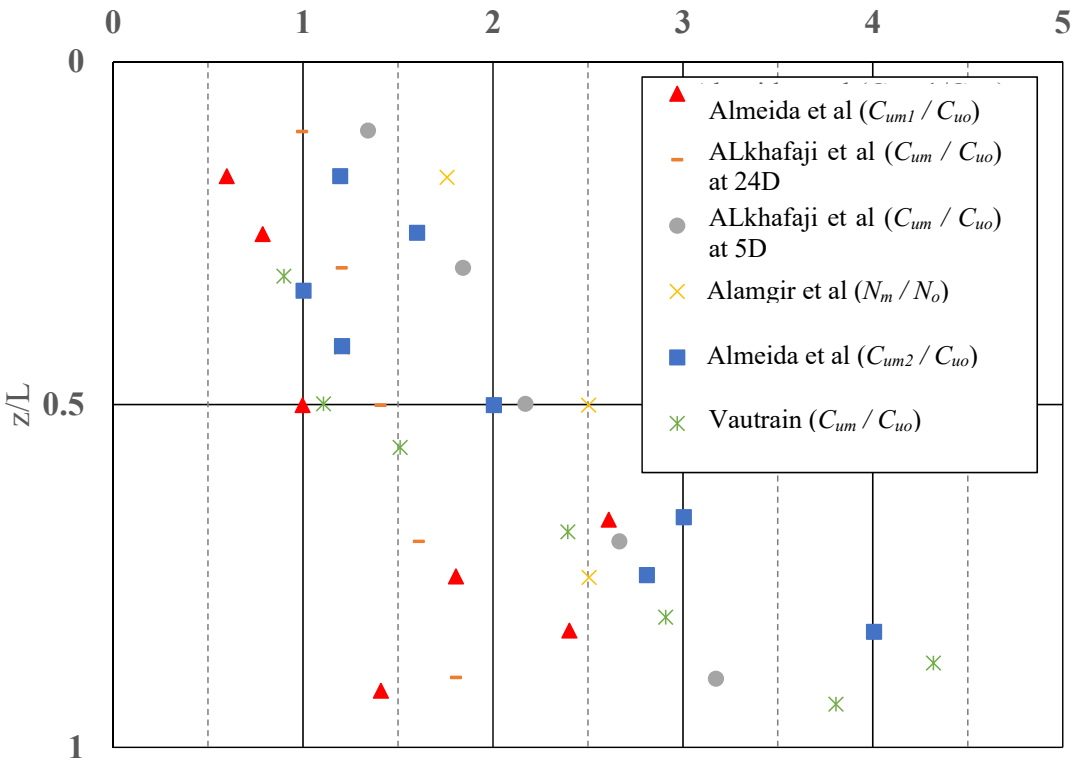

Figure 2.26 Effect of column installation on the shearing resistance of surrounding soil (Guetif et al., 2007)

Priebe (1995), Watts et al. (2000), Pitt et al. (2003), Elshazly et al. (2008), and Castro et al. (2010) reported the stone columns installation effect as an increase in the horizontal coefficient of the surrounding soil (k). The horizontal coefficient (k) is defined as the ratio between the horizontal stresses and vertical pressure. A summary of the estimated values of the horizontal coefficient after stone column installation are presented in Table 2.2. Elshazly et al. (2008) reported an inverse relation between horizontal coefficient and spacing between stone columns (S).

Moreover, displacement stone column causes a reduction in the coefficient of permeability of the clay around the column up to a distance of 0.3 of the stone column radius (Weber et al., 2010). Accordingly, the rate of consolidation is reduced, particularly in the initial stage of consolidation (Indraratna et al., 2012). Nevertheless, Castro et al. (2014) concluded that displacement stone columns have a positive effect on reducing the total settlement of reinforced clay soil.

Table 2.2. Values of horizontal coefficient (k) in the literature

References	Horizontal coefficient value (k)
(Goughnour, 1983)	From at-rest earth pressure coefficient (k) to $1/k_o$
(Priebe, 1995)	1.0
(Watts et al., 2000)	Between at rest (k_o) and passive (K_p) earth pressure coefficients.
(Pitt et al., 2003)	from 0.4 to 2.2
(Elshazly et al., 2008)	from 0.7 to 2.0
(Kirsch, 2008)	from 1 to 1.6 k_o
(Castro et al., 2010)	from 2 to 4 k_o

Based on a full-scale experimental study, Watts et al. (2000) reported that the influence of the installation extends to 2.5 times the column diameter (D). However, Kirsch (2008) stated that the influence ranges from 4 to 5 times D. Weber et al. (2010) divided the clay around the stone columns into three zones: penetration zone (0.35 to 0.5 D), smear zone (0.5 to 0.6 D), and Compaction zone (0.6 to 1.25 D). Consequently, the total affected zone ranges from 1.5 to 2.5 times the column diameter.

Even though many studies have been conducted to investigate the effect of the displacement method on clay soil, the findings are contradictory. Furthermore, the influence of this method on the bearing capacity of a group of stone columns has not been adequately investigated. Thus, an innovative approach is required to simulate the displacement method experimentally and to numerically examine its effect on the bearing capacity of a group of stone columns.

2.5 Discussion

The behaviour of stone columns depends on lateral support from the surrounding soil. For a single-column concept, when the vertical load increases, it will lead to lateral displacement in the stone column and farther bulging failure will occur. However, since stone columns are always used in groups, the vertical stress is applied to the columns and the surrounding soil, which leads to an increase in the horizontal resistance of the surrounding soil. In this case, a general shear failure is a common mechanism. However, for short columns and floating columns, punching failure may

occur due to low-end bearing resistance. Thus, the single-column concept does not represent the actual failure mechanism in a group of stone columns.

Using the group technique is closer to the actual behaviour of a group of stone columns. Nevertheless, most of the previous studies were done on small models at single gravity, and there are questions concerning the scale effect as well as the boundary problem. Changing from a low-stress level used in the laboratory to a high-stress level in the field may not be persuasive. On the other hand, large scale tests are expensive, and it is difficult too to clearly reveal the interaction between stone columns and the soil around them in a full-scale model.

The triaxial test is a technique used to study the performance of stone columns. Since the horizontal deformations are not restrained and the stresses around the sample are controllable, the behaviour of stone columns can be tested under high-stress levels. This method was therefore used in this research to examine the performance of groups of stone columns in cohesive soil. The effects of some parameters on the capacity of stone columns is still unknown, such as the stress levels in the triaxial test, the spacing between columns, and the stress concentration ratio.

Even though numerical models need calibration with experimental or field tests, they are currently one of the most powerful tools for studying such complex problems as the interaction between stone columns and the adjacent soil. However, the two-dimensional numerical analysis or homogenization method that has previously been used, makes it difficult to accurately simulate an array of stone columns under the footing (Muir Wood et al., 2000). Since existing analytical and numerical models cannot capture the actual behaviour of stone columns and the effect of all the governing parameters, it is necessary to explore 3-D modelling as a solution to the problems arising from the simplifications and assumptions needed in analytical or experimental work.

Chapter 3: Experimental Investigation

3.1 Introduction

One of the main challenges of laboratory testing of a group of stone columns is to create a prototype simulation of a clay soil reinforced with a group of stone columns. In order to tackle the influences of the major design parameters on the bearing capacity of the reinforced clay soil, the complexity of the vibro floatation method used for the installation of stone columns was simplified to a displacement method, and the non-homogeneity in the field layers was simplified to a one-dimensionally consolidated bed of homogenous clay.

In order to reduce the scale and boundary effects, the preparation of the clay soil and installation of the stone columns were conducted in a large rigid-wall tank. Nine core samples of the reinforced clay with a diameter of 10 cm were extracted from the tank and tested in a triaxial system.

3.2 Apparatus and sample preparation

3.2.1 General test requirements

The aim of experimental work was to represent a typical field simulation of stone columns using the vibro-displacement method. In order to create this model, the following were the test requirements.

1- A homogenous clay layer with an appropriate thickness and shear resistance to make it possible to create stone columns.
2- The stone columns prepared in such a way as to simulate the vibro- displacement method in the field. The installation procedure should be repeatable and consistent for all the columns.
3- A core sample of the stone columns and the clay around it should be extracted from the soil without causing any disturbance to the soil.
4- The core sample should undergo a triaxial test to investigate the effect of stone column geometric properties on the bearing capacity of the reinforced clay.

(Figure 3.1) show the setup use to prepare the clay layer and install stone columns. The setup details and the used equipment are described in the following section.

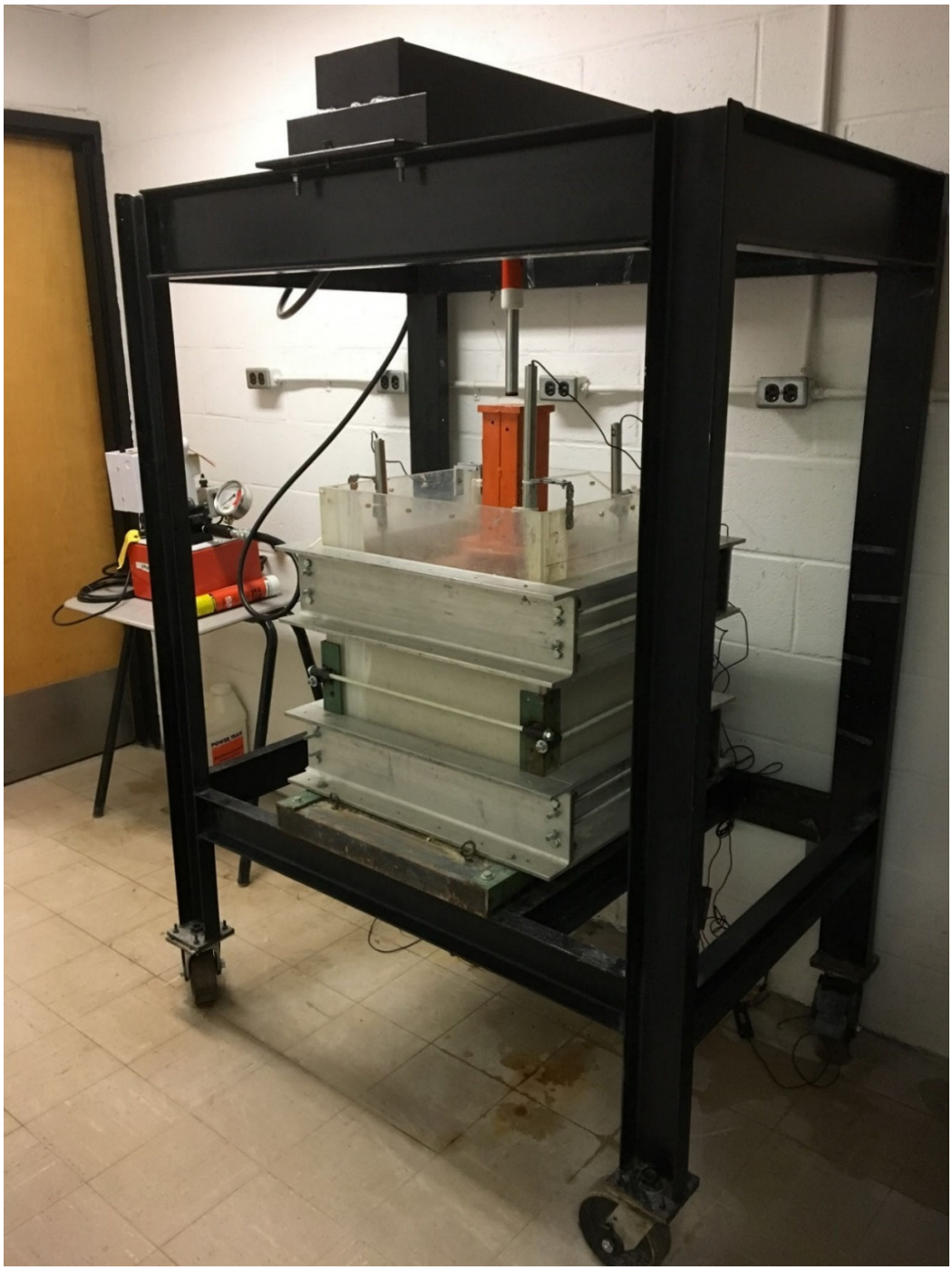

Figure 3.1 Setup for the consolidation and installation of stone columns

3.2.2 Consolidation tank and applying pressure

The triaxial test apparatus was used to apply pressure on the reinforced clay sample. It was not suitable to install the columns by the displacement method in the 10 cm clay sample that is tested in the triaxial apparatus. In addition to the installation difficulties, the displacement installation method for stone columns causes a disturbance in the clay around the columns (McCabe, 2009; Weber et al., 2010). Thus, the clay was created in a large tank with a plan dimensions of 50 X 50 cm and a height of 60 cm, as shown in Figure 3.2.

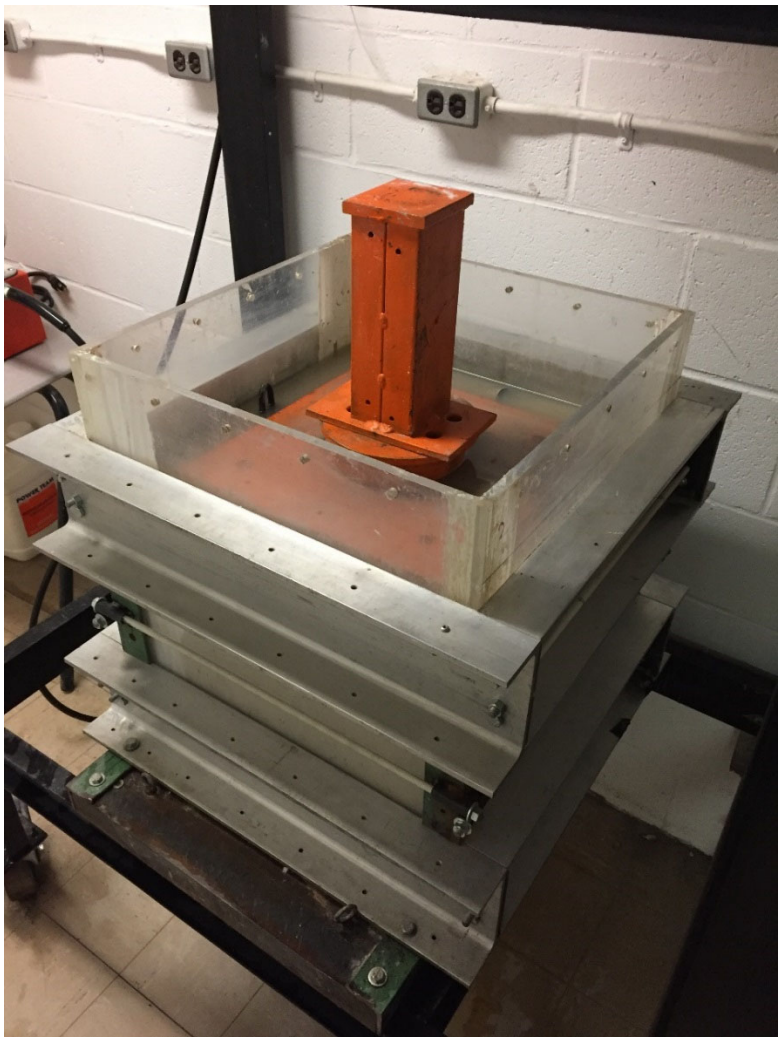

Figure 3.2. Consolidation tank

A consolidation process is required before constructing stone columns. A hydraulic loading system (Figure 3.3) attached to a steel frame was utilized to apply constant pressure on the clay

sample throughout the necessary time for the consolidation process. Also, two layers of coarse sand were placed above and below the clay layer to allow water expulsion during consolidation.

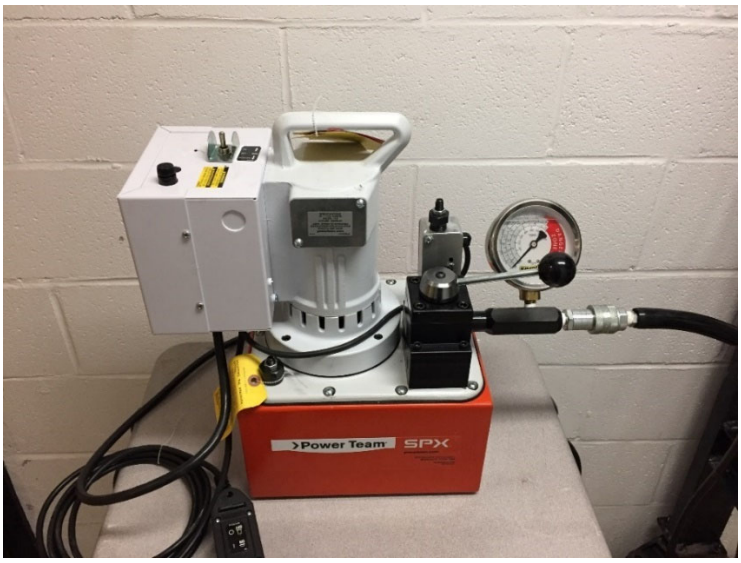

Figure 3.3 Hydraulic system

3.2.3 Sand columns installation

The displacement method was utilized for construction of the stone columns. A thin wall of steel tubes, 45 cm high and closed with a separate aluminum cone was used to create a hole in the clay. Outer diameters of 2.1 cm, 3.0 cm, 3.9 cm and 5.1 cm were utilized to achieve different replacement ratios. A constant opening angle of 60 degrees was used for all the cones to achieve a consistent effect during the driving process for all column diameters. Details of the steel tubes and solid cones are shown in Figure 3.4. The same loading hydraulic system used in the consolidation process was utilized to drive all the tubes in the clay. Stone columns were constructed in the large tank with two different arrangements, as shown in Figure 3.5. In order to distribute the columns in the tank, two wood templates shown in Figure 3.6 were used. The openings in the wood templates were larger than the diameter of the steel pipes by 1.0 mm to allow smooth movement of the steel pipes during stone column installation. There was a vertical distance of 10 cm between the two wood plates to ensure verticality of the tubes during construction of the stone columns.

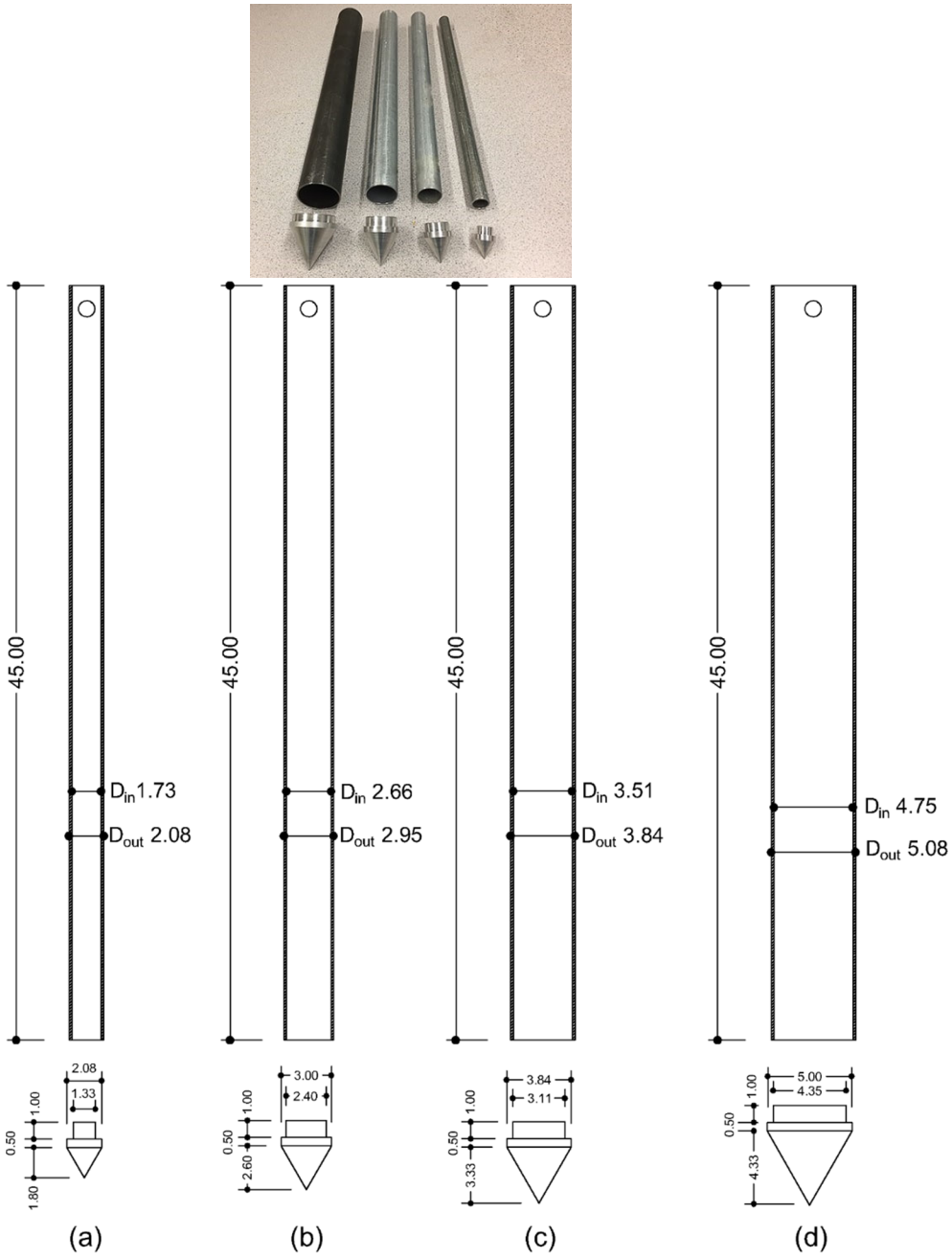

Figure 3.4 Details and dimensions (in cm) of stone columns installation tools: (a) 2 cm columns, (b) 3 cm columns, (c) 4 cm columns, and (d) 5 cm columns

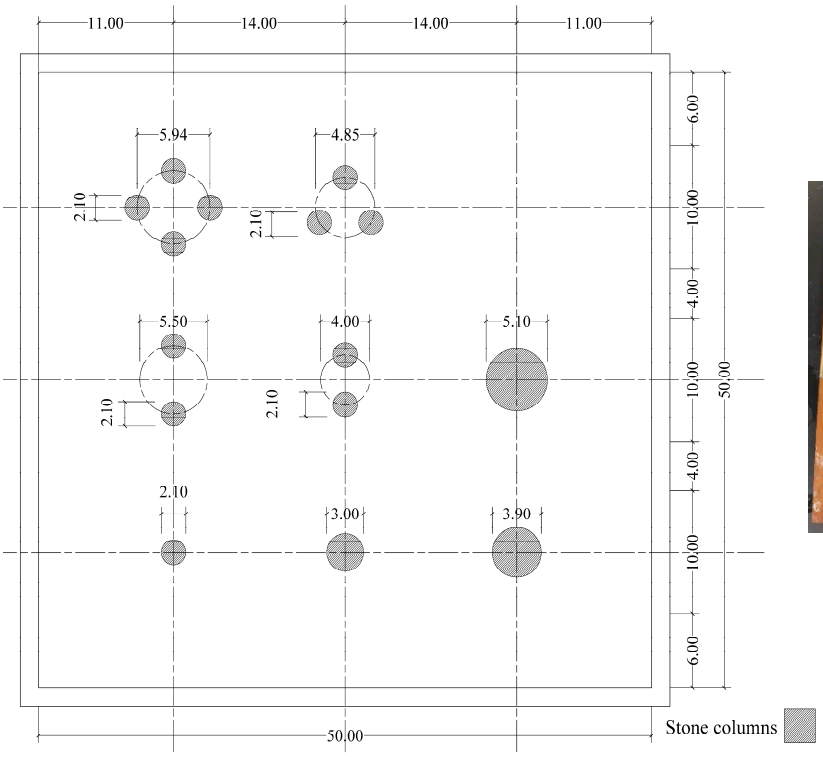

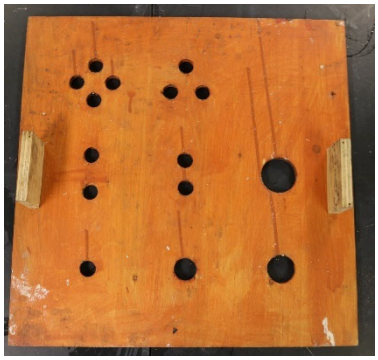

(a)

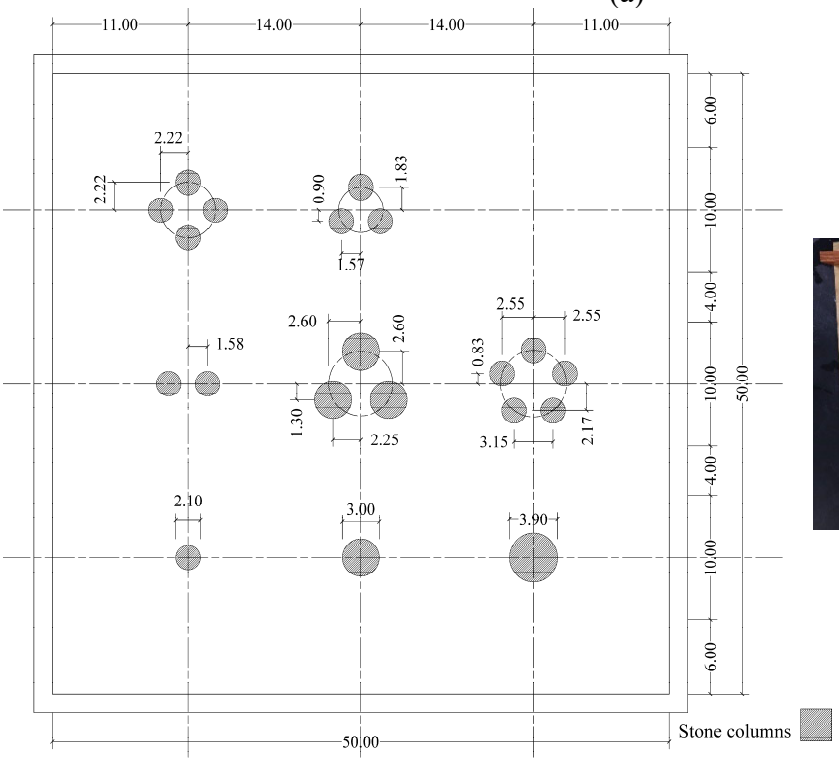

(b)

Figure 3.5 Stone columns arrangement in the consolidation tank (dimensions in cm): (a) T1 - T4 & (b) T 5

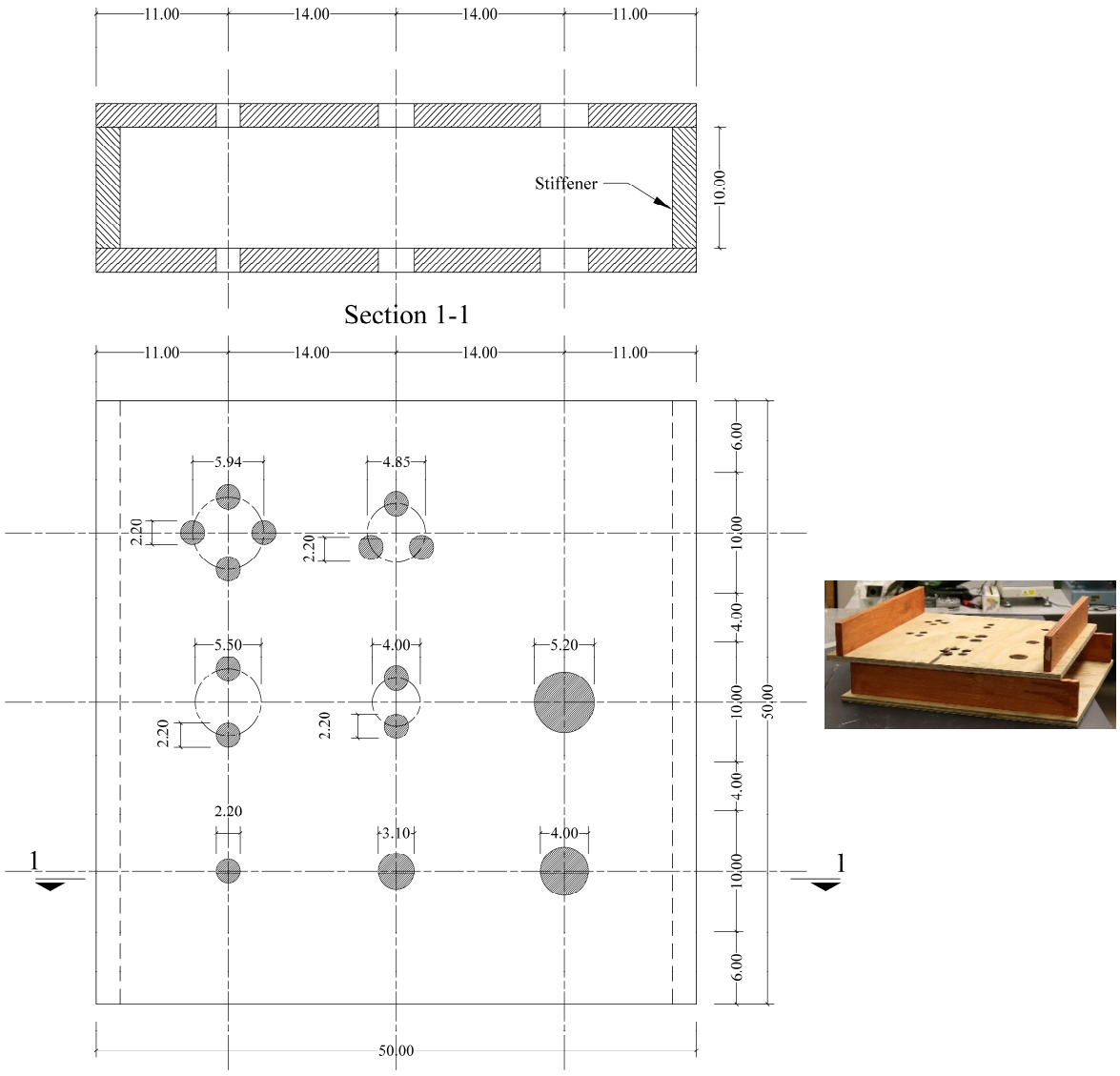

Figure 3.6 Template plate for stone columns installation for test T1-T4 (dimension in cm).

3.2.4 Triaxial system and sample preparation

Nine core triaxial samples (CTS) of the stone columns with the surrounding clay were cut from the tank. The reinforced clay samples were taken out from the reservoir by a thin wall steel tubes with an inner diameter of 9.80 cm, a thickness of 0.18 cm, and a height of 45 cm as shown in Figure 3.7. A solid PVC solid cylinder of 9.65 cm diameter and 15.00 cm height were used to extract the sample out of the cutter. A linear actuator (Figure 3.7) pushed the dolly by a constant movement rate, which was set to 3.0 cm/sec to avoid any disturbance to the samples. Two similar

template plates were used to adjust the position of each sample in the tank (Figure 3.8). The vertical distance between the two plates was set to 10 cm to confirm the verticality of the cutter during the cutting process.

The standard triaxial setup (Figure 3.9) was assembled and was used to conduct the loading test on the reinforced clay samples of 10 cm diameter and 20 cm height. A pressure panel system using air pressure and bladder pressure cylinder was used to apply cell and backpressure with a capacity of 650 kN/m^2. The water was collected in a de-airing tank which was attached to a vacuum pump to de-air the water. There was a fan at the bottom of the de-airing tank, which reduced the required de-airing time for the full capacity of the tank from more than 1 hour to 10 minutes. An automatic volume change device was used to measure the volume of water going into and out of the sample. A vertical transducer attached to the cell measured the vertical movement during the test. Also, three pressure transducers were connected to all the valves of the cell. Two pressure transducers were used to measure the internal water pressure (PWP) on top and bottom of the sample, while the third transductor was used to measure the water pressure around the sample ($\sigma 3$) during all the test steps. Data were gathered by a data acquisition system attached to a computer. In order to increase the accuracy of the test, all the measurements were collected automatically by the computer software within a predefined time period.

(a)

(b)

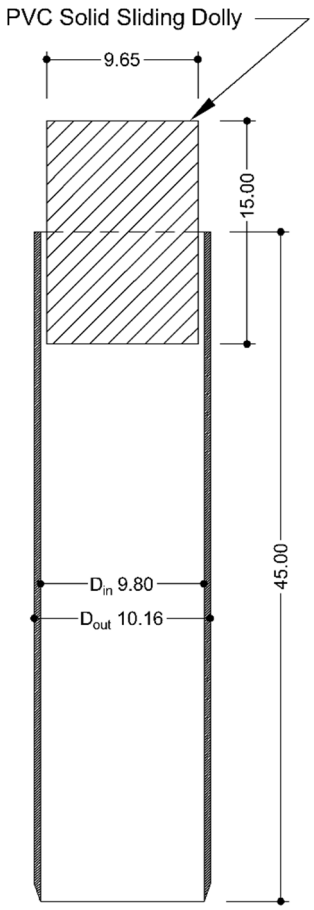

(c)

Figure 3.7 Sample preparation tools: (a) Sample Cutter, (b) linear actuator, and (c) Sample cutter and dolly dimension details (dimensions in cm)

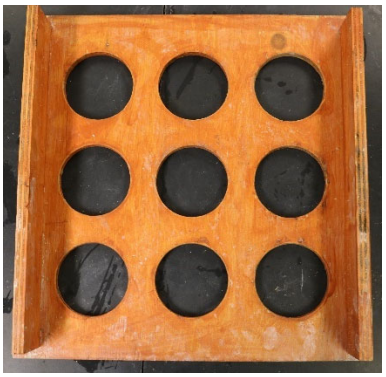

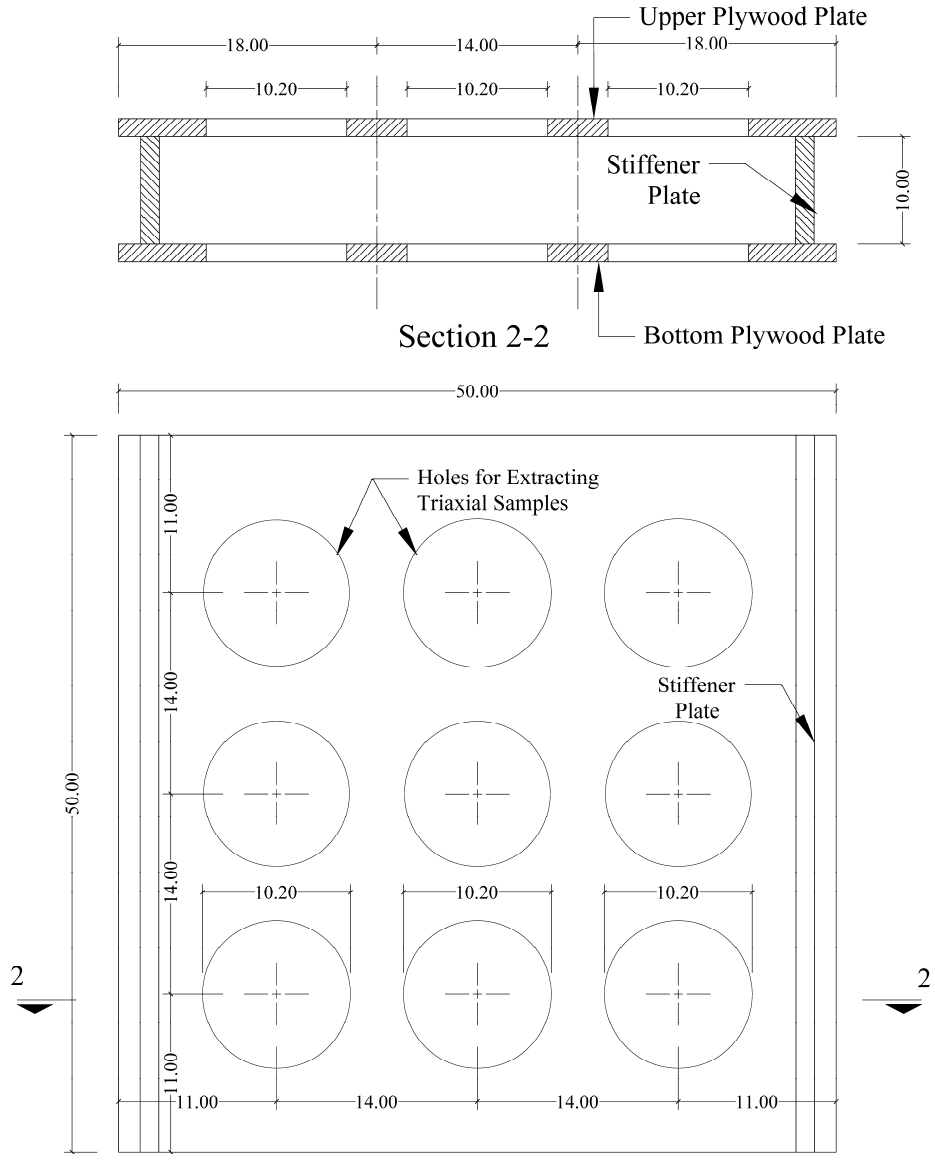

Figure 3.8 Samples extracting template plate (dimensions in cm)

Figure 3.9 Triaxial setup

3.3 Materials

3.3.1 Clay

The clay sample was prepared from a dry kaolin powder. The powder was mixed with water at 1.5 times the liquid limit of the used kaolin clay. A liquid limit test was conducted on the Kaolin clay according to BSI 1990 to calculate liquid and plastic limits. The liquid limit test results are shown in Figure 3.10. The chemical and physical properties of the clay are shown in Table 3.1, while the particle size distribution analysis obtained from the hydrometer test is shown in Figure 3.11.

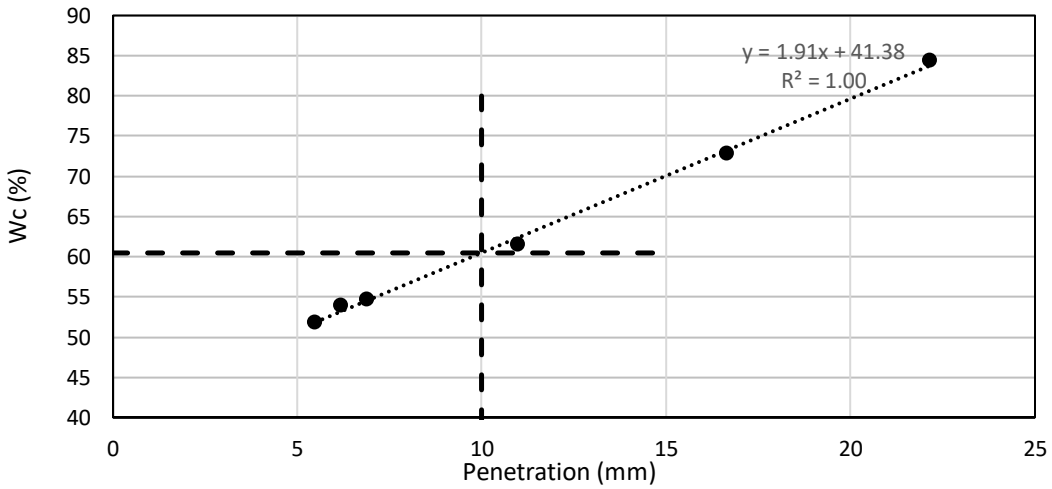

Figure 3.10 Liquid limit test results

Table 3.1 Chemical and physical properties of the used Kaolin Powder

Silicon dioxide SiO_2 (%)	46.5
Aluminum oxide Al_2O_3 (%)	37.5
Ferric oxide Fe_2O_3 (%)	1
Titanium dioxide TiO_2 (%)	1.3
Calcium oxide (quicklime) CaO (%)	0.3
Magnesium oxide MgO (%)	0.3
Potassium oxide K_2O (%)	0.2
Sodium oxide Na_2O (%)	0.1
%Carbon	0.1
%Sulfur	0.13
Dry Modulus of Rupture (mPa)	6.55
Plastic limit (%)	35
Liquid limit (%)	60
Gs	2.61

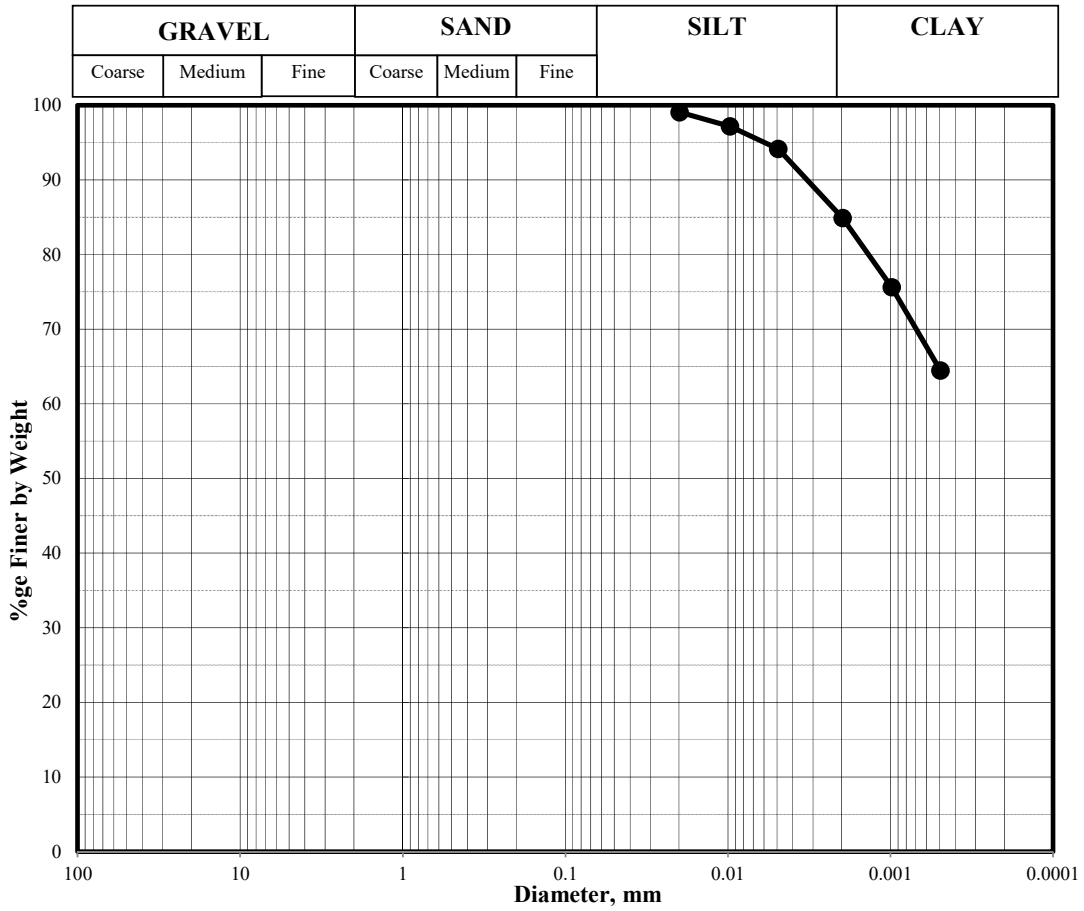

Figure 3.11 Particle size distribution for Kaolin clay

3.3.2 Sand

The material used in modelling the stone columns was coarse silica sand. The physical properties of the sand indicate that it is uniform, coarse-graded sand with particles diameters ranging from 1.2 mm to 0.8 mm. The grain size distribution curve is shown in Figure 3.12. The uniformity coefficient ($d_{60\%}/d_{10\%}$) of the used sand is 1.64, and the main particle size, $d_{50\%}$, is about 0.95 mm. The specific gravity of this sand is 2.65.

The ratio between the stone column diameter (D) to the particle size (d) influences the behaviour of stone columns. In practice, the diameter of stone columns range between 0.6 to 1.0 m and the used stone particle size d = 10 to 80 mm (Canadian Foundation Engineering Mannual, 2006). Therefore, the typical ratio (D/d) ranges between 8 and 100. In the proposed model, the stone column diameters range between 2 and 5 cm, and main sand particles size is 0.95 mm. The ratio D/d in the proposed model is 21 to 52, which is in the average range of the typical values.

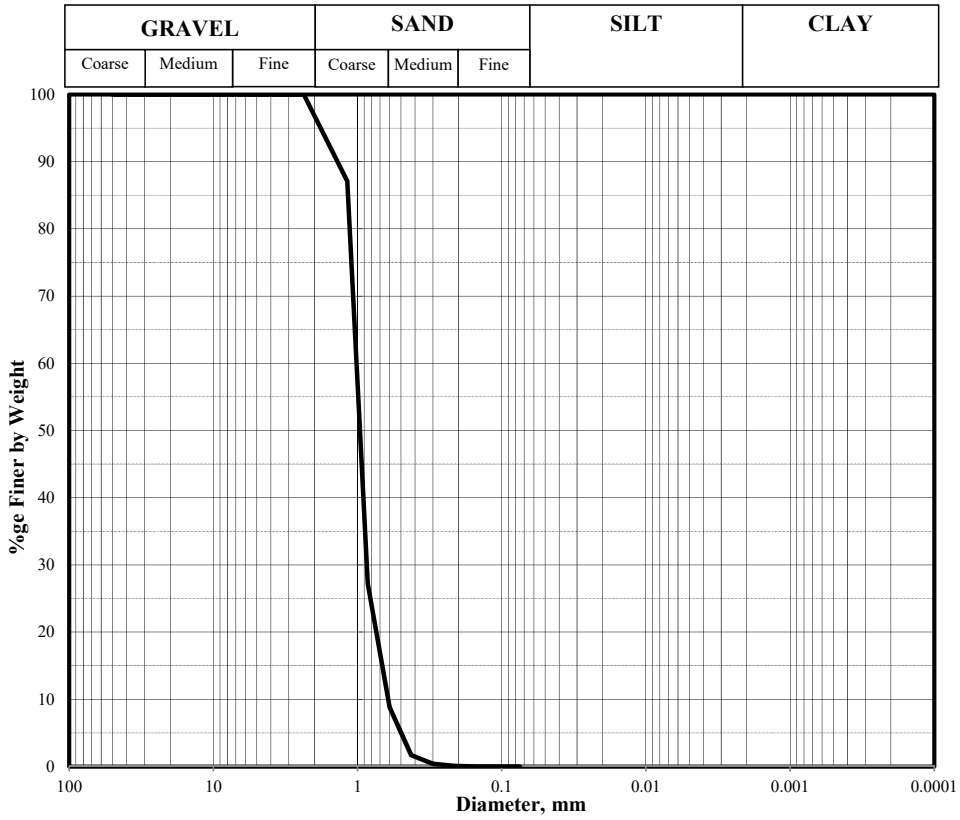

Figure 3.12 Particle size distribution for sand

A direct shear test was performed on the sand at different compaction energies, the results of which are presented in Figure 3.13. A summary of all the sand properties are shown in Table 3.2.

Table 3.2 Properties of sand soil

	Compaction energy, (kN.m/m^3)		
	112	225	657
Angle of shearing resistance, ϕ_s' (Degree)	37.02	42.82	47.18
Dry unit weight, $\gamma_{s\,dry}$ (kN/m^3)	15.07	15.20	16.00
Saturated unit weight, $\gamma_{s\,sat}$ (kN/m^3)	18.34	18.41	18.87
Voids ratio, e	0.73	0.71	0.62
At rest earth pressure coefficient, k_o	0.40	0.32	0.27

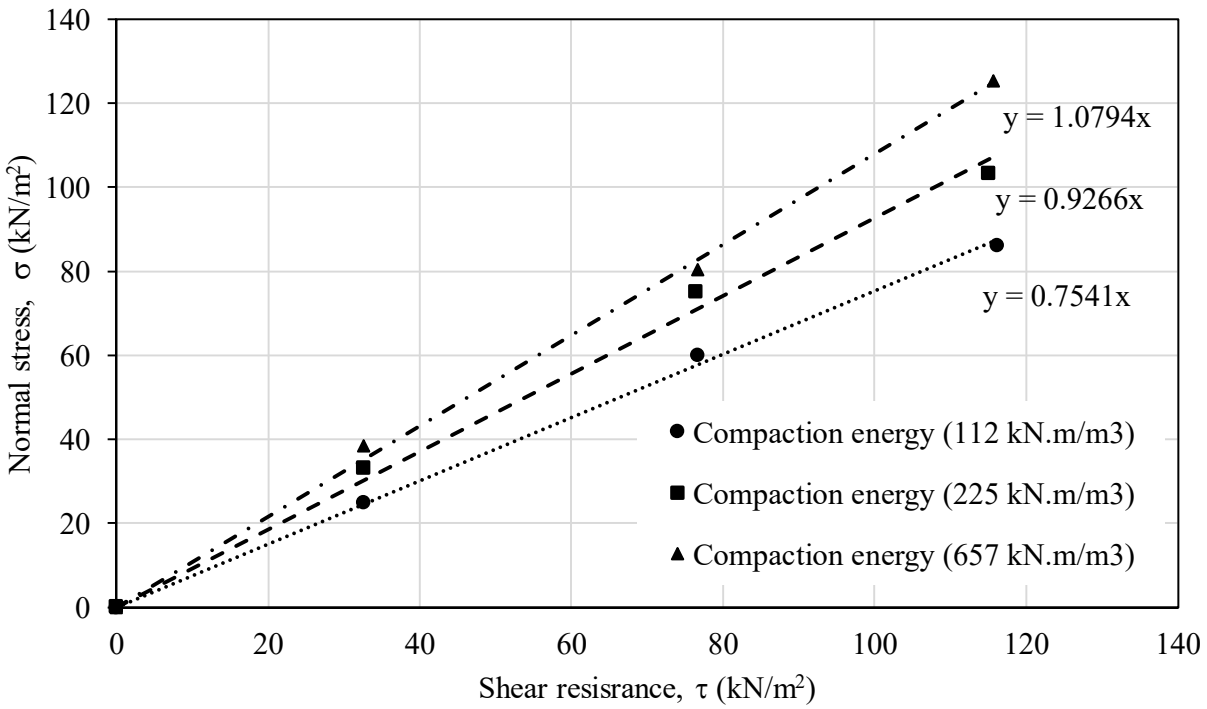

Figure 3.13 Direct shear test results for sand

3.4 Experimental procedures

Tests were carried out to examine the parameters that govern the performance of stone columns. The influence of spacing between columns and the effect of the compaction energy used during the construction process were investigated in different stone column arrangements. The experimental work was conducted in three stages:

1- Clay sample creation and consolidation.
2- Construction of stone columns and arrangement.
3- Sampling process and triaxial test.

The test program consists of creating five large clay samples with the same pre-consolidation pressure and different compaction energy for installation of the stone columns (Table 3.3). Nine core triaxial samples (CTS) (Figure 3.14) were gathered from each large clay sample; each triaxial sample has different reinforcement properties as shown in Table 3.4.

Table 3.3 Large clay samples properties

Test No.	Compaction energy (kN.m/m^3)	Pre-consolidation pressure, σ_c (kN/m^2)
T1	310	80
T2	310	80
T3	620	80
T4	310	80
T5	310	80

Table 3.4 Core triaxial samples (CTS) properties: (a) tests T1-4 & (b) test T5

(a)

Sample No.	No. of Stone Columns	Stone Columns Diameter, *D* (cm)	Stone Columns Spacing ratio, *S/D*	Replacement ratio, A_s (%)
CTS 1	1	2.10	-	4.4
CTS 2	1	3.00	-	9.0
CTS 3	1	3.90	-	15.2
CTS 4	1	5.10	-	26.0
CTS 5	2	2.10	2.0	8.8
CTS 6	2	2.10	2.75	8.8
CTS 7	4	2.10	2.0	17.6
CTS 8	3	2.10	2.0	13.2
CTS 9	-	-	-	0

(b)

Sample No.	No. of Stone Columns	Stone Columns Diameter, *D* (cm)	Stone Columns Spacing ratio, *S/D*	Replacement ratio, A_s (%)
CTS 10	2	2.1	1.5	8.8%
CTS 11	3	2.1	1.5	13.2%
CTS 12	4	2.1	1.5	17.6%
CTS 13	5	2.1	1.5	22.1%
CTS 14	3	3.0	1.5	27.0%
CTS 15	1	2.1	-	4.4%
CTS 16	1	3.0	-	9.0%
CTS 17	1	3.9	-	15.2%
CTS 18	-	-	-	0.0%

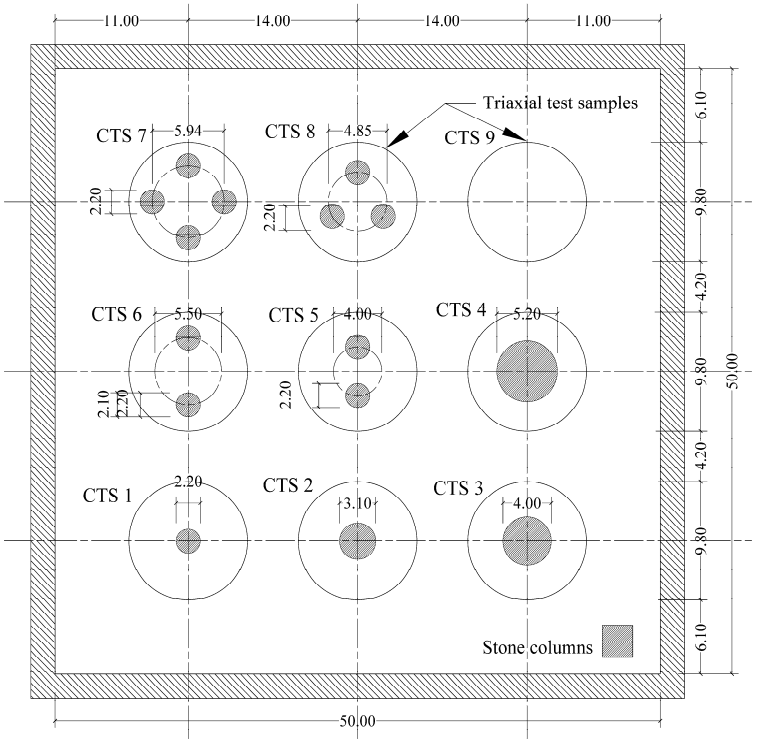

(a)

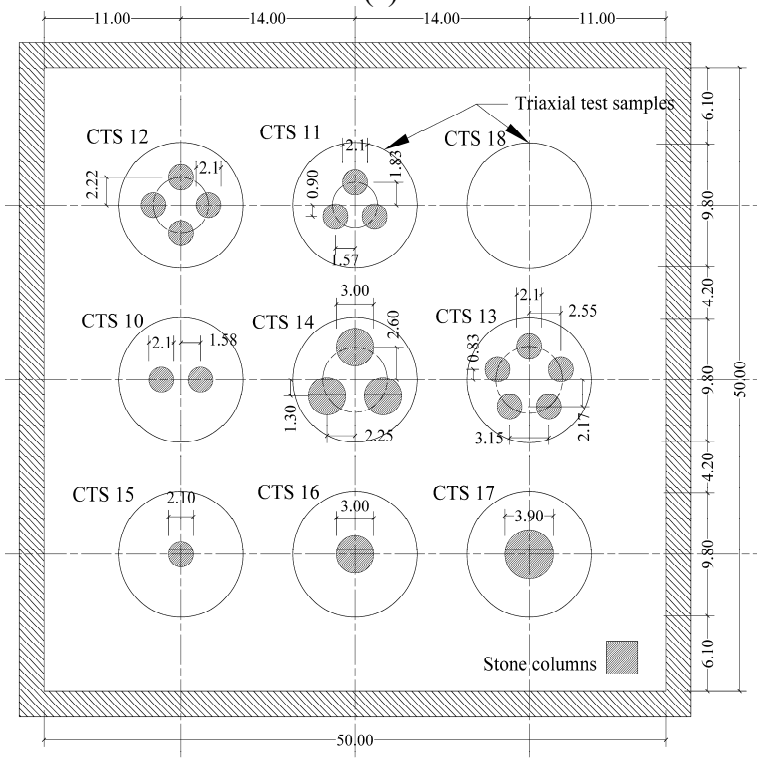

(b)

Figure 3.14 Core triaxial samples plan: (a) tests T1-4 & (b) test T5

3.4.1 Clay layer creation and consolidation

Kaolin clay powder was used for creating the clay layer, since it has low sensitivity, high consolidation rate, and it is fast to be saturated. The dry powder was mixed with water at 1.5 the liquid limit; at a high water content the particles are free to create their own structure. The liquid limit of the used kaolin clay was 60%, thus the weight of water added to the dry powder was 90% of its dry weight. Using the mixer shown in Figure 3.15, the slurry was mixed for 20 minutes until fully saturated. 10 kg of kaolin clay was mixed with 9 kg of water at one time in the mixer. It required ten mixes to fill the tank and create a layer of slurry with a total height of 50 cm. The kaolin slurry was slowly poured into the tank to avoid any air bubbles. At the end of the pouring stage, the slurry was slowly hand-mixed inside the consolidation tank to avoid any difference between the poured layers and to achieve uniform layers inside the tank.

A sand bed of 5 cm was placed below and above the Kaolin slurry layer. Two porous sheets were seated between the sand layers and the Kaolin slurry. The friction between the Kaolin slurry and the tank walls has a marked influence on transferring stress to the bottom of the clay layer. This friction causes a reduction in the bottom of the tank up to 20% of the applied stress on the top of the tank (Cairncross, 1973). In order to reduce the adhesion between the Kaolin slurry and the tank walls, all the sides of the tank were smeared with silicone grease.

Figure 3.15 Clay/water mixing machine

After preparing the soil layers in the testing tank, a consolidation process began. Consolidation occurs by gradually increasing the applied pressure on the top of the clay layer. The pressure was applied in increments and each increment was allowed to stay until the steady-state occurred, at which point the excess water pressure due to the load increment dissipated. Measuring the pore water pressure in the clay slurry was not possible. So, measuring the rate of the settlement was used as an alternatively to judge the steady state. In order to state the loading rate, a consolidation test was performed on the Kaolin slurry, the results of which are presented in Figure 3.16. Based on the consolidation properties of the Kaolin slurry, the loading rate, total final settlement, and percentage of settlement at the end of loading process were estimated (Table 3.5). The slurry was kept in the tank under its own weight for one day then an initial stress of 20 kPa was applied. The applied load was doubled every day until reaching the maximum consolidation pressure of 80 kPa, which was maintained for four days before removing all the applied pressure. In order to measure the settlement of the clay layer throughout the entire consolidation process, four linear transducers

were fixed to the consolidation tank corners, and the average value was considered. The average final settlement at the end of loading process for all tests (T1, T2, T3, T4, T5) varied from 12 cm to 15 cm, which matched the estimated settlement in Table 3.5. The setup used in the clay consolidation process is shown in Figure 3.17.

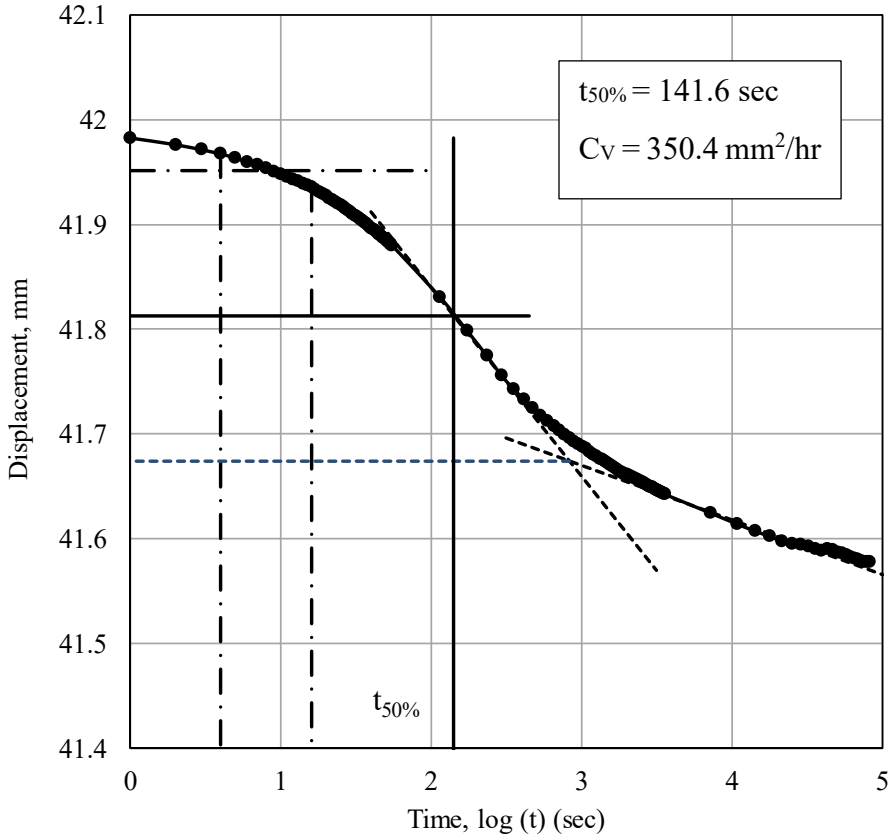

(a)

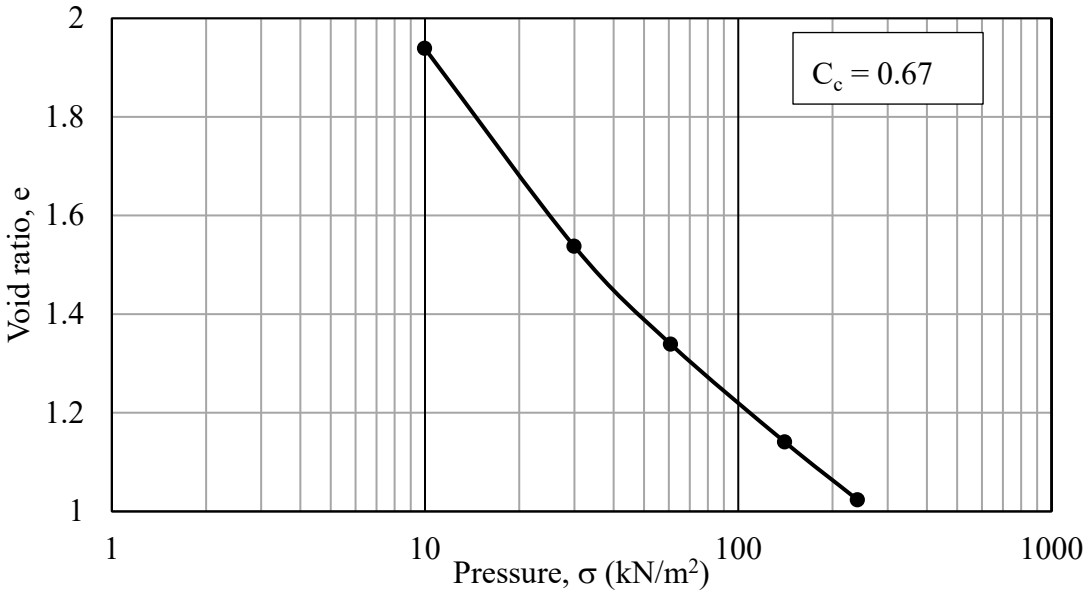

(b)

Figure 3.16 Consolidation test results for Kaolin slurry: (a) Settlement Vs log. time curve, (b) Void ratio Vs log-pressure curve

Table 3.5 Settlement calculation for the slurry layer in the consolidation tank

Applied pressure (kN/m^2)	0	20.00	40.00	60.00	80.00
Time (hr)	12	24.00	24.00	24.00	96.00
C_C	0.68	0.68	0.68	0.68	0.68
C_v (mm^2/hr)	350.00	350.00	350.00	350.00	350.00
Thickness (mm)	500.00	472.70	440.46	393.39	357.92
Initial stess (kN/m^2)	0.50	3.43	11.95	21.64	34.14
$\Delta\sigma$ (kN/m^2)	3.63	16.57	28.05	38.36	45.86
Total settlement (mm)	93.32	73.70	47.06	35.48	26.95
TV	0.07	0.15	0.17	0.22	1.05
U %	29.25%	43.76%	46.96%	52.58%	93.91%
Actual settlement (mm)	27.30	32.25	22.10	18.65	25.31
Total settlement at the end of loading process (mm)	125.60				

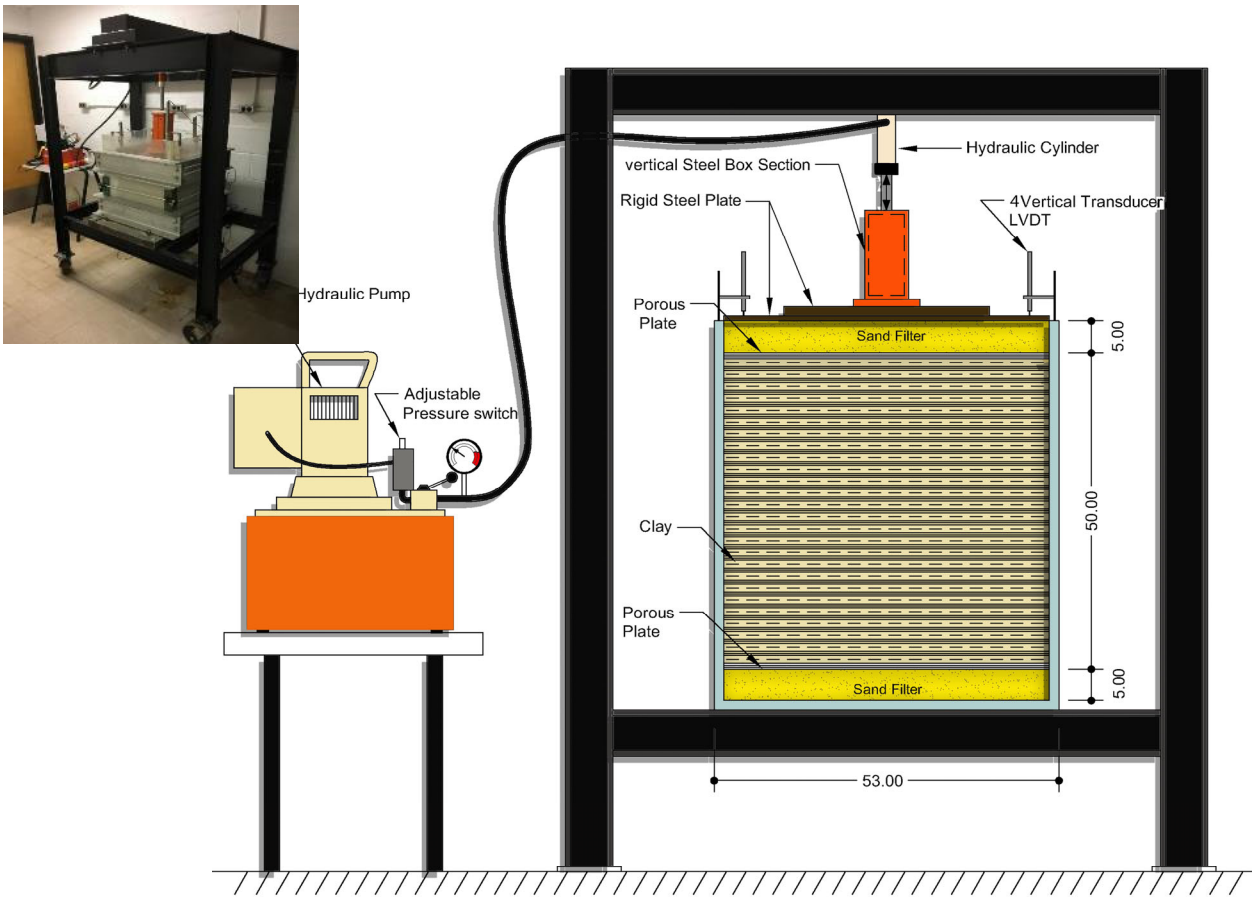

Figure 3.17 Large clay sample consolidation setup

3.4.2 Arrangement of stone columns

A drilling method was used in most of the previous studies to install the stone columns. An open-end thin tube was inserted into the soil, and an auger was used to excavate the soil inside it (Hu, 1995; Sivakumar et al., 2004). However, the excavation method does not simulate the actual installation procedure in the field, particularly for the vibro-floatation method. Therefore, a new stone column installation method was used; this approach was based on driving a tube closed with a separate cone. After driving the tube to a depth of 40 cm, the tube was gradually pulled out, and the hole filled with compacted sand (Figure 3.18). Since the method of compaction has a significant effect on the behaviour of stone columns (Miranda et al., 2015; Bergado et al., 1987), two different compaction energies were used in the experimental program. Compaction energy of 310 kN.m/m^3 was used in tests T1, T2, T4, T5, and 620 kN.m/m3 was used in test T3. The values of the compaction energy were selected to achieve two goals: to keep the sand in place after

removing samples from the tank to perform the triaxial test, and to minimize the change in the stone column diameter due to compaction. A consistent compaction method was utilized, the sand inside the columns was compacted by a weight of 300 gm freely dropped from a constant height of 240 mm. In order to achieve a constant compaction energy, the number of drops and the volume of the compacted stone was varied in each column based on the column diameter as shown in Table 3.6.

Table 3.6 Compaction properties for stone columns

Stone columns Diameter (cm)	Volume of stone in each layer (cm^3)	Height of drop (mm)	No. of drops	
			T1 & T2 & T4 &T5	T3
2.1	13.8	240	6	12
3.0	28.3	240	12	24
3.9	47.8	240	20	41
5.1	81.7	240	35	70

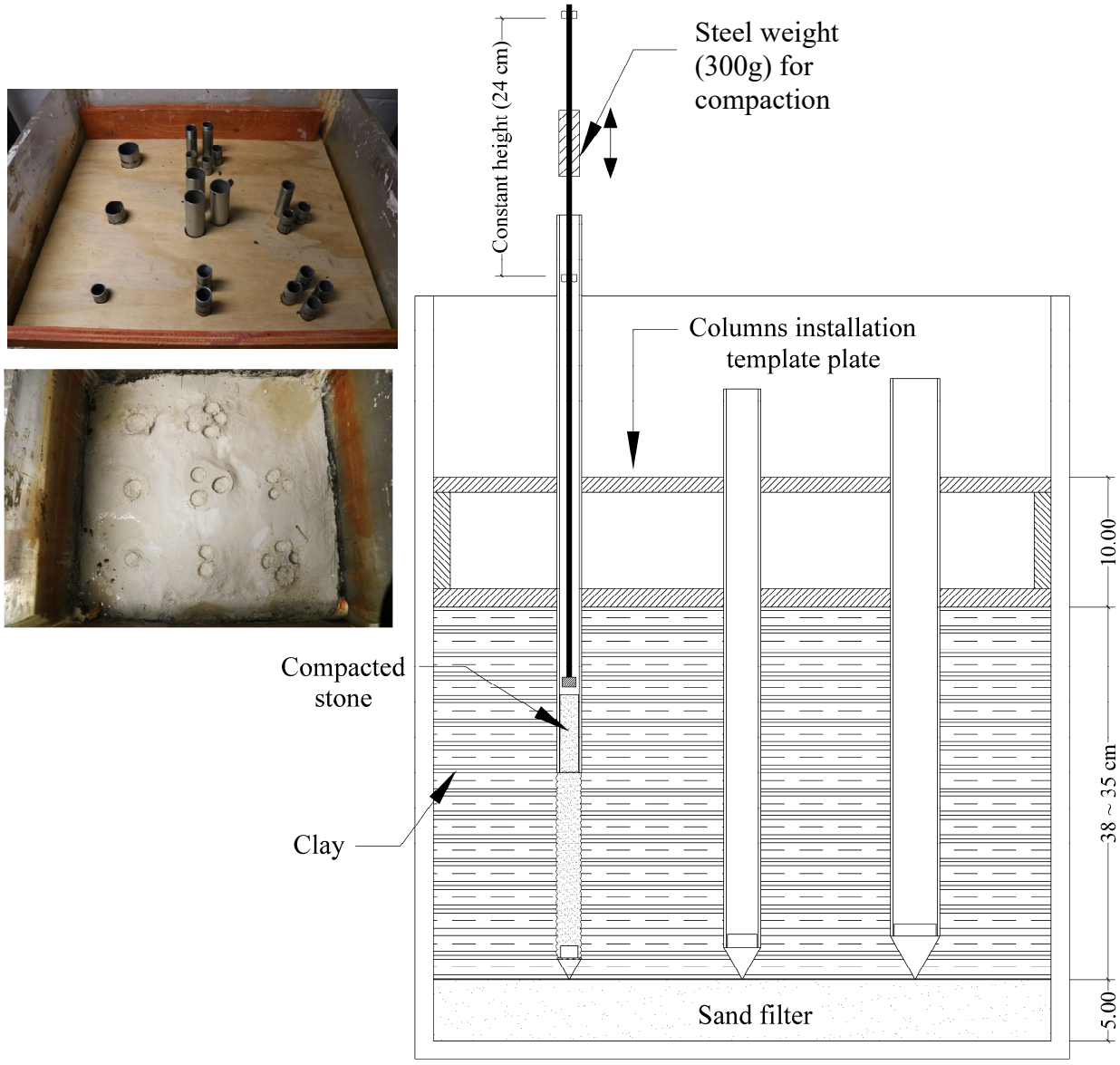

Figure 3.18 Stone column installation method

3.4.3 Triaxial test sample preparation

A group of nine core triaxial samples was cut from the large clay sample after installation of the stone columns, as described in section 3.2.4. The cutter cylinders were driven in the reinforced clay sample using the sample template plate as shown in Figure 3.19. In order to remove the clay around the cutters, one of the tank sides was disassembled and the clay around the cutter cylinders was carefully scraped off.

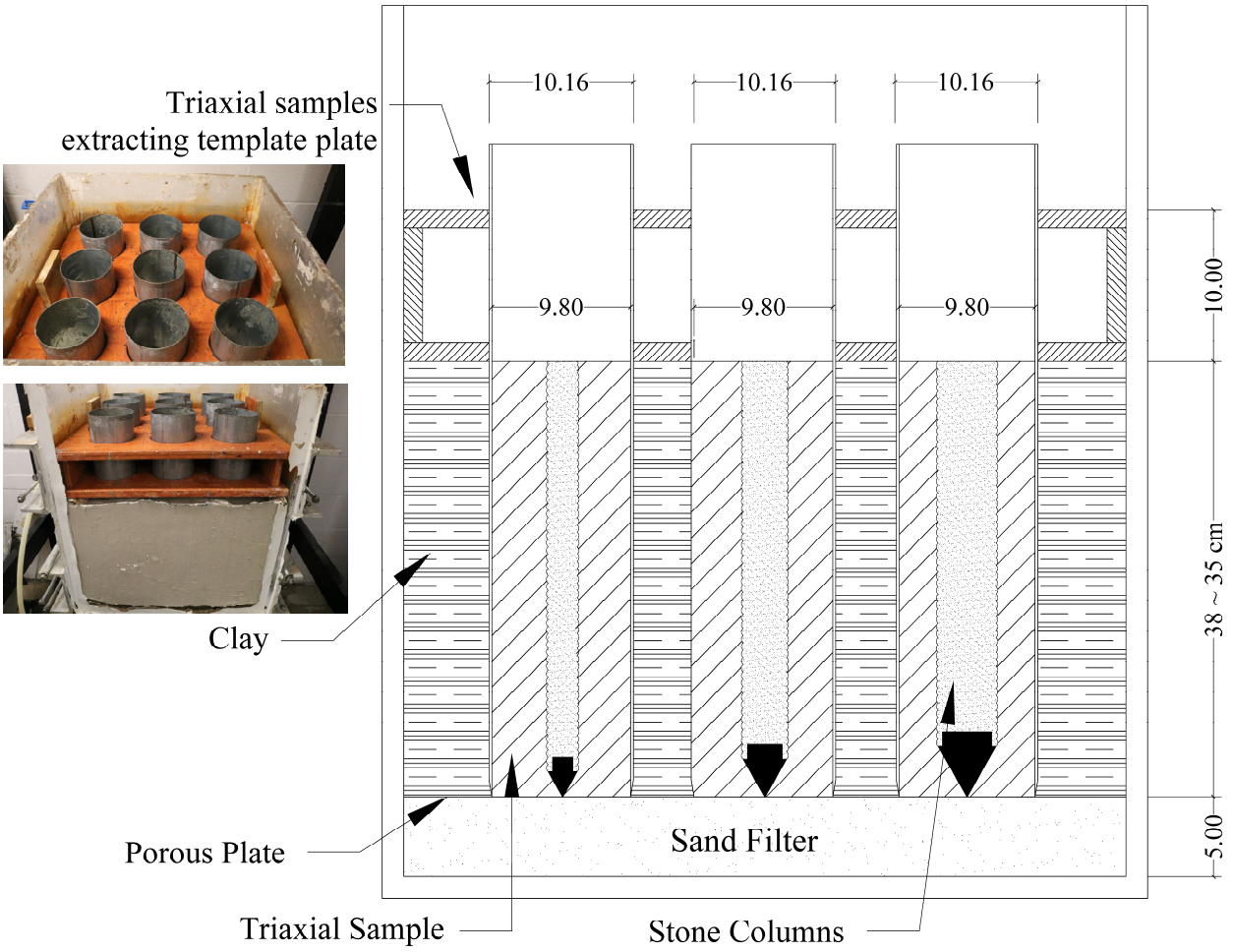

Figure 3.19 Triaxial samples cutting process

A PVC solid cylinder (Dolly) with a diameter of 9.65 cm and height of 15 cm was used to push the sample out of the cutter, and the sample was received in another half cylinder (Receiver) with a bigger inner diameter of 10.00 cm. In order to avoid any disturbance during sample extracting process, an electric linear actuator with a constant moving rate of 3 cm/min, and aligned with the centerline of the sample, was utilized to extract the triaxial samples from the cutting cylinders as shown in Figure 3.20. Nine samples were extracted from the tank and a CU triaxial test, which required 24 hours, was performed on each sample. Since it was therefore essential to store the samples in a way that prevented any disturbance or water content change, the samples were fully wrapped by two layers of thin plastic sheets and then stored in a closed cylinder that was in turn inserted in an air vacuumed plastic cover. All the steps of sample preparation and storage are shown in Figure 3.21.

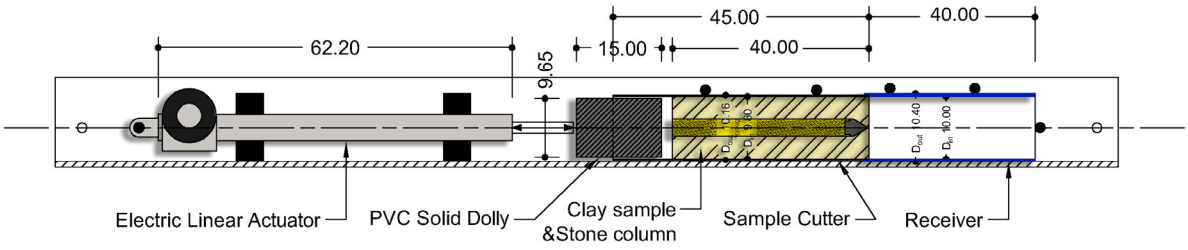

Figure 3.20 Extracting triaxial samples device

(a)

(b)

Figure 3.21 Triaxial extraction and storing process: (a) sample extraction, (b) sample storing

3.4.4 Triaxial test

The utilized triaxial test setup is shown in Figure 3.24. A consolidated undrained (CU) triaxial test was carried out on all the samples prepared as described in the previous section. The samples were placed in the triaxial cell, according to the D 4767-04 standard (ASTM, 2004). The triaxial cell and the full system were saturated by de-aired water. The triaxial test consisted of three stages:

1- Sample preparation and system saturation stage.
2- Consolidation stage.
3- Axial loading stage.

In order to place the sample in the triaxial cell, all the wrapping around the sample was removed. The length of the samples varied between 38 and 35 cm (the required minimum height for a triaxial sample is 20 cm). Also, due to the displacement installation method, there was a high disturbance in the soil around the top and bottom of the stone columns. Thus, the extra length was equally cut from top and bottom of the samples to remove any disturbed soil (Figure 3.22). After adjusting the length of the sample, it was placed in the triaxial test cell, and the rubber sleeve was installed as shown in Figure 3.23.

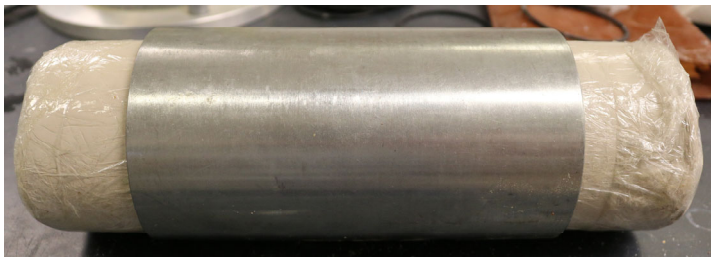

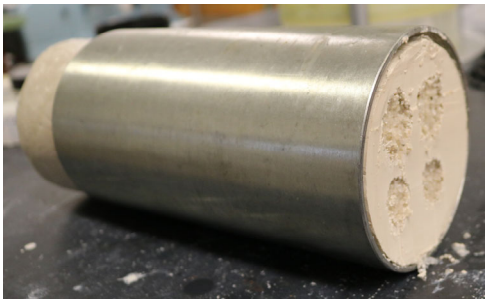

Figure 3.22 Triaxial samples length adjustment

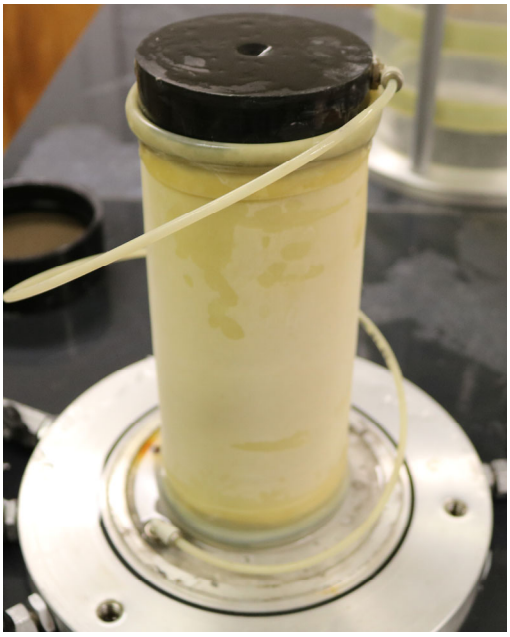

Figure 3.23 Triaxial test sample

The aim of the saturation stage was to ensure that the system was fully saturated and to drive any air out of the system. No high back pressure was required because the sample was fully saturated. In the saturation stage, a small cell pressure (σ_3) of 5 kN/m^2 was applied while the same pressure was applied as a back pressure inside the sample. The values (PT1) were kept unattached to allow for water flushing until a steady water flow came out from the valve.

After the saturation stage, the drainage valves were closed, and the confinement pressure was increased to 160 kPa in T1, T2, T3, T5 and 80 kPa in T5. The drainage valves at the top (PT1) and the bottom (PT2) were then opened again. The total volume of water driven out of the clay sample was measured by an automatic volumetric change device. Moreover, the water pressure inside and around the sample was measured by PT2 and PT3, respectively. The consolidation stage allowed 24 hr to achieve 100% primary consolidation.

Before the loading stage, all the drainage values were closed, and the initial pore water pressure was measured. The loading was applied to the sample using the strain control method. The strain rate was defined in the loading frame. The applied force was measured by an external load cell fixed to the frame and connected to the top of the sample. The strain rate was 0.5 mm/min for all the triaxial tests. During loading stage, the applied load, the pore water pressure, and the vertical deformation were automatically measured by the data acquisition system at a rate of 60 readings/min.

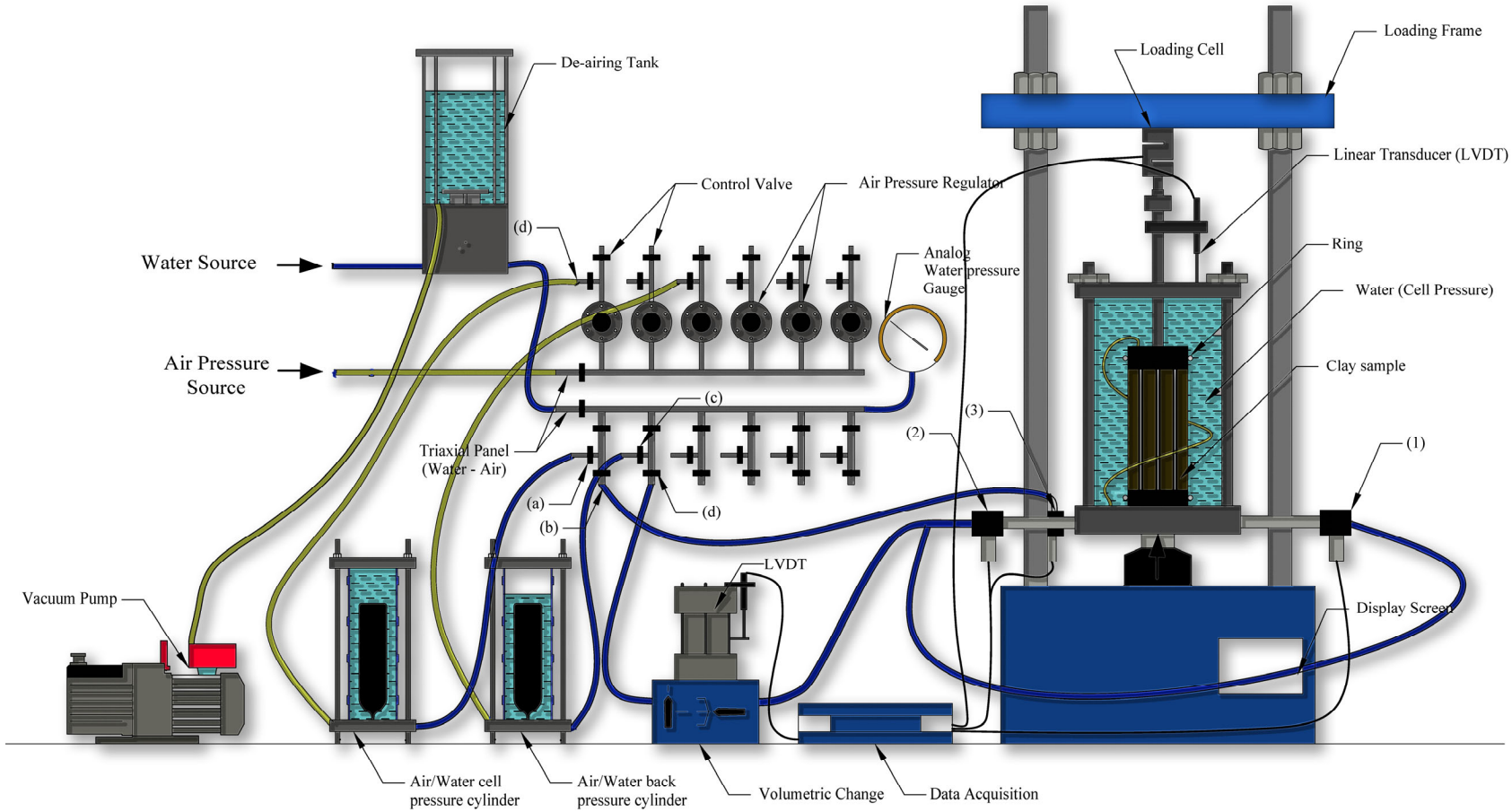

(1) Pressure Transducer (PT) for Pore Water Pressure Measurements

(2) PT for Back Pressure Measurements

(3) PT for Cell Pressure Measurements

(a) & (b) Control Valve (CV) for Applying cell pressure

(c) & (d) (CV) for Applying Back Pressure

Figure 3.24 Triaxial test details

Chapter 4: Experimental Test Results

4.1 General

Test results of the experimental investigation are presented in this chapter. The consolidation test followed D-2435 (ASTM, 2011) and was performed on a sample taken from the clay layer prepared to calculate the clay properties after the consolidation stage in the tank. As described in Chapter 3, five tests (T 1 ~ 5) were performed, a group of nine triaxial samples (CTS 1 ~ 18) were gathered from each test, and a consolidated undrained (CU) triaxial test was performed on each sample. In each group of reinforced clay samples, unreinforced samples (CTS 9 & CTS 18) were tested and used as a base for all the specimens in the same group. Table 4.1 provides a summary of the testing program.

Tests T1 & T2 were utilized to check on the repeatability and reproducibility of the test process and results. In these two tests, single and groups of stone columns were used as the reinforcement. Two spacing ratios were used for the stone columns (2 & 2.75), and three stone column groups (2, 3, and 4 columns) were used to investigate different replacement ratios. Moreover, a smaller stone column spacing ratio of 1.5 was used in test T5. In test T3, higher compaction energy was used during the installation of the stone columns to investigate the effect of the compaction energy on the performance of the stone columns. A confined pressure of 160 kN/m^2 was used for all the samples from tests T1, T2, T3 and T5. However, a smaller confinement pressure of 80 kN/m^2 was used in test T4.

Table 4.1 Summary of the testing program

Test No.	Compaction energy ($kN.m/m^3$)	confinment pressure, σ_3 (kN/m^2)	Sample no.	No. of Stone Columns	Stone Columns Diameter, D (cm)	Stone Columns Spacing ratio, *S/D*	Replacement ratio, A_s (%)
T1	310	160	CTS 1	1	2.1	-	4.4
			CTS 2	1	3.0	-	9
			CTS 3	1	3.9	-	15.2
			CTS 4	1	5.1	-	26
			CTS 5	2	2.1	2	8.8
			CTS 6	2	2.1	2.75	8.8
			CTS 7	4	2.1	2	17.6
			CTS 8	3	2.1	2	13.2
			CTS 9	-	-	-	0
T2	310	160	CTS 1	1	2.1	-	4.4
			CTS 2	1	3.0	-	9
			CTS 3	1	3.9	-	15.2
			CTS 4	1	5.1	-	26
			CTS 5	2	2.1	2	8.8
			CTS 6	2	2.1	2.75	8.8
			CTS 7	4	2.1	2	17.6
			CTS 8	3	2.1	2	13.2
			CTS 9	-	-	-	0
T3	620	160	CTS 1	1	2.1	-	4.4
			CTS 2	1	3.0	-	9
			CTS 3	1	3.9	-	15.2
			CTS 4	1	5.1	-	26
			CTS 5	2	2.1	2	8.8
			CTS 6	2	2.1	2.75	8.8
			CTS 7	4	2.1	2	17.6
			CTS 8	3	2.1	2	13.2
			CTS 9	-	-	-	0
T4	310	80	CTS 1	1	2.1	-	4.4
			CTS 2	1	3.0	-	9
			CTS 3	1	3.9	-	15.2
			CTS 4	1	5.1	-	26
			CTS 5	2	2.1	2	8.8
			CTS 6	2	2.1	2.75	8.8
			CTS 7	4	2.1	2	17.6
			CTS 8	3	2.1	2	13.2
			CTS 9	-	-	-	0
T5	310	160	CTS 10	2	2.1	1.5	8.80%
			CTS 11	3	2.1	1.5	13.20%
			CTS 12	4	2.1	1.5	17.60%
			CTS 13	5	2.1	1.5	22.10%
			CTS 14	3	3.0	1.5	27.00%
			CTS 15	1	2.1	-	4.40%
			CTS 16	1	3.0	-	9.00%
			CTS 17	1	3.9	-	15.20%
			CTS 18	-	-	-	0.00%

4.2 Consolidation test results

A fully automated consolidation test machine was utilized to perform all the consolidation tests, as shown in Figure 4.1. Consolidation test results were utilized to calculate all the clay parameter after the consolidation process occurred in the large tank, namely: unit weight (γ), Initial void ratio (e_0), consolidation coefficient (C_v), pre-consolidation pressure (σ'_c), compression index (C_c), swell index (C_s), and permeability coefficient (K).

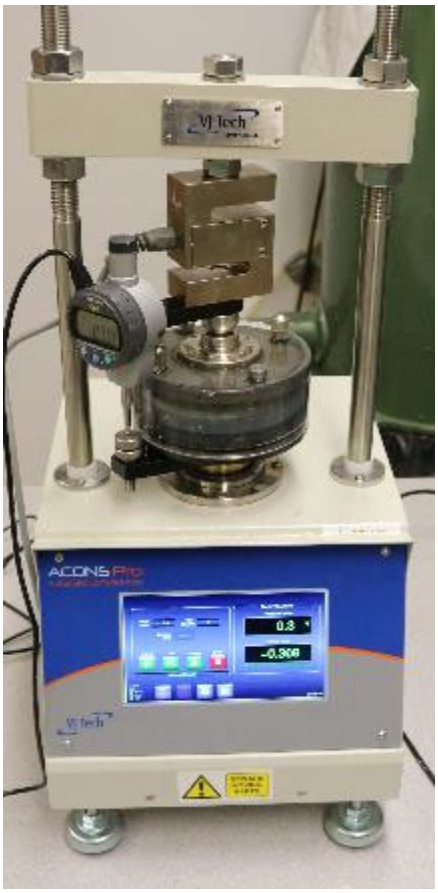

Figure 4.1 Automatic odometer apparatus

Figure 4.2- 4.6 represent e-log σ' and settlement-log t curves for tests T1~5. From the e-log σ'curves, the pre-consolidation pressure (σ'_c), compression index (C_c), and swell index (C_s) were predicted (Terzaghi et al., 1967). In addition, the consolidation coefficient (C_v) was calculated from the settlement-log t curves.

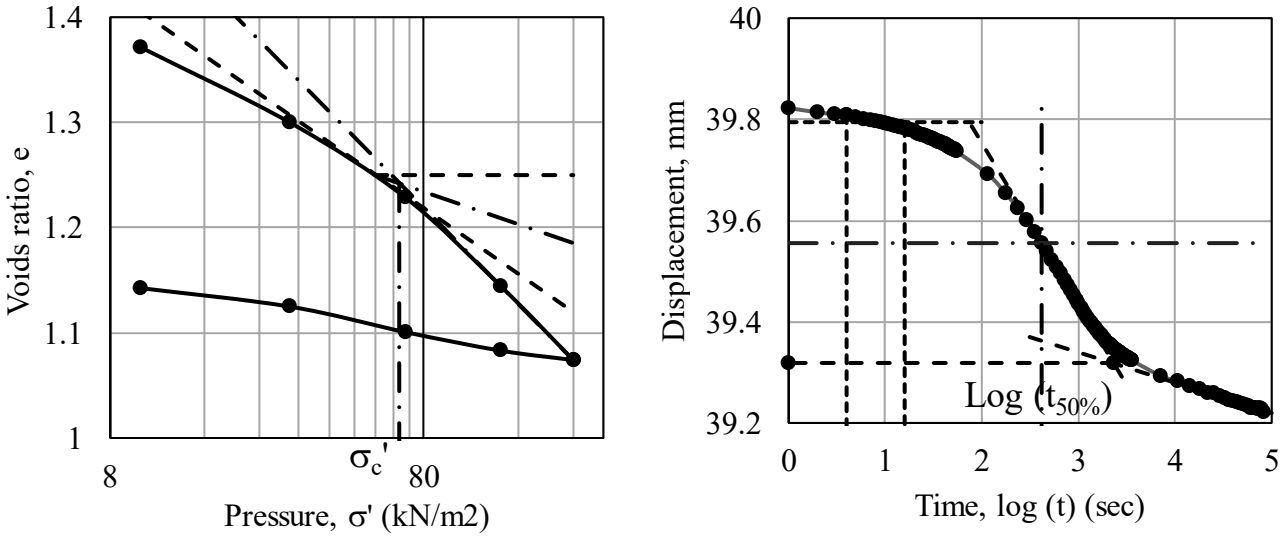

(a) (b)

Figure 4.2 Consolidation test results for clay used in T1: (a) e-log σ' curve and (b) settlement-log t curve at stress 70 kPa

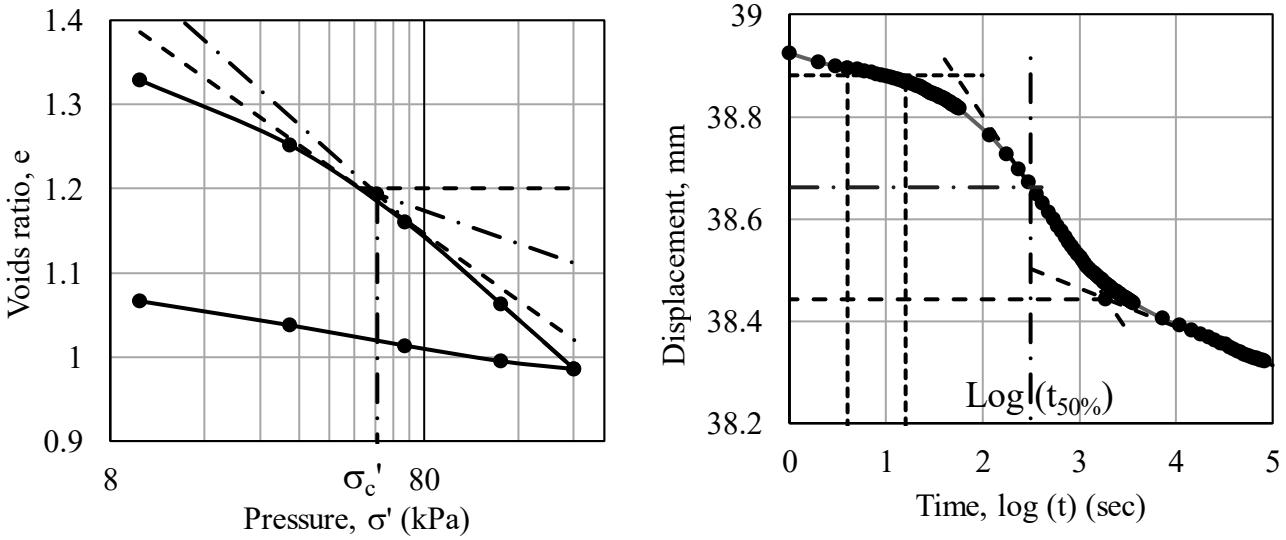

(a) (b)

Figure 4.3 Consolidation test results for clay used in T2: (a) e-log σ' curve & (b) settlement-log t curve at stress 240 kPa

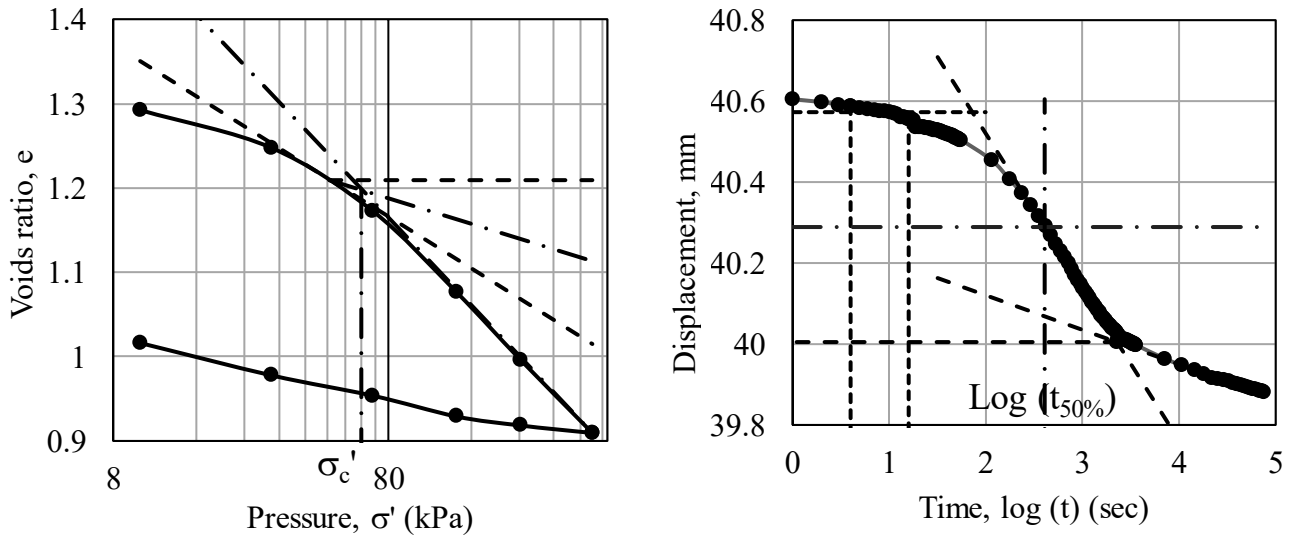

(a) (b)

Figure 4.4 Consolidation test results for clay used in T3: (a) e-log σ' curve & (b) settlement-log t curve at stress 140 kPa

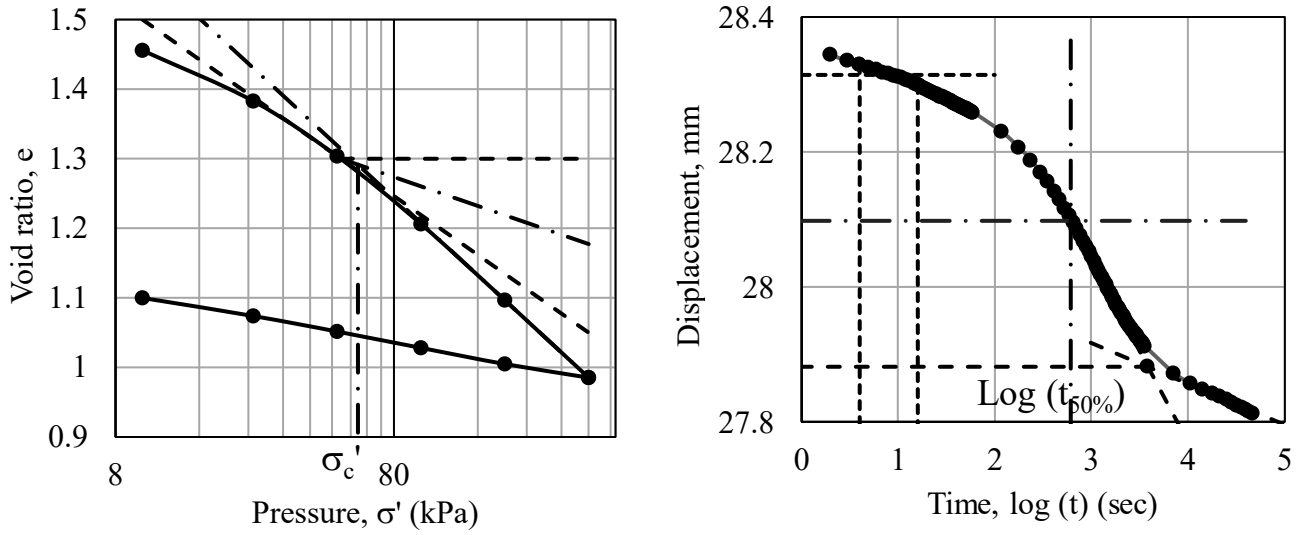

(a) (b)

Figure 4.5 Consolidation test results for clay used in T4: (a) e-log σ' curve & (b) settlement-log t curve at stress 25 kPa

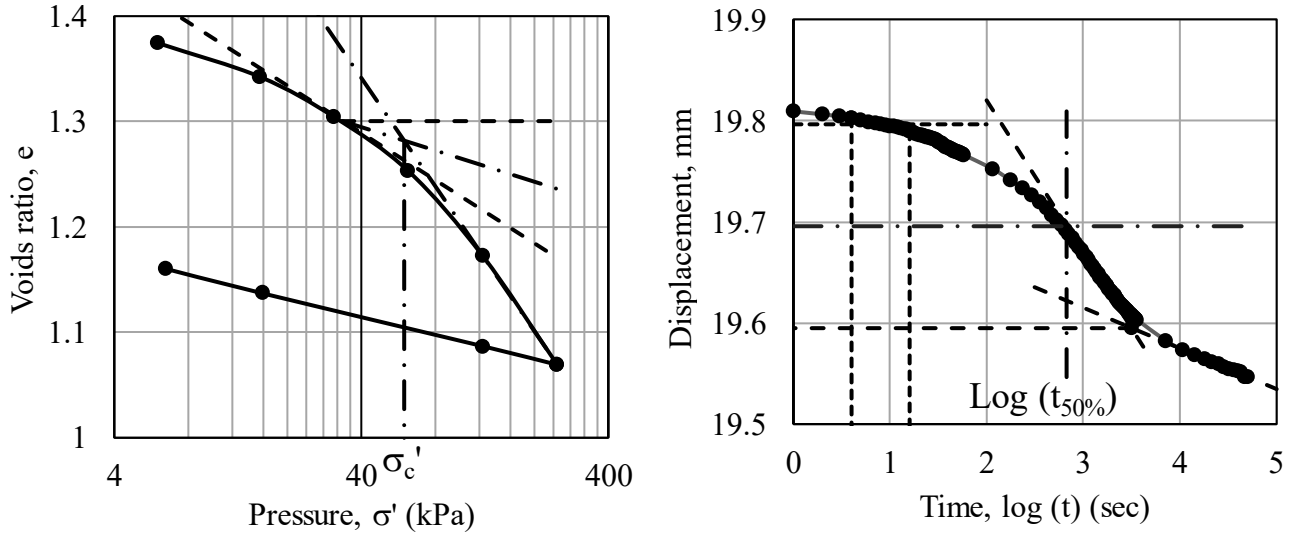

Figure 4.6 Consolidation test results for clay used in T5: (a) e-log σ' curve & (b) settlement-log t curve at stress 15.5 kPa

A summary of the properties of the clay used in each test are shown in Table 4.2. From the clay properties, there were very slight changes in the consolidation properties of the prepared clay. Therefore, it could be concluded that the clay preparation process is repeatable and reproducible.

Table 4.2 Clay properties after large tank consolidation stage

		T1	T2	T3	T4	T5
Clay Properties	e_0	1.38	1.36	1.34	1.47	1.37
	Gs	2.61	2.59	2.61	2.57	2.60
	$\gamma_{c\ sat}$ (kN/m^3)	16.43	16.43	16.55	16.03	16.44
	$\gamma_{c\ dry}$ (kN/m^3)	10.74	10.78	10.93	10.19	10.76
	C_s	0.0497	0.0599	0.0241	0.0251	0.0541
	C_c	0.3012	0.3310	0.3427	0.3685	0.3276
	σ_c' (kPa)	67.44	56.81	63.84	59.39	67.04
	C_v (mm^2/hr)	170.80	169.99	98.03	126.18	138.94
	K (m/sec)	2.462E-10	2.450E-10	1.413E-10	2.015E-10	1.931E-10

4.3 Triaxial test results

The prime intention of the experimental program was to study the effect of the arrangement of stone columns on the loading resistance of clay soil reinforced by stone columns. Also, the results were used to validate the numerical model, which is presented in Chapter 5. A conventional CU triaxial test was performed on each reinforced clay sample as described in 3.4.4. In this section the triaxial results are presented. The results are shown as the loading applied during the test, confinement pressure (σ_3) (consolidation stage), and vertical displacement (s) (loading stage).

4.3.1 Consolidation stage

A constant confinement pressure (160 kN/m^2 for T1, T2, T3, T5 and 80 kN/m^2 for T4) was applied to the sample during the consolidation stage while the drainage paths were opened. During the consolidation stage, the volumetric change (ΔV) was measured with time. The results are presented as the relation of the degree of consolidation (%) versus time (min) as shown in Figure 4.7. The degree of consolidation is defined as the ratio between the volume change (ΔV) at a time and the maximum volumetric change.

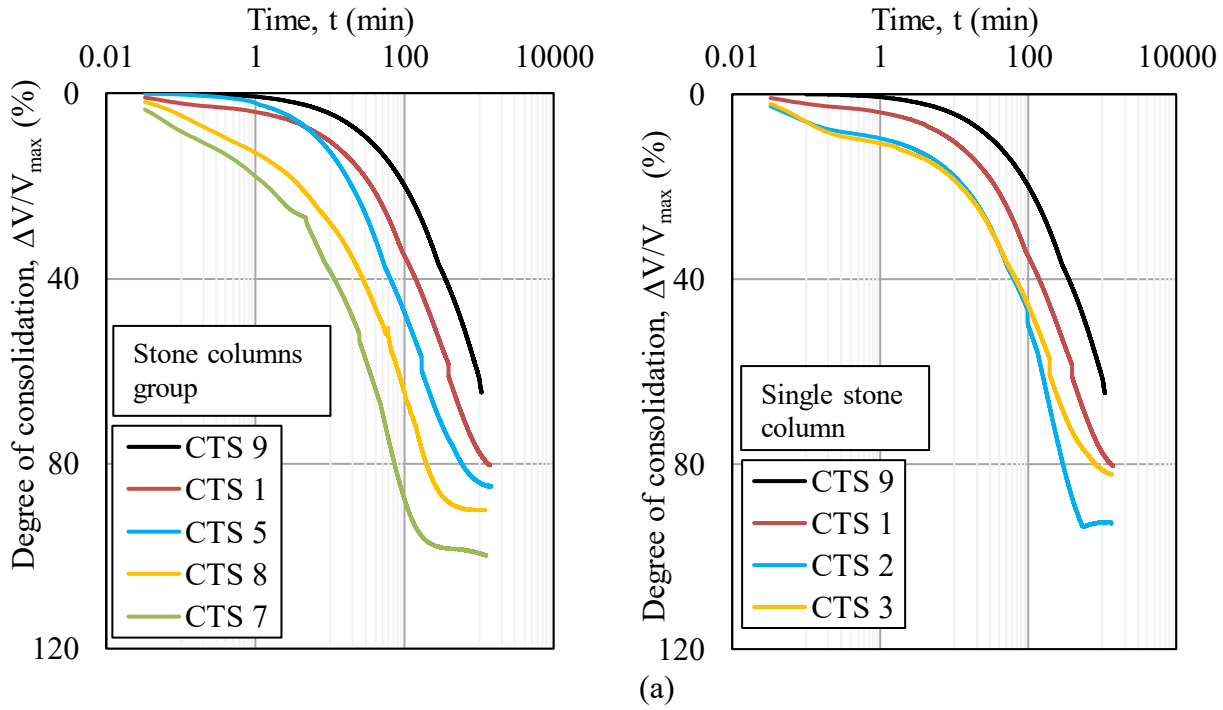

(a)

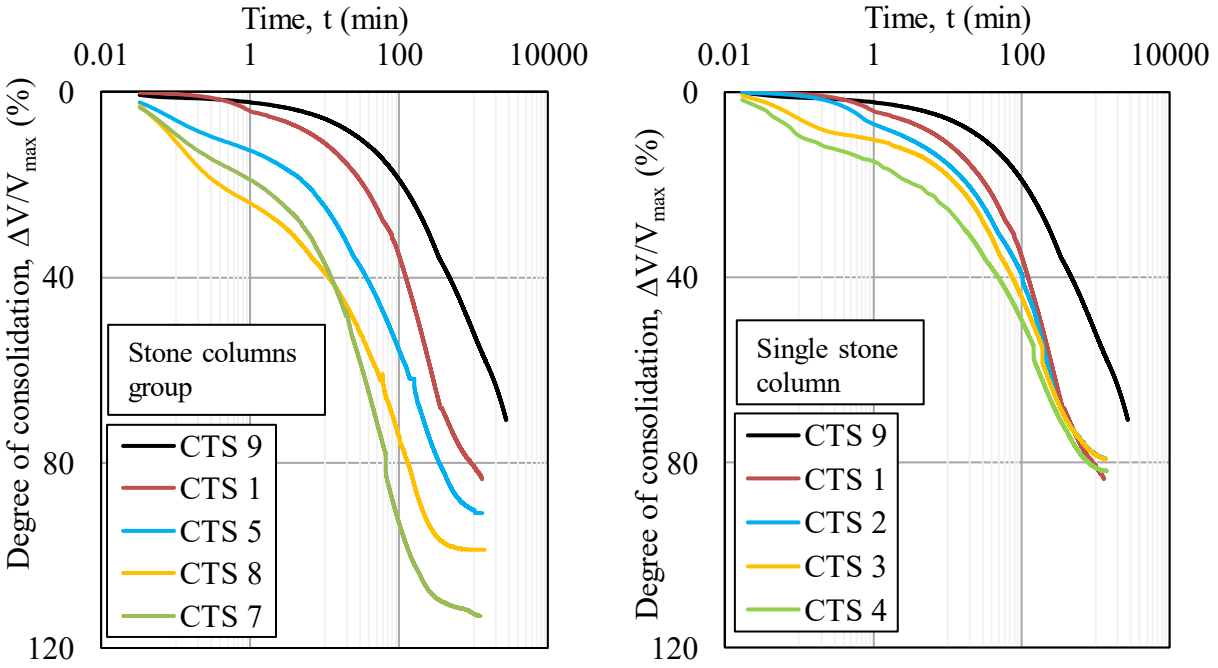
Time, t (min)
0.01
1
100
10000
0
40
80
120
Degree of consolidation, ΔV/V_max (%)
Stone columns group
CTS 9
CTS 1
CTS 5
CTS 8
CTS 7
Single stone column
CTS 9
CTS 1
CTS 2
CTS 3
CTS 4

(b)

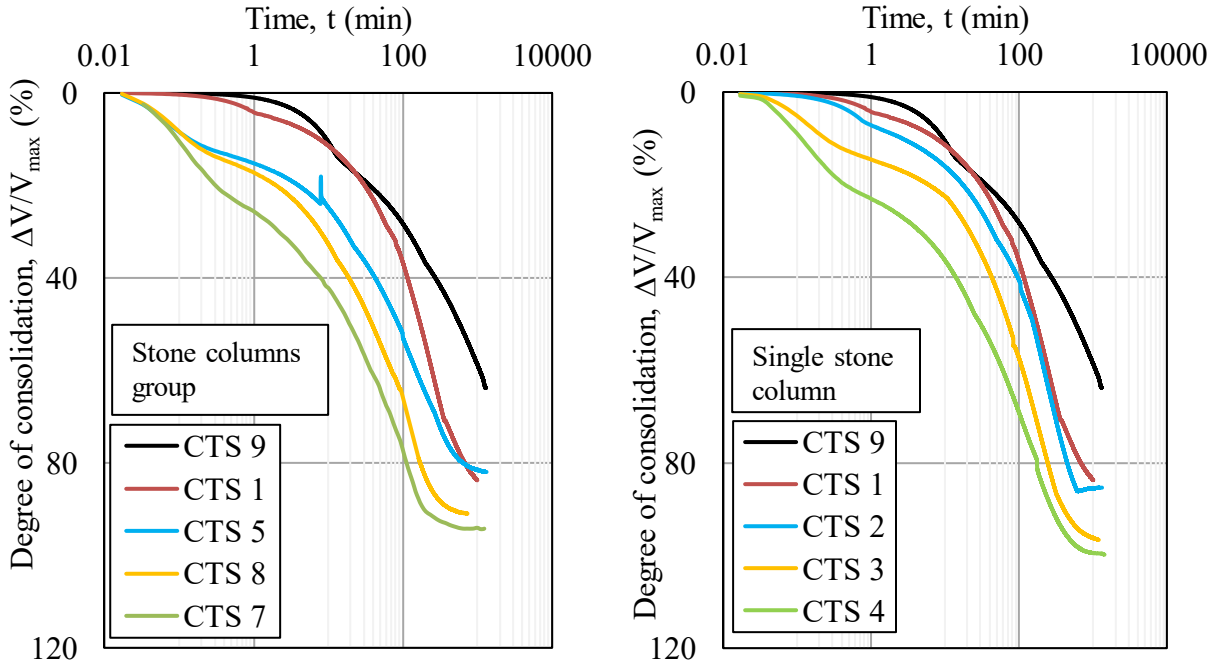
Time, t (min)
0.01
1
100
10000
0
40
80
120
Degree of consolidation, ΔV/V_max (%)
Stone columns group
CTS 9
CTS 1
CTS 5
CTS 8
CTS 7
Single stone column
CTS 9
CTS 1
CTS 2
CTS 3
CTS 4

(c)

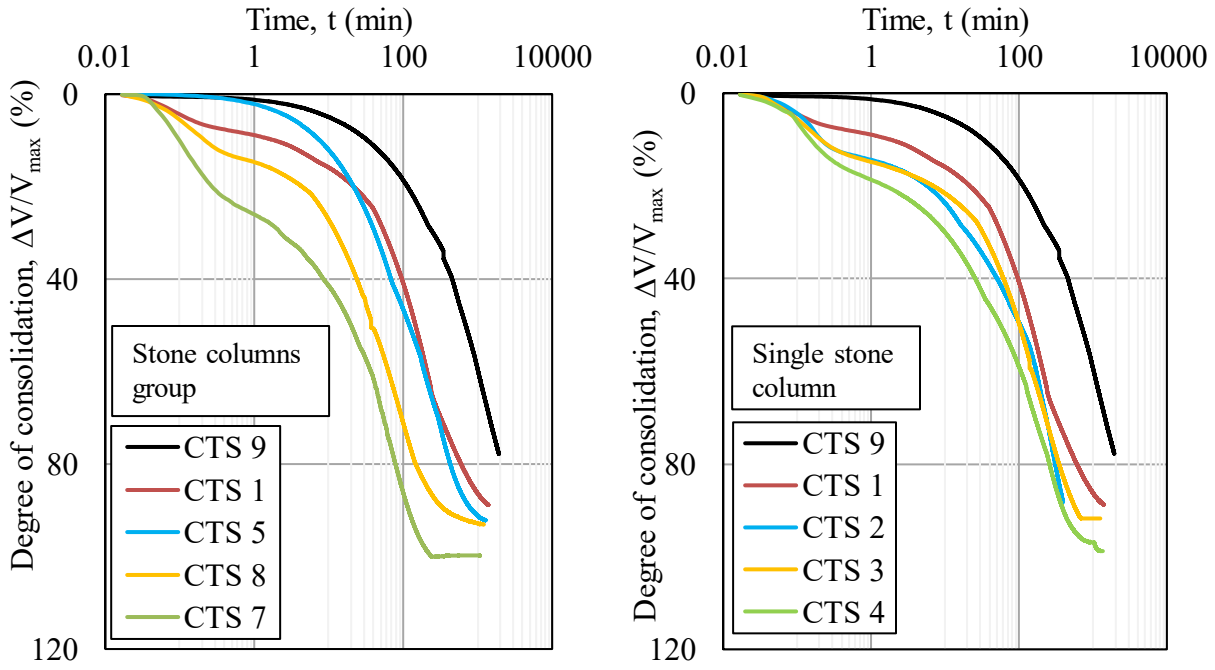

(d)

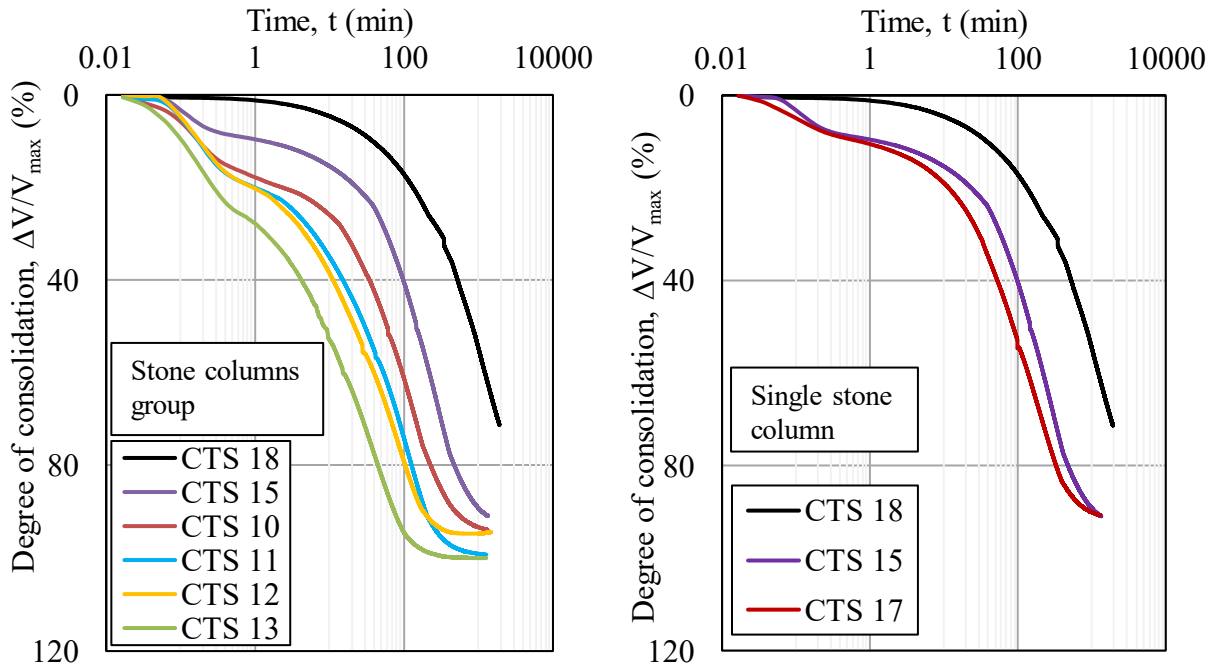

(e)

Figure 4.7 Results of consolidation stage during triaxial tests: (a) T1 & (b) T2, (c) T3, (d) T4, (e) T5

For test T1, T2, T3, T4, T5 the effect of stone columns on speeding up consolidation settlement of clay samples is quite clear. However, increasing the number of stone columns is more efficient than increasing the diameter of the stone columns. As shown in Figure 4.7 (b), after 100 min the degree of consolidation increased from 32.5 % to 95.0 % when the number of stone columns in increased from one in CTS 1 (A_s = 4.4 %) to four in CTS 7 (A_s = 17.6%). However, the degree of consolidation increased

to 50% when the diameter of the stone columns increased from 2.1cm (A_s = 4.4%) to 5.1 cm (A_s = 26%). By comparing the results of T3 and T2, it appears that the compaction energy does not have a noticeable effect on the consolidation test of the reinforced soil. Regarding T5 results, when the spacing ratio (*S/D*) reduced to 1.5, a similar consolidation rate occurred for the samples reinforced by a single or group of stone columns. In order to clearly show the effect of stone columns geometry, the consolidation behaviour of samples reinforced by two stone columns with a diameter of 2.1 cm at different spacing/diameter ratios (*S/D* = 2.00 and 2.75 for CTS5 and CTS6 respectively) are shown in Figure 4.8. In addition, Figure 4.9 shows the effect of increasing diameters of a group of three stone columns from 2.1 cm (A_s = 13.2%) to 3 cm (A_s = 27.0%). From the two figures, it could be concluded that increasing both diameters and spacing between stone columns reduces the consolidation time for the reinforced clay. However, the most economical design is achieved by uniformly distributing stone columns on the total area under the footing at a certain replacing ratio (stone column diameter).

The effect of the arrangement of stone columns on consolidation behaviour of the reinforced sample can be understood in a quantitative way by adapting Terzarghi's one-dimensional consolidation theory (Terzaghi, 1925) and Barron's two-dimensional consolidation settlement theory (Barron, 1948). For the same soil, the degree of consolidation is inversely related to the horizontal water path squared, as shown by equation (4-1), (4-2), and (4-3). Increasing the number of stone columns as well as the spacing between stone columns reduces the water bath, thereby increasing the consolidation rate of the reinforced clay.

$$T_r = \frac{C_{vr} t}{d_e^2} \tag{4-1}$$

$$U_r = 1 - \exp\left(\frac{-8T_r}{m}\right) \tag{4-2}$$

$$U_t = 1 - \left(1 - U_r\right)\left(1 - U_v\right) \tag{4-3}$$

Where

- T_r Dimensionless time factor
- C_v Horizontal coefficient of consolidation (m^2/min)
- t Time required to achieve a certain total degree of consolidation U_t (min)
- m Dimensionless factor calculated from stone columns diameter and spacing
- U_r Degree of consolidation due to horizontal drainage
- U_v Degree of consolidation due to vertical drainage

U_t Degree of consolidation due to vertical and horizontal drainage

d_e Average diameter of stone column effective zone (m)

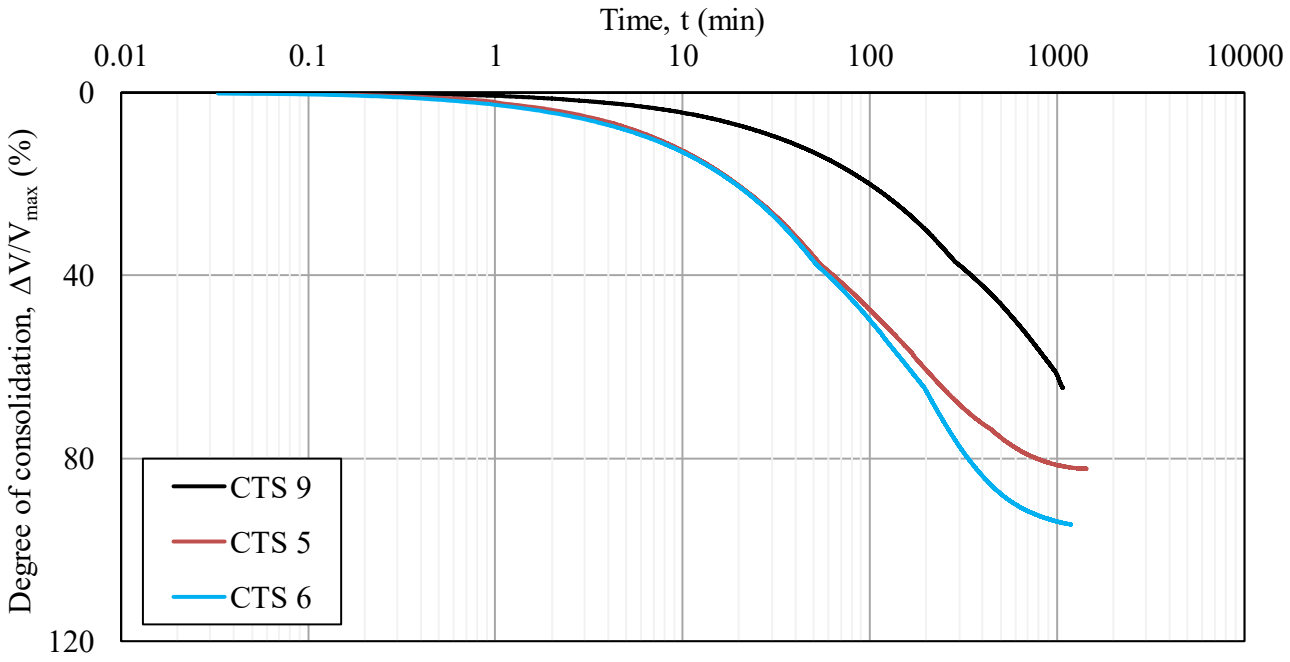

(a)

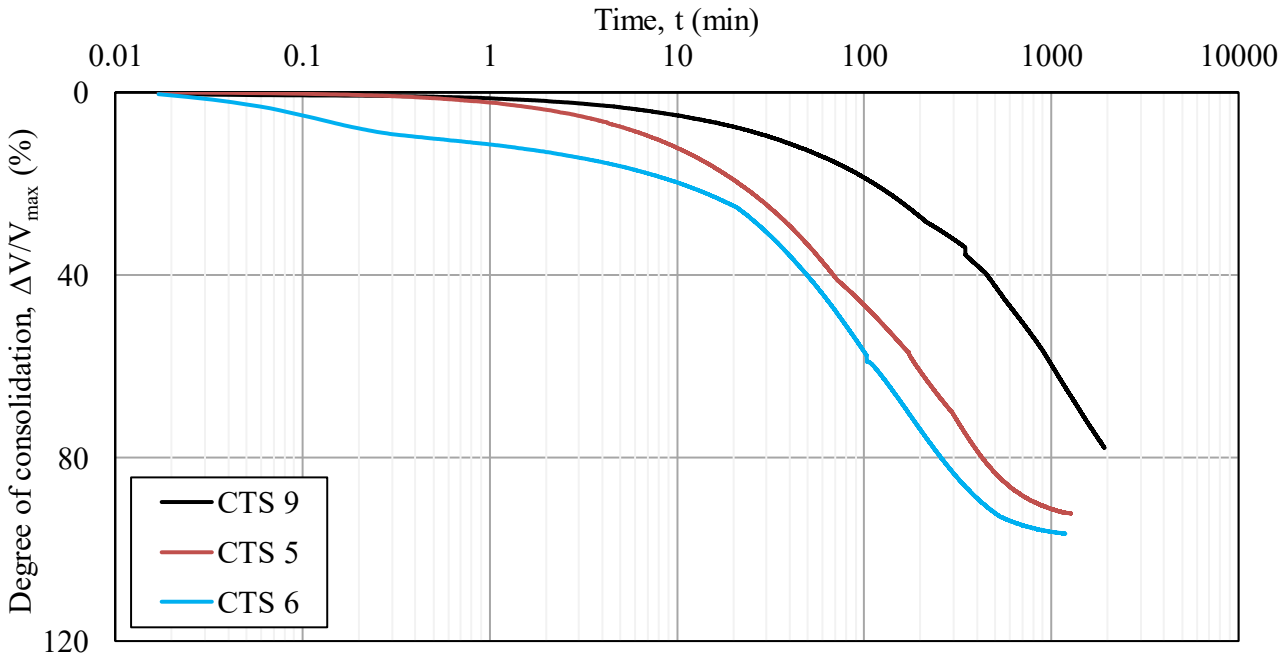

(b)

Figure 4.8 Effect of increasing spacing between stone columns on the consolidation rate of the reinforced clay: (a) T1, (b) T4

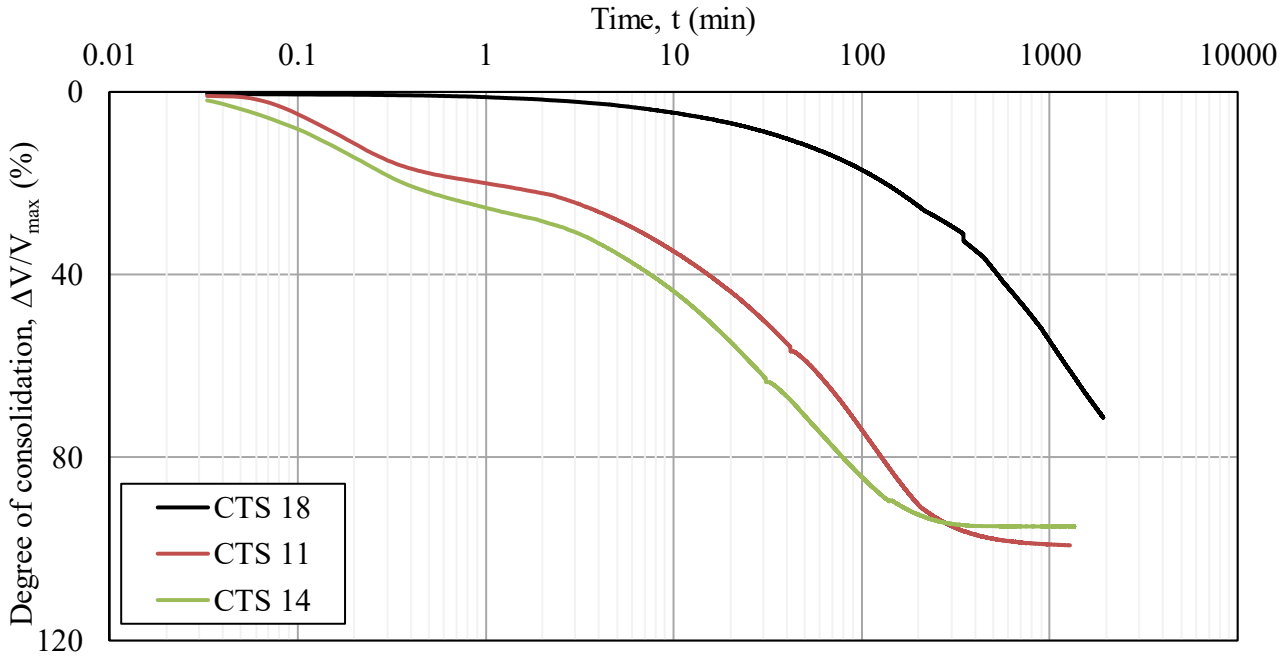

Figure 4.9 Effect of increasing the diameter of stone columns at *S/D*=1.5

4.3.2 Loading stage

At the end of the consolidation stage, all the drainage valves were closed. Therefore, there was not any volumetric change in the reinforced clay sample. The load was applied to samples by means of displacement control. The vertical deformation, s (mm), the cell pressure, σ_3 (kPa), the pore water pressure, u (kPa), and the applied load, P (kN) was measured with time. The data obtained from triaxial tests was analyzed assuming that stone columns and surrounding clay soil behave as one homogeneous soil. So, the deviator stress is the axial load divided by the average cross-section of the sample, equation (4-4), and the axial strain (ε) is the axial deformation divided by the total length of the sample. Figure 4.10, Figure 4.11, Figure 4.12, and Figure 4.14 show the loading stage results for all the samples. Also, the excess pore water pressure during loading stage was measured to evaluate the effect of stone column properties on the undrained properties of reinforced clay soil. The water pressure was measured on top and bottom of the samples, and the average values are shown in Figure 4.15.

$$A_{avg} = \frac{\left(\frac{\pi D_i^2}{4} \times L_i\right)}{L_i\left(1-\varepsilon\right)} \tag{4-4}$$

Where

A_{avg} average cross-section area of the sample (cm^2)

D_i initial sample diameter (10 cm).

L_i initial sample length (20 cm).

ε vertical strain

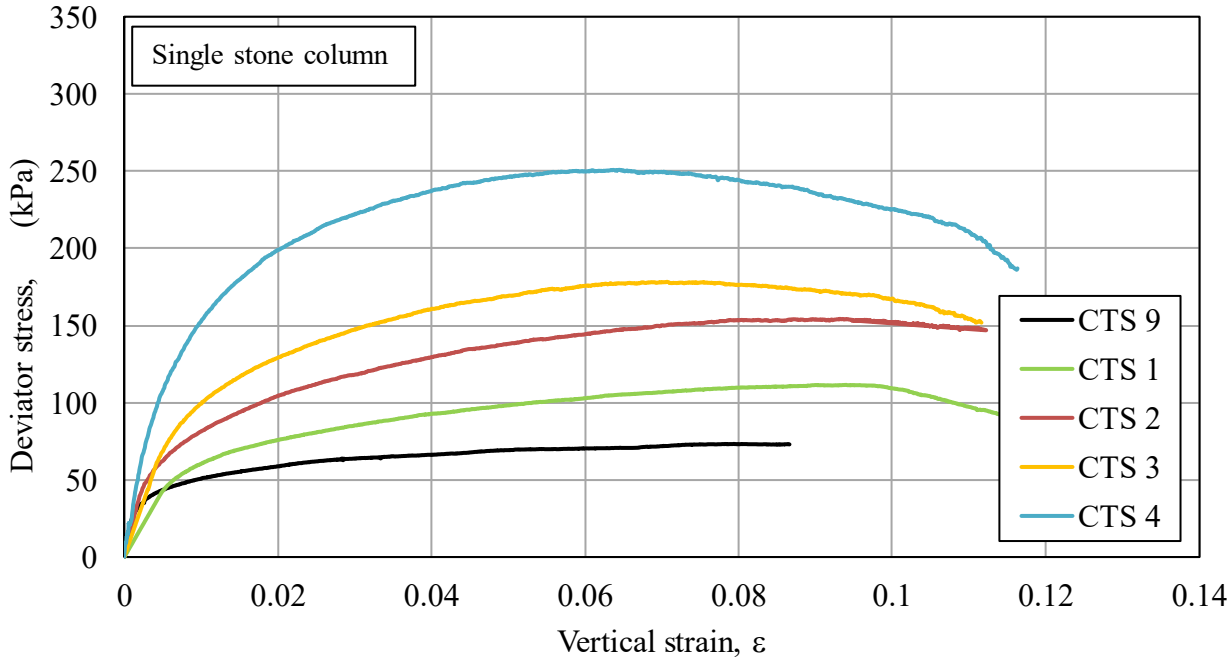

(a)

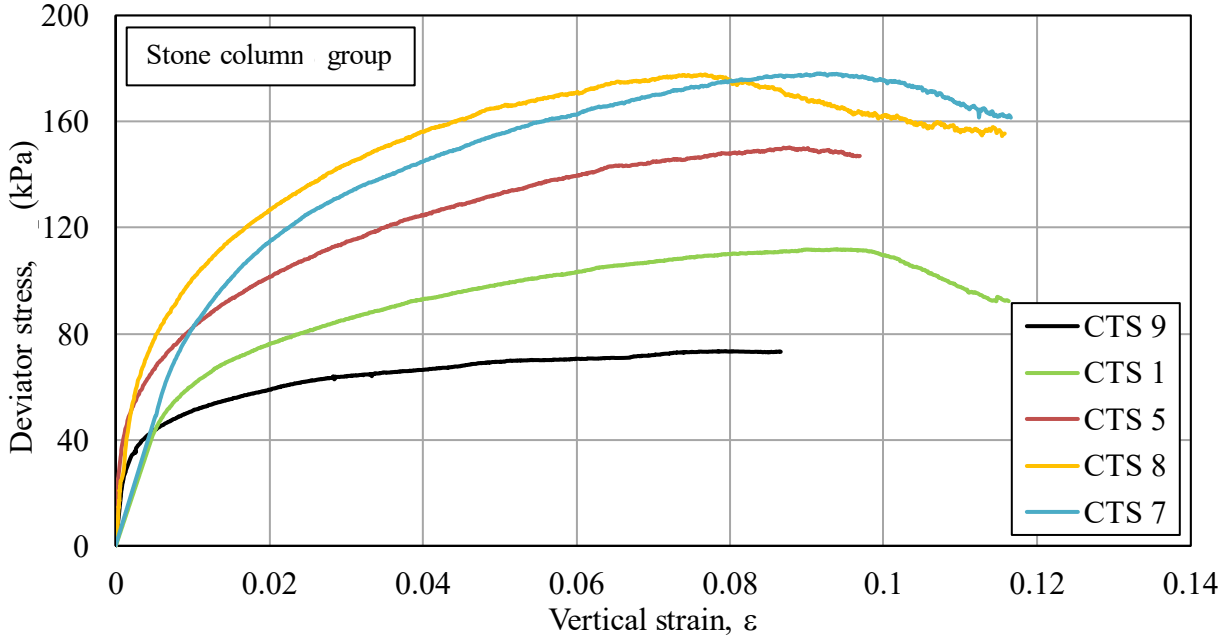

(b)

Figure 4.10 Deviator stress versus axial strain for samples in T1: (a) effect of increasing stone column diameter, (b) effect of increasing number of stone columns

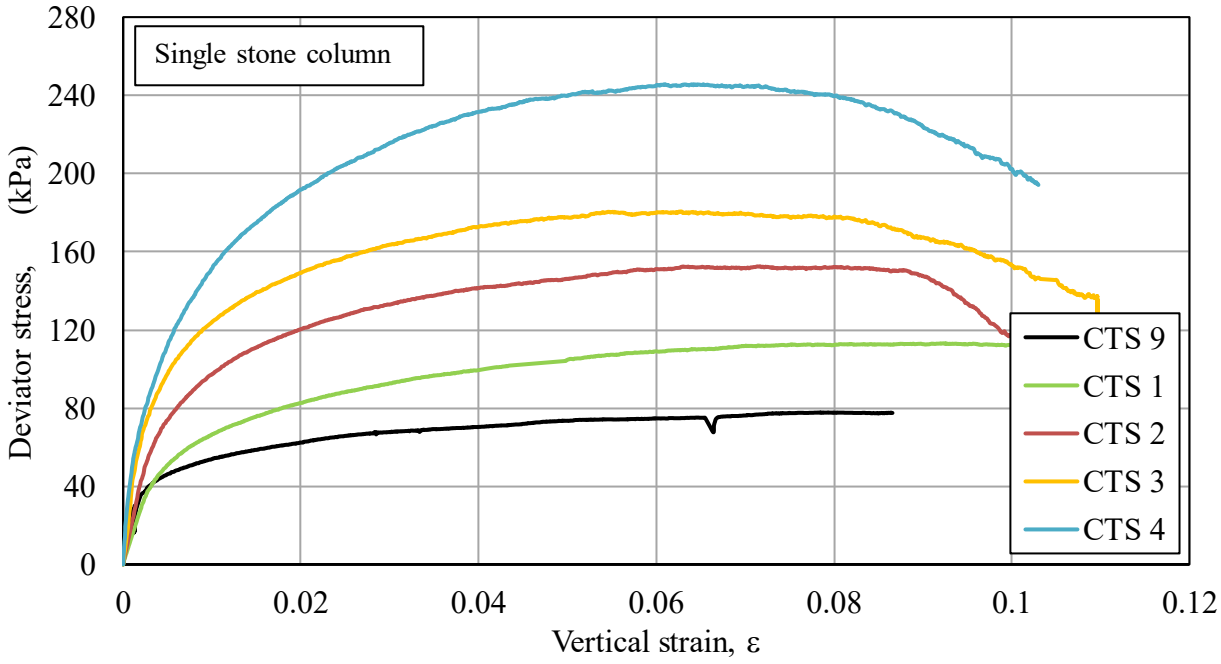

(a)

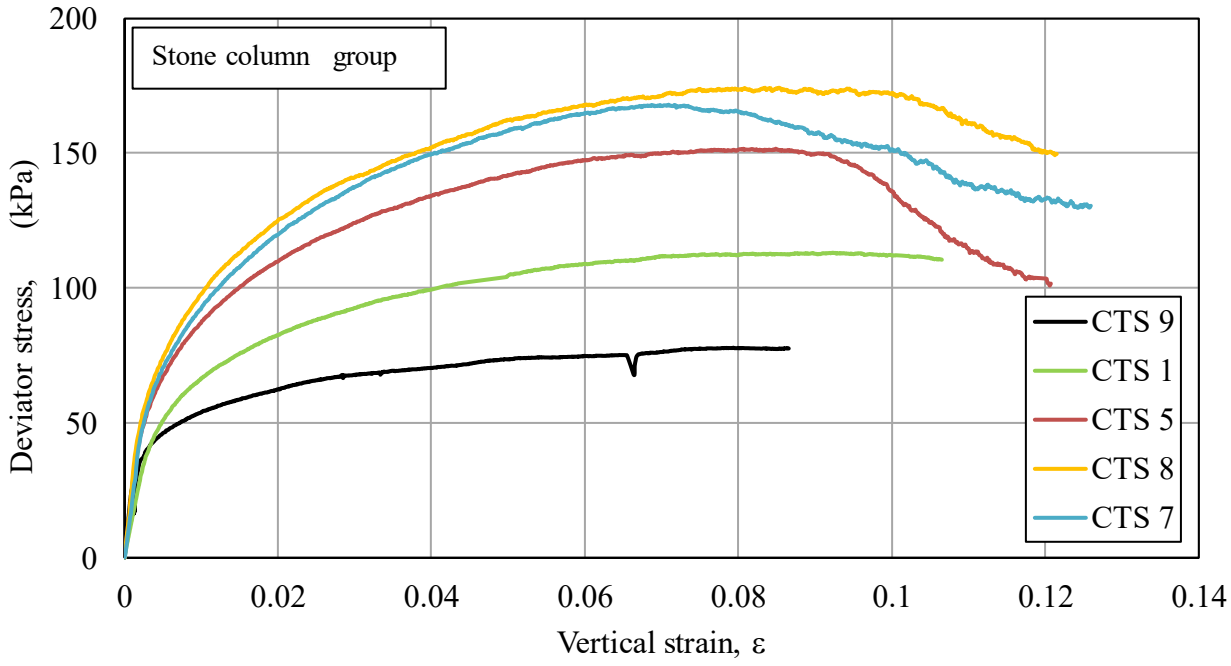

(b)

Figure 4.11 Deviator stress versus axial strain for samples in T2: (a) effect of increasing stone column diameter, (b) effect of increasing number of stone columns

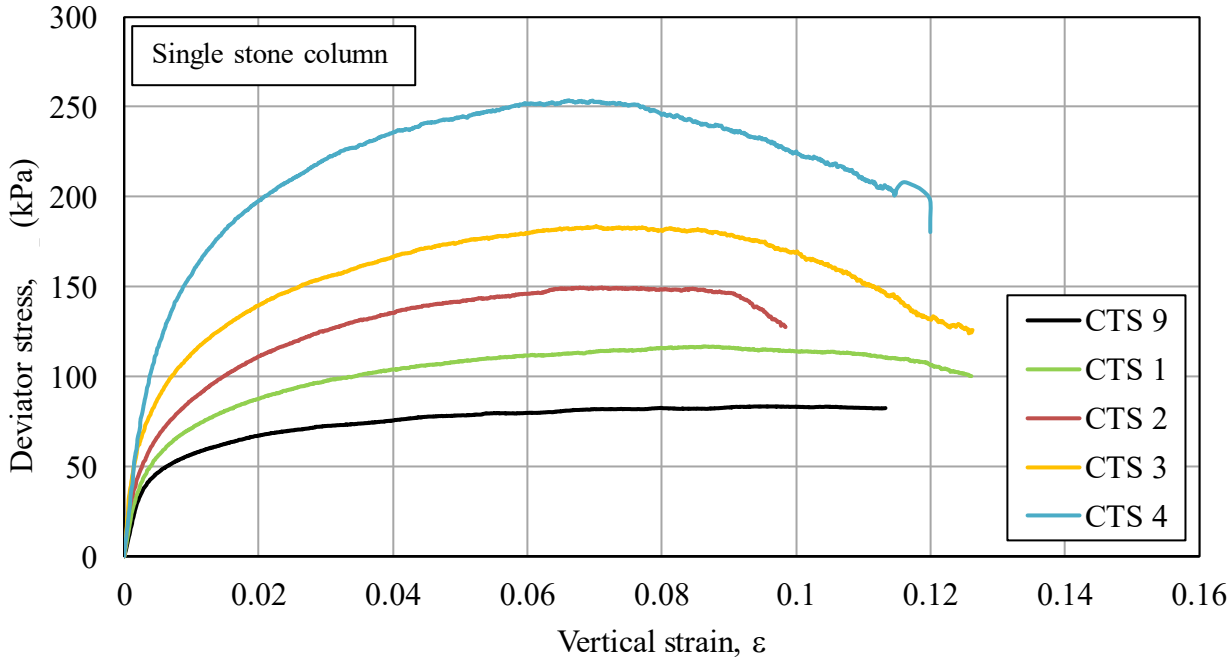

(a)

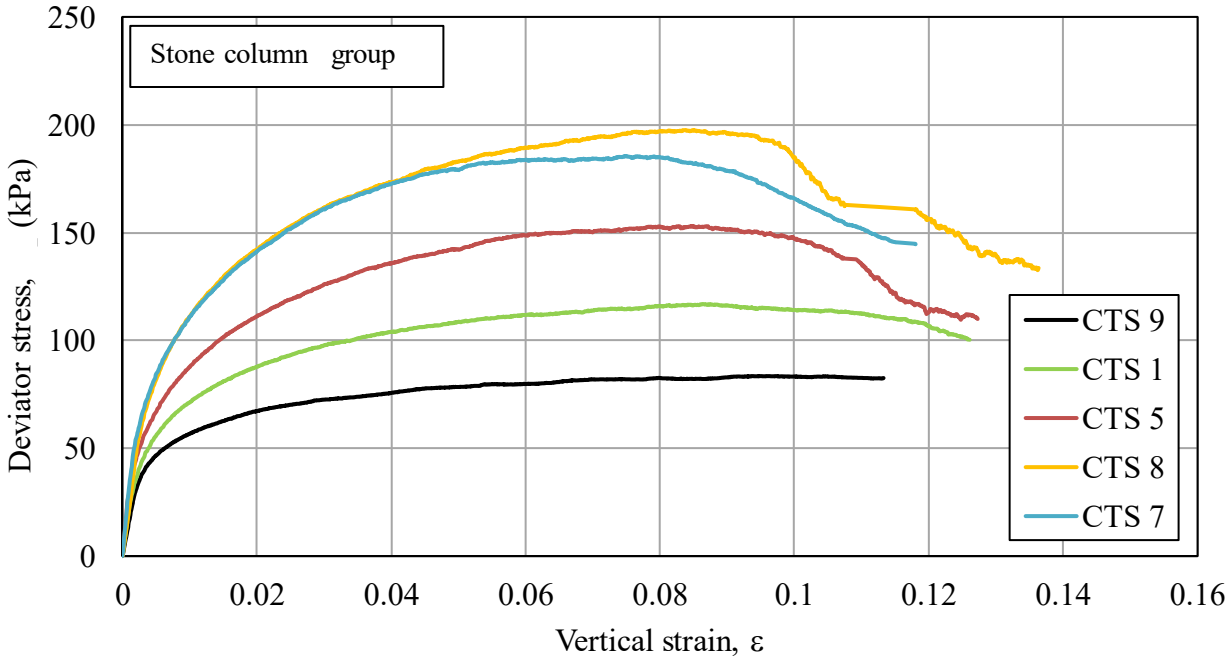

(b)

Figure 4.12 Deviator stress versus axial strain for samples in T3: (a) effect of increasing stone column diameter, (b) effect of increasing number of stone columns

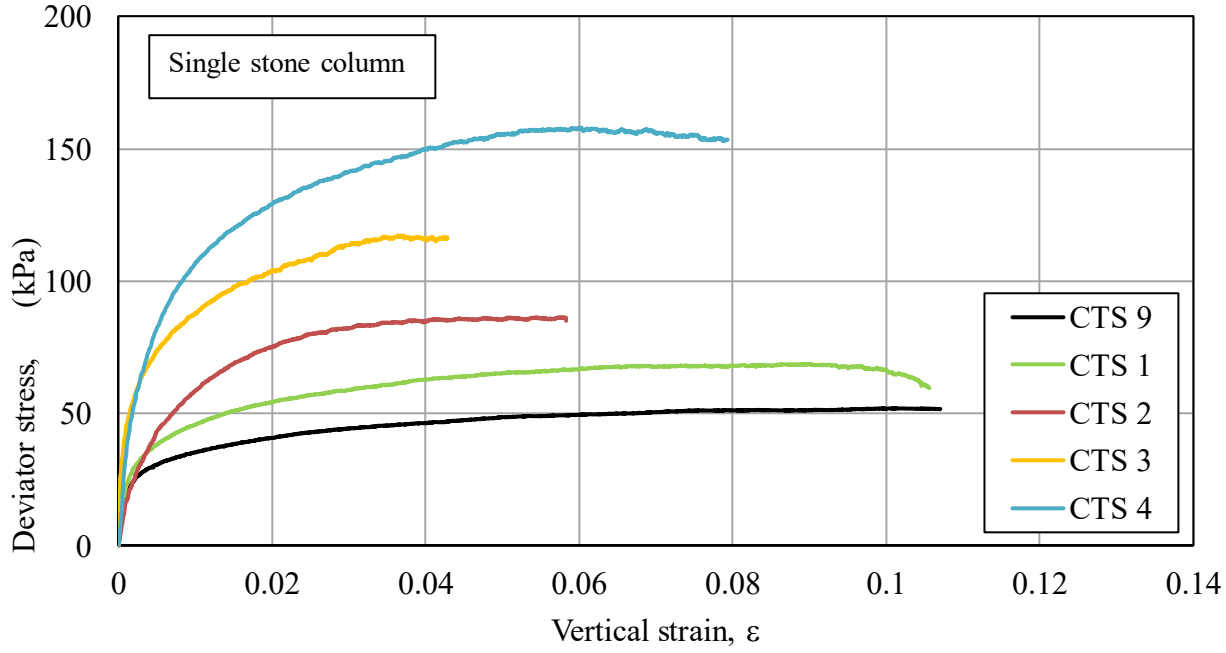

(a)

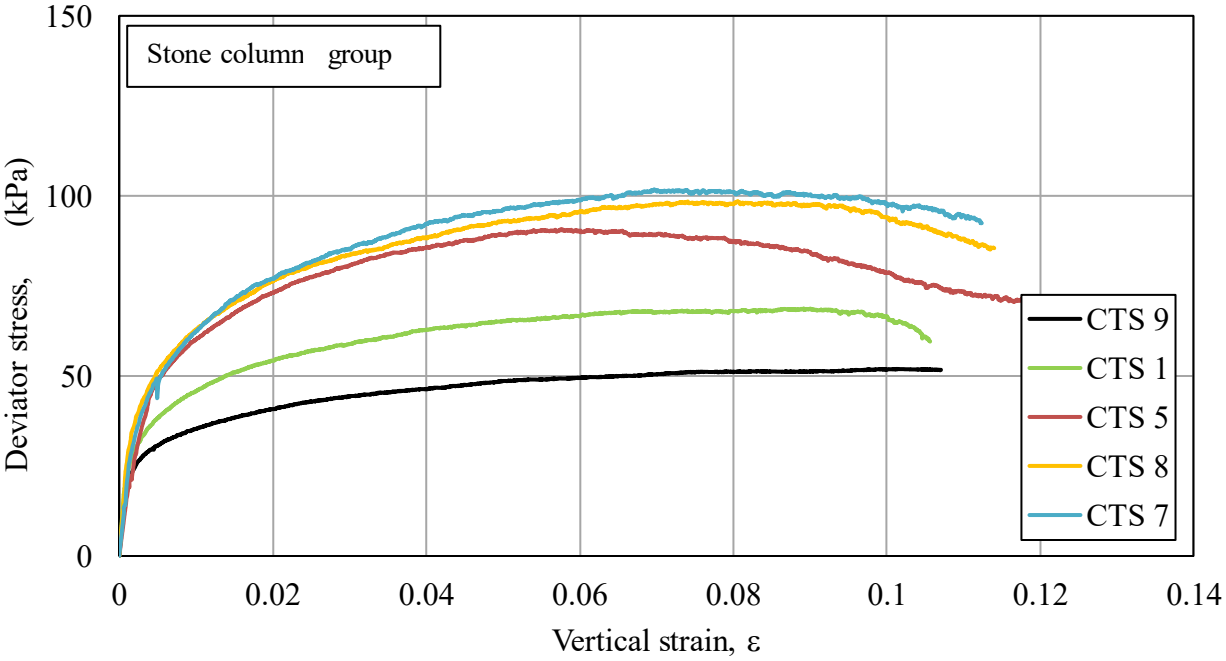

(b)

Figure 4.13 Deviator stress versus axial strain for samples in T4: (a) effect of increasing stone column diameter, (b) effect of increasing number of stone columns

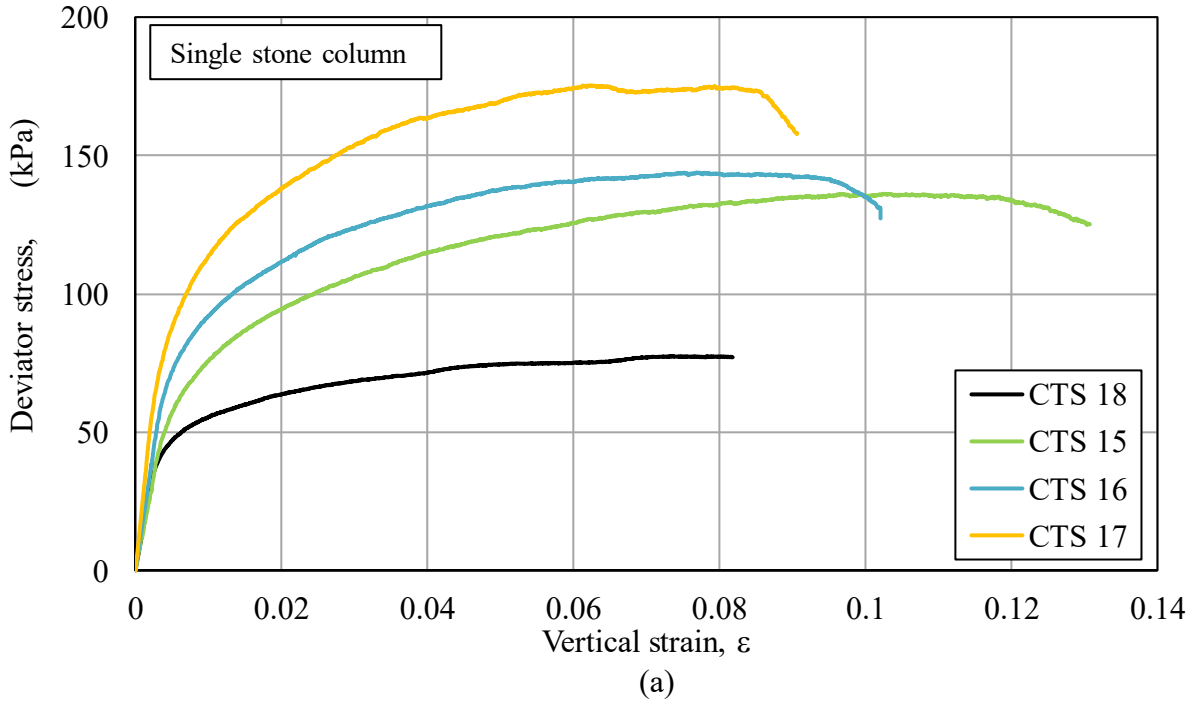

(a)

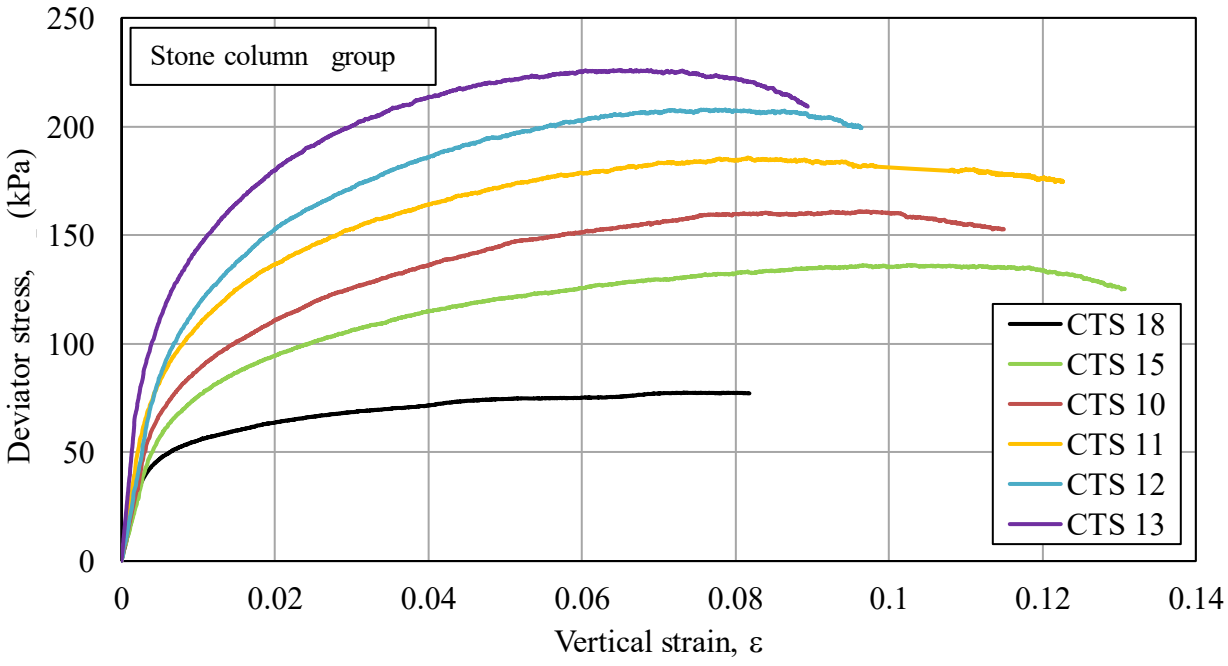

(b)

Figure 4.14 Deviator stress versus axial strain for samples in T5: (a) effect of increasing stone column diameter, (b) effect of increasing number of stone columns

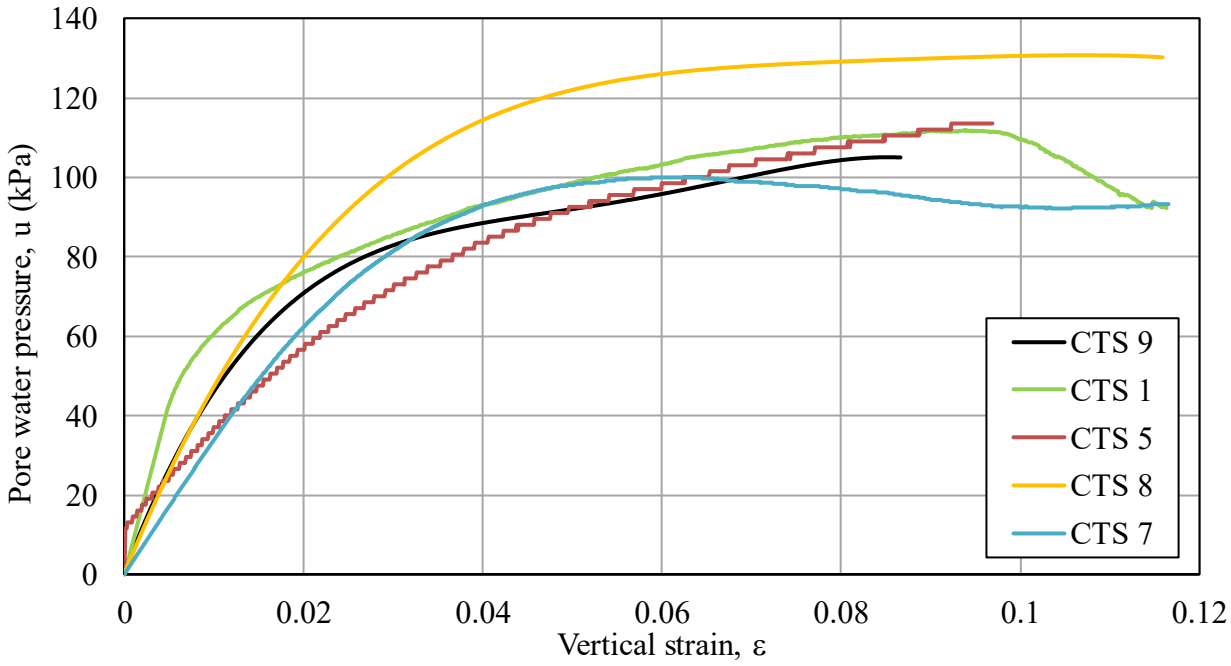
Pore water pressure, u (kPa)
140
120
100
80
60
40
20
0
0
0.02
0.04
0.06
0.08
0.1
0.12
Vertical strain, ε
CTS 9
CTS 1
CTS 5
CTS 8
CTS 7

(a)

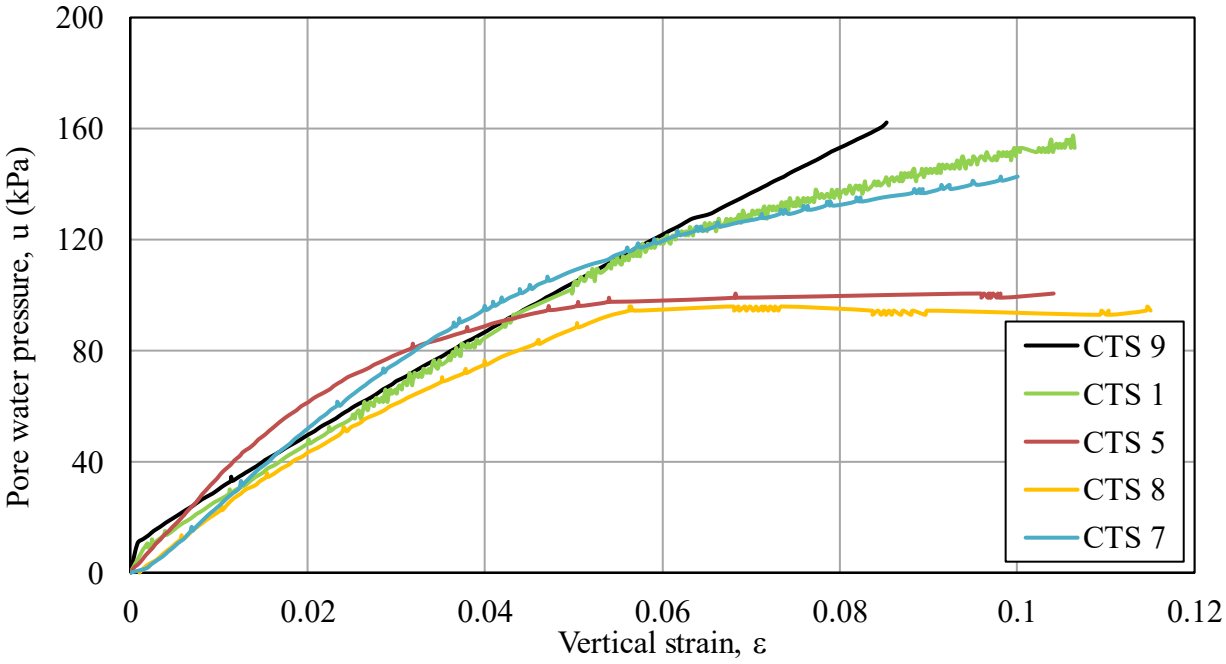
Pore water pressure, u (kPa)
200
160
120
80
40
0
0
0.02
0.04
0.06
0.08
0.1
0.12
Vertical strain, ε
CTS 9
CTS 1
CTS 5
CTS 8
CTS 7

(b)

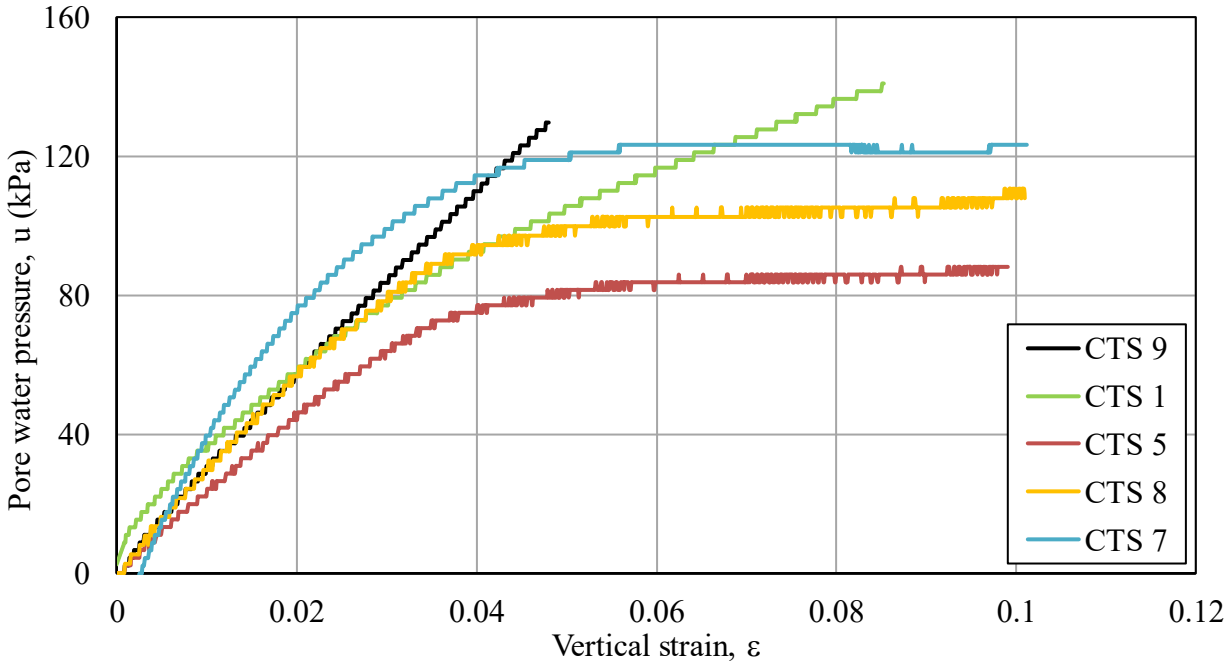
160
120
80
40
0
Pore water pressure, u (kPa)
0
0.02
0.04
0.06
0.08
0.1
0.12
Vertical strain, ε
CTS 9
CTS 1
CTS 5
CTS 8
CTS 7

(c)

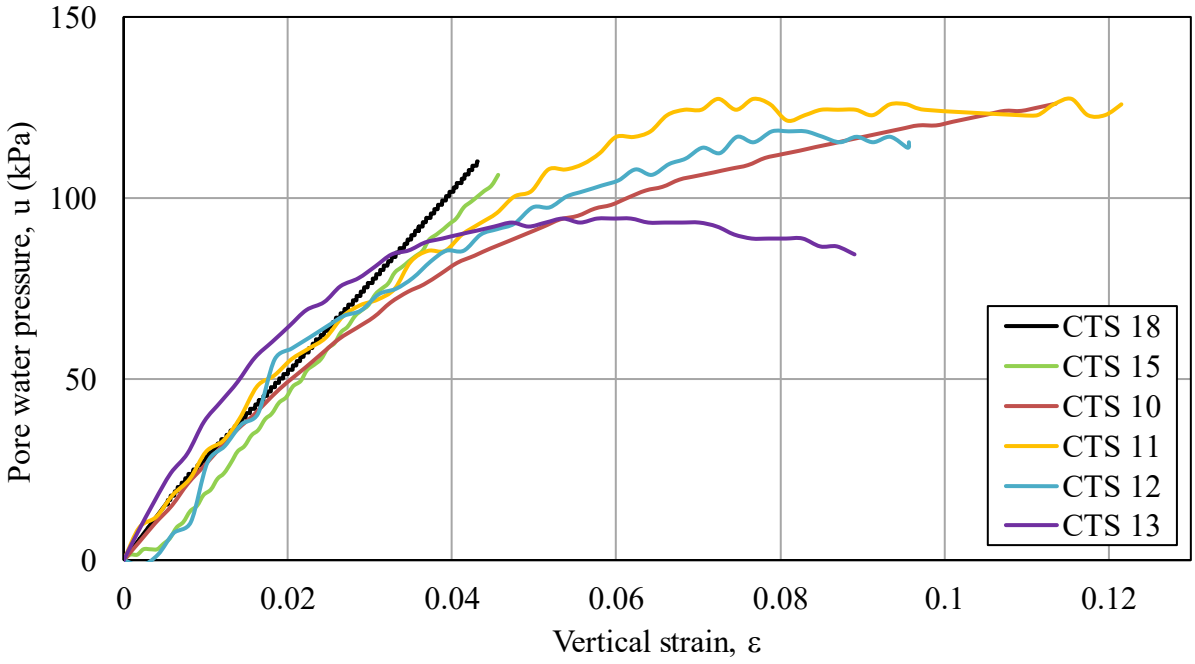
150
100
50
0
Pore water pressure, u (kPa)
0
0.02
0.04
0.06
0.08
0.1
0.12
Vertical strain, ε
CTS 18
CTS 15
CTS 10
CTS 11
CTS 12
CTS 13

(d)

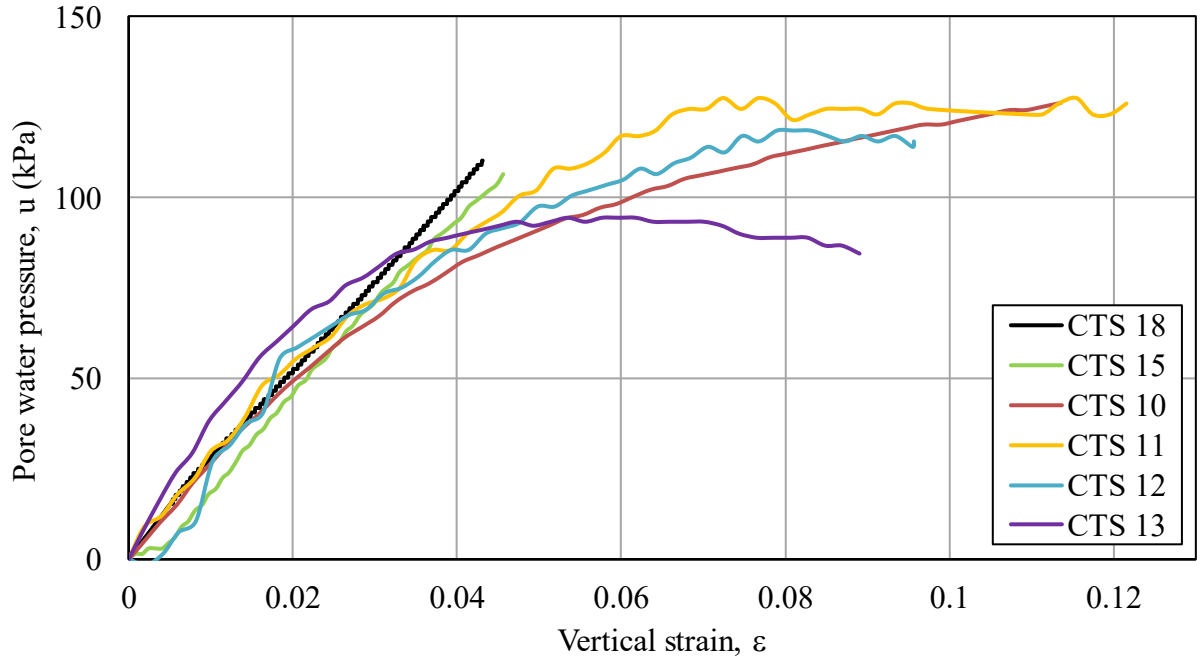

(e)

Figure 4.15 Pore-water pressure versus axial strain: (a) T1, (b) T2, (c) T3, (d) T4, (e) T5

It is clearly noticeable from all test results that increasing the replacement ratio enhances reinforced soil capacity. However, the increasing percent varies according to the arrangement of stone columns and testing parameters. A comparison between the test results is presented in the following sections to explicitly present the effect of each parameter on performance of reinforced clay soil.

4.3.2.1 Repeatability and reproducibility of test data

Test T1 and T2 were performed to illustrate the repeatability and reproducibility of the test procedures. The results of T1 and T2 for samples reinforced by a single and group of stone columns are presented in Figure 4.16 and Figure 4.17, respectively. Both figures show that the results were almost identical for all samples.

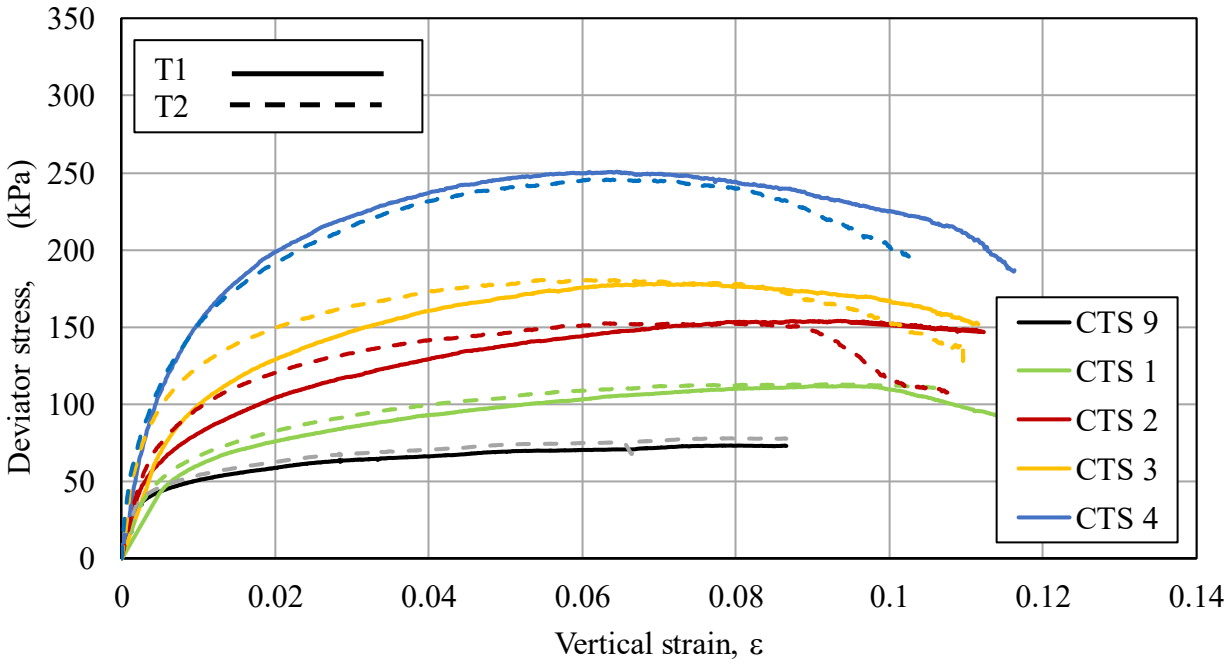

Figure 4.16 Test T1 and T2 results for clay samples reinforced by a single stone column

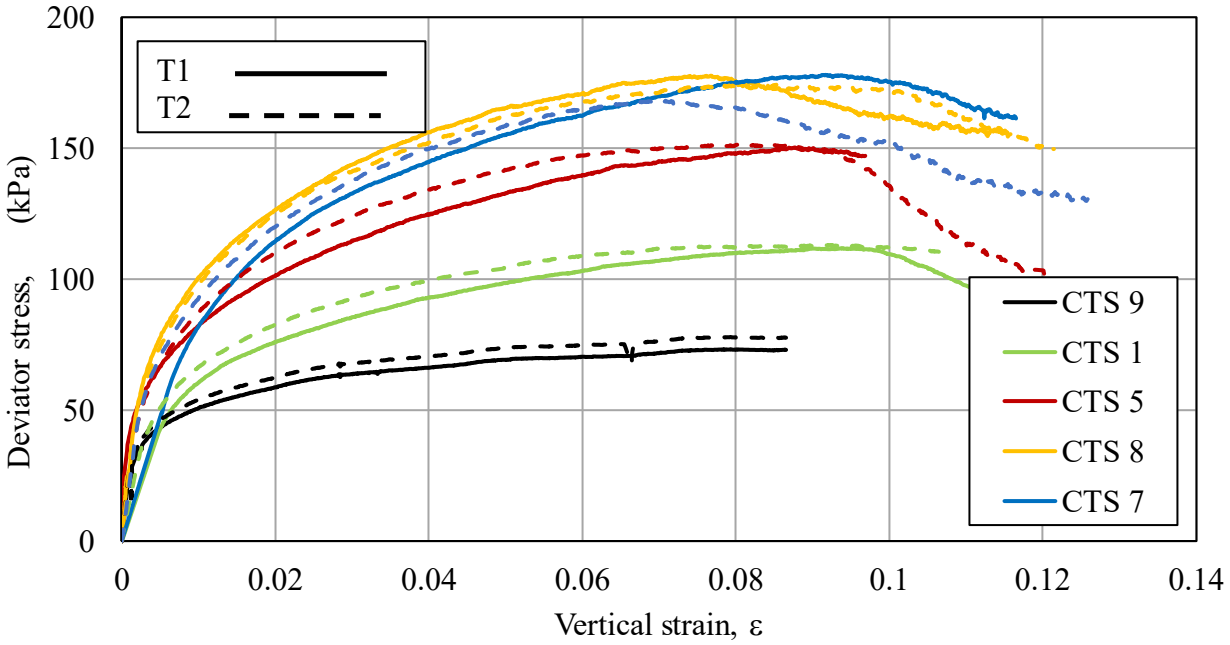

Figure 4.17 Test T1 and T2 results for clay samples reinforced by a group of stone columns

4.3.2.1 Effect of Compaction energy

Two different compaction energies of 310 kN.m/m^3 and 620 kN.m/m^3 were utilized to compact the sand inside the stone columns. The values of the compaction energy were selected to achieve two criteria: keep the sand in place after removing the samples from the tank to perform the triaxial test and minimize the change in the stone column replacement ratio due to compaction. In order to show the effect of

increasing the compaction energy, the results of T2 and T3 are presented in Figure 4.18 and Figure 4.19. There was a slight increase of 1 % to 3% in the reinforced clay resistance when a single stone column was used. However, the effect of increasing the compaction energy is noticeable in CTS 8 and CTS 7 with 3 and 4 stone columns respectively, as the deviator stress was improved by 15%. This increase was expected due to the lateral compaction, which enhances the strength of clay confined by a group of stone columns. However, this enhancement was not noticeable in clay samples reinforced by a single stone column because the stone columns were installed in a large tank so that there was no boundary effect and the clay around the stone column was unconfined. Therefore, the effect of the lateral compaction was not obvious.

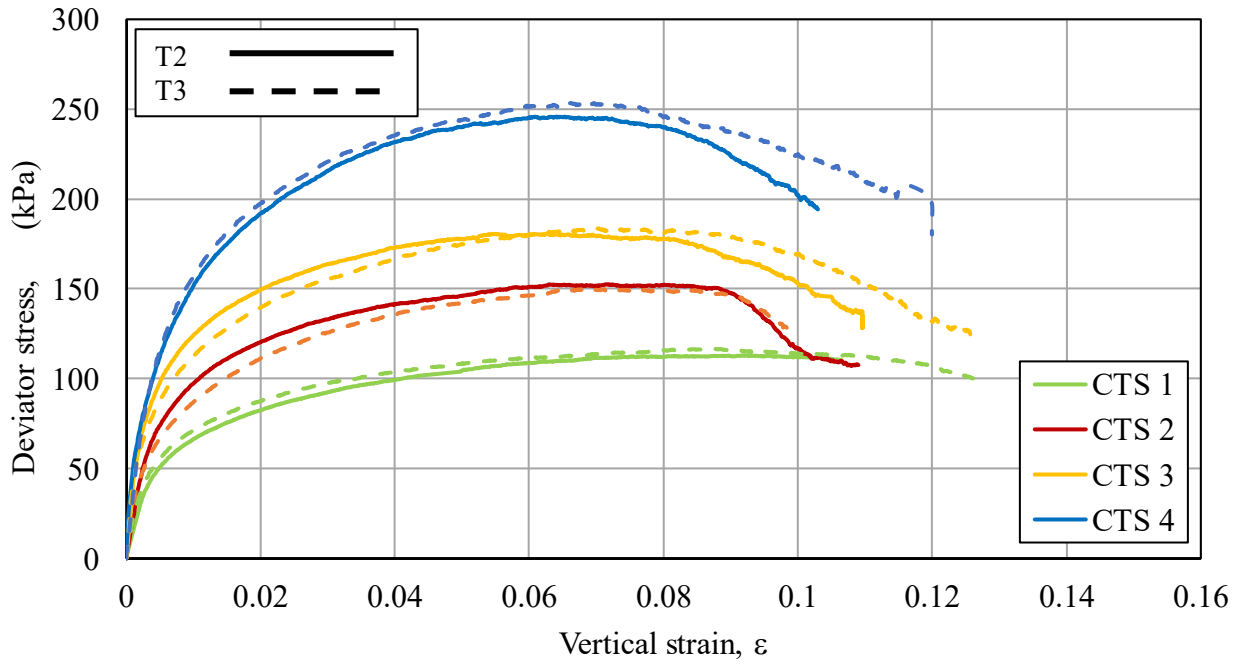

Figure 4.18 Effect of increasing the compaction energy used to install stone column in clay samples reinforced by a single stone column

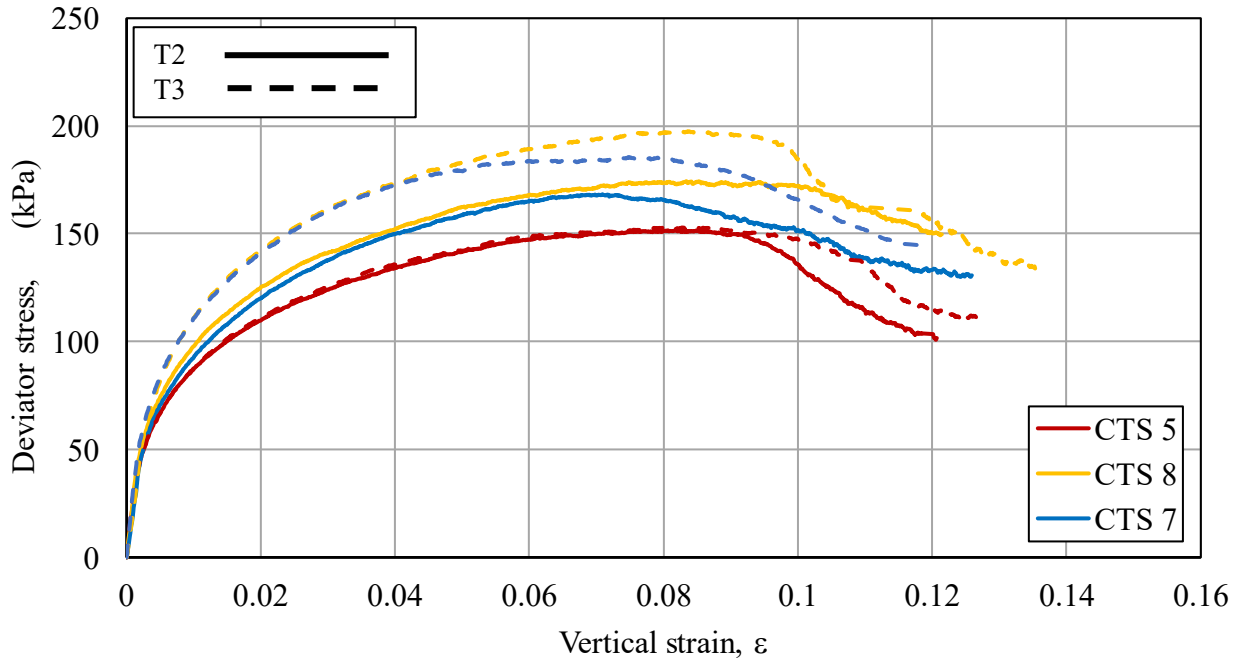

Figure 4.19 Effect of increasing the compaction energy used to install stone column in clay samples reinforced by a group of stone columns

4.3.2.2 Effect of spacing between stone columns

Figure 4.20 (a) presents the stress-strain behaviour for samples CTS 10 in T5 and CTS 5, CTS 6 in T2, which have the same replacement ratio of 8.8 % and *S/D* of 1.50, 2.00 and 2.75. It can be noted that increasing the spacing between columns at the same replacement ratio reduces the resistance of the reinforced soil, which agrees well with the observations of Khalifa et al. (2017) and Castro (2014). The resistance reduces with the increase of the column spacing/diameter ratio (*S/D*), which confirmed that for small spacing between columns the lateral support from the surrounding soil increases and accordingly shows improvement. The same behaviour could be concluded from the results of CTS 5 and CTS 6 in test T3 and T4, as shown in Figure 4.20 (b) and (c) respectively.

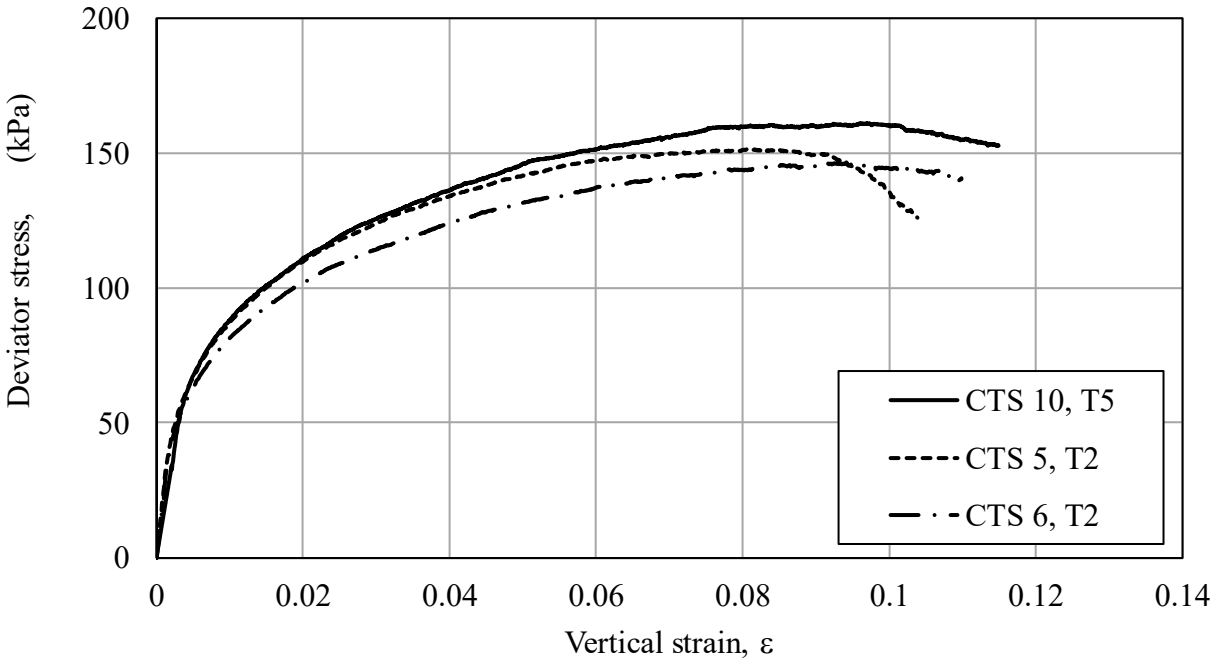
200
150
100
50
0
Deviator stress, (kPa)
0
0.02
0.04
0.06
0.08
0.1
0.12
0.14
Vertical strain, ε
CTS 10, T5
CTS 5, T2
CTS 6, T2

(a)

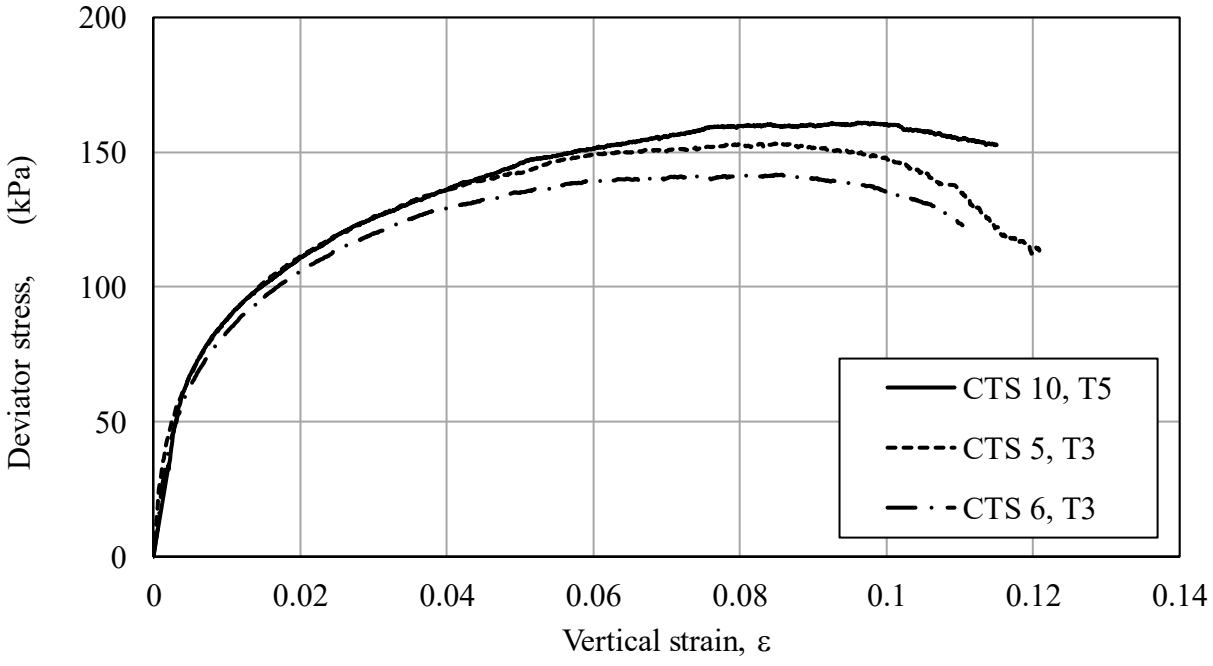
200
150
100
50
0
Deviator stress, (kPa)
0
0.02
0.04
0.06
0.08
0.1
0.12
0.14
Vertical strain, ε
CTS 10, T5
CTS 5, T3
CTS 6, T3

(b)

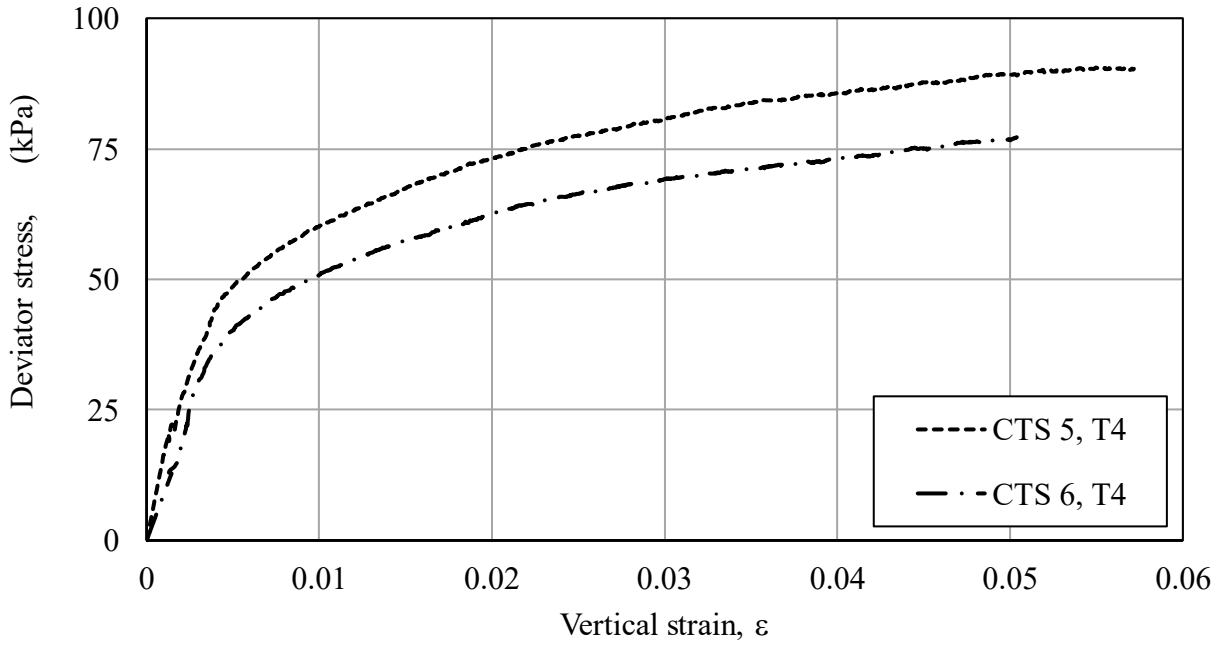

(c)

Figure 4.20 Effect of spacing/diameter ratio (*S/D*) for clay sample reinforced by two stone columns on the performance of stone columns: (a) T2 and T5, (b) T3 and T5, (c) T4

4.3.3 Comparison between single and group of stone columns

The primary output from the loading stage is improvement in the loading capacity of reinforced clay soil. Consequently, the relation between the axial strain (ε) and the deviator stress (σ_2) for all the samples was utilized to estimate the improvement factor (IMF). IMF is defined as the maximum deviator stress of the reinforced sample divided by the maximum deviator stress of the unreinforced sample.

Figure 4.21 (a) shows a summary of test T2 results when the confinement pressure was 160 kN/m^2, a spacing ratio of 1.5, and compaction energy of 310 kN.m/m^3. For samples reinforced by a single stone column, there is a linear relationship between the replacement ratio and IMF. The rate of the improvement was found to be almost the same in all tests conditions: 8.3, 7.7, 8.5, and 7.8 for T2, T3, T4, and T5 respectively. For clay samples reinforced by a group of stone columns, for replacement ratio less than 14% and *S/D* of 2.0 the capacity of clay samples reinforced by a group slightly increased compared to others reinforced by a single stone column. However, the capacity of the group significantly decreased for a replacement ratio higher than 13.2%.

The compaction energy increased to 620 kN.m/m^3 in test T3, and the capacity of the group slightly increased compared to test T2 as shown in Figure 4.21 (b). However, the capacity of the group reduced

at a replacement ratio of 13.2% as test T2. When the confinement pressure reduced to 80 kN/m^2 in test T4, the same reduction occurred in the group capacity. However, the reduction started at a smaller replacement ratio of 10% as shown in Figure 4.21 (c). For a closer spacing between stone columns in test T5 (S/D =1.5) the reduction in the group capacity did not occur, and the capacity of the group is higher than the single stone columns at the same replacement ratio as shown in Figure 4.21 (d).

Findings from all the tests suggest that the main reason behind the reduction that occurred in the resistance of samples reinforced by a group of stone columns at high replacement ratio (A_s > 10%), is the confinement around stone columns. In order to fully understand this reduction, the failure mechanism of the stone columns in different samples was compared. Three failure mechanizes were noticed in all the samples: bulging, shear, and bending (Figure 4.22). The same failure mechanisms were found experimentally by Hu (1995) and numerically by Etezad et al. (2015). For the samples reinforced by single stone columns, only bulging failure was noticed. However, shear and bending failure mechanisms occurred when a group of stone columns was used. For tests T2, T3 and T4, a spacing ratio of 2.00 was utilized, and the clay around the stone columns was not confined particularly for the sample reinforced by four stone columns (A_s = 17.6%). Also, the stiffness difference between soil and the column materials led to a stress concentration in the columns (Vautrain, 1978; Lee et al., 1994; Siahaan et al., 2018). Therefore, samples failed due to the bending that occurred in stone columns, as shown in Figure 4.22 (c). On the other hand, for samples reinforced by stone columns with a smaller spacing ratio of 1.5, the clay between the stone columns were additionally confined with the consequence that the total resistance of the samples increased and shear failure mechanism occurred, as shown in Figure 4.22 (b).

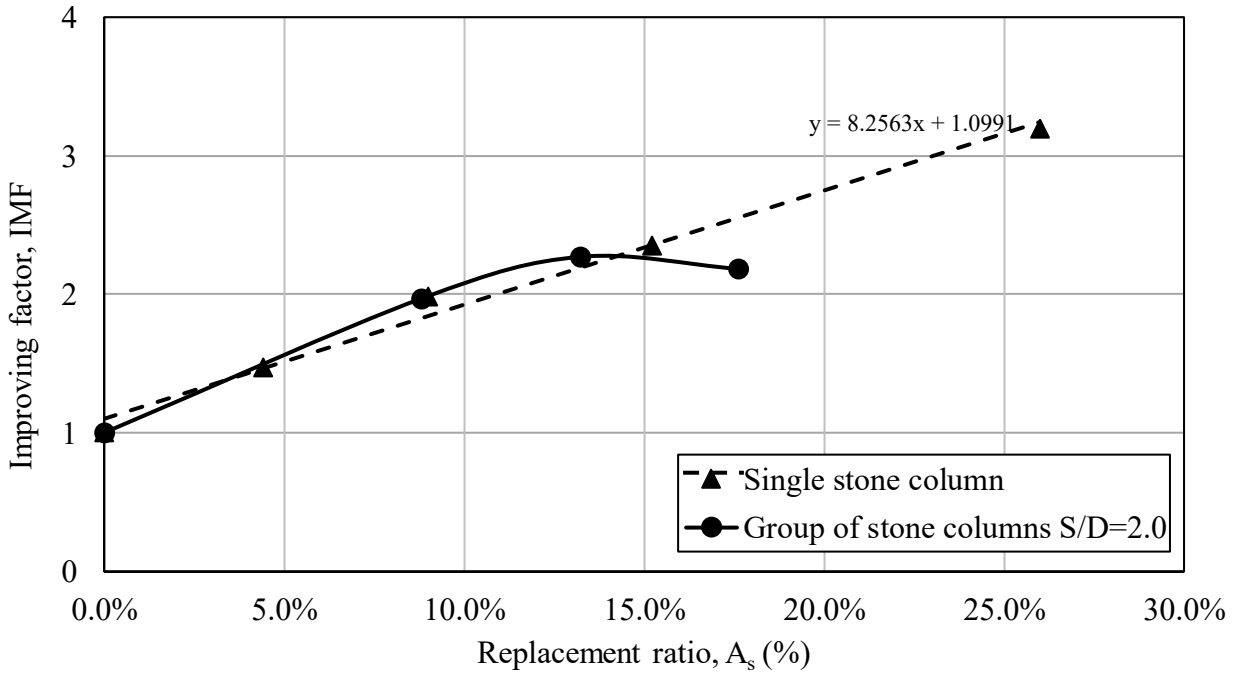
y = 8.2563x + 1.0991
Improving factor, IMF
Replacement ratio, A_s (%)
Single stone column
Group of stone columns S/D=2.0
0
1
2
3
4
0.0%
5.0%
10.0%
15.0%
20.0%
25.0%
30.0%

(a)

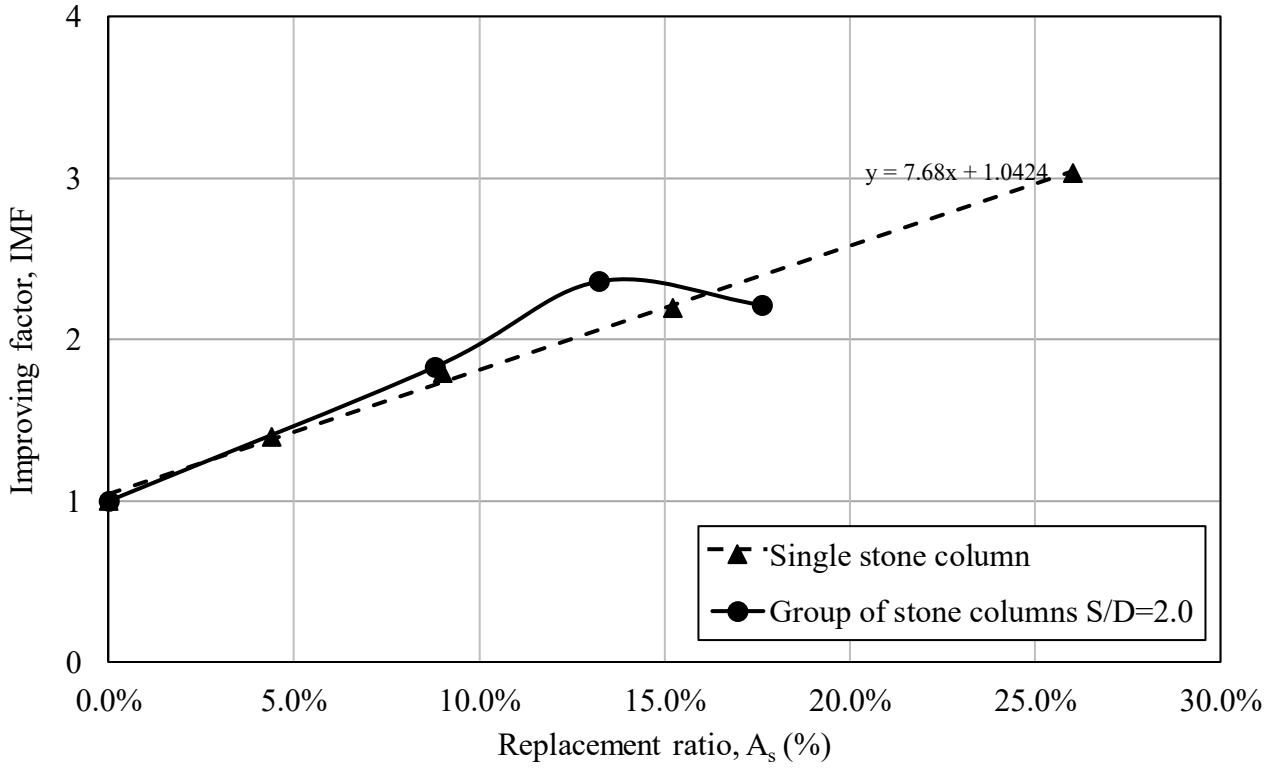
y = 7.68x + 1.0424
Improving factor, IMF
Replacement ratio, A_s (%)
Single stone column
Group of stone columns S/D=2.0
0
1
2
3
4
0.0%
5.0%
10.0%
15.0%
20.0%
25.0%
30.0%

(b)

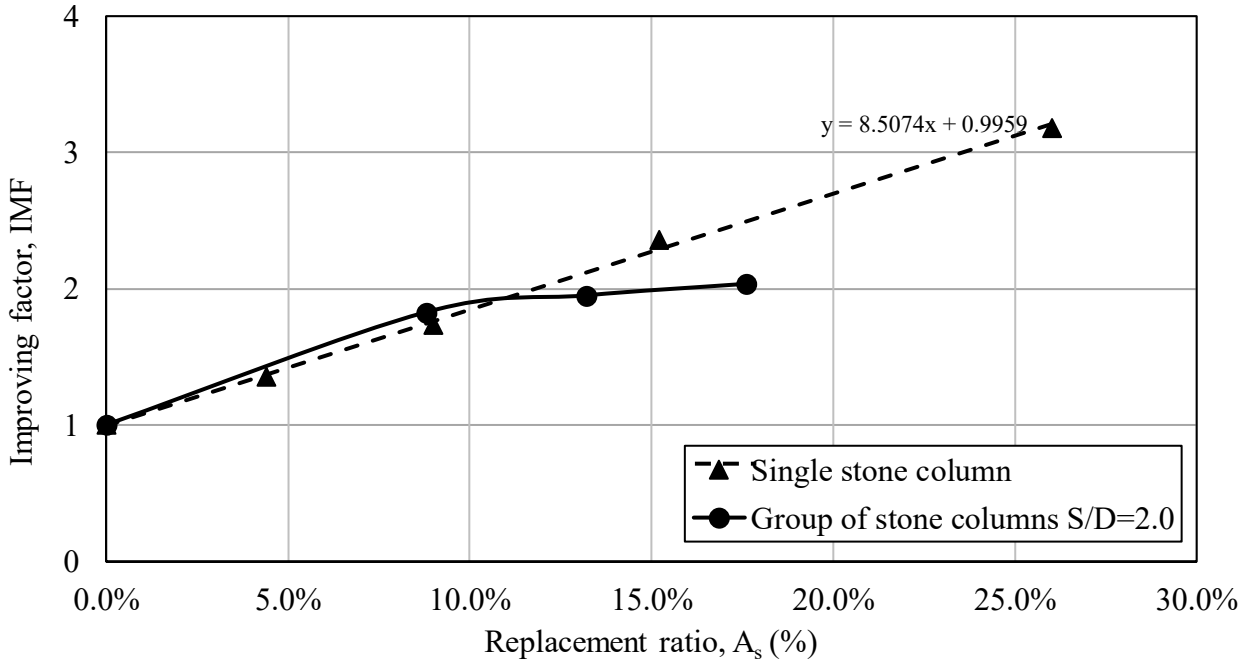

(c)

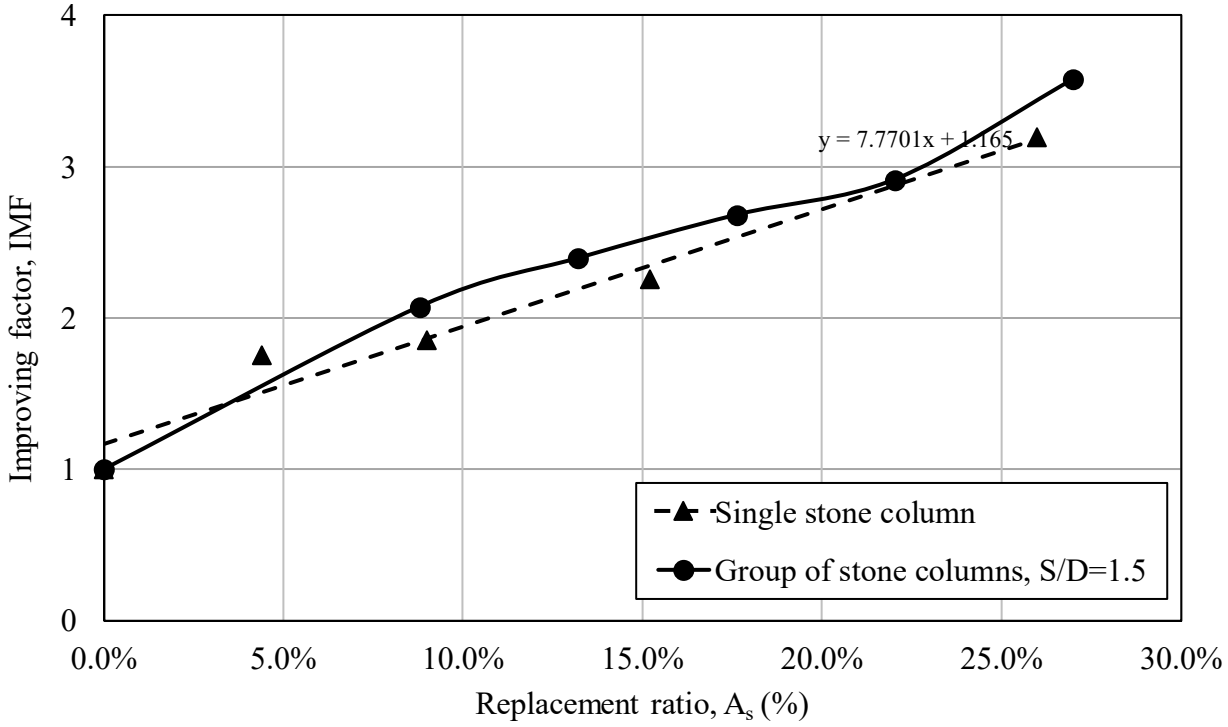

(d)

Figure 4.21 Improving factor versus the replacement ratio for clay samples reinforced by single and group of stone columns: (a) T2, (b) T3, (c) T4 and (d) T5

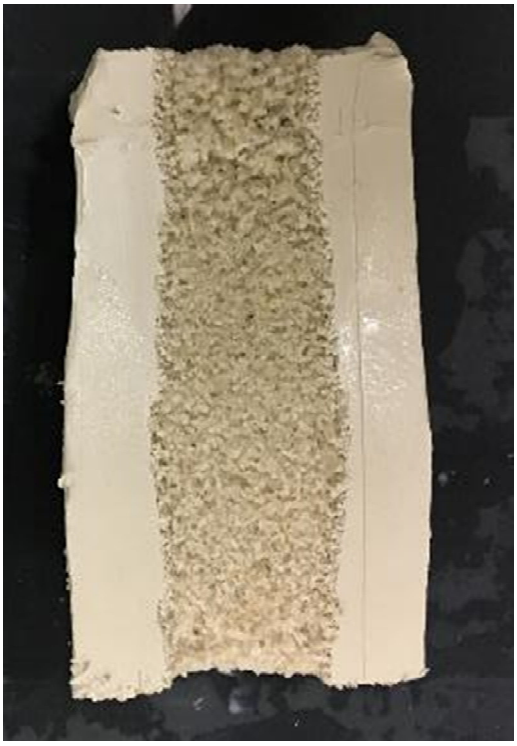

(a) Bulging failure (CTS 4, T2)

(b) shear failure (CTS 12, T5)

(c) bending failure (CTS 7, T2)

Figure 4.22 Observed failure mechanisms for stone columns in triaxial test samples

Chapter 5: Numerical Analysis

5.1 General

Numerical modelling is one of the most powerful tools for examining geotechnical engineering problems. The interaction between stone columns and the surrounding soil is no exception. In the literature, the assumptions used to examine the interaction between columns are based on two-dimensional numerical modelling and homogenized columns and the surrounding soil, which does not accurately represent the physical condition of the system. In this chapter, 3-D finite element models (FE) are developed to capture the behaviour of a group of stone columns surrounded by soft soil and to examine the influence of the parameters governing its performance. The models are validated against the experimental results presented in Chapter 4.

In this investigation, the effect of the installation of columns on the results produced was examined. A numerical model was developed to simulate the installation of the columns in order to examine its influence on the adjacent soil. A full-scale 3-D finite element model was developed for a rigid square footing on clay reinforced with stone columns. The results produced were used to establish the failure mechanism of the system, which was utilized to develop design theory and design charts for predicting the bearing capacity of these footings.

5.2 Finite element approaches

In developing the numerical model, emphasis was placed on assigning proper boundary conditions, material constitutive models, and the size and type of the elements used to simulate stone columns and the surrounding clay soil. The commercial finite element software "ABAQUS" Ver. 6.11, 2011, was used to perform this analysis.

5.2.1 Material constitutive models

In order to simulate the changes in the pore water pressure and capture the time dependency of the clay soil, the constitutive model of elastic-hardening plastic modified by Drucker-Prager/cap plasticity (Drucker et al., 1952) was used to simulate the clay soil in all the finite element approaches. The plastic properties of the material were defined by the angle of friction (β_c) and cohesion (d_c), which were calculated from the drained friction angle (ϕ_c') and cohesion of clay (c_c') as given in equations (5-1) and (5-2), respectively (Genna et al., 1994; Chen et al., 2012; Sinha et al., 2016). In order to complete the

definition of the plastic yield surface shown in Figure 5.1 and Figure 5.2, the cap eccentricity (R), transition surface factor between Drucker-Prager shear line and the cap (α), and the flow stress ratio (K) were defined as 1.3, 0.05, and 1, respectively for all models. The consolidation parameters of clay soil were used to define the cap hardening curve using equation (5-3) (Genna et al., 1994; Helwany, 2007). Figure 5.3 presents the cap hardening curve for the clay used in test T2. The elastic behaviour of clay soil was simulated using the porous elastic nonlinear-isotropic model. The porous elastic model was defined by the bulk modulus (κ) which is linked to the swelling index (C_s) as given in equation (5-4), and Poisson's ratio (ν). In addition, the properties that control the porous properties of the clay soil are defined as: the permeability coefficient (k), initial void ratio (e_o), specific gravity of water (γ_w), and saturated density of clay ($\rho_{c\text{-}sat}$).

$$\tan\beta_c = \frac{6\sin\phi_c'}{3-\sin\phi_c'} \tag{5-1}$$

$$d_c = \left(1-\frac{1}{3}\tan\beta_c\right)\frac{2c_c'\cos\phi_c'}{1-\sin\phi_c'} \tag{5-2}$$

$$\varepsilon_v^P = \frac{C_c - C_s}{2.3(1+e_0)}\ln\frac{\sigma'}{\sigma_c'} \tag{5-3}$$

$$\kappa = \frac{2c_s}{2.3\times(1+e_0)} \tag{5-4}$$

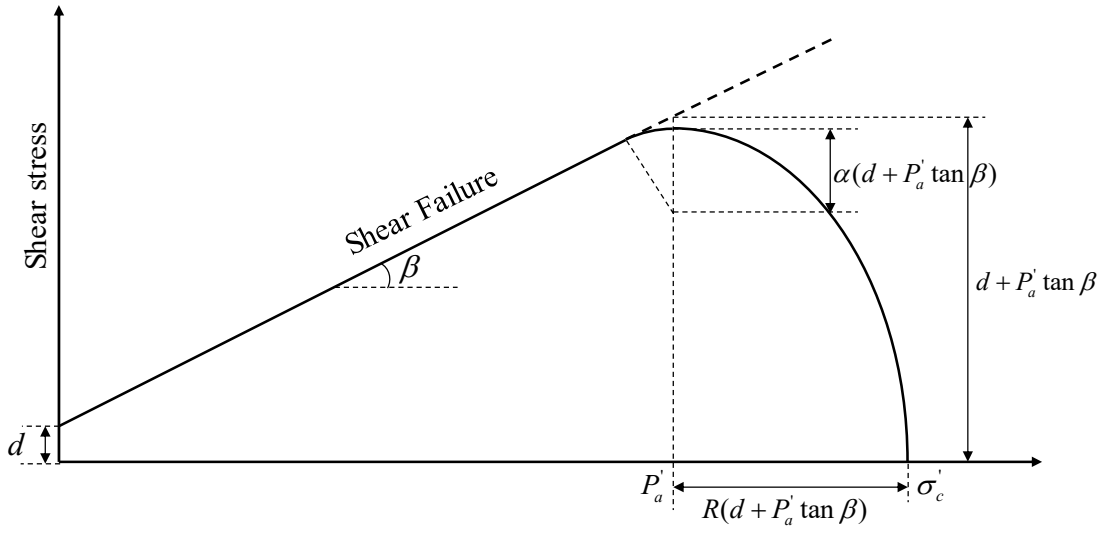

Figure 5.1 Yield surface of the modified Drucker-Prager/cap model

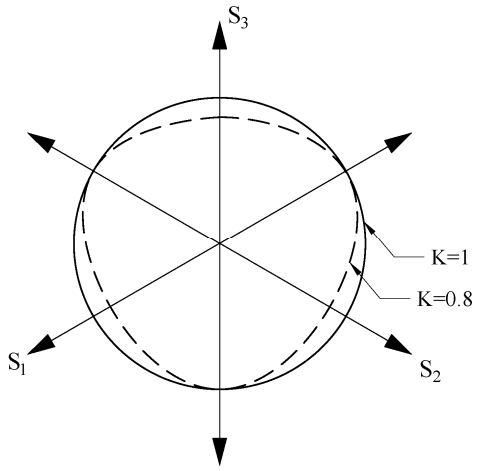

Figure 5.2 Projection of modified cap plasticity yield-flow surface

Drucker-Prager constitutive model is restricted to the value of $K \geq 0.788$, which is equivalent to Mohr-Coulomb friction angle of 22^o (ABAQUS, 2011). Since the angle of friction of the material of the stone columns is relatively higher than 22^o, the elastic-perfect plastic Mohr-Coulomb constitutive model was used in all finite element models. The friction angle (ϕ_s') was determined from the results of the direct shear test, given in section 3.3.2 and the dilation angle (δ) was determined according to Bolton (1986) and Mohanty et al. (2015). A linear elastic model was utilized in stone material by defined Young's modulus (E) and Poisson's ratio (ν). The permeability properties of the clay and stone materials were defined using the permeability coefficient (k), initial void ratio (e_o), and the unit weight of the water (γ_w). Furthermore, the saturated densities of the material of the stone columns (ρ_s), permeability coefficient (k), initial void ratio (e_o) were provided in the material definition.

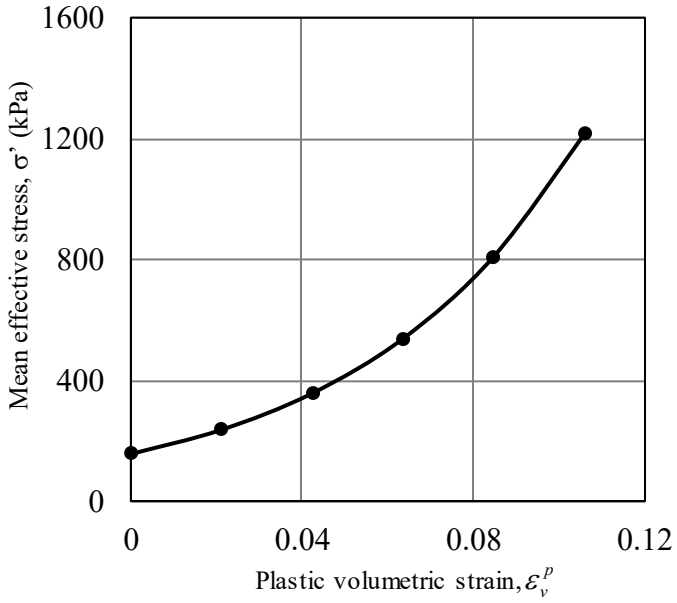

Figure 5.3 Modified cap model hardening curve for clay soil in test T2

5.2.2 Element type and mesh properties

In this investigation, an 8-node brick element with linear pore pressure and linear displacement was used in the FE models. Furthermore, different element sizes were used in each model based on the model size and number of stone columns. However, there are general rules that were considered in all models such as the mesh was very dense around the stone columns, and its size was gradually increased around the boundaries. The stone column was divided into at least ten elements at the cross-section. The aspect ratio of all the elements ranged between 1 and 3. A mesh sensitivity analysis was conducted in order to minimize the mesh effect on the results.

5.3 Experimental FE model approach (EFE)

In this section, a modelling approach is proposed to examine the influence of the stone columns properties (replacement area A_s %, spacing S, no. of columns N) on the vertical stress capacity of reinforced soil. This approach is validated against the present experimental results. The EFE model was utilized to simulate the triaxial tests in the experimental program conducted on the reinforced clay sample with a diameter of 10 cm and a total length of 20 cm, as shown in Figure 5.4. The stone column diameter (D_s), number and spacing/diameter ratio (S/D) was used as presented in the experimental program (Table 4.1). The effect of stone columns installation was neglected in this model, but it is investigated separately in the next IFE approach. The finite element model is divided into three steps. The first step was defined

as geostatic, where all the initial conditions were defined and the gravity load was applied. The second step represented the confinement due to external cell pressure (σ_3) in the triaxial test; the duration of this step was set to 24 hours as presented in the experimental program. The vertical load was applied in the last step, using displacement control from the top surface of the sample. Each time step was set in order to satisfy the movement rate of the triaxial deviator, which was set to 0.5 mm/min during the triaxial test.

Due to the high compaction energy used during the installation of the columns, the stone particle squeezes inside the clay soil creating a penetration zone as shown in Figure 5.5. This interaction prevents any relative deformation between stone columns and the clay soil. Therefore, most of the finite element models utilized in the literature to simulate laboratory and field tests of single and group of stone columns, assumed a full contact between stone columns and the surrounding soil (Goughnour et al., 1979; Mitchell et al., 1985; Ambily et al., 2007; Domingues et al., 2007; Elshazly et al., 2008; Hanna et al., 2013; McCabe et al., 2016). Consequently, full contact between the stone columns and the clay soil was utilized in the proposed EFE model.

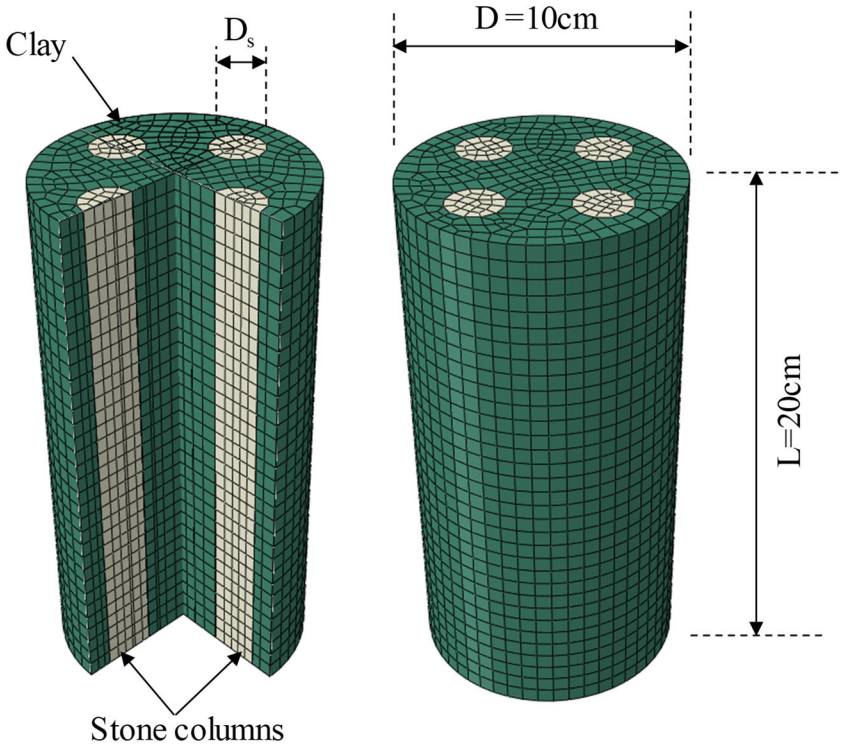

Figure 5.4 Details of EFE model approach (CTS 7)

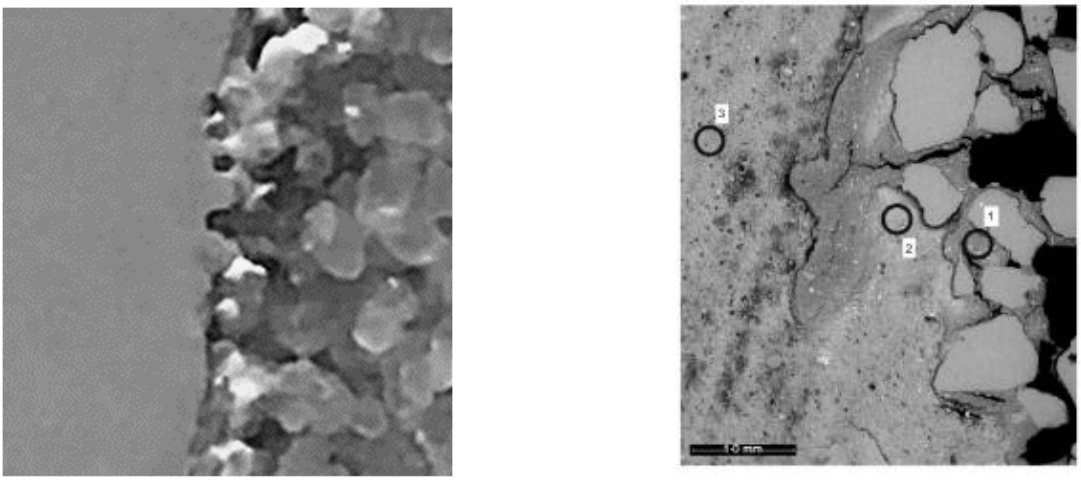

(a) (b)

Figure 5.5 Penetration zone around the stone column: (a) current study (b) Weber et al., (2010)

5.3.1 Material properties

All Drucker-Prager/cap plasticity model parameters for the clay soil were calculated from the clay properties presented in Table 4.2. However, the Mohr columns shear parameters were calculated from the triaxial test performed on the unreinforced clay sample (CTS 9) in tests T2 and T4 under a confinement pressure of 160 kN/m^2 and 80 kN/m^{2,} respectively. Mohr-Coulomb circle of the two samples are shown in Figure 5.6. The drained and undrained shear strength parameters of the clay soil are obtained based on Mohr-Coulomb failure line are shown in Table 5.1. The drained shear parameters were used to calculate Drucker-Prager cap plasticity model parameters, which are used for all the numerical models in the EFE approach.

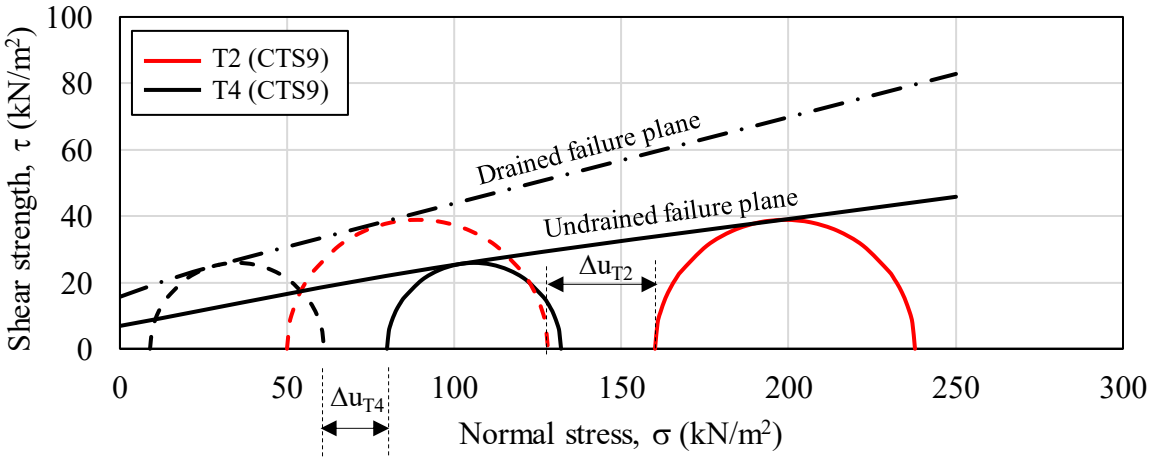

Figure 5.6 Drained and undrained Mohr-Columns failure planes for clay soil used in the experimental program

Table 5.1 Mohr-Coulomb shear strength parameters of the clay soil used in the experimental program

Shear strength parameters	Drained	Undrained
Angle of shear resistance, ϕ_c°	18.30	10.30
Cohesion, c_c (kN/m^2)	15.80	6.50

A direct shear test was conducted on the coarse sand used for filling the stone columns under different compaction energies as described in section 3.3.2. The test results are summarized in Figure 5.7. Based on the relation between the compaction energy and the angle of friction, an angle of friction of 44° was used for the stone columns material in numerical models simulating tests T2, T4, and T5. Regarding numerical models simulating test T3, an angle of friction of 46.8° was used. The modulus of elasticity of the stone columns material is one of the factors that has a significant effect on the performance of the reinforced clay soil. The ratio between the elastic modulus of stone column material and the clay soil was considered to have a lower range of 10 and upper limit of 40 (Balaam et al., 1981; Balaam et al., 1985). The modulus of elasticity of dense sand ranged from 48,000 to 81,000 kN/m^2 (Bowles, 1996). A parametric study was conducted by Hanna et al. (2013) using numerical analysis, and the elastic modulus of the stone columns ranged from 35,000 to 175,000 kN/m^2. Ambily et al. (2007) and Mohanty et al. (2015) presented a numerical analysis to study the response of stone columns in layered soil using a modulus of elasticity of 50,000 kN/m^2 for the stone column materials. In the current study, the modulus of elasticity of the stone column material in models related to tests T2, T4, and T5 was 50,000 kN/m^2. Since higher compaction energy was used in test T3, a modulus of elasticity of 60,000 kN/m^2 was used in all numerical models simulating triaxial samples in test T3.

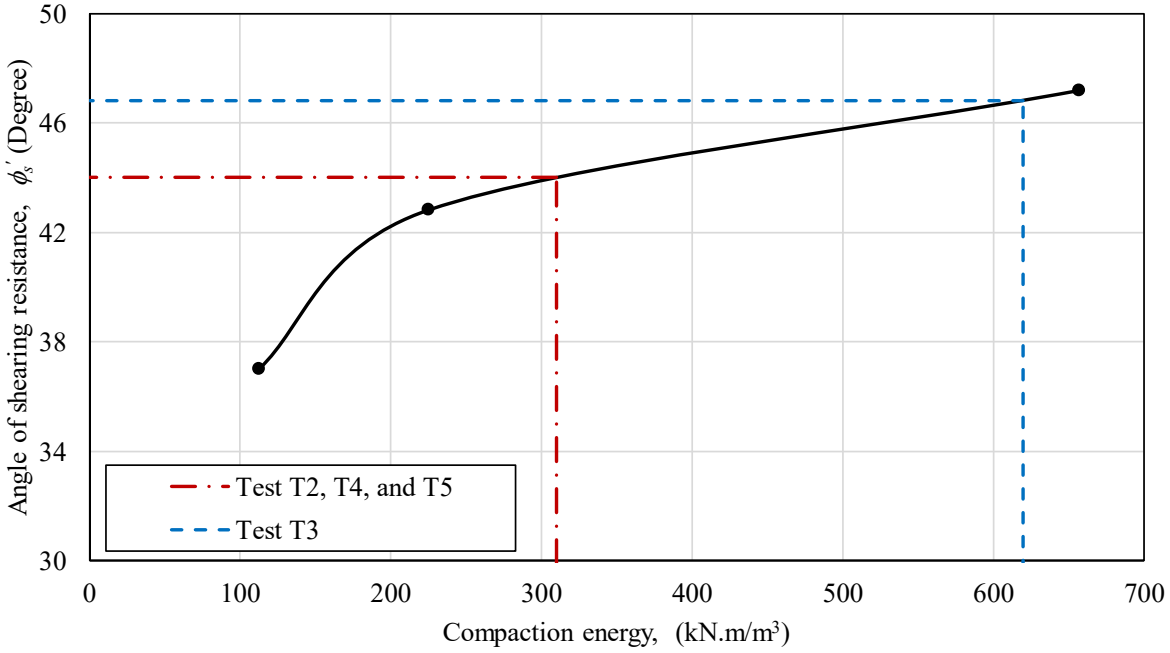

Figure 5.7 Relation between compaction energy and friction angle of stone columns materials used in the experimental program

A Poisson's ratio (ν) of 0.3 and 0.4 was used for the stone column material and clay soil for all models, respectively (Kulhawy et al., 1990; Hanna et al., 2013; Mohanty et al., 2015).

The permeability coefficient for clay soil was calculated from the consolidation test presented in the experimental program, the values of which are presented in Table 4.2. The permeability coefficient of the stone column material was assumed to be 0.01 m/sec (Bowles, 1996).

5.3.2 Boundary conditions

The EFE modelling approach was presented based on the triaxial test conducted in the experimental program, having a test sample of 10 cm diameter and a length of 20 cm. In order to simulate top and bottom rigid plates used to support the sample in the triaxial test, fixed boundary conditions were applied to the base of the model during all the model steps. However, a constraint condition using predefined equations was defined to control the movement of the top surface. In this constraint, a reference point was defined at the center of the model top surface, and the predefined equations were used to set the displacements (*Ux, Uy, Uz*) of all points on this surface to match the displacements of the reference point.

During the geostatic step, no constraints were applied to the top surface of the sample; however, the horizontal displacements (*Ux, Uy*) of the sides were restrained as shown in Figure 5.8 (a). The

confinement pressure was applied to the top and sides of the model in the second step (confinement step). Accordingly, constrains on the sides of the model were inactive due to the applied stresses on the sample and the friction between the triaxial sample material and porous plates between the sample and the rigid supporting plates. It was noticed that there was not any relative deformation between the top and the bottom surfaces of the sample and the rigid plates (Figure 5.9). Therefore, the horizontal displacements (*Ux, Uy*) of the reference point were restrained as shown in Figure 5.8 (b).

In the last step (loading step), all the restraints were kept as the confinement step. Moreover, a vertical displacement was applied to the reference point in order to simulate the deviator load as shown in Figure 5.8 (c).

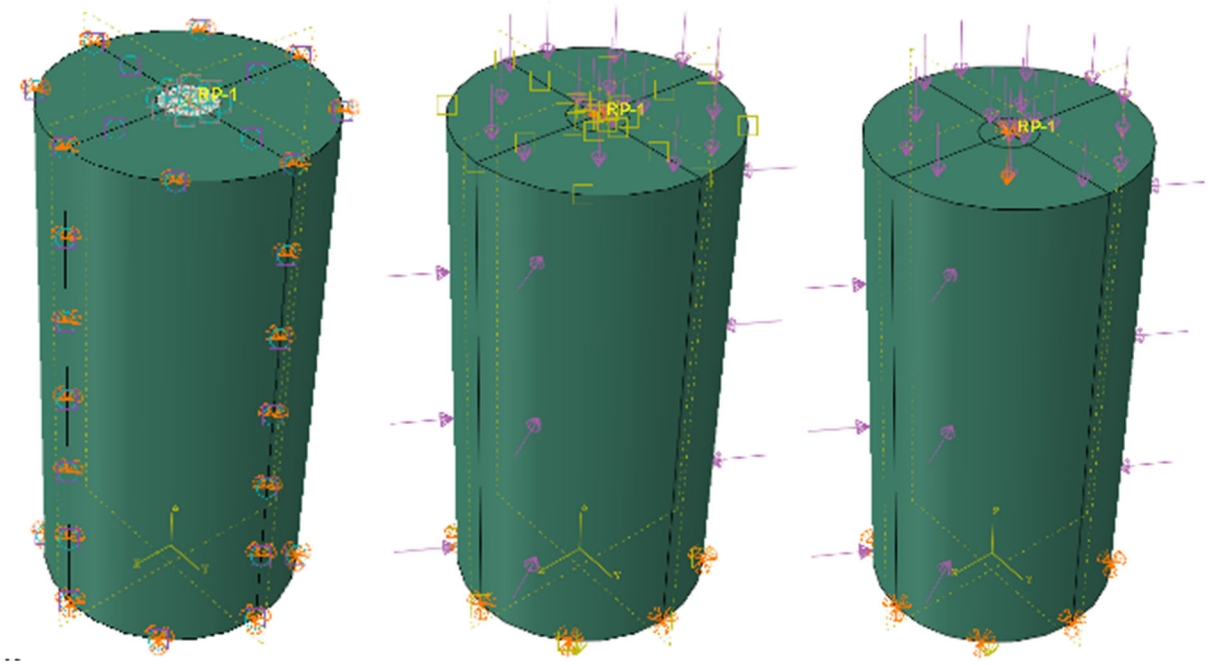

(a) (b) (c)

Figure 5.8 Boundary condition applied to the EFE model: (a) geostatic step, (b) confinement step, (c) loading step

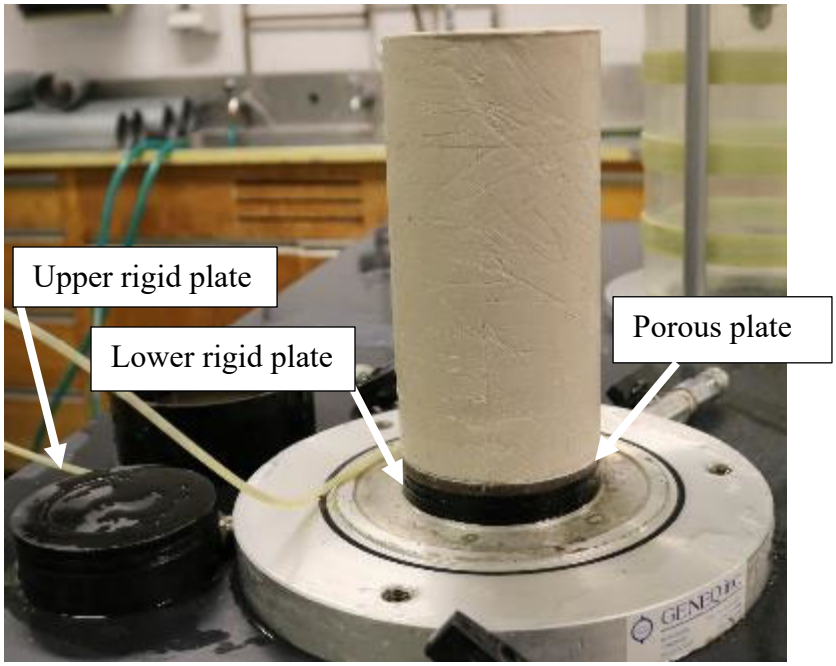

(a)

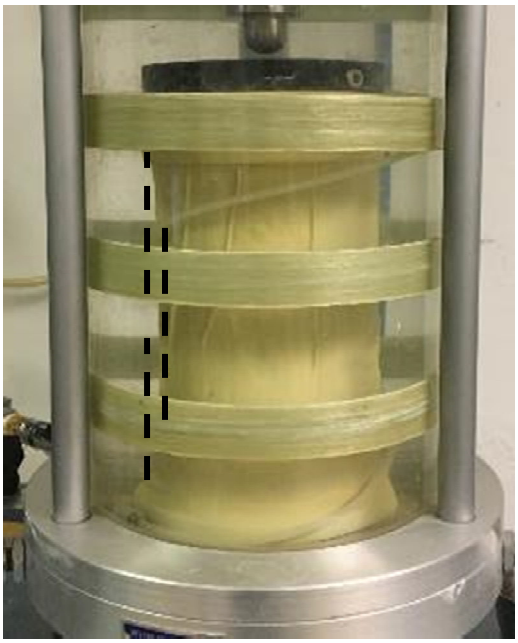

(b)

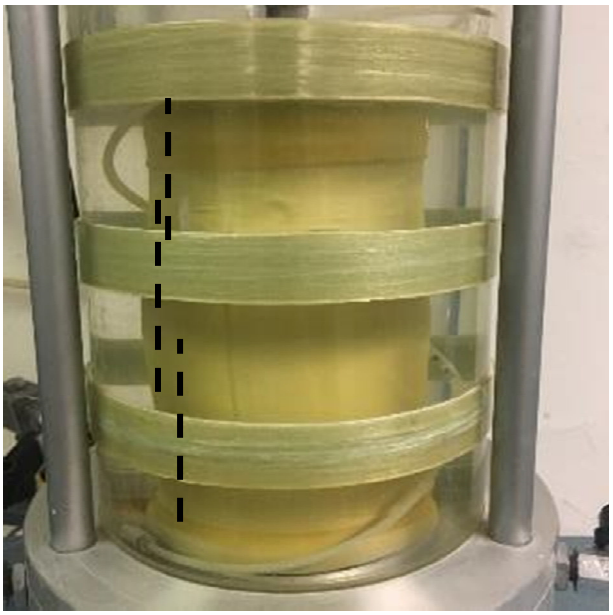

(c)

Figure 5.9 Triaxial test sample: (a) preparation, (b) sample deformation at the end of confinement step, (c) sample deformation at the end of the loading step

5.3.3 Initial conditions

Predefined fields were defined in the proposed FE model, namely: Geostatic stress for clay and stone material, initial pore water pressure, initial void ratio of clay and stone columns materials, and degree of saturation. The initial pore water pressure was defined for the whole model, and it was assumed to be linearly distributed along with the model with a maximum value of 1.962 kN/m^2 at the model base as

shown in Figure 5.10. The total stresses at the base of the model were calculated separately for stone columns and the clay soil according to saturated unit weights calculated in the experimental program (Table 3.2 and Table 4.2). Accordingly, the effective geostatic stresses at the base of the model were calculated and defined for the clay soil and stone columns separately, as shown in Figure 5.11. Also, at rest earth pressure coefficient (K_o) was defined for stone column material according to equation (5-5). The model was assumed to be fully saturated; thus, a degree of saturation of 100% was predefined in the model. Finally, the void ratio of the stone columns material and the clay soil was defined based on the properties presented in Table 3.2 and Table 4.2, as shown in Figure 5.12.

$$k_o = 1 - \sin\left(\phi'\right) \tag{5-5}$$

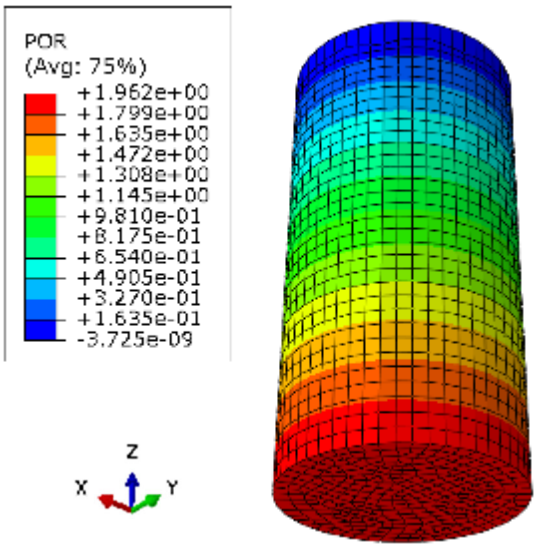

Figure 5.10 Initial pore water pressure (kPa) (CTS 8, T2)

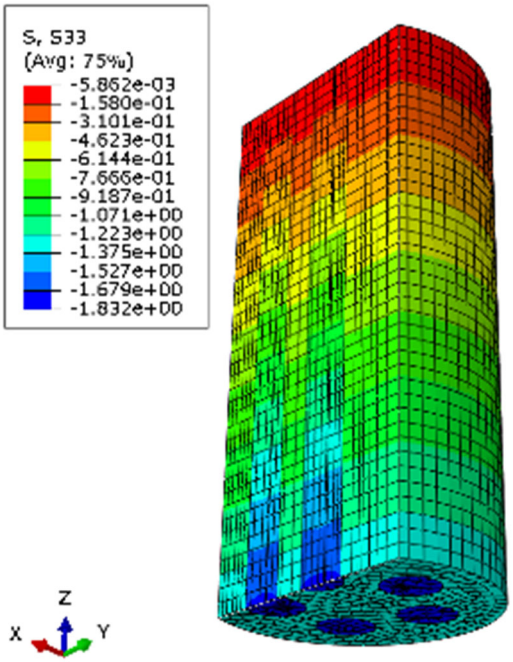

Figure 5.11 Initial effective stress (kPa) (CST13, T5)

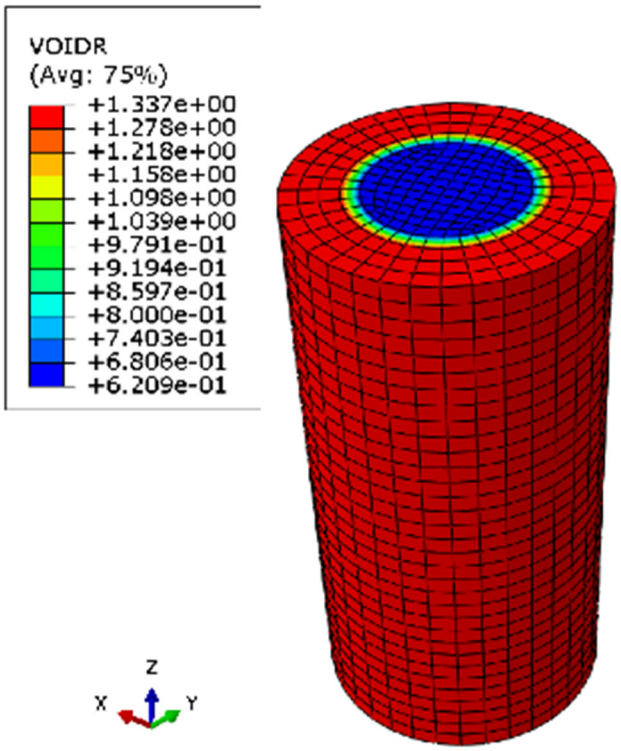

Figure 5.12 Initial void ratio (CTS 5, T3)

5.3.4 Finite element type, meshing, and mesh sensitivity analysis

The 8-nodes brick, trilinear displacement, trilinear pore pressure (C3D8P) element was used in the EFE model approach. This element can capture the change in the effective stresses and pore water pressure

of the reinforced soil. In order to find the optimum mesh size, a mesh sensitivity analysis was conducted that examined the accuracy of the predicted results. In this analysis, the model of (CTS 9, T2) was meshed using a constant element size. The element sizes ranged from 0.05 m to 0.006 m. The results of the mesh analysis are presented in Figure 5.13. Based on the mesh sensitivity analysis results, the mesh size effect is negligible for element size less than 0.008 m. Thus, all the models in the EFE approach were meshed using elements with a maximum element side length of 0.008 m.

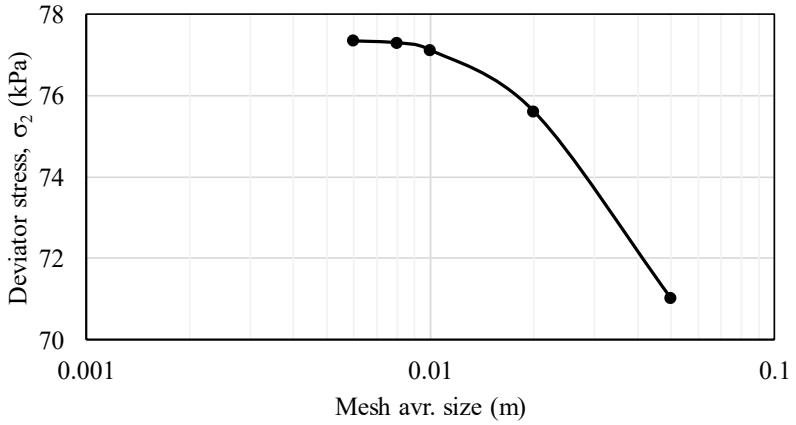

(a) Effect of mesh size on the deviator stress at failure

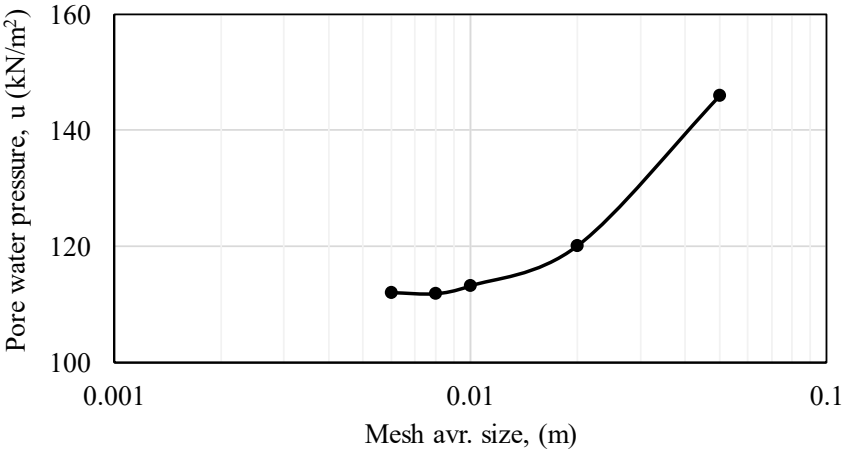

(b) Effect of mesh size on the average PWP at failure

Figure 5.13 Mesh sensitivity analysis results

5.3.5 Model run and outputs

The average number of elements and variables was found to be 20,000 and 85,000, respectively. Numerous variables were calculated from the numerical model but the focus for this study was on the load resistance of the reinforced clay soil. So, the results of the vertical reaction due to applied displacement and the pore water pressure on the top and the bottom of the reinforced clay sample during the loading stage is presented in this chapter.

5.3.6 EFE models results and validation

The main purpose of the EFE modelling approach is to validate the experimental data obtained from the triaxial testing on clay sample reinforced by single and group of stone columns discussed in Chapter 4. In order to validate the EFE modelling approach, the model of failure obtained from the numerical analysis was compared with the failure mechanism observed in the experimental program. Figure 5.14 shows a comparison between the failure mechanisms realized in the testing program and the numerical models. It should be emphasized that although the finite element model could predict bulging and bending failure mechanisms that occur in the reinforced clay soil, the shear failure was not clearly highlighted in the numerical models.

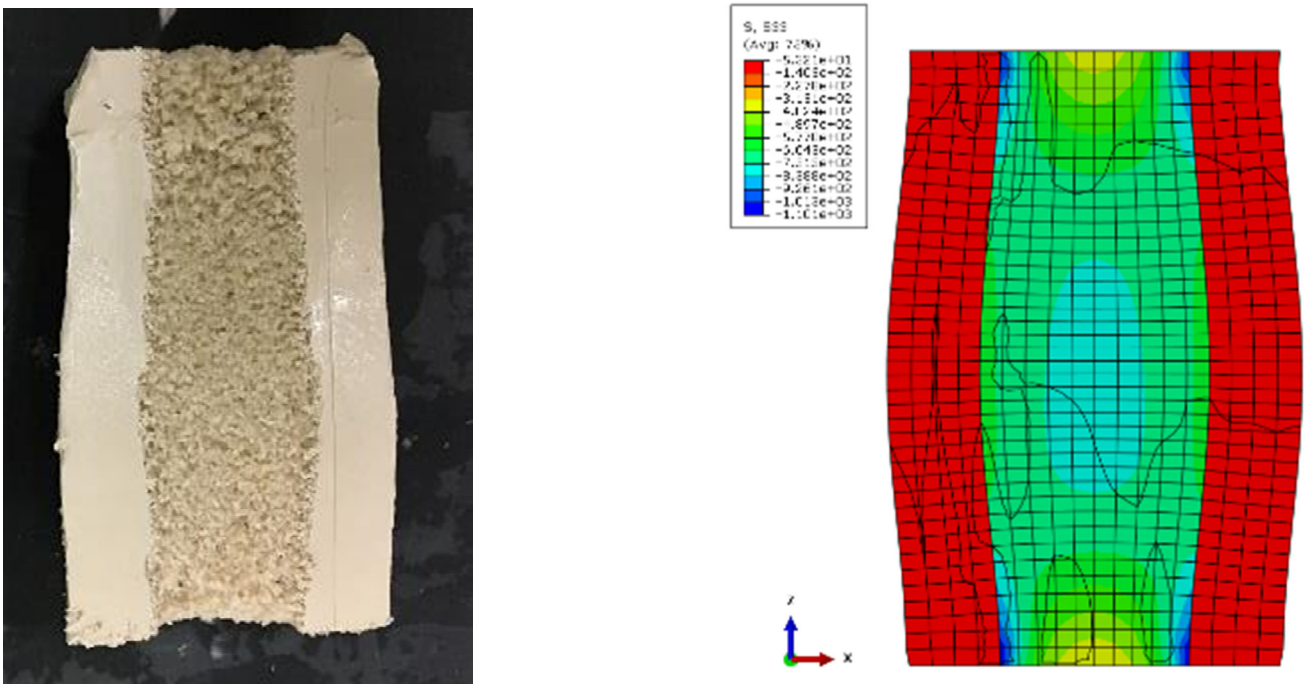

(a) Bulging failure (CTS 4, T4)

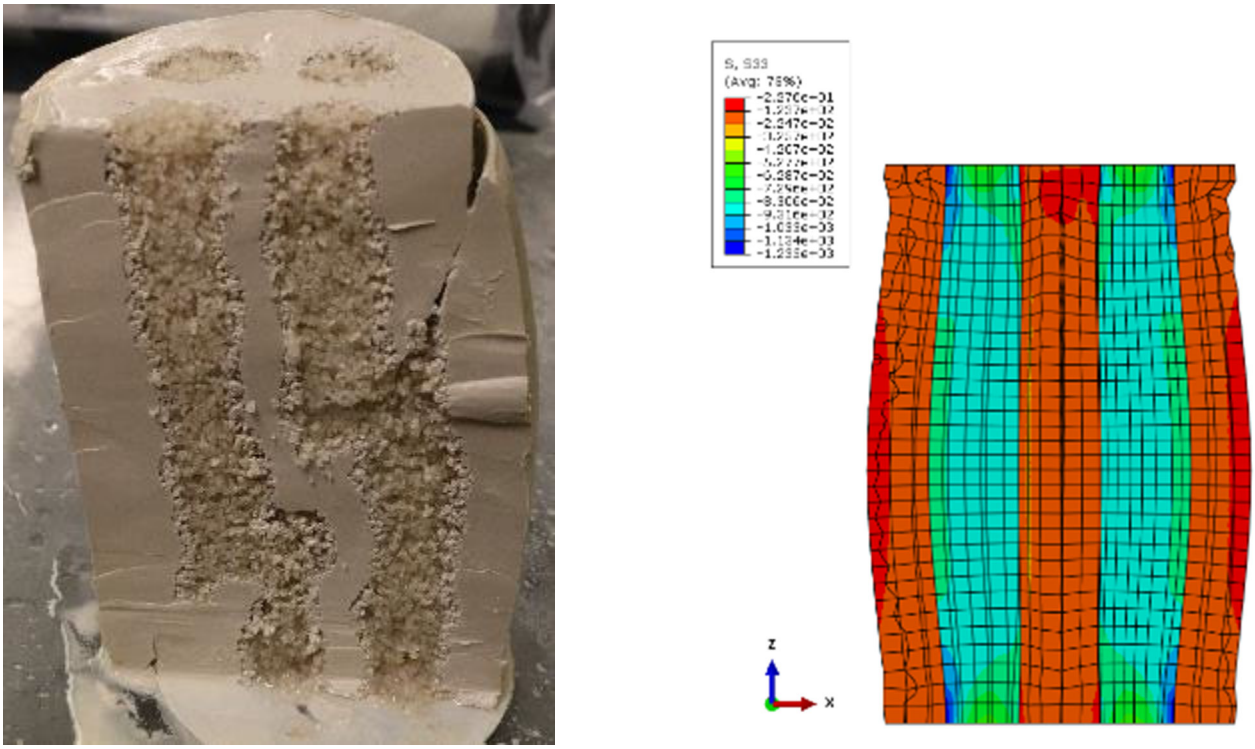

(b) Shear failure (CTS 12, T5)

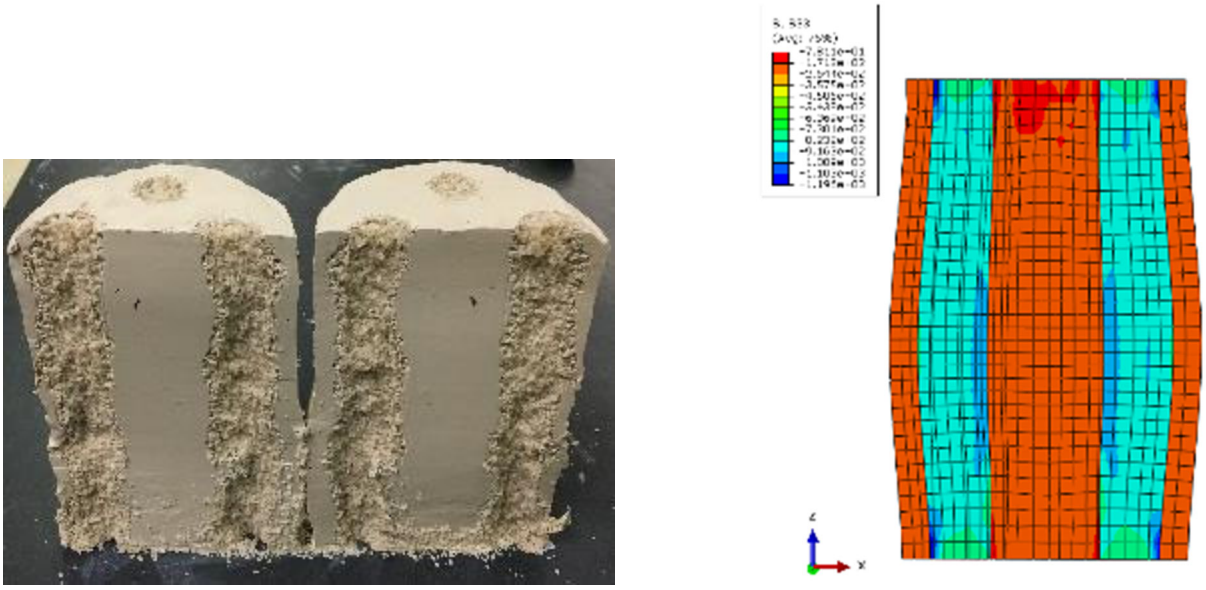

(c) Bending failure (CTS 7, T2)

Figure 5.14 Comparison between failure mechanisms and deformations observed in triaxial test and predicted from the numerical analysis

Furthermore, the relation between the deviator stress and the stain of the reinforced samples is validated against the triaxial test results discussed in Chapter 4. The deviator stress was calculated as the ratio

between the vertical reaction force at the reference point divided by the average area of the sample during the loading stage. The average area was calculated as described in section 4.3.2. Figure 5.14, Figure 5.15, Figure 5.16, Figure 5.17, and Figure 5.18 show a comparison between the numerical and experimental results for test T2, T3, T4, and T5, respectively. From all these figures even though the installation effect was not considered, the proposed finite element approach is able to predict the vertical loading capacity of a clay soil reinforced by single and group of stone columns. Since all the clay properties were determined from laboratory tests, the model can accurately predict the behaviour of an unreinforced clay sample. For reinforced samples, the numerical model underestimated the capacity of the reinforced soil. The difference between the experimental test results and the estimated values from the numerical analysis was found to be less than 15%.

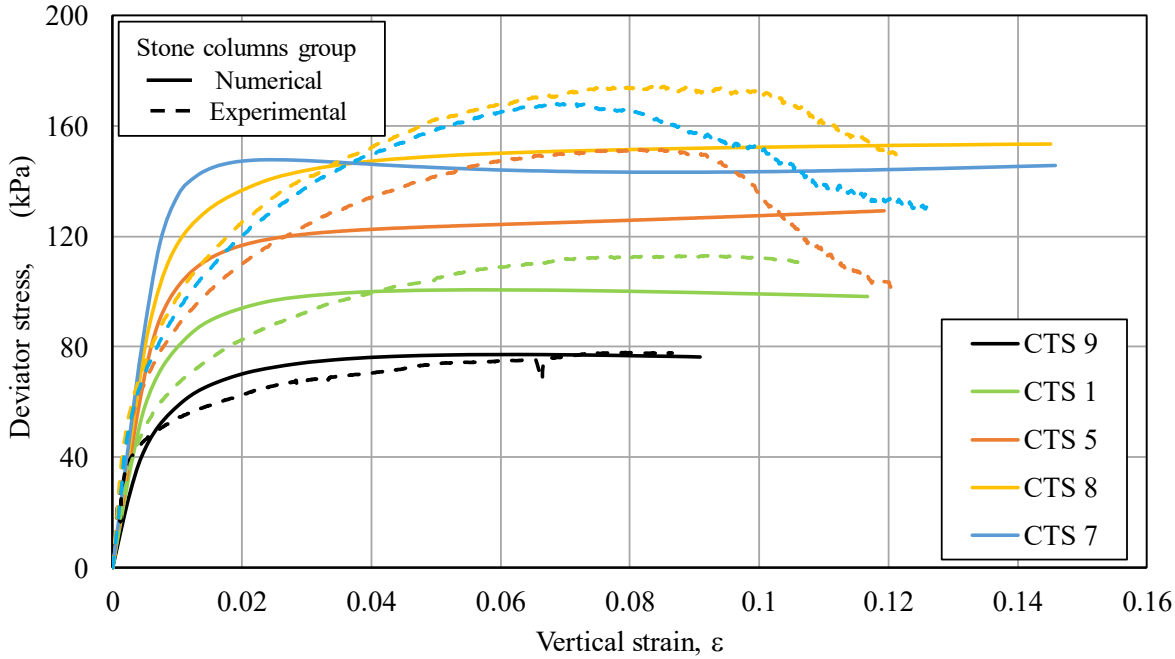

(a)

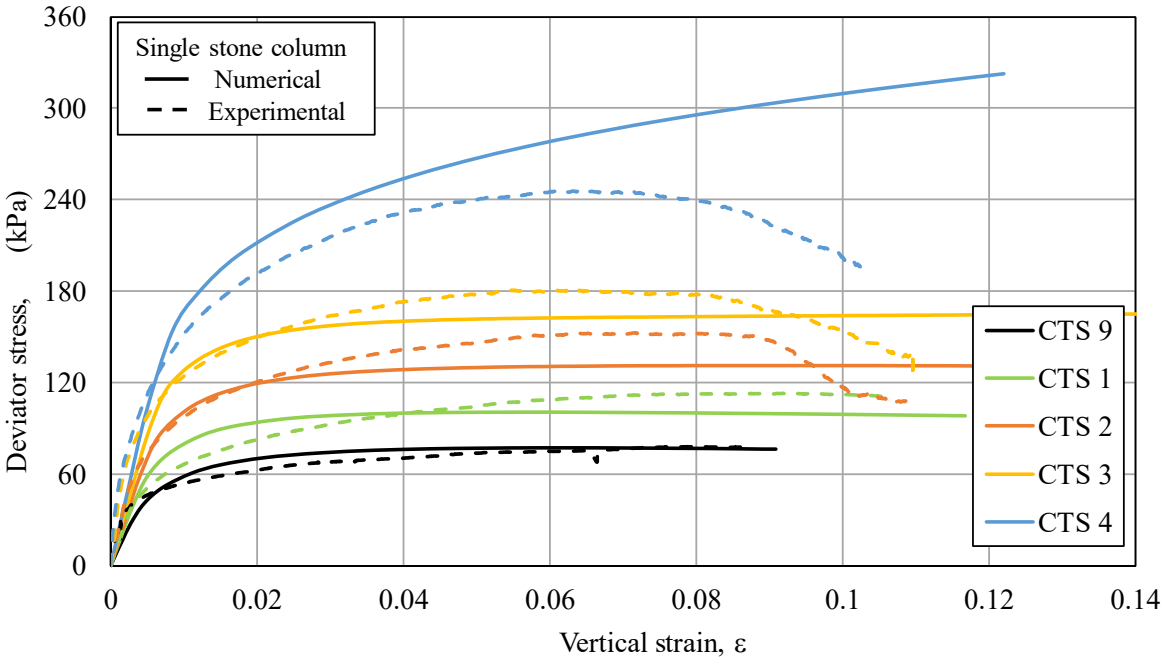

(b)

Figure 5.15 Comparison between experimental and finite element results for samples in T2: (a) group of stone columns, (b) single stone column

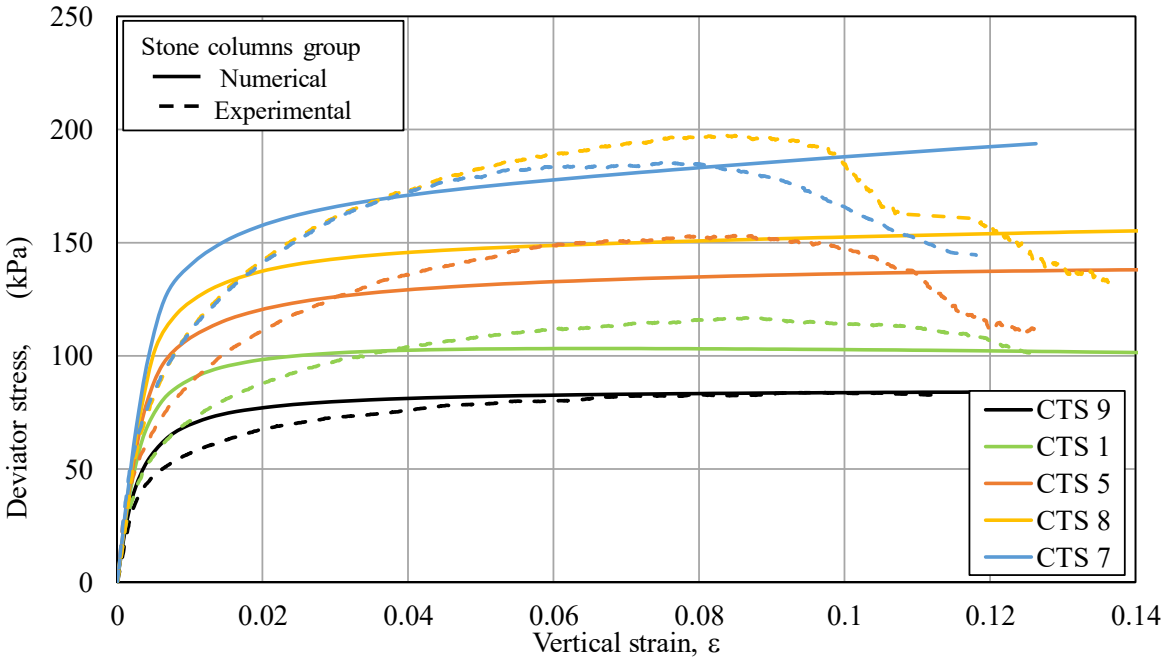

(a)

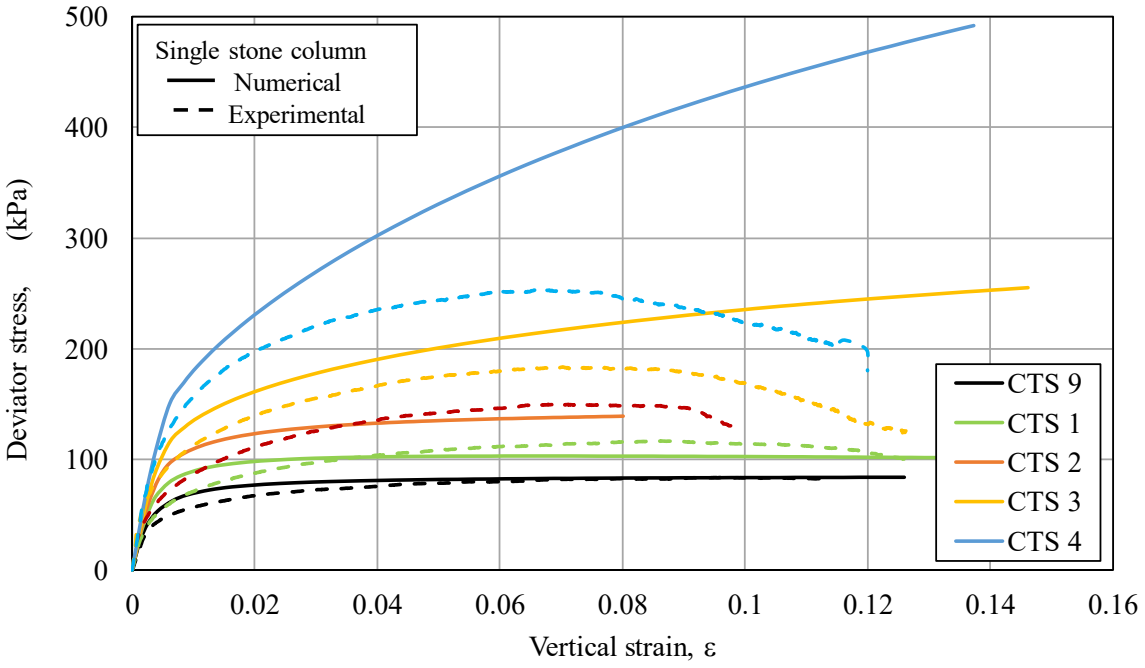

(b)

Figure 5.16 Comparison between experimental and finite element results for samples in T3: (a) group of stone columns, (b) single stone column

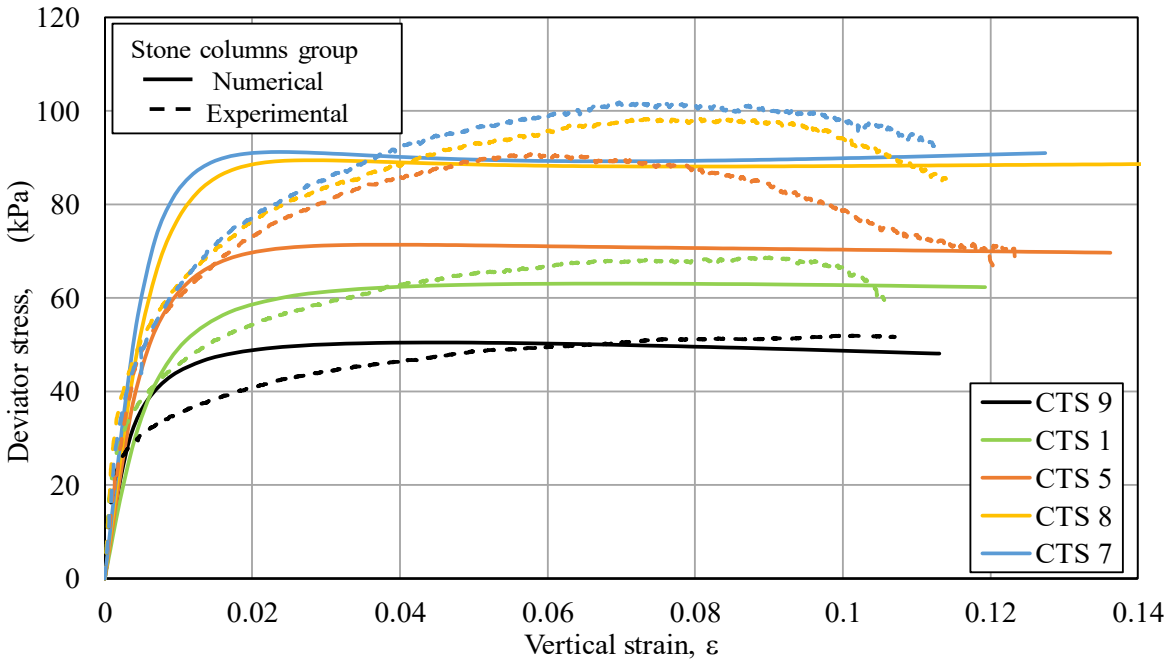

(a)

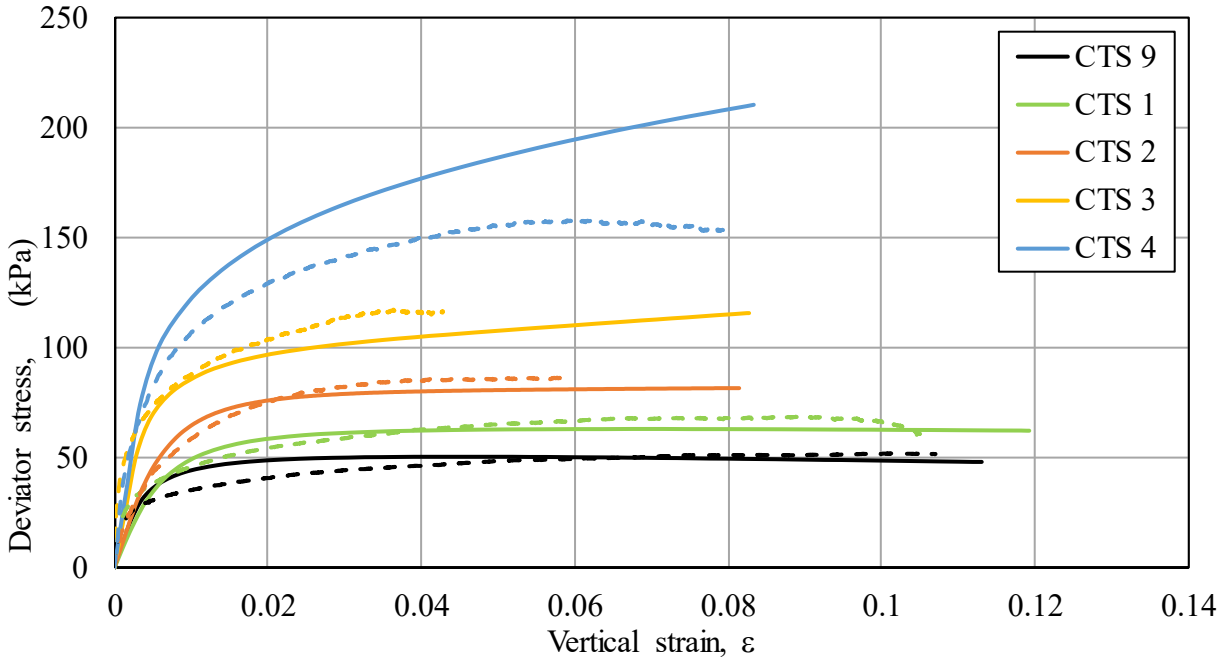

(b)

Figure 5.17 Comparison between experimental and finite element results for samples in T4: (a) group of stone columns, (b) single stone column

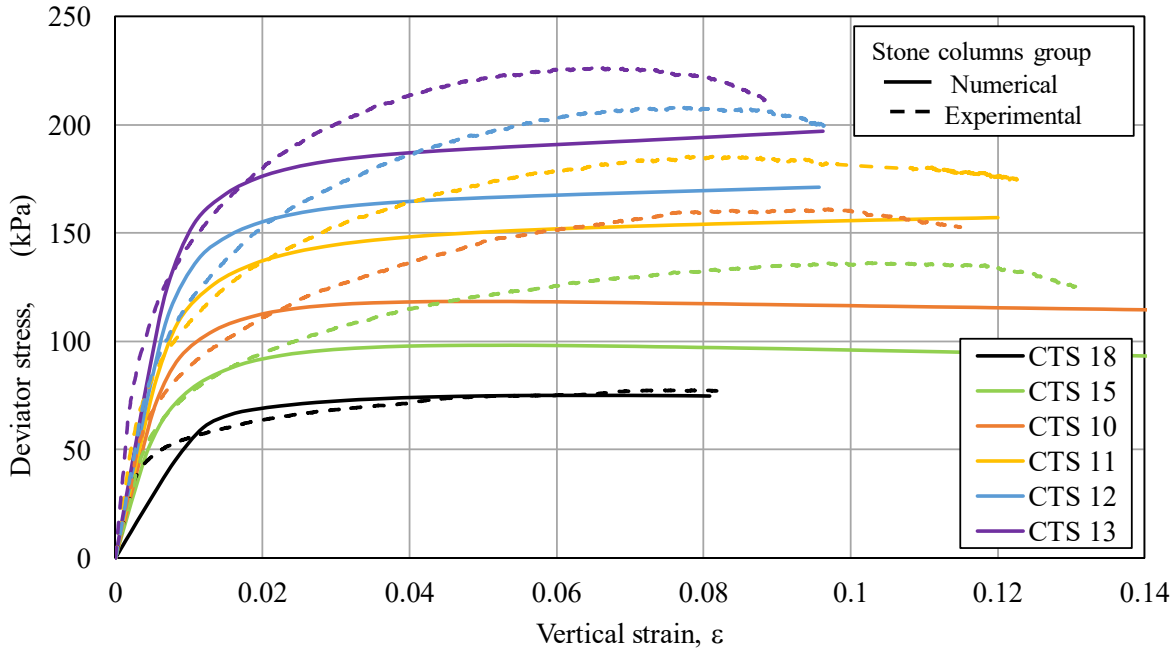

(a)

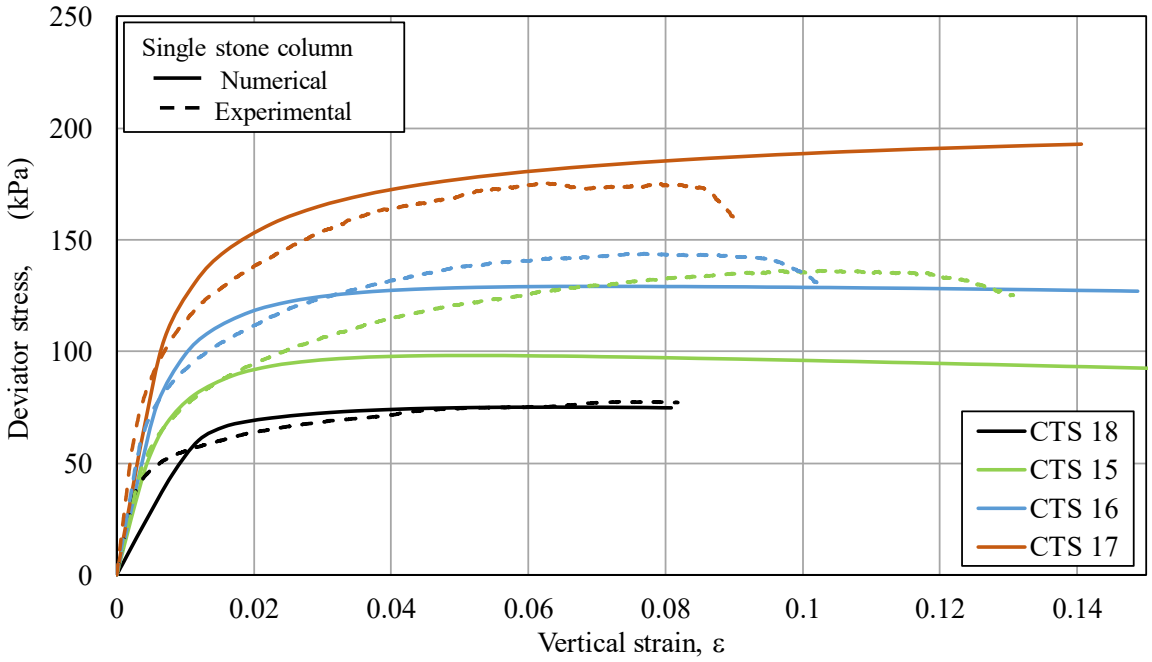

(b)

Figure 5.18 Comparison between experimental and finite element results for samples in T5: (a) group of stone columns, (b) single stone column

For the purpose of the enhancement that occurred in resistance of the reinforced clay soil to the vertical stresses, the maximum deviator stress at failure for all finite element models was obtained and compared with the experimental results. The deviator stress at failure was defined as the maximum value during the loading stage. This definition was considered when the deviator stress remained constant with increasing vertical strain (i.e., CTS 1 & 5 in test T2 and CTS 2 in test T3). For samples with high replacement ratio (i.e., CTS 4 in test T2 & T3 and CTS 13 in test T5), the deviator stress was observed to be linearly increasing. So, the tangential method was used in order to obtain the deviator stress at failure for these samples (Figure 5.19). Table 5.2 presents a summary of deviator stresses at failure obtained from the numerical models and compared with the experimental results. As discussed in section 4.3.3, the IMF factor was calculated based on the data obtained from the finite element models. Figure 5.20 shows a comparison between IMF obtained from the experimental program and the finite element analysis. The proposed finite element approach shows a better agreement with the experimental results for samples reinforced by a single stone column than those reinforced by a group. This observed difference in the total capacity is attributed to the installation of the stone columns. As discussed in section 2.4, it was found that the installation enhanced the cohesion and horizontal coefficient of the adjacent clay soil, thereby increasing its resistance to vertical stresses. In addition, the effect of installation extends to a distance ranging from 1.25 to 2.5 times the columns diameter (Watts et al., 2000;

Weber et al., 2010). This installation effect justified the underestimation of that capacity, particularly for soil reinforced by a group of stone columns. As described in section 3.4.2, the stone columns were installed in a large tank. Therefore, the influence of a single column installation was insignificant since the clay around the columns was free to deform. However, in the case of installing a group of stone columns with a spacing ratio ranging between 2 to 1.5, the clay between the columns is confined thereby increasing its resistance to vertical stresses. Therefore, the influence of stone columns installation enhanced the resistance of the clay sample reinforced by a group of stone columns more than a single stone column.

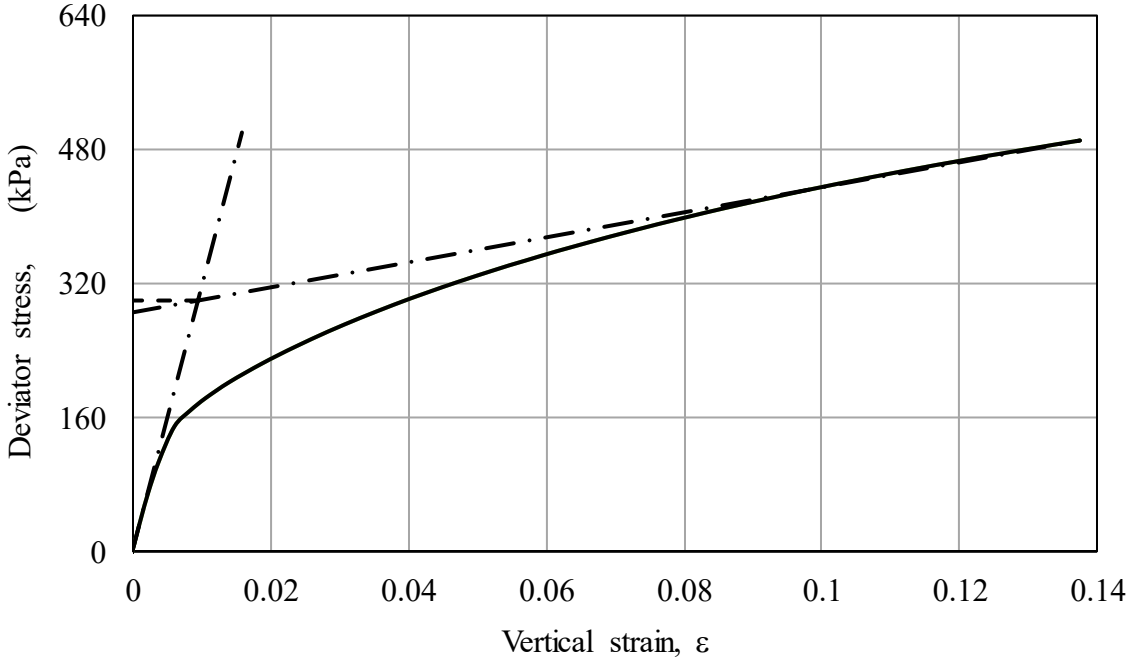

Figure 5.19 Tangential method used to calculate the deviator stress at failure for CTS 4 in test T3

Table 5.2 Summary of the numerical approach validation

Test No.	Compaction energy (kN.m/m^3)	Confinement pressure, σ_3 (kN/m^2)	Sample no.	No. of Stone Columns	Stone Columns Diameter, D (cm)	Stone Columns Spacing ratio, *S/D*	Replacement ratio, *As* (%)	Deviator stress at failure, (kN/m^2)		Error
								FE analysis	Experimental	
T2	310	160	CTS 1	1	2.1	-	4.4	100.56	113.03	-11.03%
			CTS 2	1	3.0	-	9.0	131.16	152.60	-14.05%
			CTS 3	1	3.9	-	15.2	165.10	180.78	-8.68%
			CTS 4	1	5.1	-	26.0	255.19	245.70	3.86%
			CTS 5	2	2.1	2	8.8	129.20	151.48	-14.71%
			CTS 6	2	2.1	2.75	8.8	119.29	145.98	-18.28%
			CTS 7	4	2.1	2	17.6	147.68	168.10	-12.15%
			CTS 8	3	2.1	2	13.2	153.38	174.73	-12.22%
			CTS 9	-	-	-	0.0	77.17	77.96	-1.01%
T3	620	160	CTS 1	1	2.1	-	4.4	103.17	116.79	-11.66%
			CTS 2	1	3.0	-	9.0	139.14	124.88	11.42%
			CTS 3	1	3.9	-	15.2	193.73	183.61	5.51%
			CTS 4	1	5.1	-	26.0	299.44	253.37	18.18%
			CTS 5	2	2.1	2	8.8	138.15	153.13	-9.78%
			CTS 6	2	2.1	2.75	8.8	135.63	141.50	-4.15%
			CTS 7	4	2.1	2	17.6	166.64	185.30	-10.07%
			CTS 8	3	2.1	2	13.2	155.53	197.37	-21.20%
			CTS 9	-	-	-	0.0	86.16	83.71	2.92%
T4	310	80	CTS 1	1	2.1	-	4.4	63.07	67.12	-6.04%
			CTS 2	1	3.0	-	9.0	81.67	86.35	-5.42%
			CTS 3	1	3.9	-	15.2	101.00	118.00	-14.41%
			CTS 4	1	5.1	-	26.0	154.67	158.06	-2.15%
			CTS 5	2	2.1	2	8.8	71.39	90.75	-21.33%
			CTS 6	2	2.1	2.75	8.8	70.79	79.04	-10.44%
			CTS 7	4	2.1	2	17.6	91.21	101.04	-9.72%
			CTS 8	3	2.1	2	13.2	89.45	96.88	-7.67%
			CTS 9	-	-	-	0.0	50.48	51.98	-2.87%
T5	310	160	CTS 10	2	2.1	1.5	8.8	125.97	161.03	-21.77%
			CTS 11	3	2.1	1.5	13.2	157.14	185.81	-15.43%
			CTS 12	4	2.1	1.5	17.6	171.20	207.99	-17.69%
			CTS 13	5	2.1	1.5	22.1	197.03	226.16	-12.88%
			CTS 14	3	3.0	1.5	27.0	215.44	277.44	-22.35%
			CTS 15	1	2.1	-	4.4	98.24	136.23	-27.89%
			CTS 16	1	3.0	-	9.0	129.19	143.90	-10.23%
			CTS 17	1	3.9	-	15.2	192.82	175.39	9.94%
			CTS 18	-	-	-	0.0	75.12	77.56	-3.15%

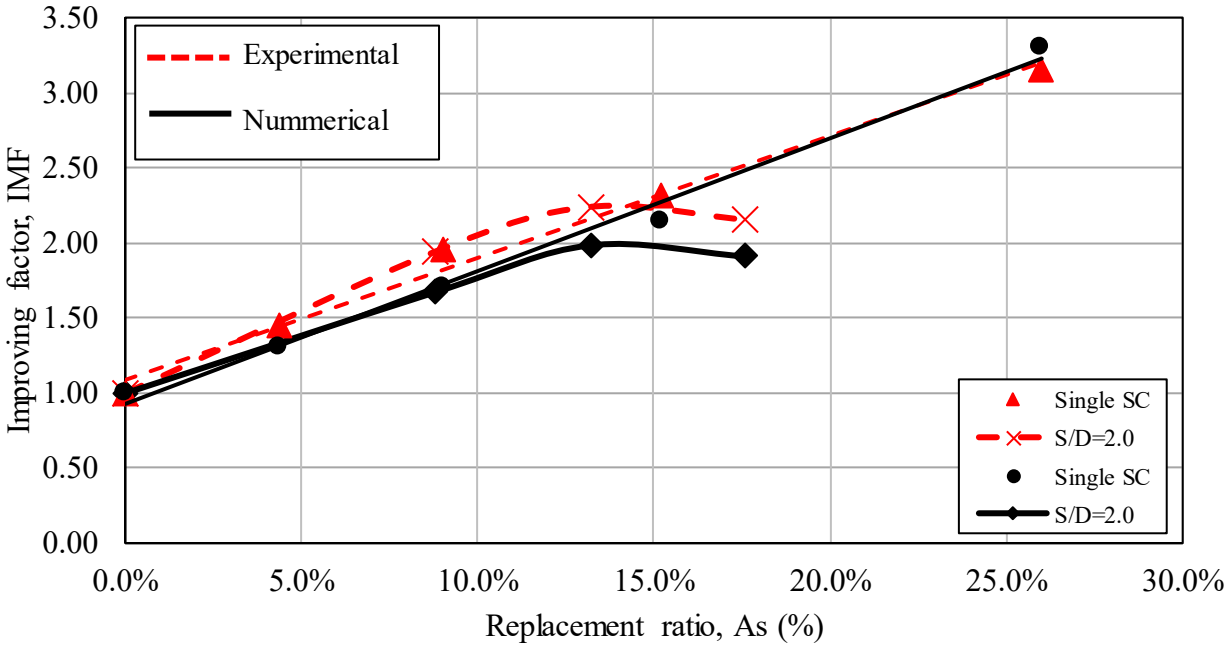
Experimental
Nummerical
Single SC
S/D=2.0
Single SC
S/D=2.0
Improving factor, IMF
Replacement ratio, As (%)
0.00
0.50
1.00
1.50
2.00
2.50
3.00
3.50
0.0%
5.0%
10.0%
15.0%
20.0%
25.0%
30.0%

(a)

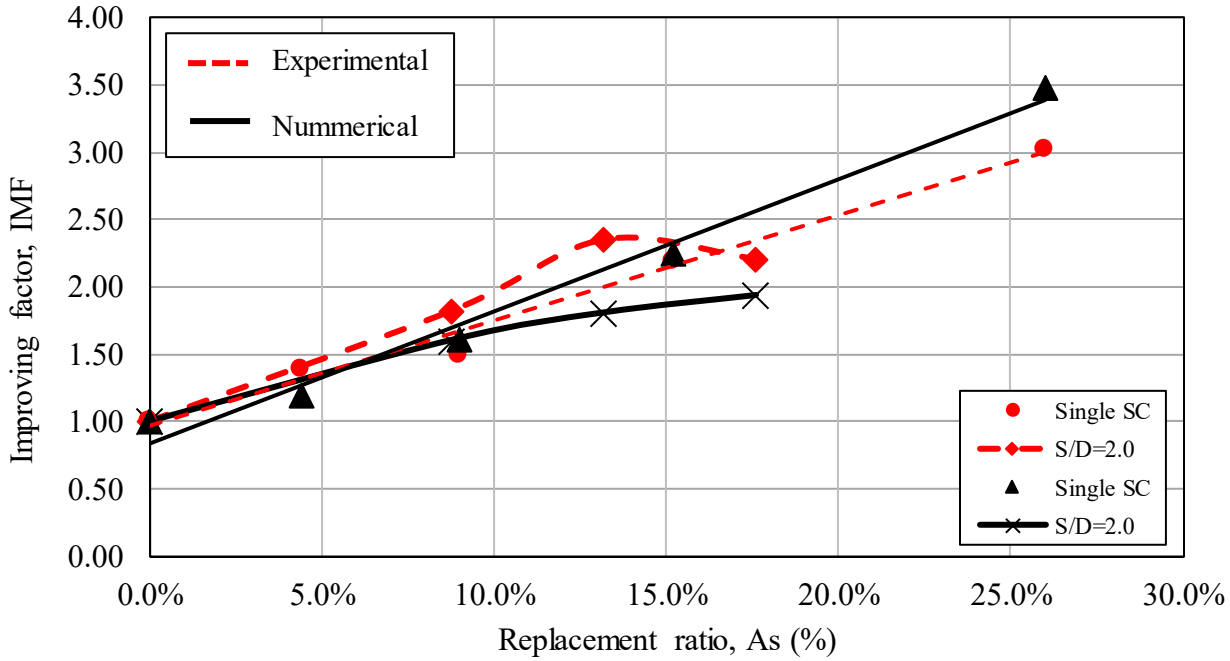
Experimental
Nummerical
Single SC
S/D=2.0
Single SC
S/D=2.0
Improving factor, IMF
Replacement ratio, As (%)
0.00
0.50
1.00
1.50
2.00
2.50
3.00
3.50
4.00
0.0%
5.0%
10.0%
15.0%
20.0%
25.0%
30.0%

(b)

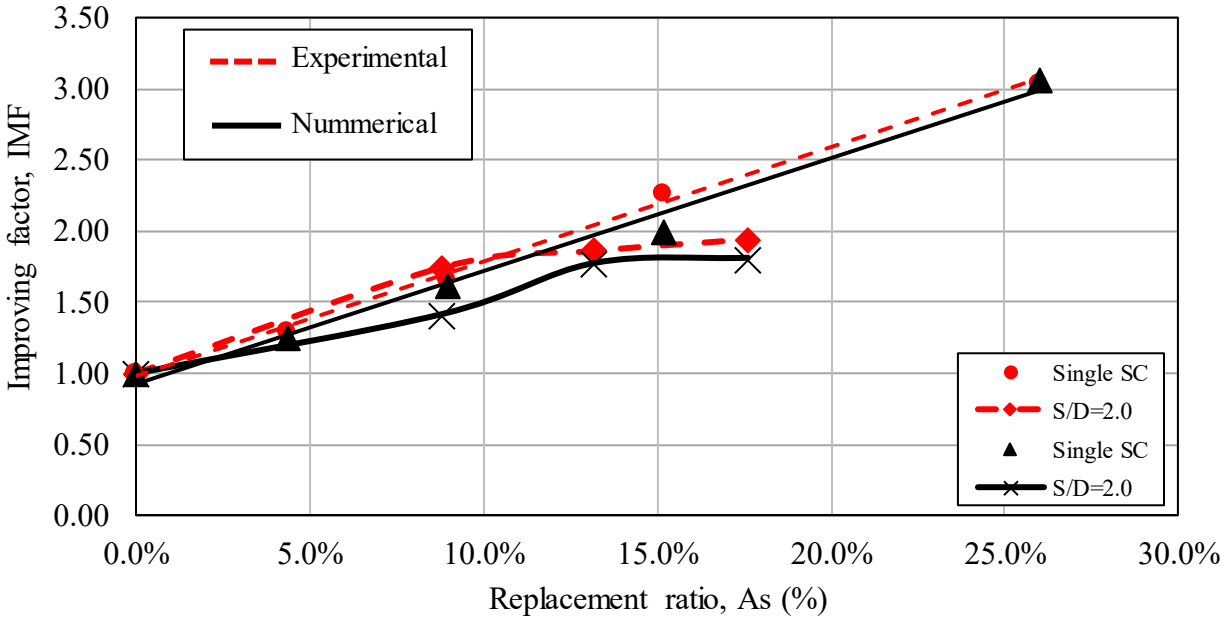

(c)

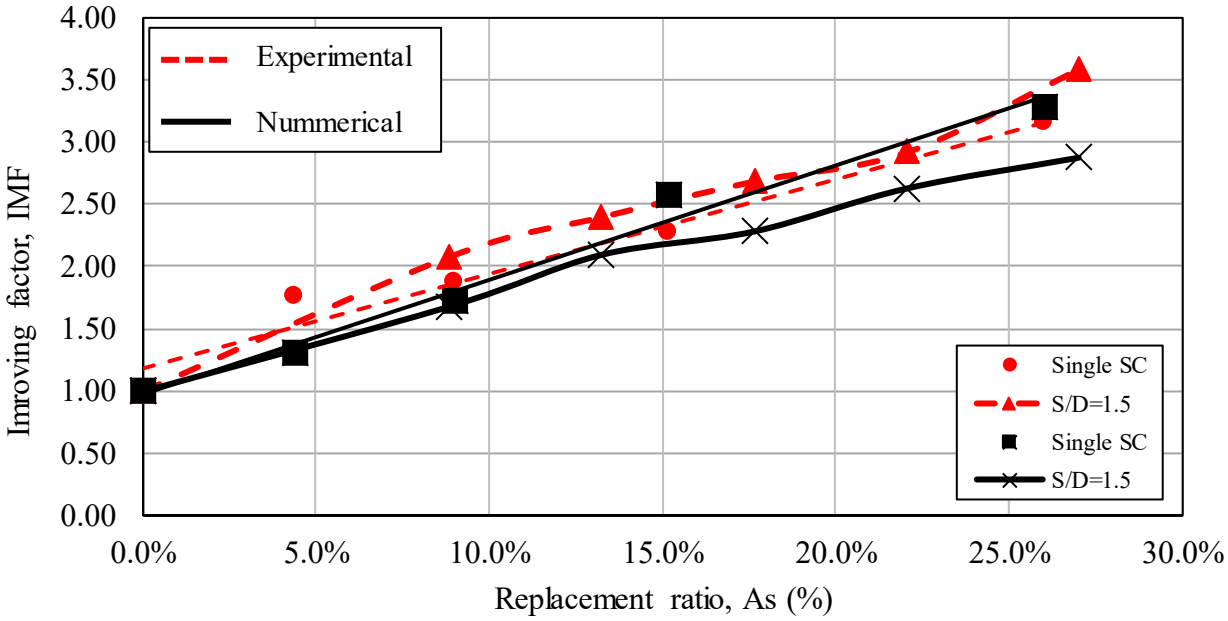

(d)

Figure 5.20 Comparison between the improvement factors obtained from the experimental study and the numerical study: (a) T2, (b) T3, (c) T4 and (d) T5

5.3.7 Validation of the FE model approach with the data available in the literature

Black et al. (2007) conducted triaxial test on clay samples reinforced by single and group of stone columns. In this study, in order to minimize the effect of the installation, the stone columns were installed

by driving a thin steel wall cylinder in the triaxial sample (D = 10cm, L = 20cm). The clay inside the steel cylinder was then removed by a small auger and the prepared hole filled with material for the stone columns. Two methods were used: wet compacted sand columns, and frozen sand columns. The results of these experimental tests ware used to validate the proposed FE model. Figure 5.21 shows a comparison of the predicted deviator stress and pore water pressure for the reinforced sample and the measured values. The predicted behaviour showed an excellent agreement with the experimental results when a frozen stone column was used. However, the predicted values slightly underestimated the capacity of stone columns installed by the wet compaction method. In the wet compaction method, a wet sand soil was compacted inside the clay sample, which applied redial pressure to the adjacent clay thereby enhancing the clay properties around the stone column. On the other hand, the frozen sand column was created and compared outside the clay sample, and it was only inserted in the hole. This method minimized the installation effect, but it does not represent the actual field conditions.

Figure 5.20 and 5.21 demonstrate that the proposed FE approach described above is general and capable of capturing the behaviour of the clay soil reinforced by single and group of stone columns. Therefore, the modelling approach is further used in the next sections to extend the study to predict the bearing capacity of a clay soil reinforced by stone columns under a rigid footing.

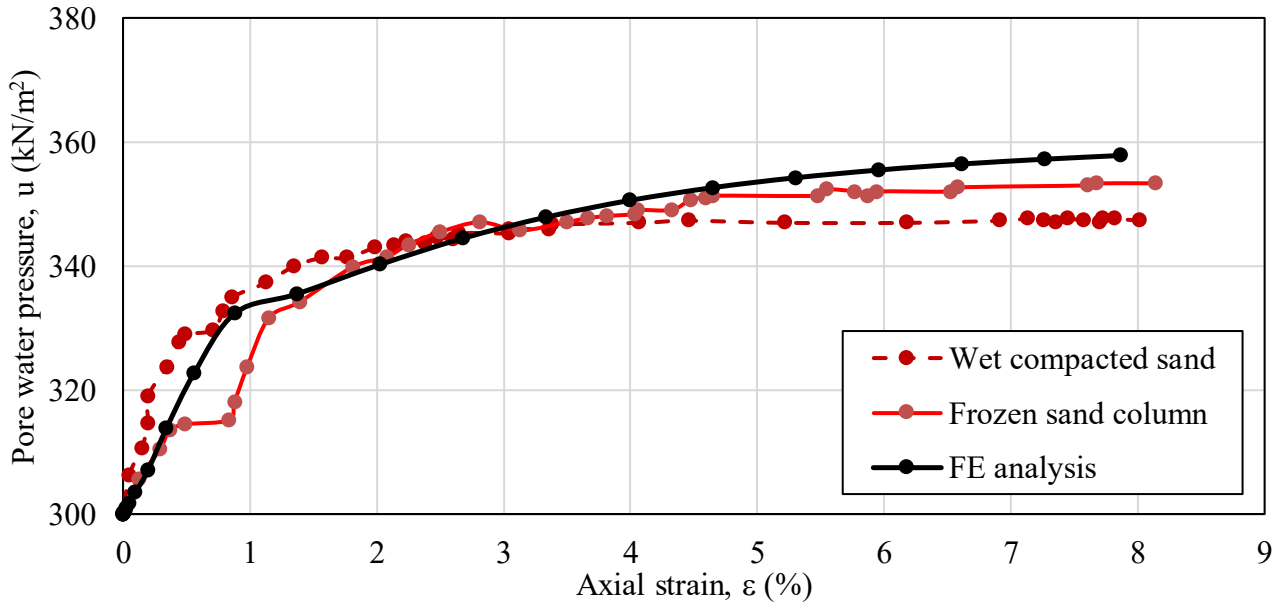

(a)

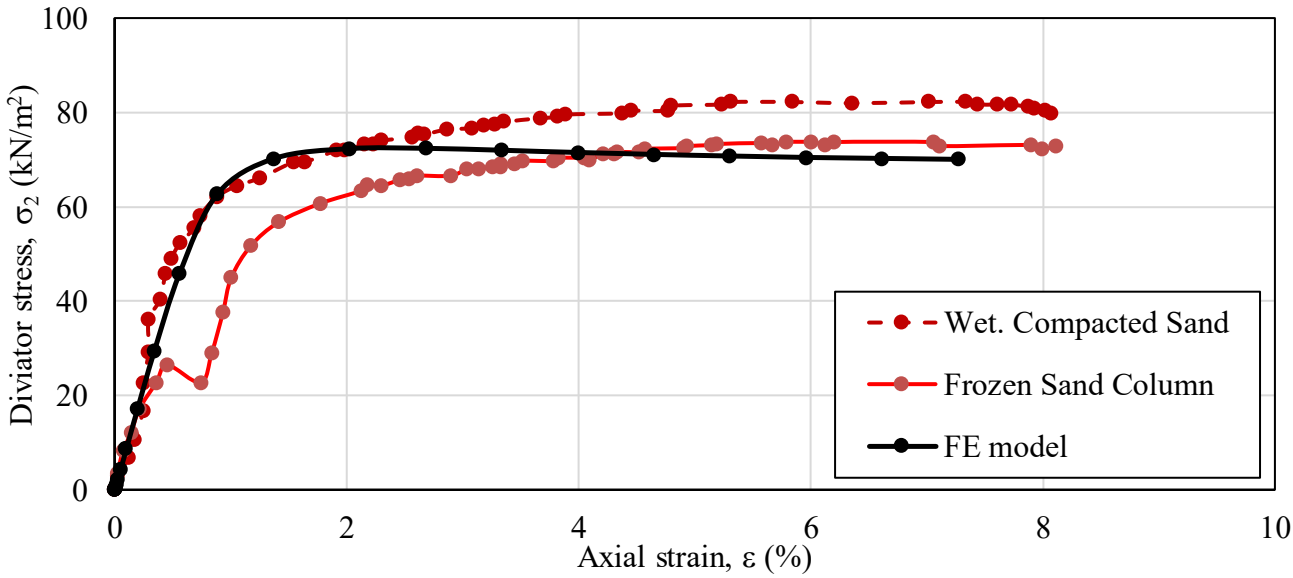

(b)

Figure 5.21 Comparison between measured results from triaxial testing (Black et al., 2007) and FE model prereductions

5.4 FE Model approach for column installation (IFE)

In the literature, numerical models are available to simulate the installation of stone columns. This was achieved by imposing a uniform lateral displacement using a 2-D FE model (Kirsch, 2006; Guetif et al., 2007; Castro et al., 2010). Nevertheless, 3-D finite element modelling is recommended by Elshazly et al. (2008), Indraratna et al. (2012), and Al Ammari et al. (2018).

In order to understand the installation effect, a 3-D finite element model was utilized to simulate the installation process that was used in the experimental program. The model consists of a section of clay soil 20cm x 20cm x 40cm and a steel prop with a conic shape at the bottom with an angle of 60^0 and a length of 30 cm. The steel prop was driven in the soil to create a hole, which was filled by stone column material as described in section 3.4.2. In order to penetrate a continuous material like soil, a unique technique called “Zipper-type” was used (Mabsout et al., 1994; Henke et al., 2006; Qiu et al., 2011). A rigid tube of 2 mm diameter was modelled below the steel prop. During the penetration stage, the tube was free to establish a contact pressure between the prop and the soil, as illustrated in Figure 5.22.

The analysis was divided into two stages. In the first stage, the gravity load and predefined geostatic stress were applied (geostatic step). A vertical displacement equal to the stone columns length was implemented on top of the steel prop in the second stage (moving step). This model will be used to

determine the radius of influence due to the installation process in the clay soil as well as estimating the change in the lateral pressure coefficient (K_o).

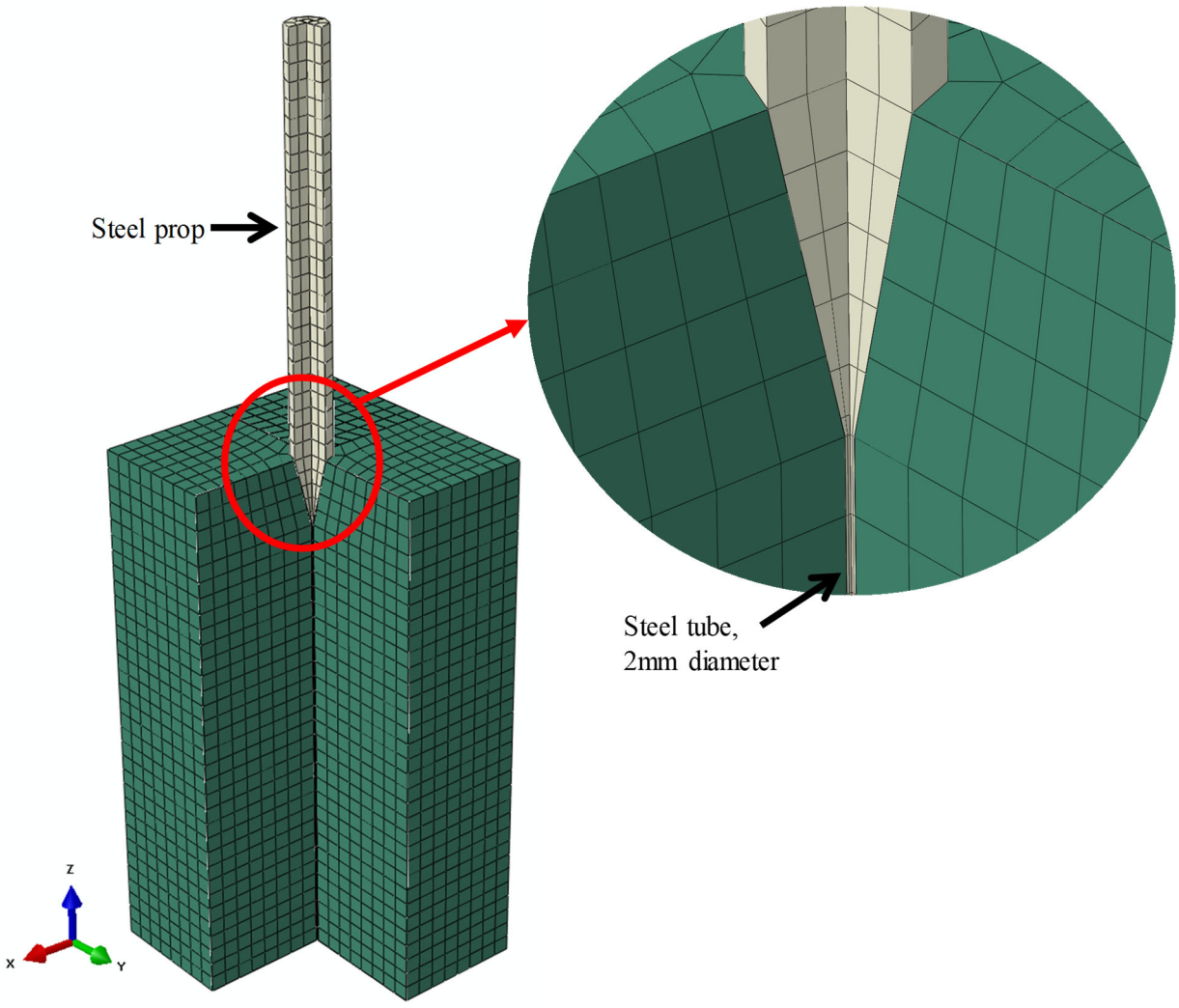

Figure 5.22 Installation FE model details

5.4.1 Material properties

The modified Drucker-Prager/cap plasticity with hardening soil model was used for the clay soil, as described in section 5.2.1, the properties of the soil used in this model are shown in Table 5.3 The steel prop was simulated using an elastic material model. The modulus of elasticity and the Poisson's ratio was 2.1E8 kPa and 0.3, respectively.

Table 5.3 Soil properties in IFE model

Parameter	Value
Saturated unit weight, $\gamma_{c\,sat}$ (kN/m^3)	16.43
Dry unit weight, $\gamma_{c\,dry}$ (kN/m^3)	10.78
Initial void ratio, *eo*	1.36
Permeability, K (m/sec)	2.45E-10
Preconsolidation pressure, σ_c' (kPa)	56.81
Consolidation index, C_c	0.331
Swelling index, C_s	0.0599
Coefficient of consolidation, C_v (mm^2/hr)	169.99
Cap eccentricity, R	1.3
Transition surface factor, α	0.05
Flow stress ratio	1
Poisson's ratio, ν	0.4
drained riction angle, ϕ_c'	18.3
drained cohesion, c_c' (kN/m^2)	15.8

5.4.2 Boundary conditions

The boundary conditions were defined as fixed at the bottom (i.e. *Ux*=*Uy*=*Uz*=0), and the displacement was constrained in the perpendicular direction on each side of the model. During the geostatic step the steel prop was removed, and the horizontal displacement was constrained on the surfaces in contact with the steel prop and tube, as shown in Figure 5-23 (a). The prop was reactivated at the beginning of the moving step, and a displacement of 30 cm was applied on the prop to drive it into the soil mass, as shown in Figure 5.23 (b). In order to simulate the drained condition, the pore water pressure was set to zero on top of the soil mass and the surface between the clay soil and the steel prop.

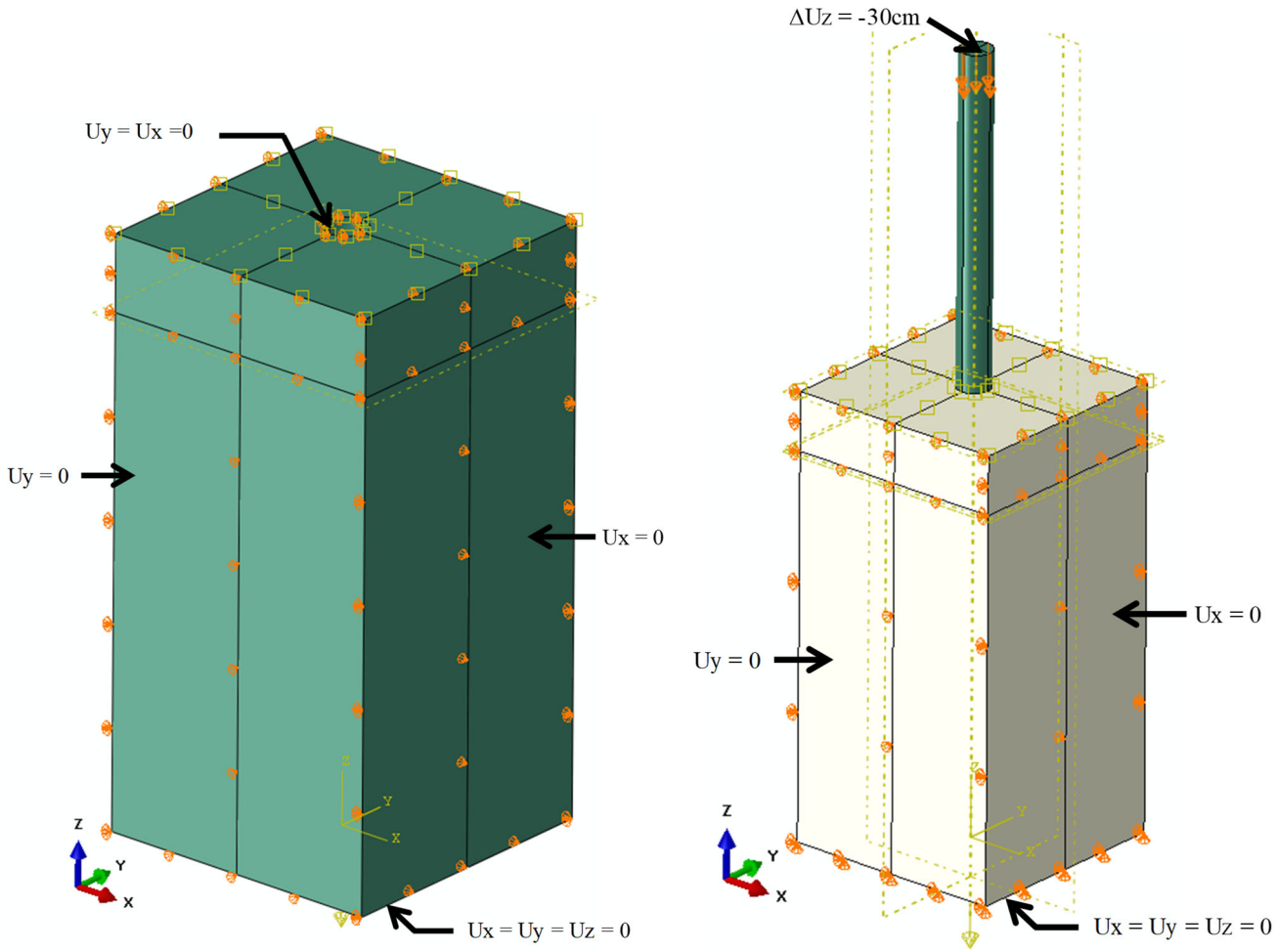

(a) (b)

Figure 5.23 Boundary conditions in IFE model: (a) Geostatic step, (b) Moving step

5.4.3 Interaction definition

Due to the large deformations caused by the penetration of the prop, a kinematic interaction formulation was utilized between the vibrator and the adjacent soil. These formulations are based on the concept of master-slave contact, which is implemented in ABAQUS. Two parameters define the interaction between the steel prop and the adjacent soil. In a direction perpendicular to the surface, hard contact was considered. In the tangential direction, two interaction properties were defined. A friction coefficient of 0.2 was used between the steel prop and the clay soil; however, a frictionless condition was defined between the soil and the thin steel tube under the prop.

5.4.4 Meshing and element type

Since the model dimensions are close to the EFE model and the same material constitutive model was used, the same element type (i.e., 8-node brick, trilinear displacement, trilinear pore pressure C3D8P) was used for the soil. Since the steel prop was not defined as a porous material, a non-pore pressure 8-node brick element was used (i.e., C3D8). The mesh element largest dimension was set to 0.01 m, which was defined based on the mesh sensitivity analysis described in section 5.3.4.

5.4.5 IFE modelling approach results

In order to investigate the effect of stone column installation on samples tested in the experimental program, three stone columns diameters were investigated, i.e. 5cm, 3cm and 2cm. All the results are presented as a function of normalized distance ratio, which is the distance to the centerline of the installed columns (r) divided by the stone column diameter (*D*) at different depths (H) as shown in Figure 5.24. Figure 5.25 presents the effect of stone column installation on increasing the horizontal stress around the column. The horizontal stress increase is presented as the stress increase ratio, which is the ratio between the horizontal stress before $(\sigma_h)_{int.}$ and after $(\sigma_h)_{fin}$ stone column installation. Figure 5.26 (a) shows that the stress increase reduces with depth and that the maximum stress ratio is 18 for H = 0, although it dropped to 9.7 for H = 30cm. The horizontal stress ratio increased with decreasing the diameter of stone columns (i.e. 18 for *D* = 5cm, 27 for *D* = 3cm, 30 for *D* = 2cm). Based on the Horizontal stress increase, the installation effect changed from 1.9*D* to 1.4*D* for stone columns diameters 2 cm and 5 cm, respectively.

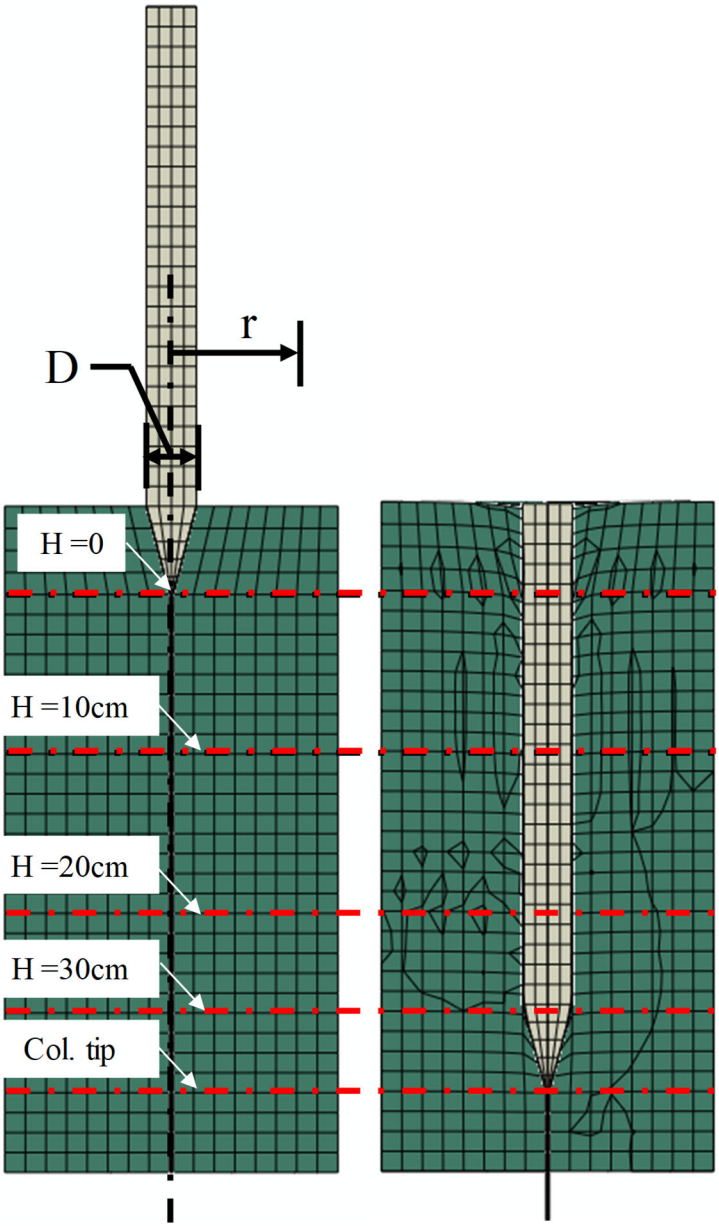

Figure 5.24 Results parameters for IFE models

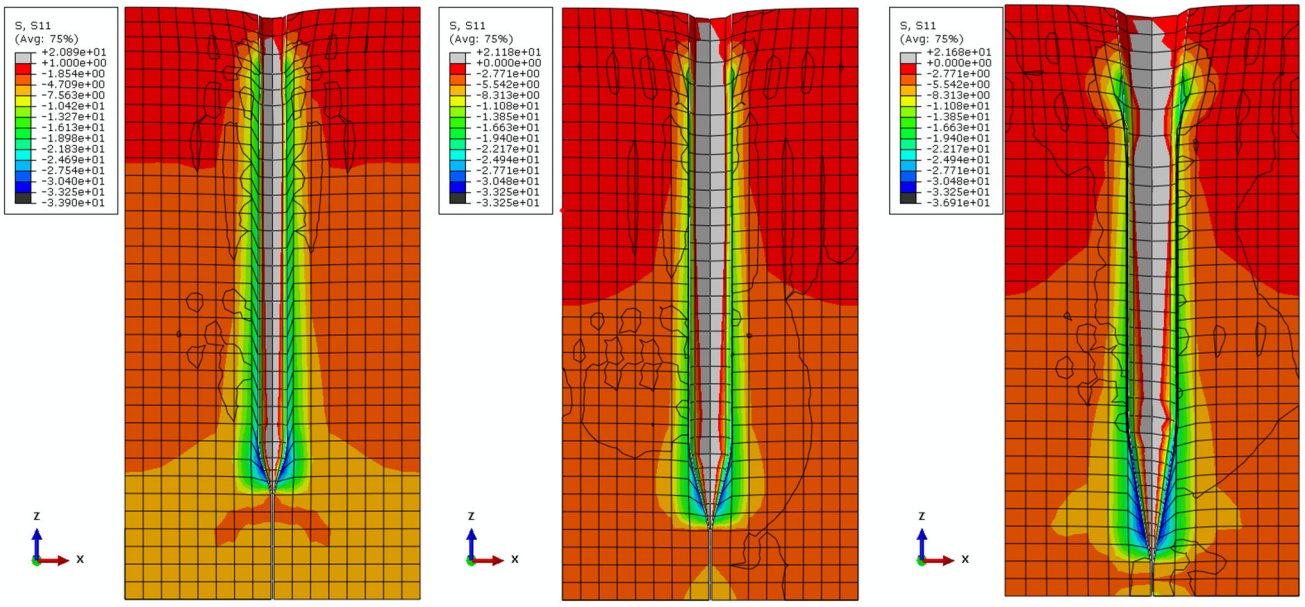

(a) (b) (c)

Figure 5.25 Contour plot of horizontal stresses around the stone column after installation: (a) D = 2cm, (b) D = 3 cm, (c) = 5 cm

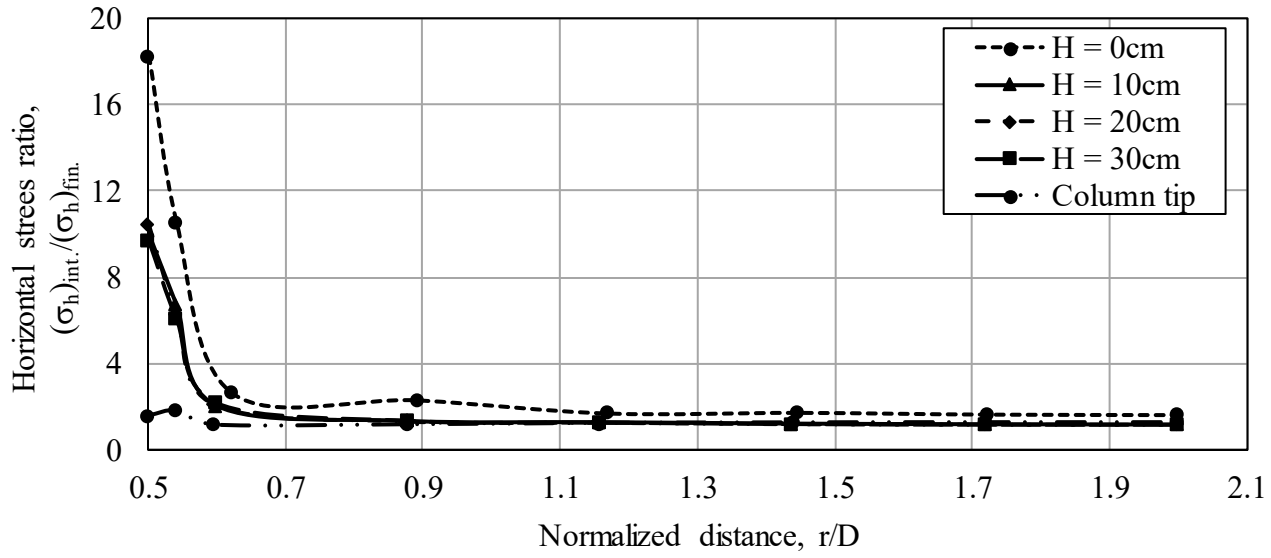

(a)

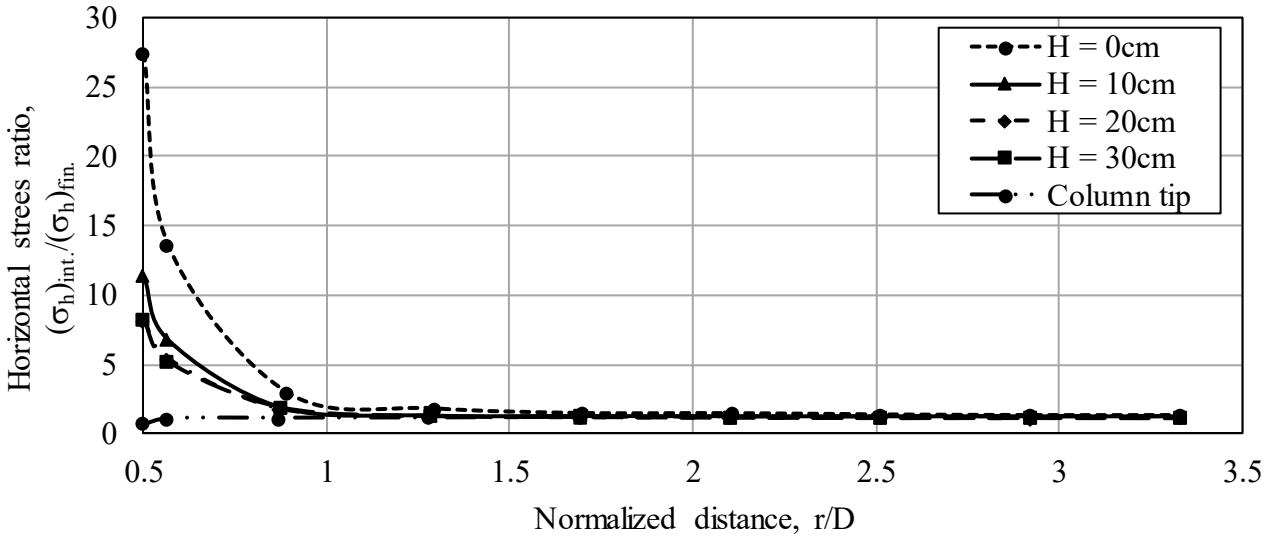

(b)

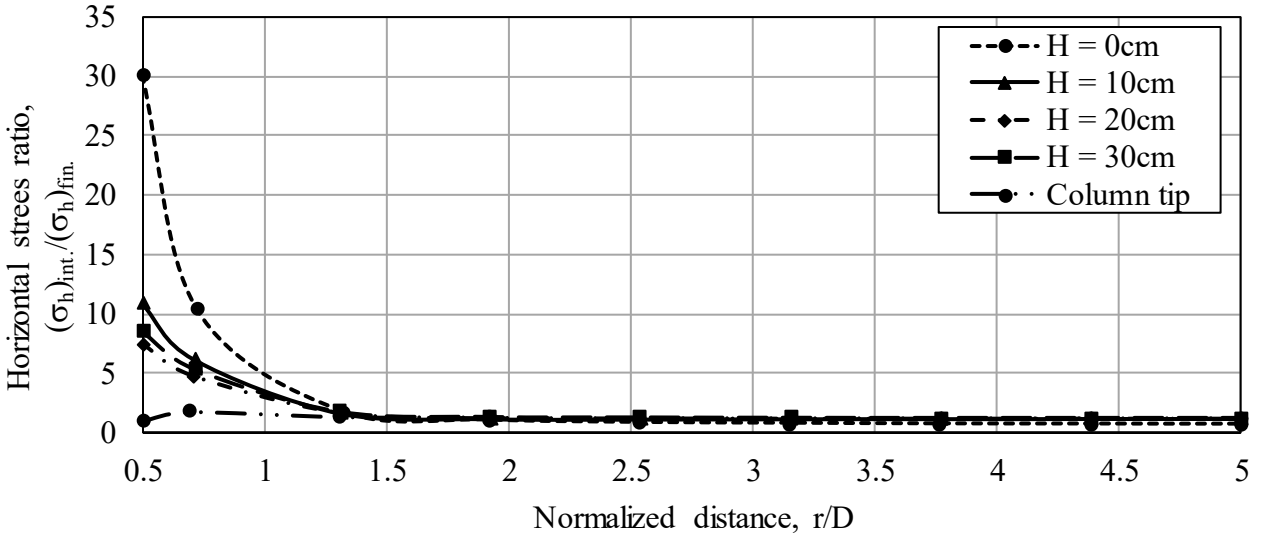

(c)

Figure 5.26 Horizontal stress increase in the clay soil after stone column installation: (a) D = 5cm, (b) D = 3cm and (c) D = 2cm

Due to the friction applied between the steel prop and the adjacent soil, the change in the clay soil around stone columns is divided into three zones: smear zone, compacted zone, and undisturbed zone (Weber et al., 2010). As shown in Figure 5.27, the smear zone was represented as the reduction in vertical stress after installation in the soil extended to a distance varying from 0.54D to 0.7D for stone columns with diameters of 5 cm and 2 cm, respectively. This reduction was followed by an increase in the vertical

stresses, which is defined as the compacted zone. The compacted zone extended to distances of 0.9*D*, 1.2*D*, and 1.9*D* for stone columns with diameters of 5cm, 3cm, and 2cm, respectively. The extension of the smear zone and compacted zone were given as 0.65*D*, 1.25*D*, respectively, for stone columns with a diameter of 0.6 m at prototype scale (Weber et al., 2010). Based on experimental and cavity expansion numerical analysis, the total effect of stone columns installation extended to a distance of 2.5*D* (Indraratna et al., 1998). Similar behaviour was decided from the change in the void ratio for the clay soil around stone columns as shown in Figure 5.28.

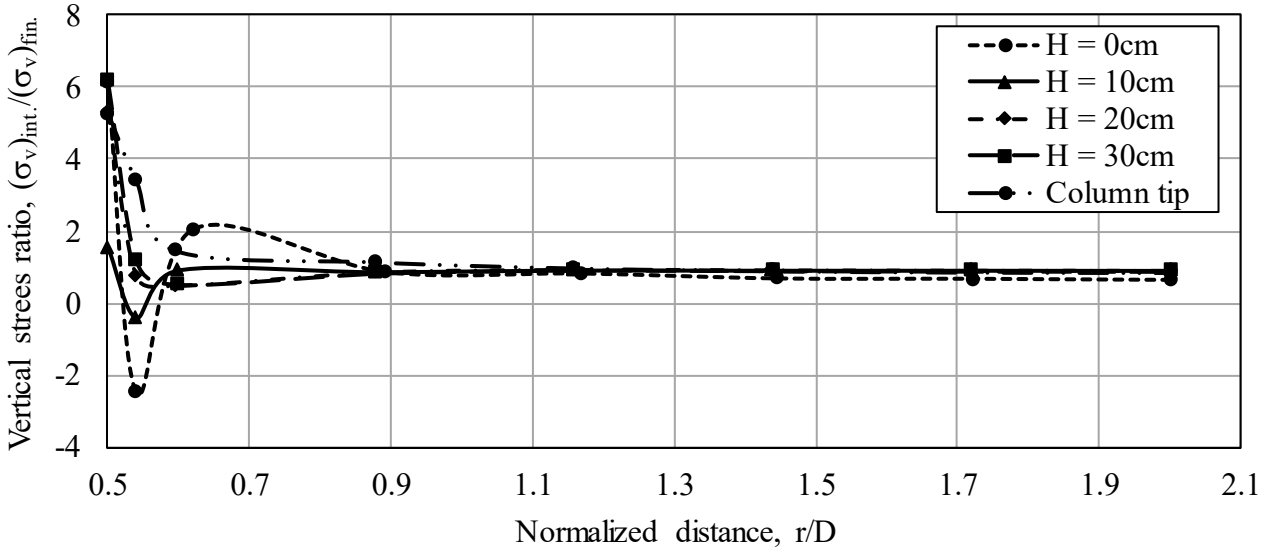

(a)

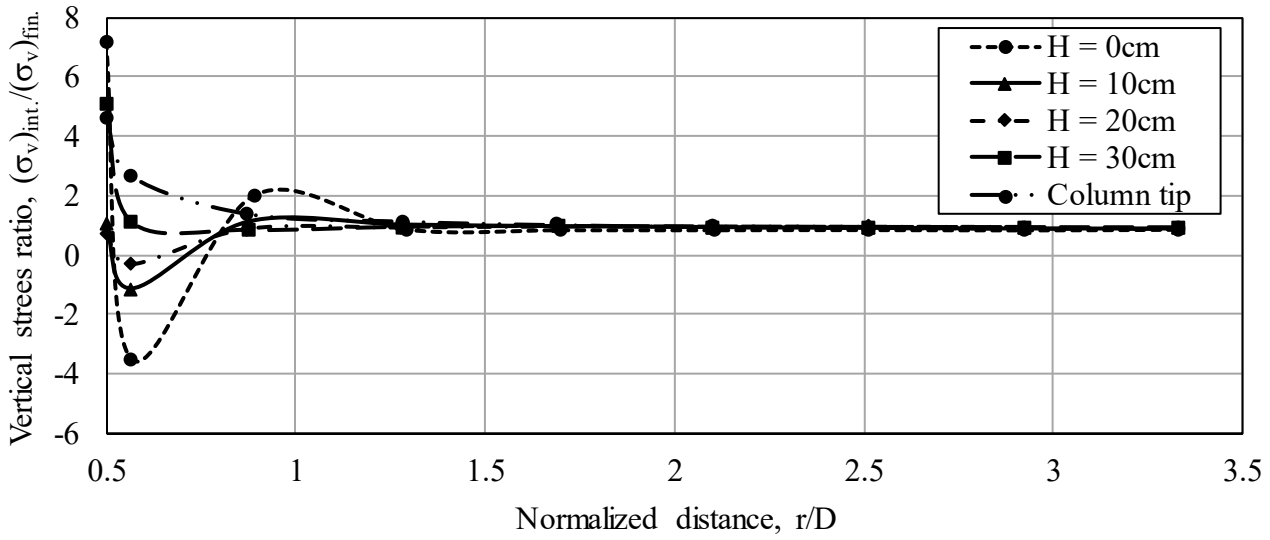

(b)

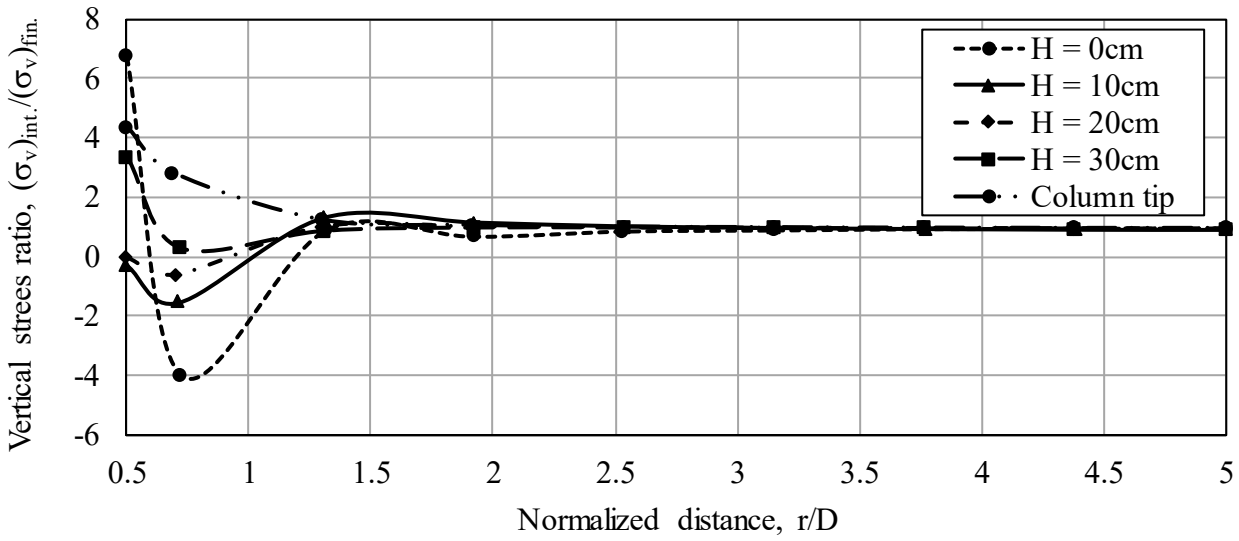

(c)

Figure 5.27 Effect of stone column installation on vertical stress of the adjacent clay soil: (a) *D* = 5cm, (b) *D* = 3cm, (c) *D* = 2cm

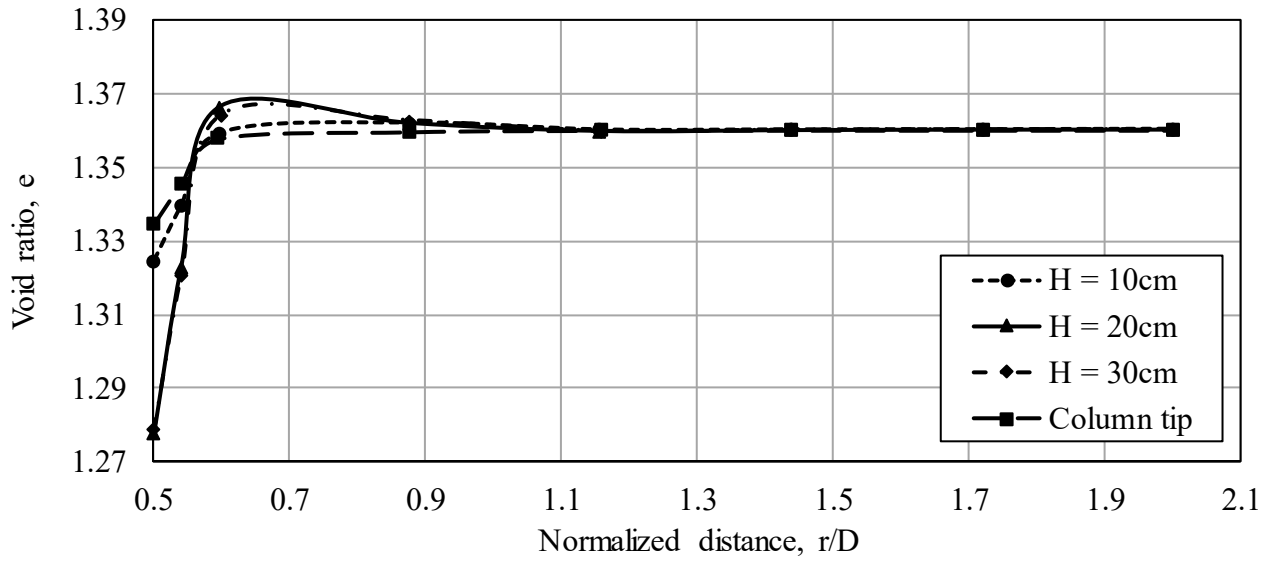

(a)

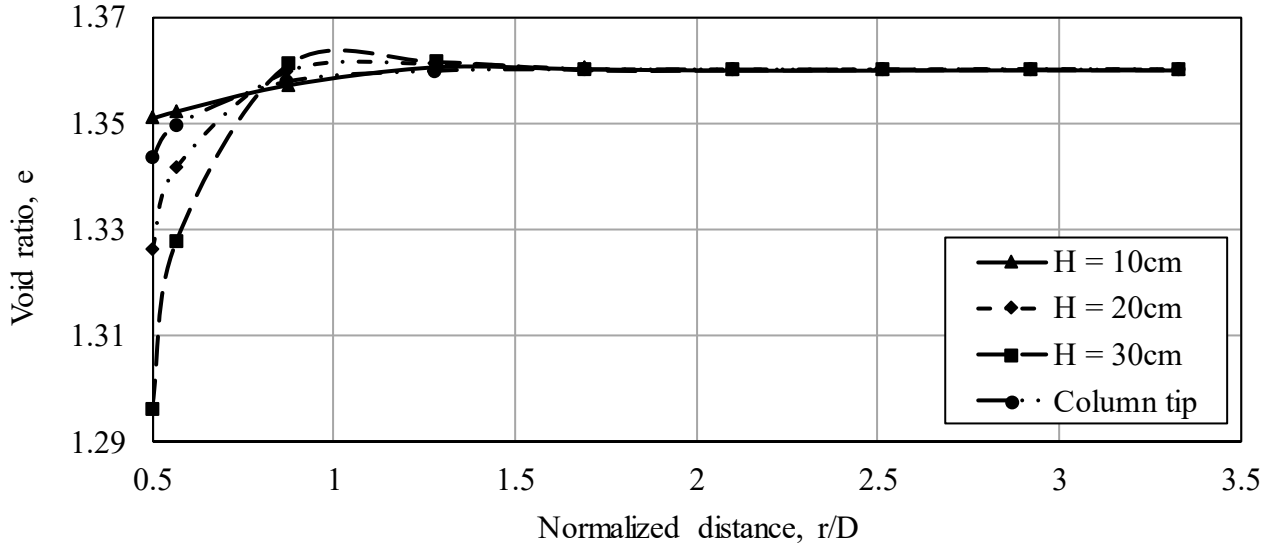

(b)

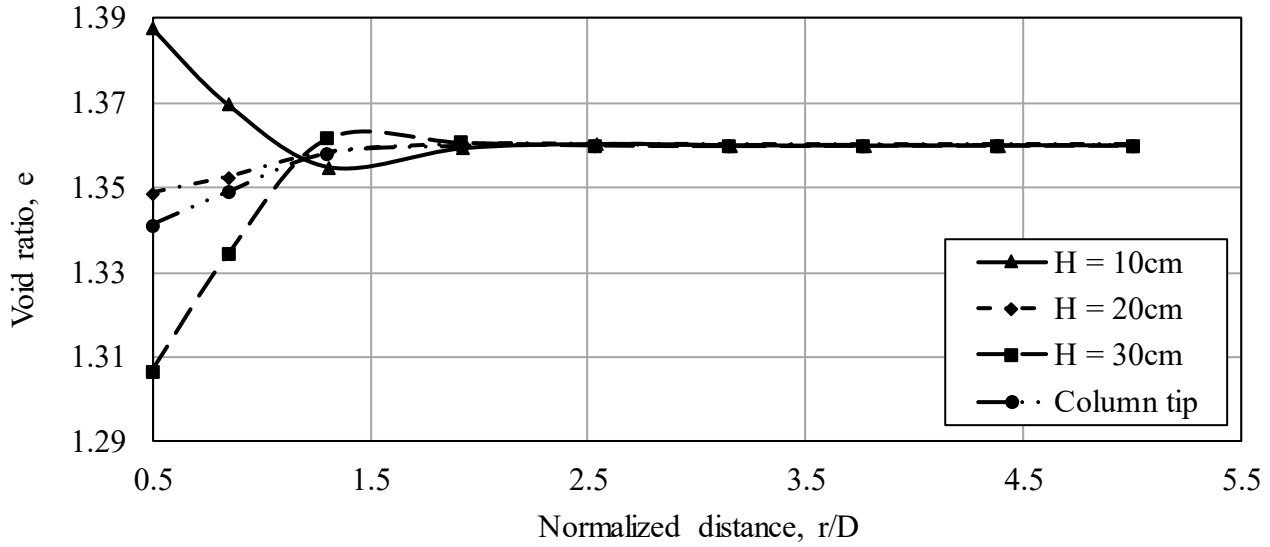

(c)

Figure 5.28 Effect of stone column installation on the void ratio of the clay soil: (a) D = 5cm, (b) D = 3cm, and (c) D = 2cm

From the stress change, the lateral pressure coefficient of the clay soil (k) can be estimated around the stone column after installation. Since the steel prop driving process was fast (10 min. maximum), the clay state was assumed to be in the undrained condition. Thus, the lateral pressure coefficient of the clay soil was set to 1. Due to the installation process, the lateral pressure coefficient of the clay around the stone columns increased, as shown in Figure 5.29. The value of the lateral pressure coefficient decreased with reducing the stone column diameter; i.e. k was 2 at a depth of 10cm for stone columns with a

diameter of 5cm, and dropped to 1.1 for stone columns with a diameter of 2 cm. However, it increased with depth; i.e. *k* increased from 1.3 at a depth of 10 cm to 1.95 at a depth of 30 cm for stone columns with a diameter of 3 cm. This increase in the lateral pressure coefficient of the clay soil upgrades the lateral support for stone columns, which improves the reinforced soil resistance to vertical stresses.

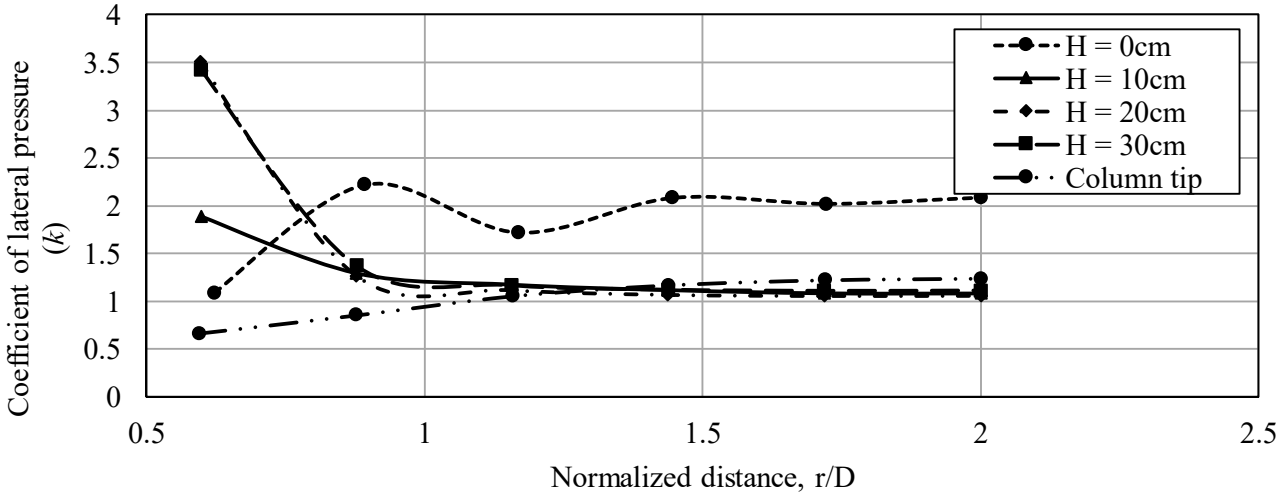

(a)

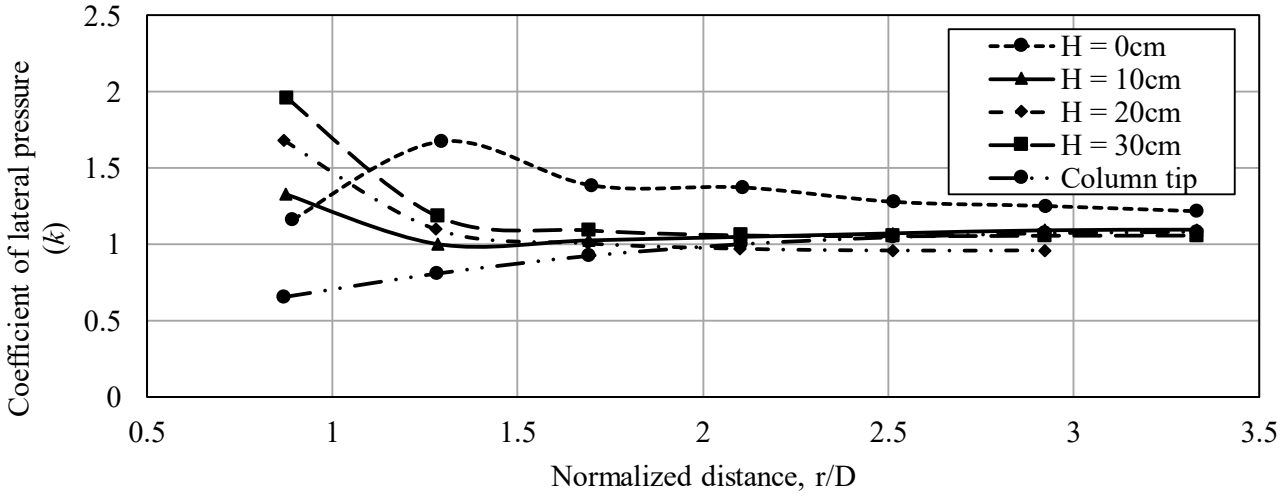

(b)

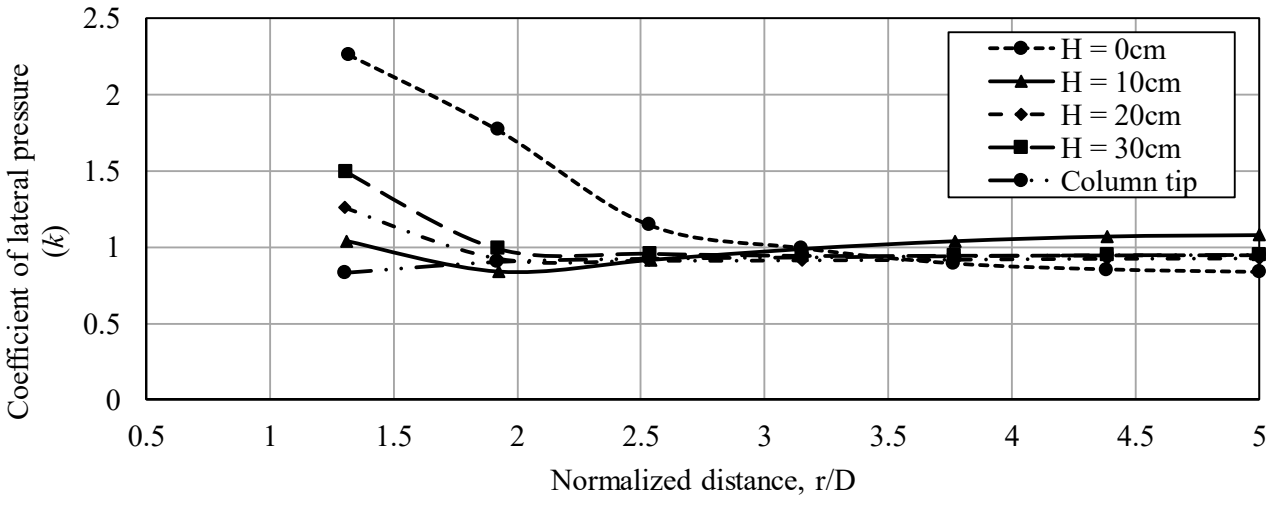

(c)

Figure 5.29 Effect of stone column installation on the lateral pressure of the clay soil: (a) D = 5cm, (b) D = 3cm, (c) D = 2cm

According to the results of the IFE approach, the maximum installation effect occurred in the top and bottom part of the stone column (i.e. H = 0cm, and H = 30cm). In the experimental program, the top and bottom 5 cm of all the sample were removed to reduce the effect of the installation. This assumption was confirmed from the numerical results. Also, the installation effect extended to a distance of 0.9D to 1.9D for stone columns with diameters of 5 cm and 2 cm. The experimental samples were reinforced by one stone column of 5.1cm, which means the diameter of the affected area at 9.18 cm is less than the sample diameter (10 cm). Therefore, the installation influences 60% of the triaxial sample reinforced by a single stone column. Regarding samples reinforced by more than one column with a spacing of 2D and 2.75D, the effect of installation does not overlap with the adjacent sample, but the influenced area increased to 100% of the sample size as shown in Figure 5.30 (a). The increase in the influenced area between the clay samples reinforced by single and group of stone columns at the same replacement ratio describes the change between the numerical and experimental results presented in section 5.3.6. For the sample reinforced by a group of stone columns with a spacing of 1.5D, the interaction between the influenced areas increased particularly for the clay soil surrounded by stone columns, as shown in Figure 5.30 (b). Therefore, the lateral pressure coefficient of the clay soil was enhanced and led to a better resistance for the entire system. All the above findings were confirmed by the experimental and the EFE numerical model approach results.

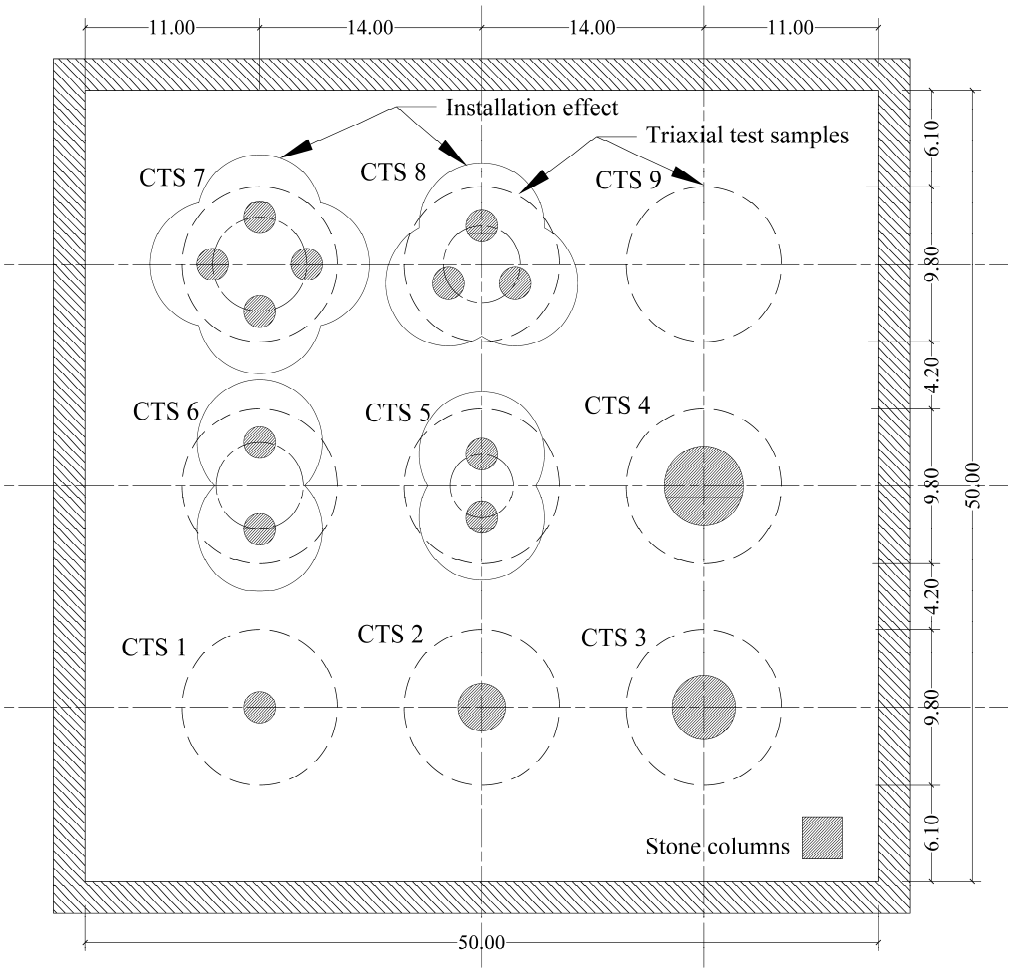
11.00
14.00
14.00
11.00
Installation effect
Triaxial test samples
CTS 7
CTS 8
CTS 9
CTS 6
CTS 5
CTS 4
CTS 1
CTS 2
CTS 3
Stone columns
6.10
9.80
4.20
9.80
4.20
9.80
6.10
50.00
50.00

(a)

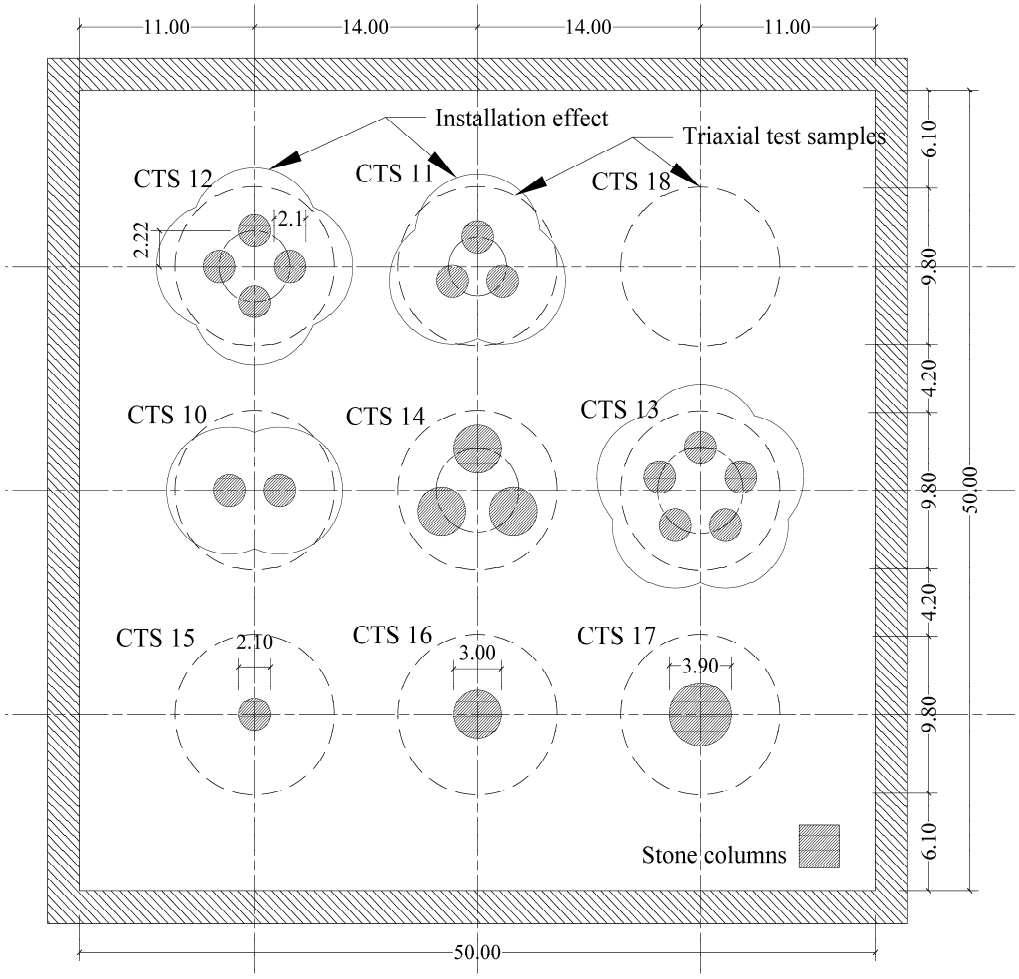

(b)

Figure 5.30 Effect of installation in triaxial samples based on IFE approach: (a) T2, (b) T5

A parametric study was conducted to estimate the effect of installation for different clay soils. The drained internal friction angle of the clay (ϕ_c') was changed from 10° to 30°; although all other parameters kept constant as calculated by the triaxial test. Figure 5.31 shows that the vertical stress ratio increased in the clay soil due to installation of the stone columns. The vertical stress ratio increased by increasing the drained internal shear resistance angle of the clay soil; i.e. at depth 30 cm, the vertical stress ratio was 4.6, 5.2, 5.4 for internal friction angle of 10°, 20°, and 30°, respectively. Installations of the stone columns also increased the horizontal stresses in the clay soil, although the effect is more noticeable in the clay soil with less internal friction angle (Figure 5.32); i.e. at depth 10 cm, the vertical stress ratio was 3.05, 4.7, 6.6 for internal friction angle of 10°, 20°, and 30°, respectively. As the shear resistance of the clay soil increased, more force is required to drive the steel prop in the soil. Therefore, the internal horizontal and vertical stresses increased. Regarding the lateral pressure coefficient, there is a slight

increase in the lateral pressure coefficient for clay soil with an internal angle of 10°, as shown in Figure 5.33 (a). On the other hand, the shear resistance of the clay soil does not have any influence on the radius of the influenced zone around the stone column; i.e. the influence on stone columns extend to 2.5*D* regardless of the clay drained friction angle as shown in Figure 5.33 (a), (b), and (c).

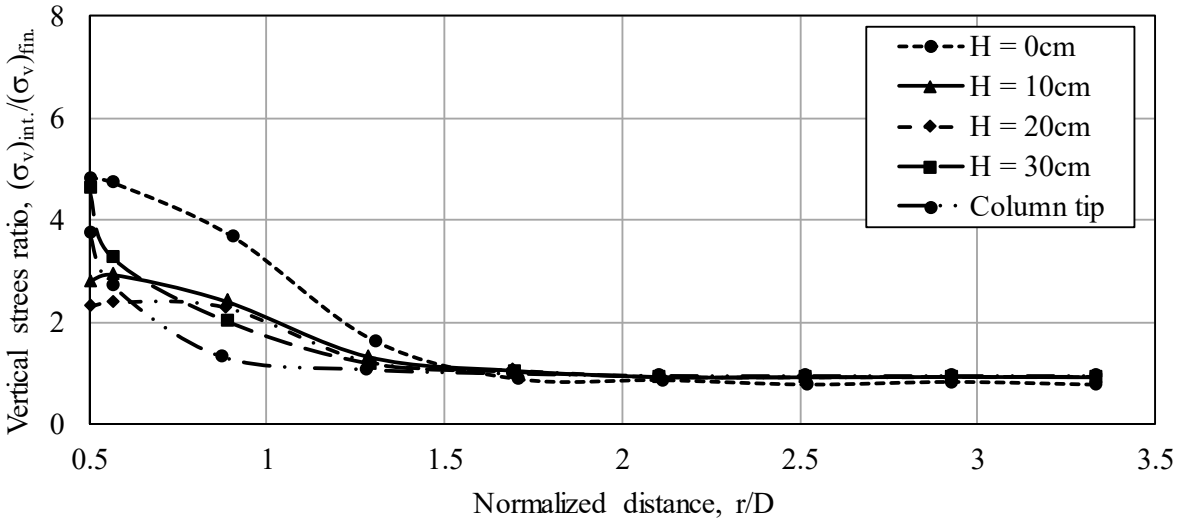

(a)

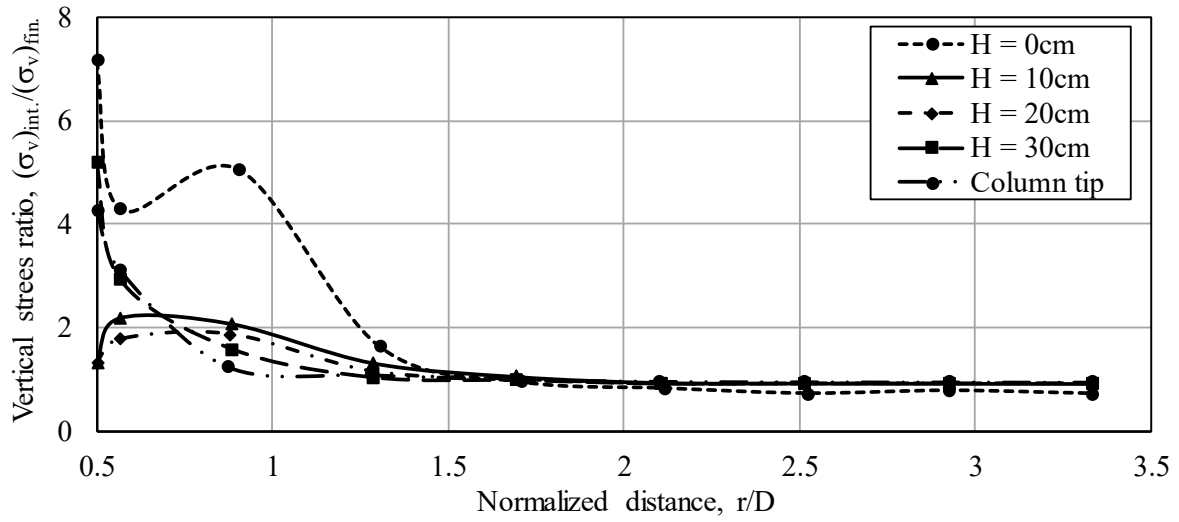

(b)

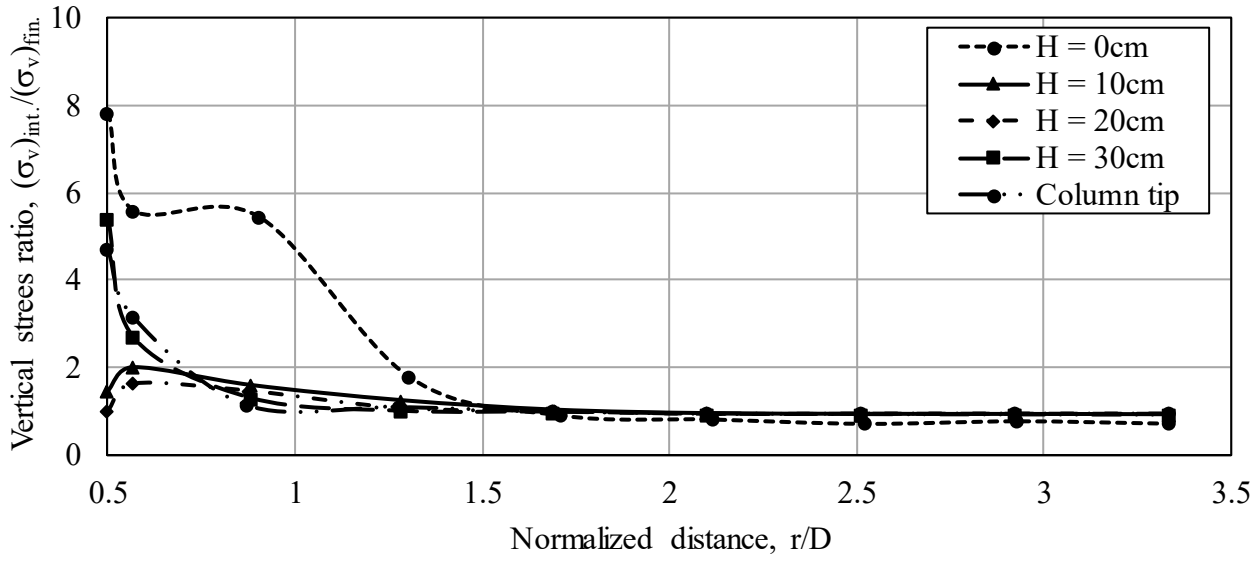

(c)

Figure 5.31 Effect of stone column (D = 3cm) installation on the vertical stresses in the adjacent clay soil: (a) ϕ_c' = 10°, (b) ϕ_c' = 20°, (c) ϕ_c' = 30°

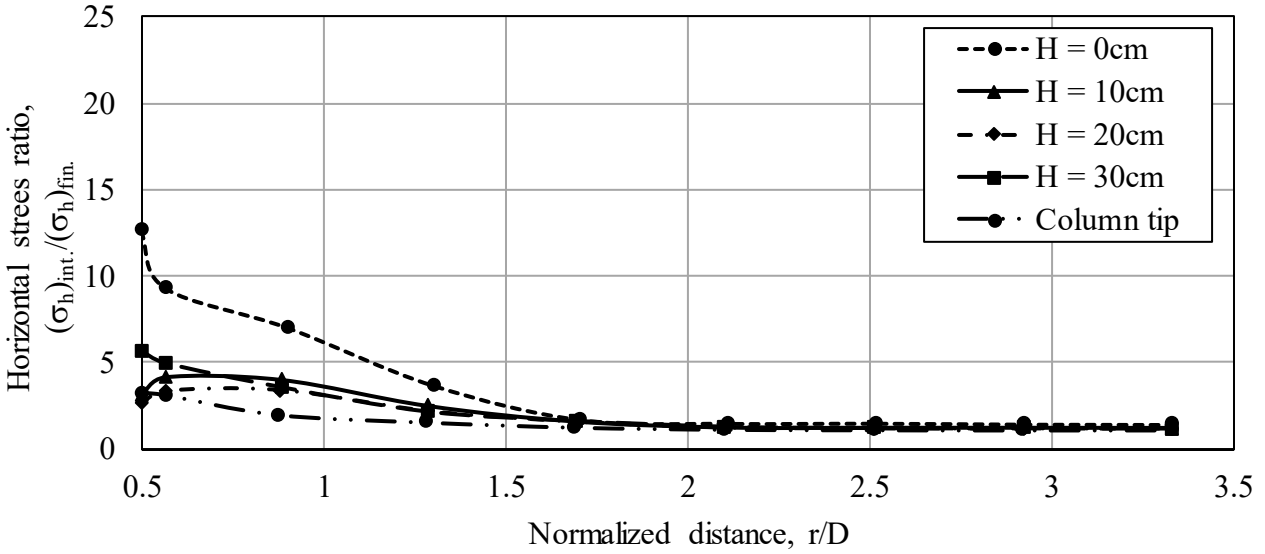

(a)

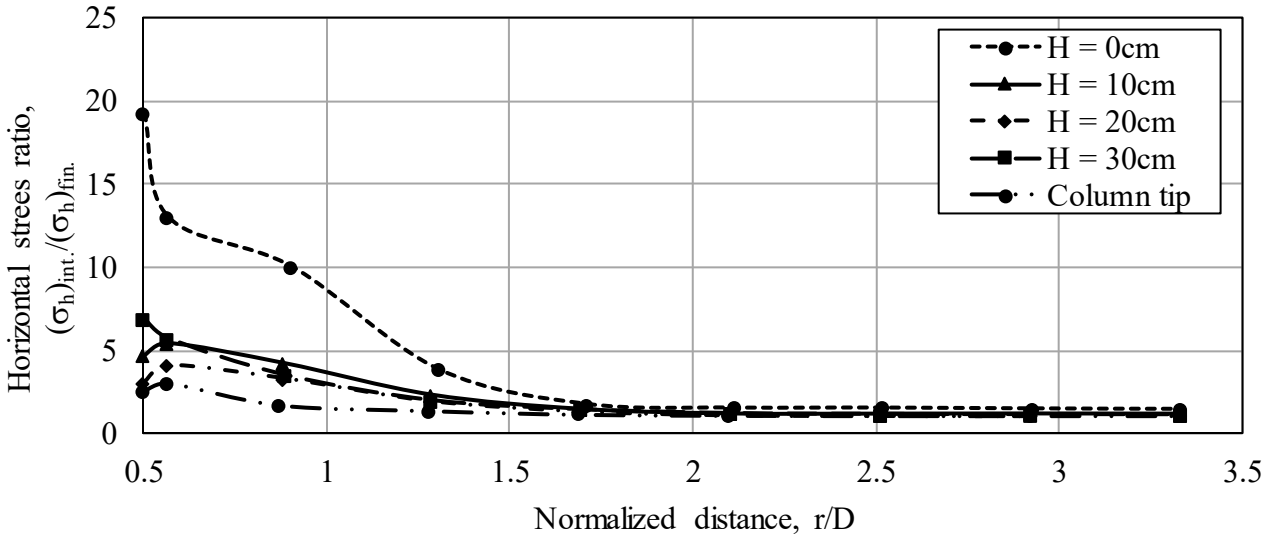

(b)

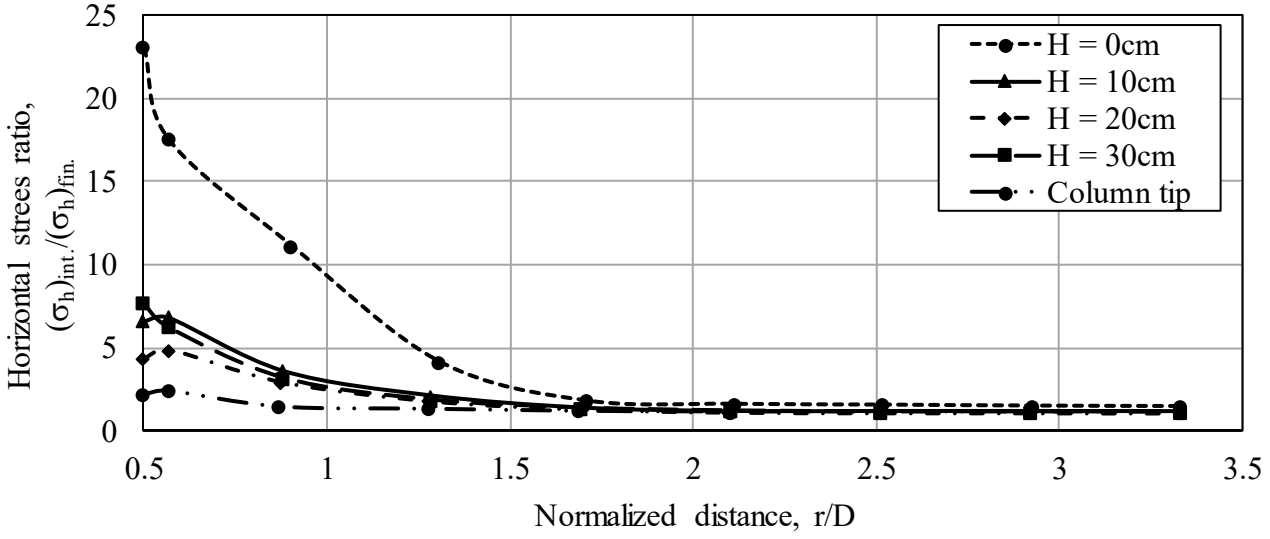

(c)

Figure 5.32 Effect of stone column (D = 3cm) installation on the horizontal stresses in the adjacent clay soil: (a) ϕ_c' = 10°, (b) ϕ_c' = 20°, (c) ϕ_c' = 30°

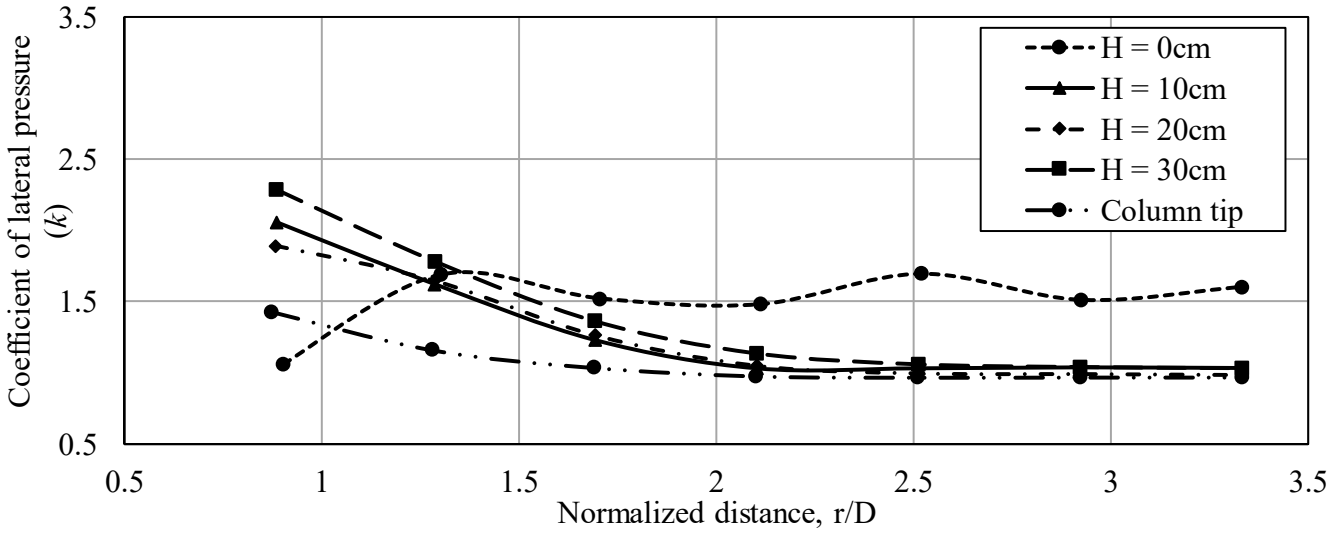
Coefficient of lateral pressure (k)
Normalized distance, r/D
H = 0cm
H = 10cm
H = 20cm
H = 30cm
Column tip
3.5
2.5
1.5
0.5
0.5
1
1.5
2
2.5
3
3.5

(a)

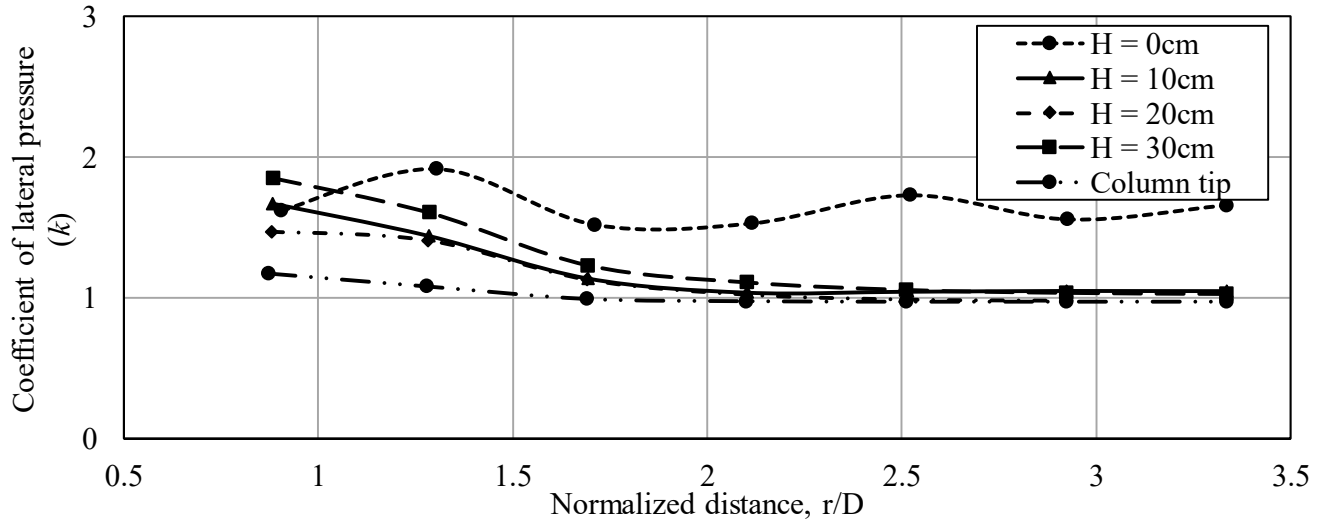
Coefficient of lateral pressure (k)
Normalized distance, r/D
H = 0cm
H = 10cm
H = 20cm
H = 30cm
Column tip
3
2
1
0
0.5
1
1.5
2
2.5
3
3.5

(b)

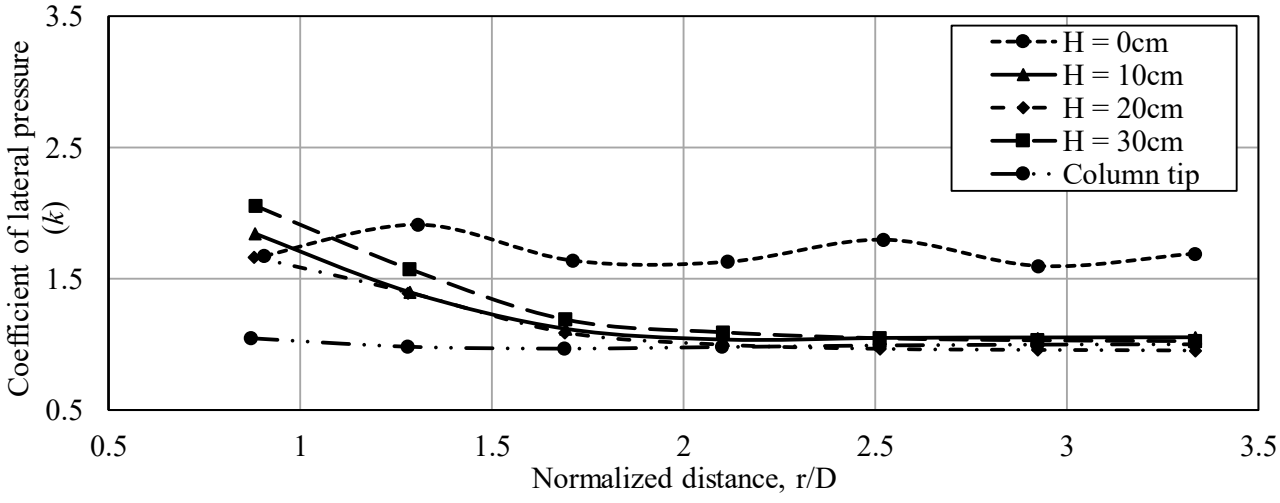

(c)

Figure 5.33 Effect of stone column (D = 3cm) installation on the coefficient of lateral pressure of the adjacent clay soil: (a) ϕ_c' = 10º, (b) ϕ_c' = 20º, (c) ϕ_c' = 30º

5.5 Full-scale FE model approach (FFE)

The approach used in the EFE, which was validated against the present experimental results, was used in a full-scale finite element model (FFE) to simulate a rigid square footing supported by a clay soil reinforced by single and groups of stone columns. The main purpose of this model is to come up with a new method to estimate the bearing capacity of a clay soil reinforced by different stone columns geometry. Therefore, the FFE model was used to find the actual plane of failure in the reinforced soil. Accordingly, the bearing capacity of the reinforced soil could be estimated based on the obtained failure plane. All the current bearing capacity theories were developed based on a strip footing assumption (Terzaghi, 1943; Meyerhof, 1951; Hansen, 1970; Griffiths, 1982). However, the presented FFE model was used to examine the bearing capacity of a square (Figure 5.34). The stone columns were assumed to be supported by a rigid stratum at the column tip. Since the assumed problem was symmetric in X and Y directions, a quarter of the model was built in the programme to optimize both the accuracy and the solving time of the FE model. Details of the FFE approach are provided in the following sections.

The same constitutive models used in the validated EFE model was utilized to simulate the clay and stone column materials. So, an elastic-hardening plastic modified Drucker-Prager/cap plasticity (Drucker et al., 1952) constitutive model was used to simulate the clay soil, and the elastic-perfect plastic Mohr-Coulomb constitutive model used for the stone column material as described in section 5.2.1.

5.5.1 Soil and geometry parameters

For practical use, the bearing capacity of the reinforced soil is presented as an improvement factor (*IR*), which is defined as the ratio of the capacity of improved soil to the capacity of the unimproved soil. Accordingly, design charts have been developed for the *IR* estimation incorporating the physical properties of the stone columns (unit weight (γ_s), internal shearing resistance angle (ϕ_s)) as well as the geometric properties of stone columns (spacing (*S*), and replacement ratio (A_s%)). The replacement ratio was calculated as the area of stone columns divided by the total area of the footing.

Table 5.4 Rang of all the parameters examined in the FFE model

Parameter	Range of value
Drained angle of shear resistance clay soil, ϕ_c' (Degree)	10, 20, and 30
Saturated unit weight of clay soil, $\gamma_{c\,sat}$ (kN/m^3)	18
drained angle of shear resistance of stone, ϕ_s' (Degree)	30, 40, and 50
Saturated unit weight of stone, $\gamma_{s\,sat}$ (kN/m^3)	20
Normalized spacing, S/D	1.5, 2, 2.5, 3, and 4
Stone column diameter D, (m)	0.6, 0.8, 1.0, 1.2, and 2.4
Number of stone columns, N	1, 2, 4, 9, and 16
Replacement ratio, A_s (%)	5 ~ 28
Footing width, B (m)	2, 4, 8

In order to eliminate the effect of the boundary conditions of the numerical model, the clay soil extended around the footing to a distance of 3B (Castro, 2014). Since the clay soil was assumed to be normally consolidated, the pre-consolidation pressure of the soil should be equal to the overburden stress. In ABAQUS, it was not possible to change the pre-consolidation pressure on the same material with depth. Therefore, the clay soil was divided into five layers, each layer with a thickness of 2m. New material was assigned to each layer. The properties of all the materials were identical except the pre-consolidation

pressure. A constant pre-consolidation pressure was defined in each material based on the effective overburden pressures at the end of the layer, as shown in Figure 5.34.

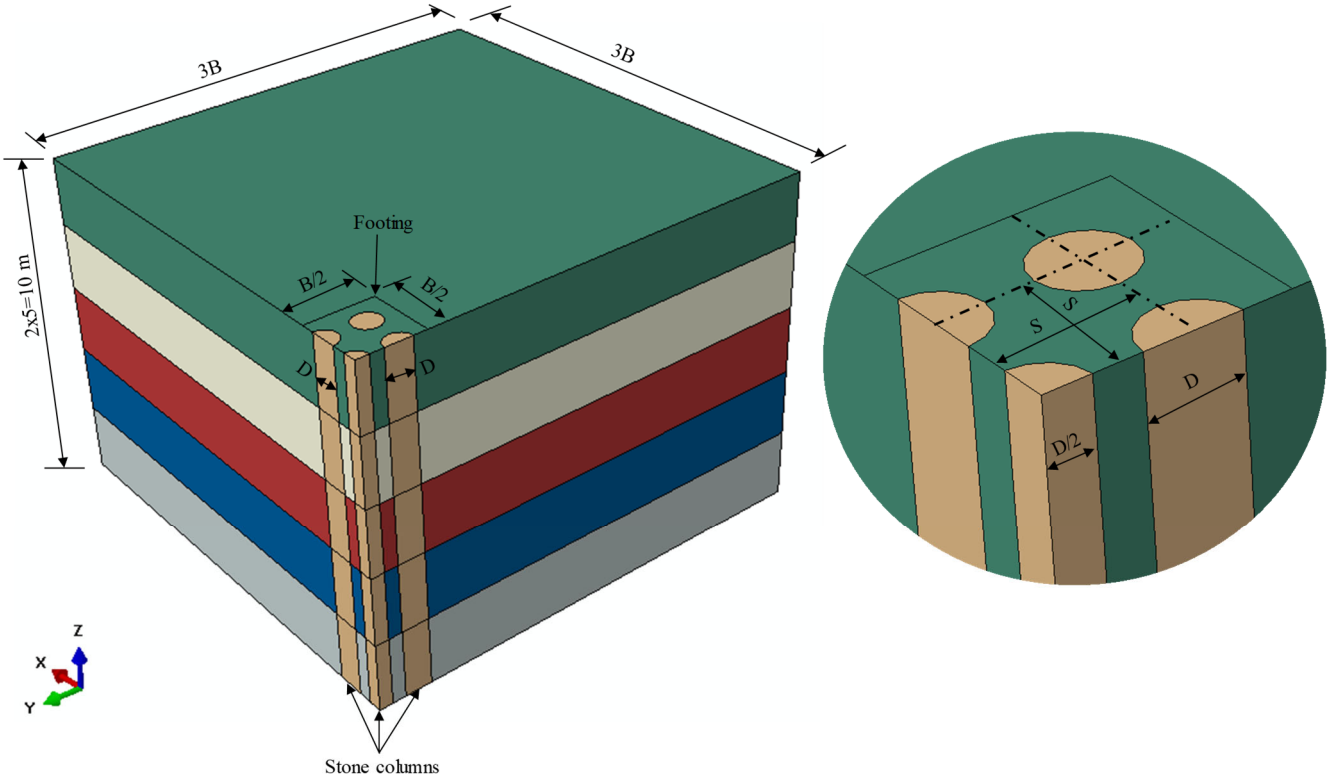

Figure 5.34 Geometric details of FFE model

5.5.2 Boundary conditions, interaction, and applied loads

As described previously, only a quarter of the problem was built in the numerical model. So, symmetric boundary conditions were used on the inside surfaces of the model, and regular boundary conditions were used elsewhere. For the symmetric boundary conditions, the displacement in a perpendicular direction to the surface (i.e. *Ux, Uy*), rotation in the vertical direction (*URz*), and the direction parallel to the surface direction (i.e. *URx, URy*) are restrained. For outside surfaces, the displacement is restricted in the perpendicular direction of the surface. Details of the used boundary conditions are shown in Figure 5.35.

In order to simulate the rigid footing, a constraint was applied to the soil surface under the footing, which connected the displacement of all the points in this surface to the reference point (RP-1). Accordingly, all the point deformations in the footing area were controlled by the reference point. The load was applied by defining a vertical distance of -0.5m in Z direction at the reference point. In order to simulate a real undrained situation, the full displacement was applied to the soil over a 24-hour period. In addition, the

pore water pressure was set to zero on the top surface of the model except for the area under the footing. A rough footing surface was also assumed; thus, the displacement in x and y directions were restrained (i.e. Ux=Uy=0) but the constraint was only activated during the loading stage.

A geostatic step was defined in the model before applying the footing displacement to make sure that equilibrium was satisfied within the soil under the overburden pressure. The stone columns were assumed to be in full contact with the soil, as described in section 5.3.

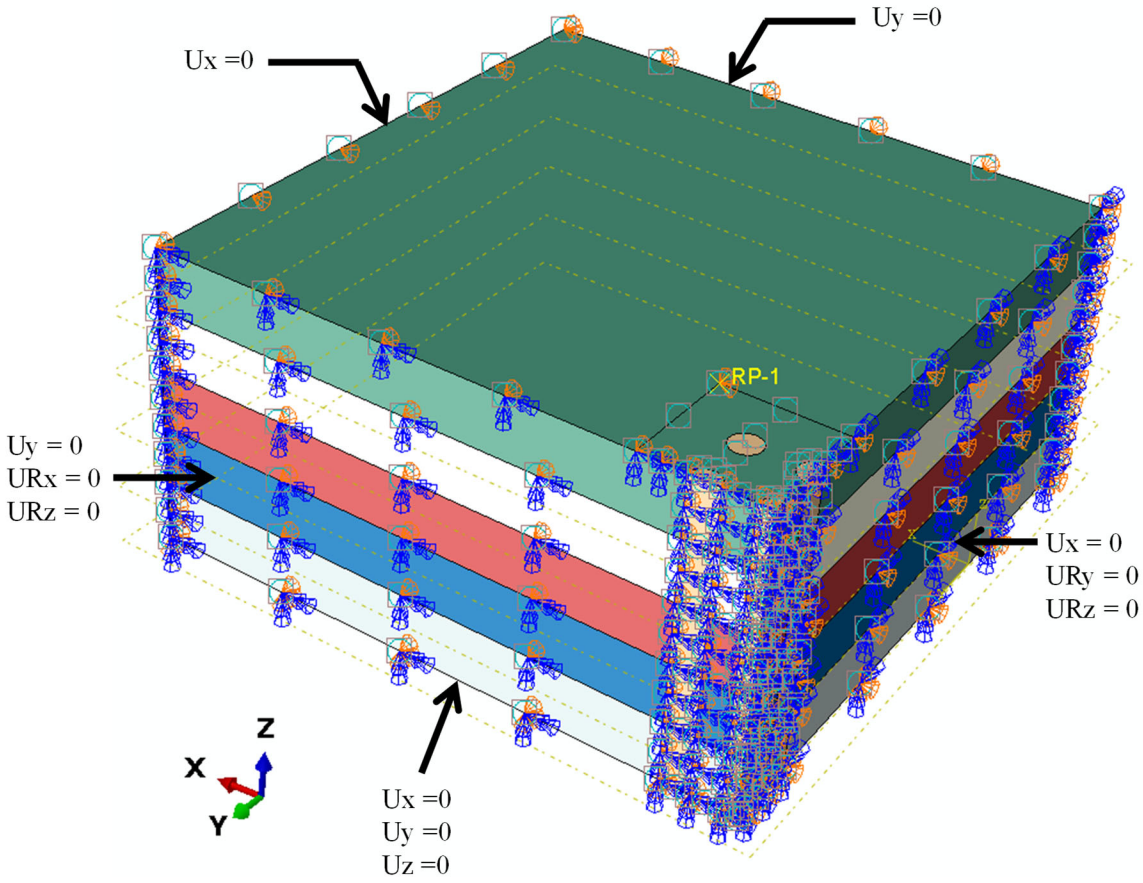

Figure 5.35 Boundary conditions details for FFE model approach

5.5.3 Initial conditions definition

Initial conditions are significant in FE numerical modelling. In the FFE model approach, four initial conditions were predefined in the model (geostatic stress, initial void ratio, initial pore water pressure, and degree of saturation). The geostatic stresses were defined for the clay soil and the stone columns separately, since a different unit weight was used in each material. The geostatic stresses were calculated from the effective stresses at the base of the model, assuming that the soil was fully saturated. Accordingly, a degree of saturation of 100% was defined for the whole model, and the pore water

pressure was defined as the hydrostatic pressure. The initial void ratio (e_o) was defined for clay soil and stone columns separately, and it was calculated using equation (5-6) where (γ_w) is the unit weight of water (9.81 kN/m3), (γ_{sat}) is the saturated unit weight of the soil, and (G_s) is the specific gravity of the soil (assumed to be 2.6 for clay and stone columns). The lateral pressure coefficient (K_o) of the clay soil and the stone columns was also defined in the model. Since the soil was assumed to be normally consolidated, the lateral coefficient was calculated based on the drained internal friction angle of the soil.

$$e_o = \frac{\gamma_w G_s - \gamma_{sat}}{\gamma_{sat} - \gamma_w} \tag{5-6}$$

5.5.4 Element size and mesh sensitivity analysis

The capability of the C3D8P element to capture the change in the effective stresses and pore water pressure of reinforced clay soil was confirmed by the EFE model in section 5.3.6. Therefore, the same element was used in the FFE model. A mesh sensitivity analysis was conducted in order to optimize the solving time and the accuracy of the results. A model of a rigid square footing (B = 2m) on clay soil was used in the mesh sensitivity analysis. The model was meshed using a constant element size of 2, 1, 0.5, 0.3, and 0.2

Figure 5.36 presents the effect of the mesh size on the model results. The bearing capacity and the pore water pressure significantly reduced when the mesh size dropped from 2 to 1. The changing rate reduced as the mesh size decreased from 0.5 to 0.2. Therefore, the element size range in all the FFE models was from 0.5 to 0.2. The smallest mesh size was used in the footing area, and the largest size was used in the model edges. The same element size distribution was used in horizontal and vertical directions as shown in Figure 5.37. Based on this meshing technique, the number of elements varied from 33000 and 150000 for models with footing width 2m and 8m, respectively.

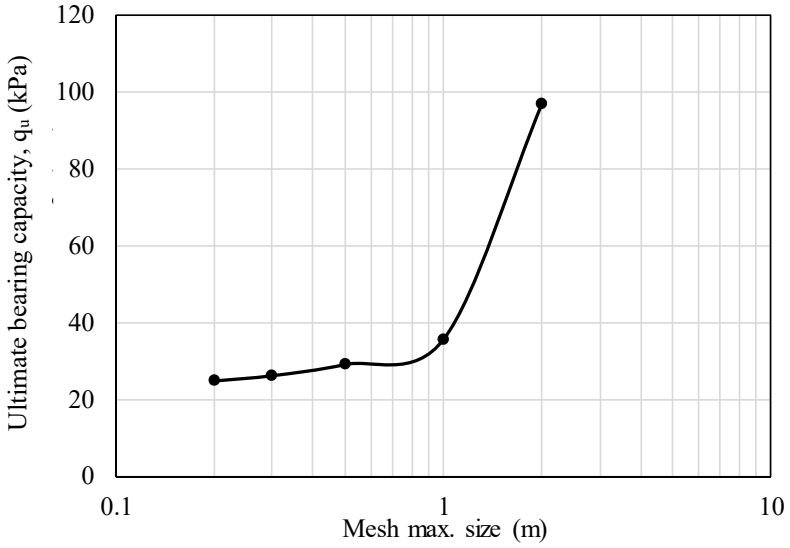

(a)

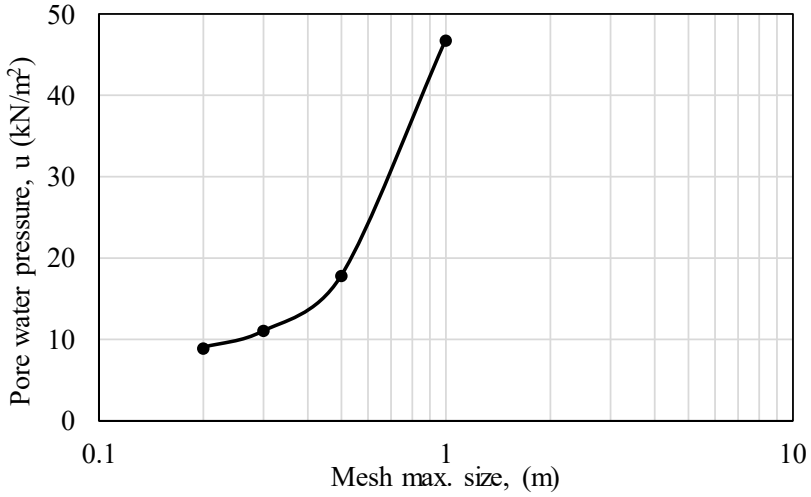

(b)

Figure 5.36 Effect of mesh size on the results of the FFE numerical model: (a) Ultimate bearing capacity, (b) Average pore water pressure under the footing

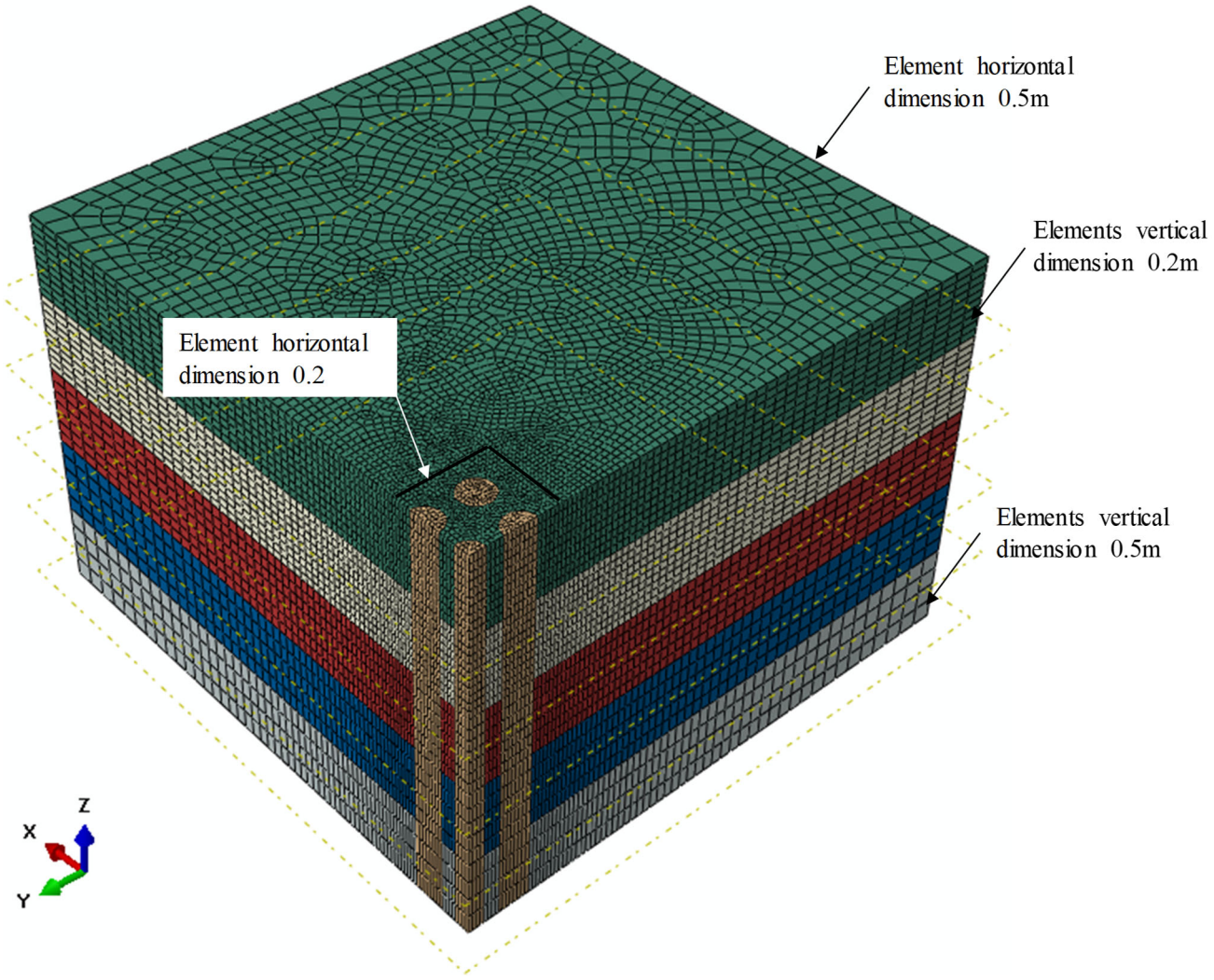

Figure 5.37 Typical meshing technique for FFE models

5.5.5 FFE modelling approach results

In this section, the results of more than 200 finite element simulation are summarized. The results are used to evaluate the performance of stone columns under rigid footings. Design charts are presented for the refinement of the bearing capacity calculations for the reinforced clay soil.

5.5.5.1 Effect of footing size

In order to evaluate the FFE model results, a model of unreinforced soil was built for the three footings (2m, 4m, and 8m) used in the analysis. To evaluate the behaviour of the clay soil under the footings, the failure plane was defined under all the footings for different drained angle shear resistance (ϕ_c'= 10°, 20°, and 30°). Since the load was applied over a relatively short 24-hour period, an undrained condition was expected to occur at failure. Therefore, a punching shear failure was observed under all the footings

as shown in Figure 5.38. The angle between the footing and the failure plane (θ_l) was 45° regardless of the footing size and the drained internal friction angle, which confirm an undrained loading case.

Figure 5.39 (a) to 5.39 (c) show vertical stress - displacement (σ_z - u) curves for different footing sizes (i.e. B = 2m, 4m, and 8m) and for different drained internal friction angles (i.e. ϕ_c'= 10°, 20°, and 30°). The ultimate bearing capacity (q_u) was calculated based on the tangential method described in section 5.3.6. All the models show the same bearing capacity regardless of the footing width (i.e. q_u = 15.01 kN/m^2 for ϕ_c' = 10°, q_u = 28 kN/m2 for ϕ_c' = 30°), which confirms that the model represents an undrained loading condition. The ultimate bearing capacity estimated from the model was compared with Meyerhof's bearing capacity equation (Meyerhof, 1951). In order to use Meyerhof's equation, the drained shear resistance of the clay soil (ϕ_c') should be converted to the undrained shear resistance (c_u). Equations (5-7) to (5-9) were used to calculate the undrained shear resistance of the clay soil (Sorensen et al., 2013). Table 5.5 shows the correlation between drained and undrained shear resistance of the clay. Since a punching shear failure was detected at failure, the estimated bearing capacity values from FFE model was 0.5 times the calculated bearing capacity using Meyerhof's equation for general shear failure (i.e. for ϕ_c' = 20, q_u (F.E. analysis) = 22.19 kPa & q_u (Meyerhof, 1951) = 46.26 kPa). This observation matches Terzaghi's recommendation for bearing capacity reduction in case of bunching and local shear failure (Terzaghi, 1943).

$$c_u = \frac{q_f' - p_f' \sin\phi_c'}{\cos\phi_c'} \tag{5-7}$$

$$q_f' = \frac{1}{\sqrt{2}}\sqrt{\left(\sigma_x' - \sigma_y'\right)^2 + \left(\sigma_y' - \sigma_z'\right)^2 + \left(\sigma_x' - \sigma_z'\right)^2} \tag{5-8}$$

$$p_f' = \frac{\sigma_x' + \sigma_y' + \sigma_z'}{3} \tag{5-9}$$

Where

q_f' effective shear stress at failure (kPa)

p_f' effective mean stress at failure (kPa)

σ_x' horizontal effective stress (in X-X direction) (kPa)

σ_y' horizontal effective stress (in Y-Y direction) (kPa)

σ_z' vertical effective stress (in Z-Z direction) (kPa)

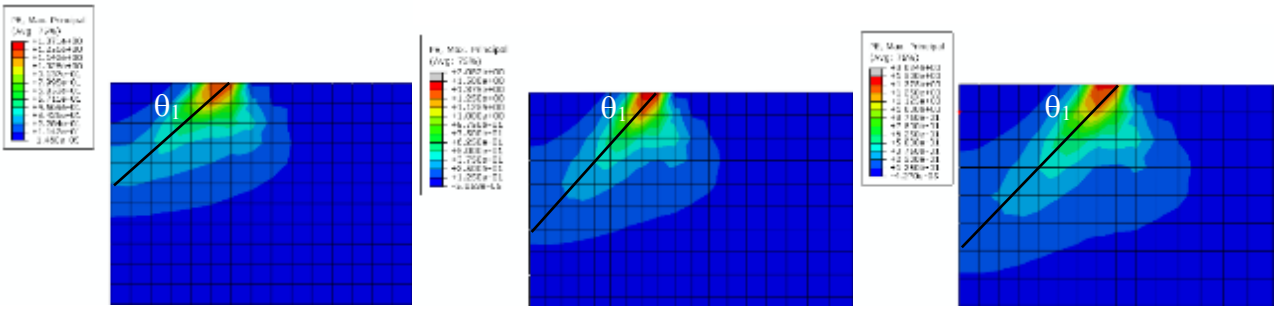

(a) ϕ_c' = 10º (b) ϕ_c' = 20º (c) ϕ_c' = 30º

B=2

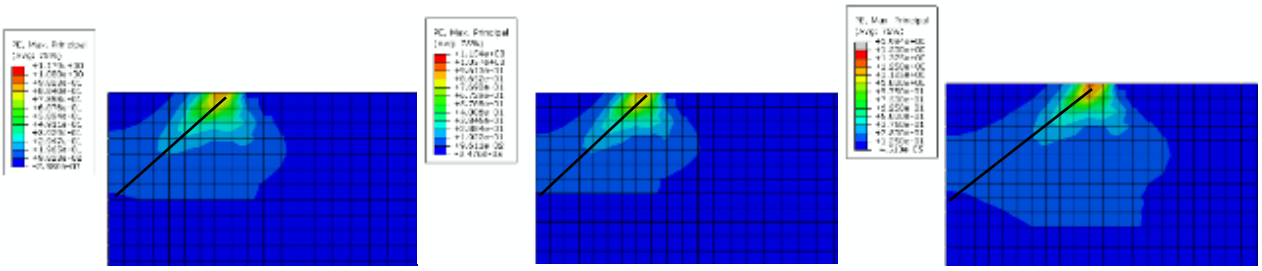

(a) ϕ_c' = 10º (b) ϕ_c' = 20º (c) ϕ_c' = 30

B=4

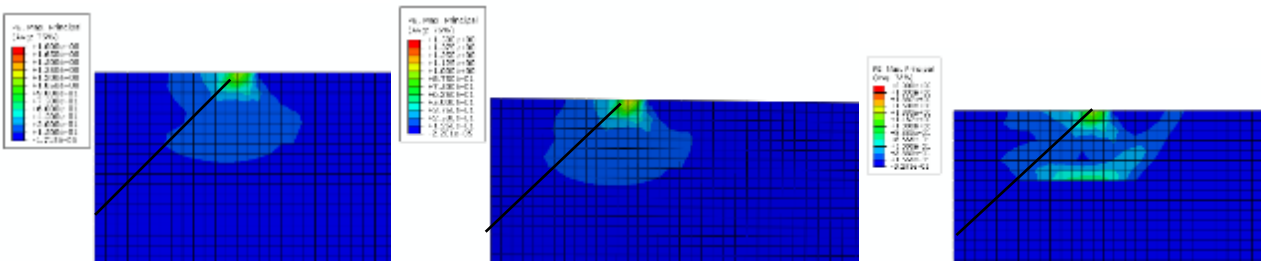

(a) ϕ_c' = 10º (b) ϕ_c' = 20º (c) ϕ_c' = 30

B=8

Figure 5.38 Failure plane under a rigid footing on unreinforced clay soil

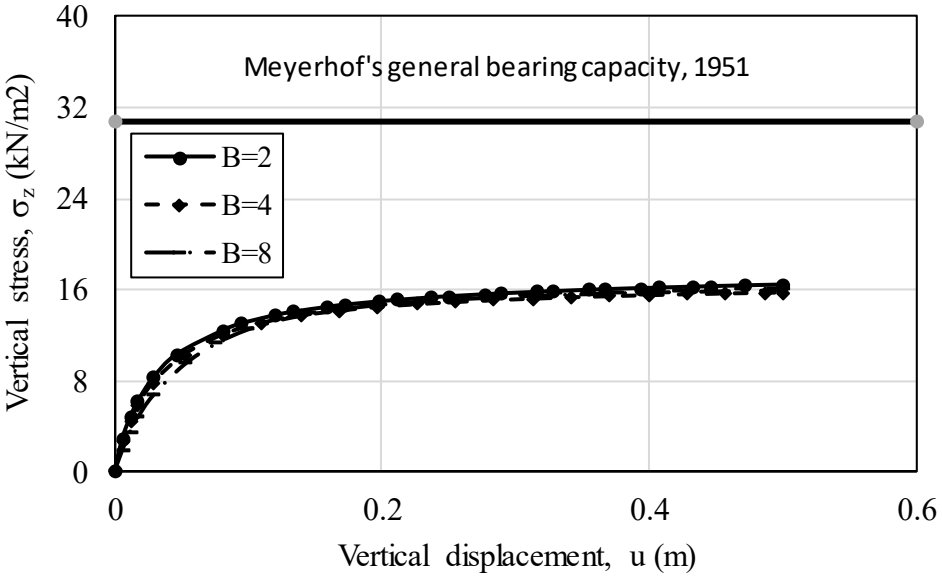
Meyerhof's general bearing capacity, 1951
B=2
B=4
B=8
Vertical stress, σz (kN/m2)
Vertical displacement, u (m)
0
8
16
24
32
40
0
0.2
0.4
0.6

(a)

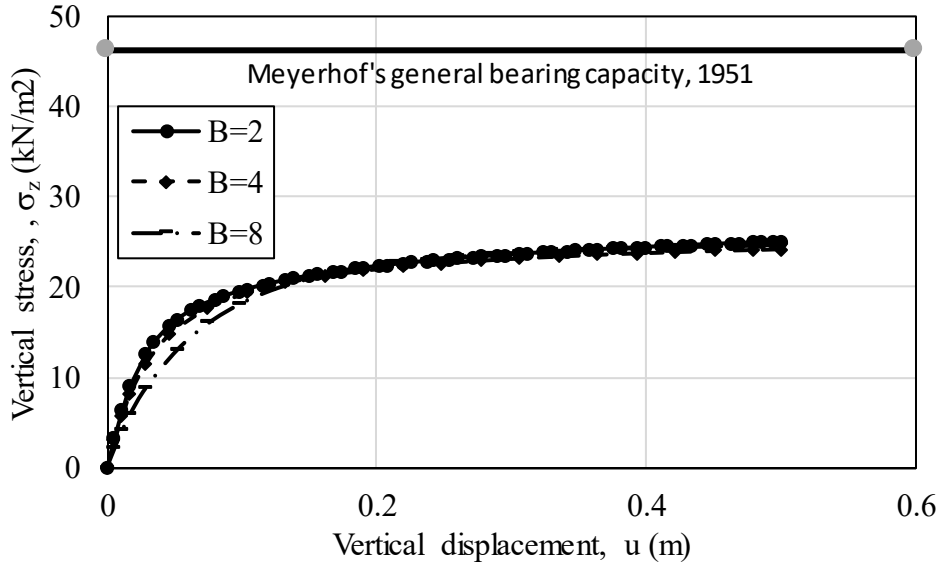
Meyerhof's general bearing capacity, 1951
B=2
B=4
B=8
Vertical stress, , σz (kN/m2)
Vertical displacement, u (m)
0
10
20
30
40
50
0
0.2
0.4
0.6

(b)

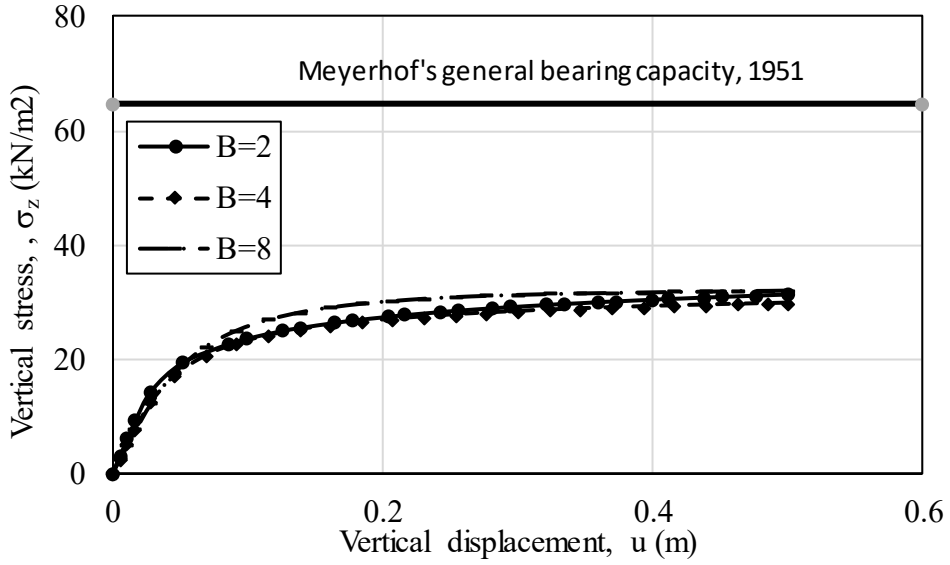

(c)

Figure 5.39 Vertical stress-displacement curve for rigid footing supported by unreinforced soft clay

Table 5.5 Correlation between drained and undrained shear values of clay soil

Drained internal friction angle, ϕ_c' (Degrees)	Vertical stress under the footing, σ_z' (kPa)	Horizontal stress under the footing, $\sigma_y' = \sigma_x'$ (kPa)	Undrained cohesion, C_u (kN/m^2)
10	15.2	8.7	4.97
20	15.2	5.2	7.54
30	15.0	3.3	9.35

5.5.5.2 Stress ratio

Under rigid footings supported by reinforced soil, the stress is concentrated on the column due to its high stiffness compared to clay soil (Black et al., 2007; Hanna et al., 2013). The ratio between the stresses on stone columns to the clay soil is defined as stress ratio (*n*). In the literature, the suggested stress ratio ranges from 2 to 6 at the surface of the soil (Mitchell, 1981; McKelvey et al., 2004; Ambily et al., 2007). In this study, the stress ratio was represented as a function of the normalized depth (Z/B), where B is the footing width and Z is the depth. The stress was measured at the center of the stone column at distance of 1.0*D* and 1.5*D* from the centerline of the stone column in the clay soil as shown in Figure 5.40. The position of measuring the stressed clay does not have an effect on the stress ratio except for the maximum value. For these results, the stresses of the clay were measured at a distance of 1.5*D*.

Figure 5.41 represents the effect of the replacement ratio on the stress ratio for a clay soil reinforced by a single stone column. It is obvious that the stress ratio increased by increasing the replacement ratio

(i.e. n = 2.3, 13.0 for A_s = 7.1%, 28.3% respectively). The stress ratio significantly increased with depth and the maximum value was found at Z/B of 0.25, 0.4 for a replacement ratio of 7.1 and 28.3%, respectively. In a higher normalized depth, the stress ratio dramatically reduced to around 8 at a normalized depth of 0.8 to 1.2 for replacement ratio of 7.1% and 28.3% respectively. At the stone column tip, the stress ratio reduced to a minimum value of 2.5 and 4 for a replacement ratio of 7.1% and 28.3% respectively.

Figure 5.42 (a) to (d) show the stress ratio for a clay soil reinforced by a group of two stone columns (A_s = 6.3%) with spacing ratio changed from 1.5 to 3. The clay stress was measured between the stone columns and around the group at a distance of 1.5D. The replacement ratio for the two columns was 6.3%. Generally, it was noticed that the stress ratio for a group of stone columns are less than a single stone column at the same replacement ratio. For a small spacing/diameter ratio (S/D = 1.5), the stresses in the clay soil between stone columns were less than the external clay soil. For a small spacing ratio, the amount of clay between stone columns is small, and the stone columns are deformed in the horizontal direction toward the edge of the footing (Figure 5.43); so, the clay between stone columns is not totally confined. When the spacing ratio increased (i.e. $S/D \geq 2$), the stress applied on the clay soil also increased, while the vertical stress in the stone columns decreased. Thus, the stress ratio decreased as the spacing between the stone columns increased (i.e. n_{max} = 24, 20.5, 20.3, 20.2 for S/D = 1.5, 2.0, 2.5, 3.0). The same trend is observed for clay soil reinforced by four stone columns at a replacement ratio of 12.6%, as shown in Figure 5.44.

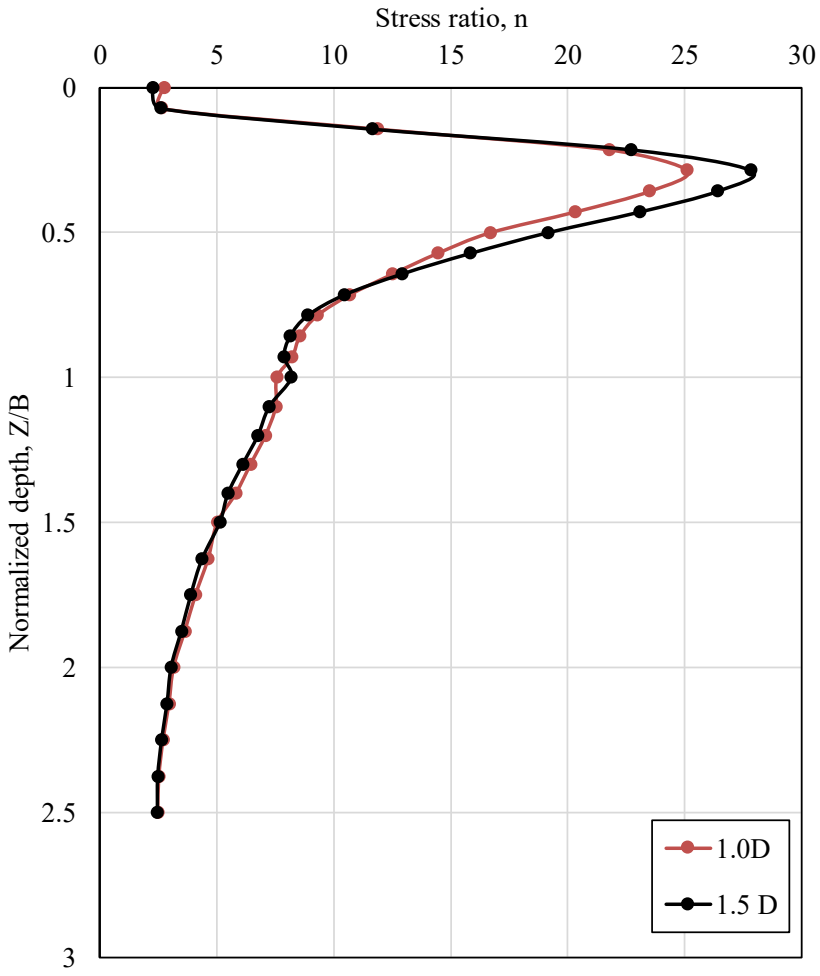

Figure 5.40 Relation between stress ratio and normalized depth of single stone column at A_s 7.1%

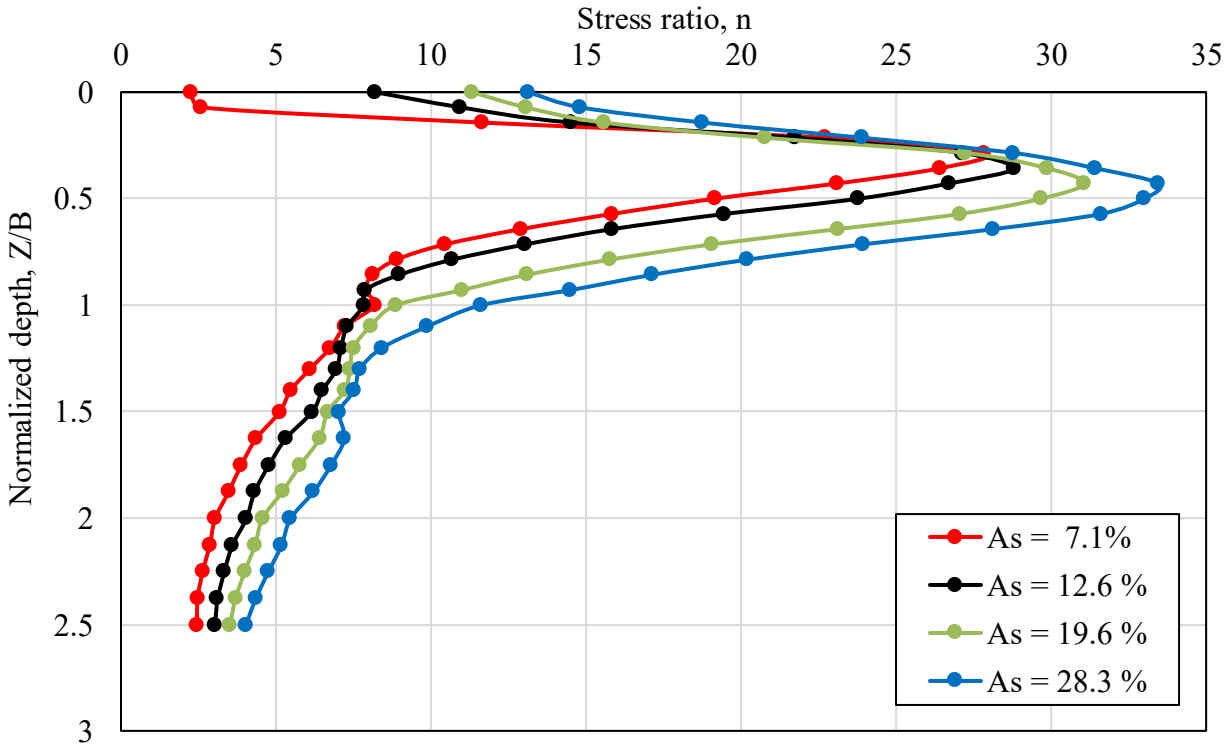

Figure 5.41 Effect of replacement ratio on the stress ratio for clay soil reinforced by a single stone column

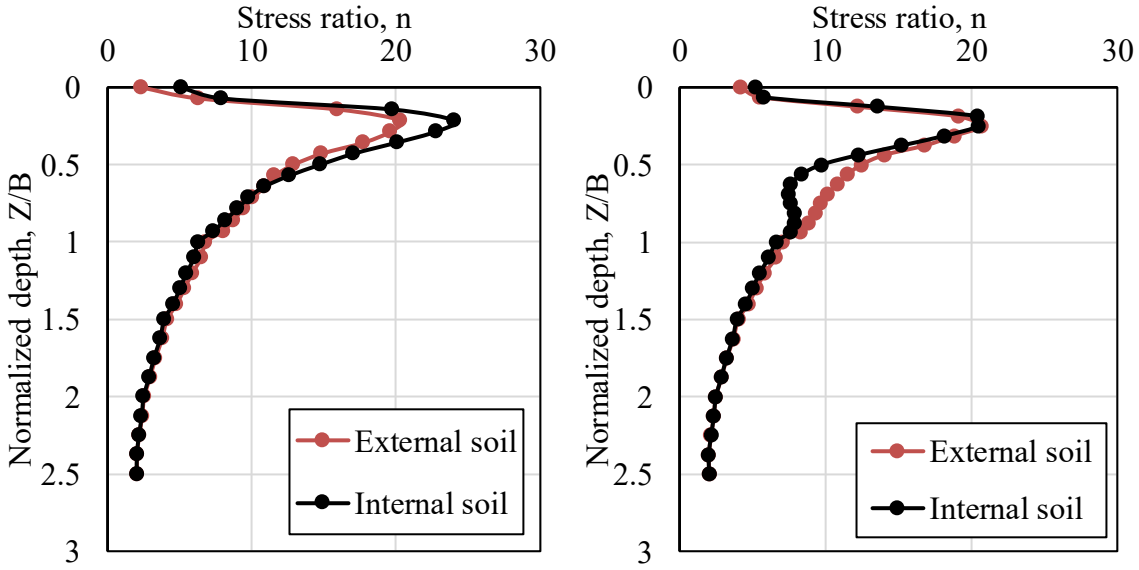

(a) (b)

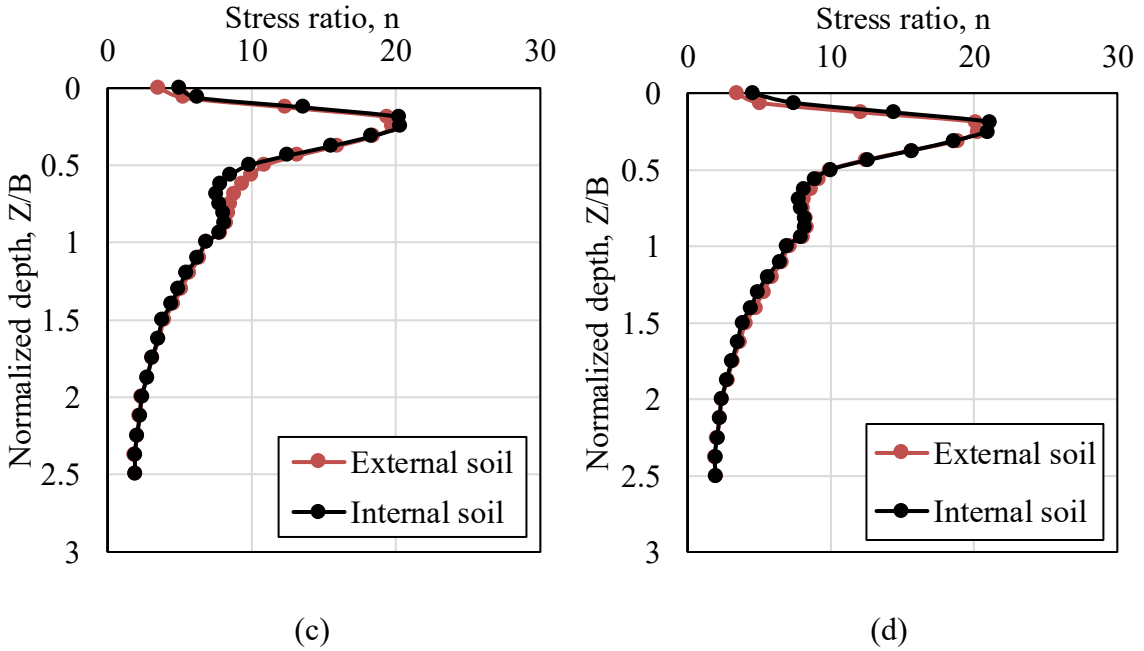

(c) (d)

Figure 5.42 Stress ratio for clay soil reinforced by 2 stone columns, A_s = 6.3%: (a) *S/D* = 1.5, (b) *S/D* = 2.0, (c) *S/D* = 2.5, (d) *S/D* = 3.0.

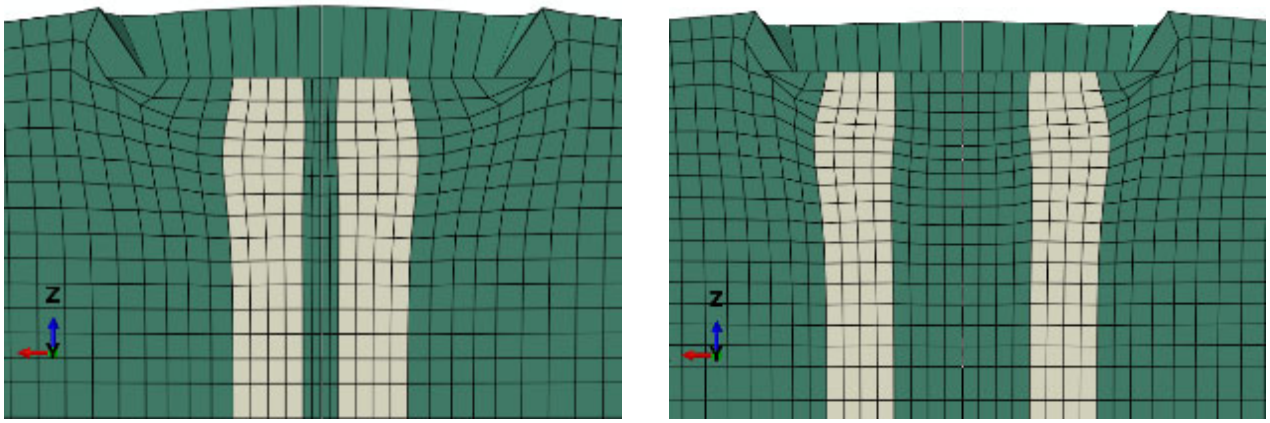

(a) (b)

Figure 5.43 Deformation shape for clay soil reinforced by 2 stone columns: (a) *S/D* = 1.5, (b) *S/D* = 3.0

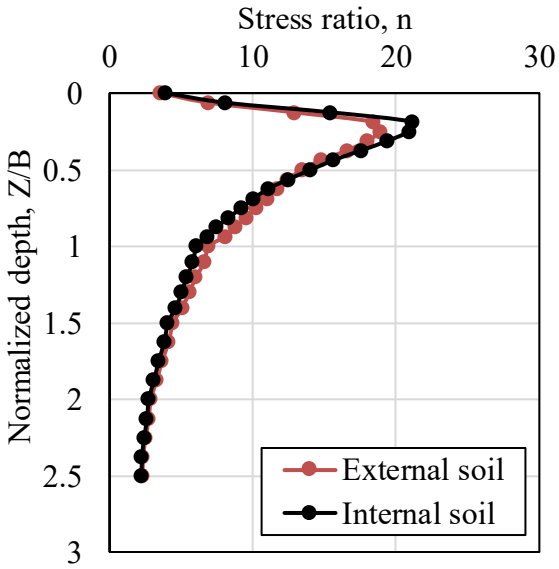
Stress ratio, n
0
10
20
30
Normalized depth, Z/B
0
0.5
1
1.5
2
2.5
3
External soil
Internal soil

(a)

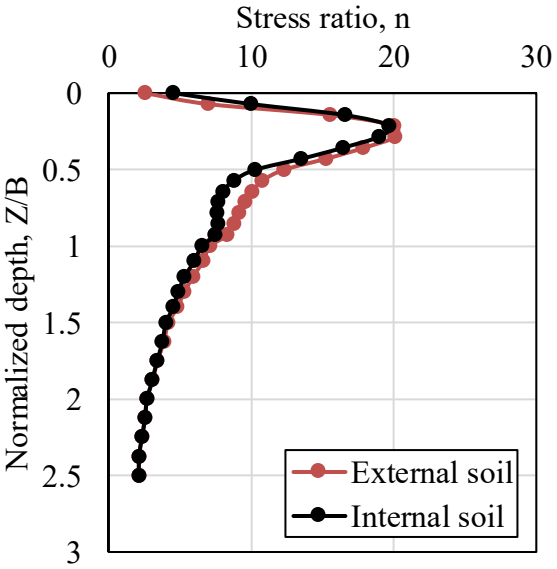
Stress ratio, n
0
10
20
30
Normalized depth, Z/B
0
0.5
1
1.5
2
2.5
3
External soil
Internal soil

(b)

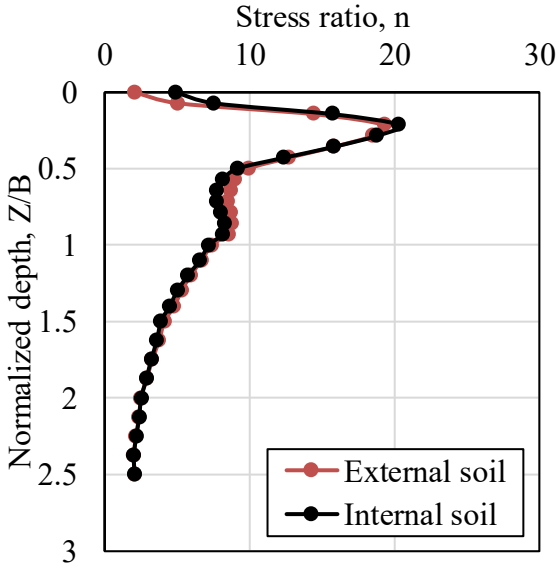
Stress ratio, n
0
10
20
30
Normalized depth, Z/B
0
0.5
1
1.5
2
2.5
3
External soil
Internal soil

(c)

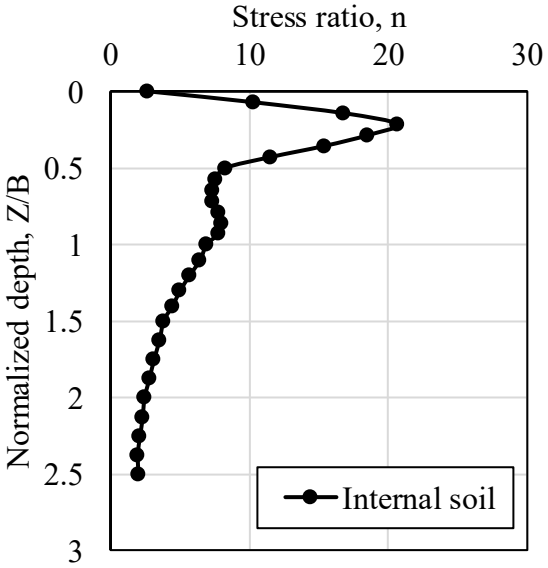
Stress ratio, n
0
10
20
30
Normalized depth, Z/B
0
0.5
1
1.5
2
2.5
3
Internal soil

(d)

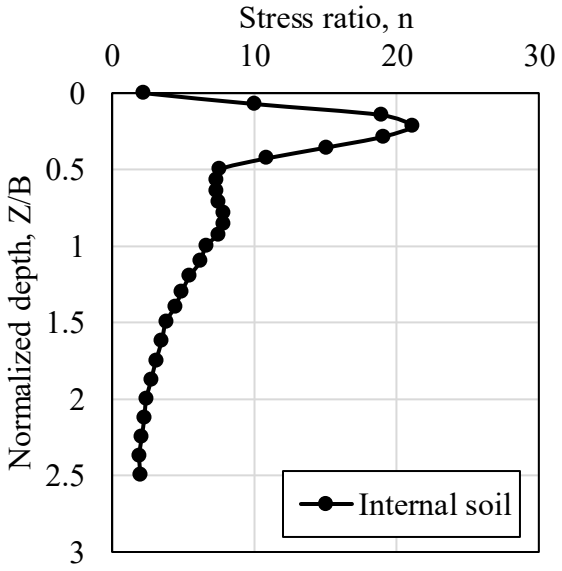

(e)

Figure 5.44 Stress ratio for clay soil reinforced by 2 stone columns, A_s = 12.6%: (a) *S/D* = 1.5, (b) *S/D* = 2.0, (c) *S/D* = 2.5, (d) *S/D* = 3.0, (e) *S/D* = 3.5

Figure 5.45 shows the effect of replacement ratio on the maximum stress ratio for clay soil reinforced by single and group of stone columns. For single stone columns, the stresses carried by the stone column increased by increasing the replacement ratio. Thus, the maximum stress ratio increased by increasing the replacement ratio. However, the maximum stress ratio decreased by increasing the replacement ratio for a clay soil reinforced by a group of stone columns. In order to keep the same spacing ratio constant, the number of stone columns should increase. By increasing the number of stone columns under the footing, the stresses will be distributed between the soil and stone columns, which reduces the stress ratio.

Figure 5.46 presents the effect of the spacing ratio between stone columns on the maximum stress ratio. For spacing ratios less than two, the stress ratio reduced by increasing the spacing ratio. For a spacing ratio higher than two, the stress ratio does change by increasing the spacing ratio. The same behaviour occurred in clay soil reinforced by 2 and 4 stone columns at the replacement ratio of 6.3% and 12.6%, respectively. For spacing ratio 1.5, the stress ratio for clay soil reinforced by two stone columns is higher than four stone columns. For two stone columns, the replacement ratio is small, and the columns are closer to the footing center, which allows more stresses to be carried by the stone columns compared with the adjacent soil. In case of four stone columns, the columns are distributed on the full area of the footing, which improves the stress distribution between the clay and stone columns.

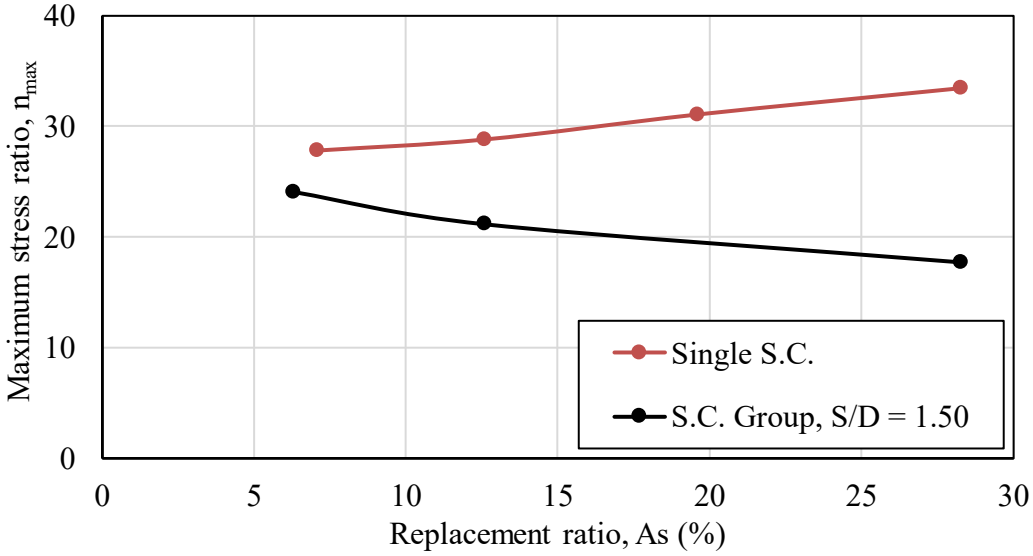

Figure 5.45 Comparison between maximum stress ratio for clay soil reinforced by single and group of stone columns, D = 0.8 m

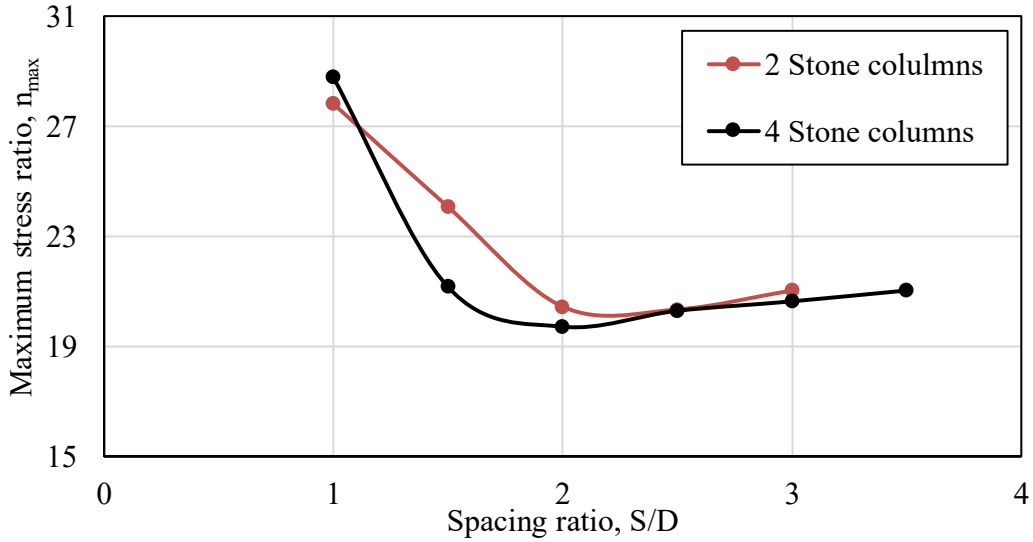

Figure 5.46 Effect of spacing ratio (*S/D*) on the stress ratio

The replacement and spacing ratios are not the only factors that control the stress ratio. The diameter of the stone columns also affects the resistance of soft clay soil reinforced by stone columns. In the numerical analysis, three global modes of failure mechanism were observed in the reinforced soil, namely: general shear failure, local shear failure, and punching shear failure (Figure 5.47). These failure mechanisms are confirmed by Hu (1995) and Hanna et al. (2013). In addition, there is an internal bulging failure that occurs in stone columns during all the global shear failures, and it matches Hu's (1995) findings from an experimental analysis as shown in Figure 5.48. The diameter of the stone columns is

one of the main factors that control the ultimate vertical stress capacity of a single stone column and ultimately a local bulging failure (Gibson et al., 1961; Barksdale et al., 1983a). In the literature, the footing size was assumed to be consistent, since it does not have an influence on the bearing capacity of the reinforced soil. In the current analysis, different footing widths were used in order to investigate the effect of a change in the diameter of the stone columns at the same replacement ratio. Figure 5.49 shows the effect of using the same replacement ratios for different stone column diameters. The maximum stress ratio increased by increasing the diameter of the stone columns at the same replacement ratio (i.e. for A_s = 7.1%, n_{max} = 16.8 for D = 0.6 m & n_{max} = 27.1 for D = 1.2 m).

Figure 5.50 presents the effect of changing the number of stone columns on the stress ratio at the same replacement ratio and diameter. When the diameter and replacement ratio are constant, the number of stone columns does not affect the stress ratio.

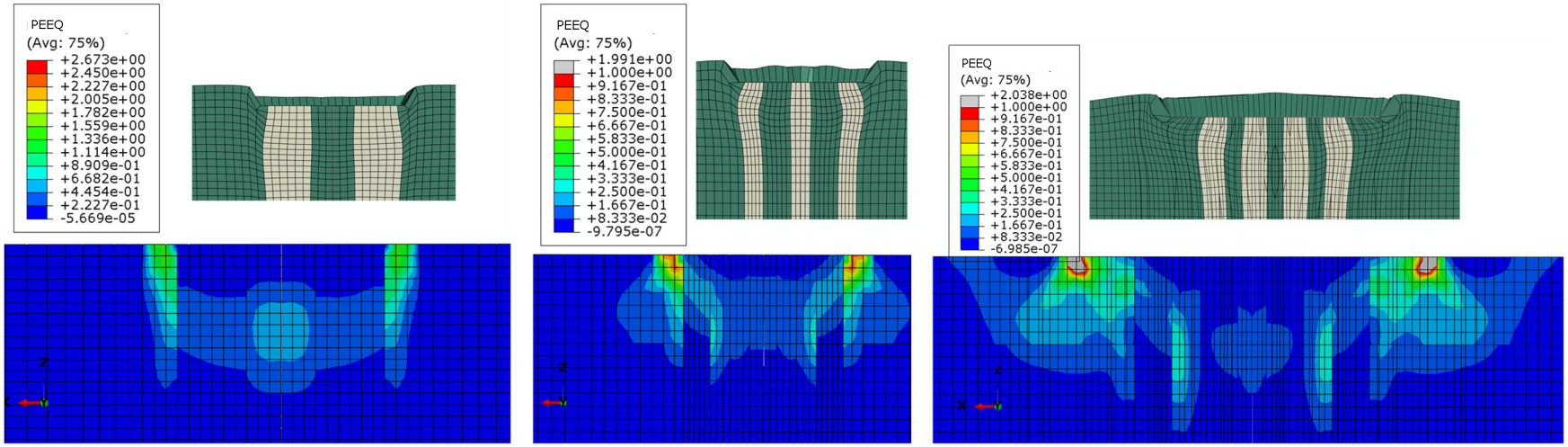

(a) (b) (c)

Figure 5.47 Failure mechanisms in reinforced clay soil: (a) punching shear failure, A_s = 14.1 %, D = 0.6 m, (b) local shear failure, A_s = 15.9 %, D = 0.6 m, (c) General shear failure, A_s = 19.6 %, D = 1.00 m

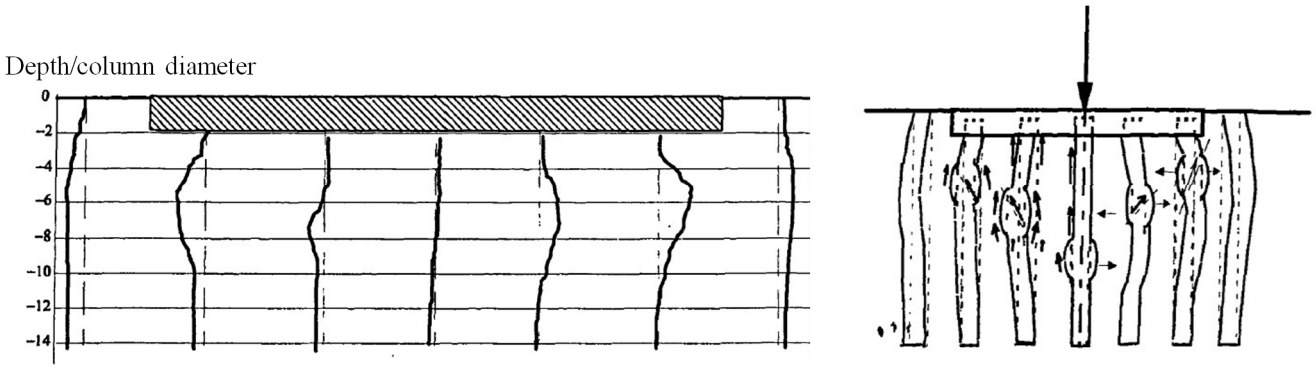

Figure 5.48 Stone columns deformation under rigid footing at failure, after (Hu, 1995)

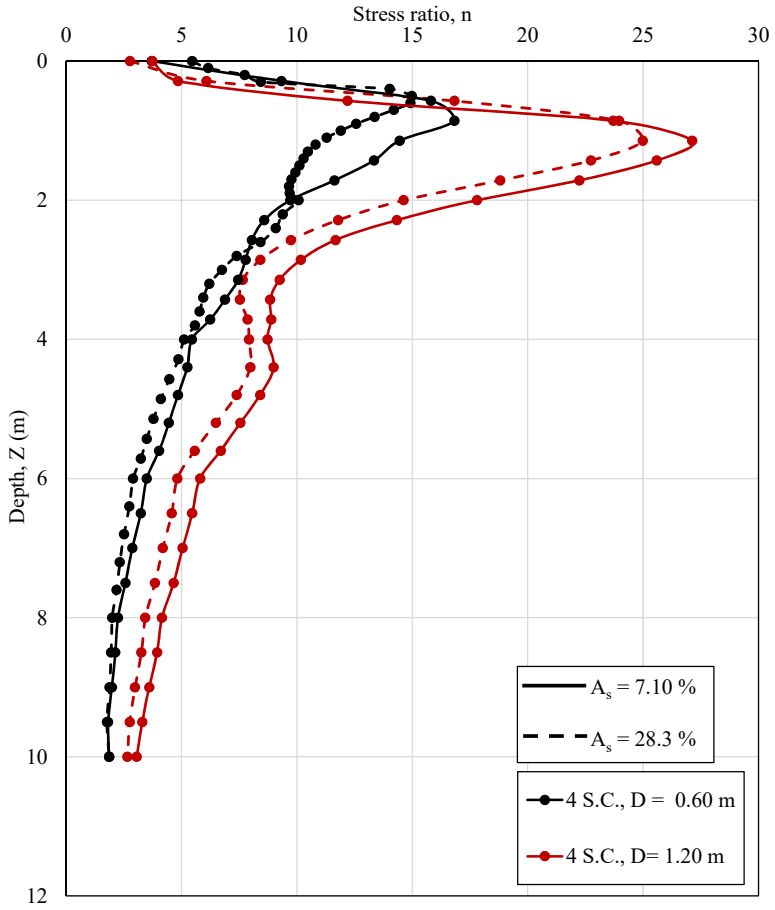

Figure 5.49 Effect of stone columns diameter on stress ratio at the same replacement ratio

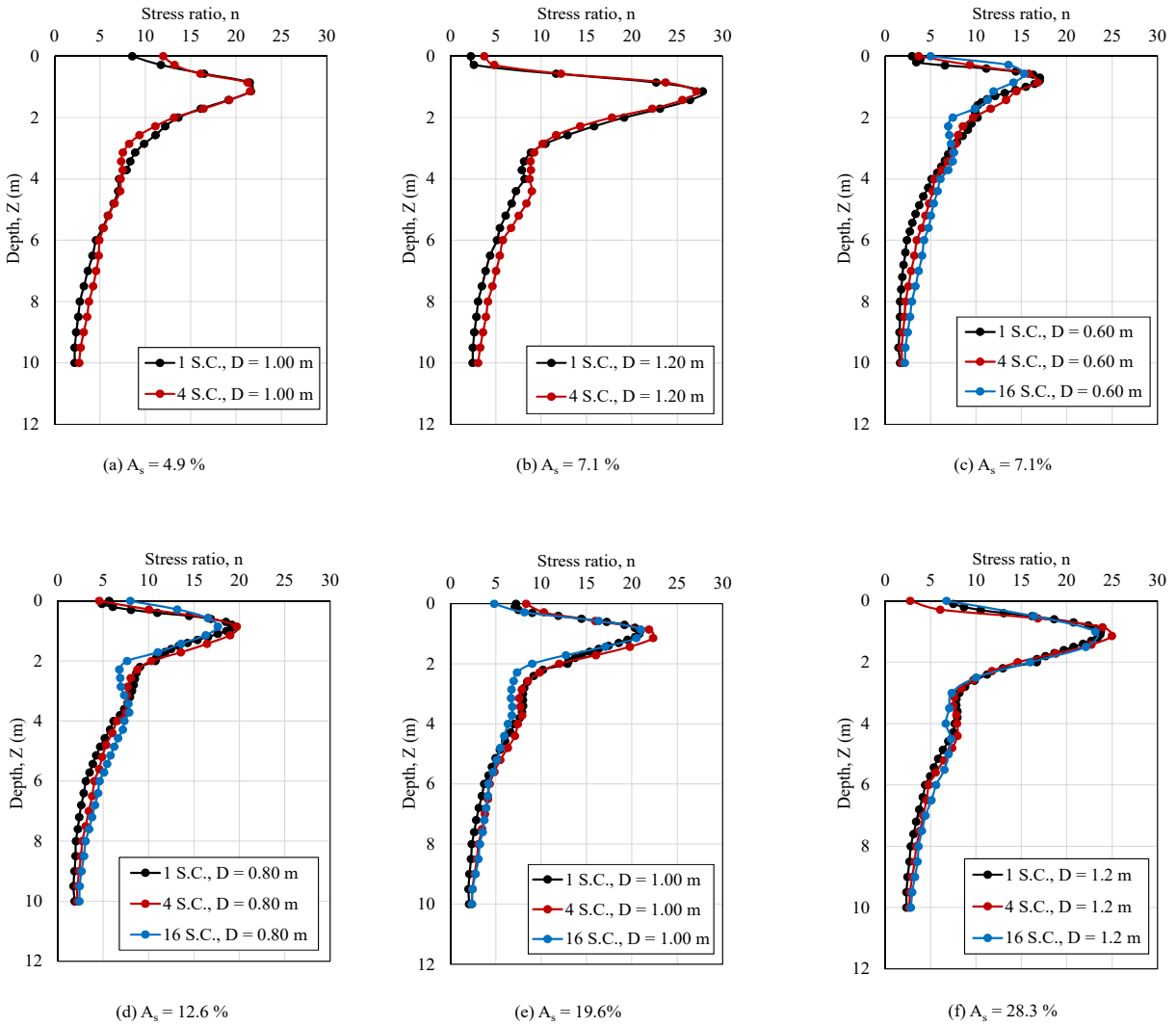

Figure 5.50 Effect of number of stone columns with the same diameter and replacement ration on the stress ratio

Increasing the drained shearing resistance of stone column material ($\phi_{s'}$) is expected to increase the stress ratio. Figure 5.51 shows the effect of increasing the stone friction angle from 30° to 50°. A significant increase happened in the shallow part (Z/B ≤1), then the rate of increase reduced with depth.

In practice, the stone columns are more efficient in soft clay soil, so the drained shear resistance of the clay soil changes normally between 10° to 20°. Since a large percent of vertical stress is carried by stone columns, increasing the drained shear resistance of clay soil will slightly increase the total resistance of the reinforced soil as well as the stress ratio.

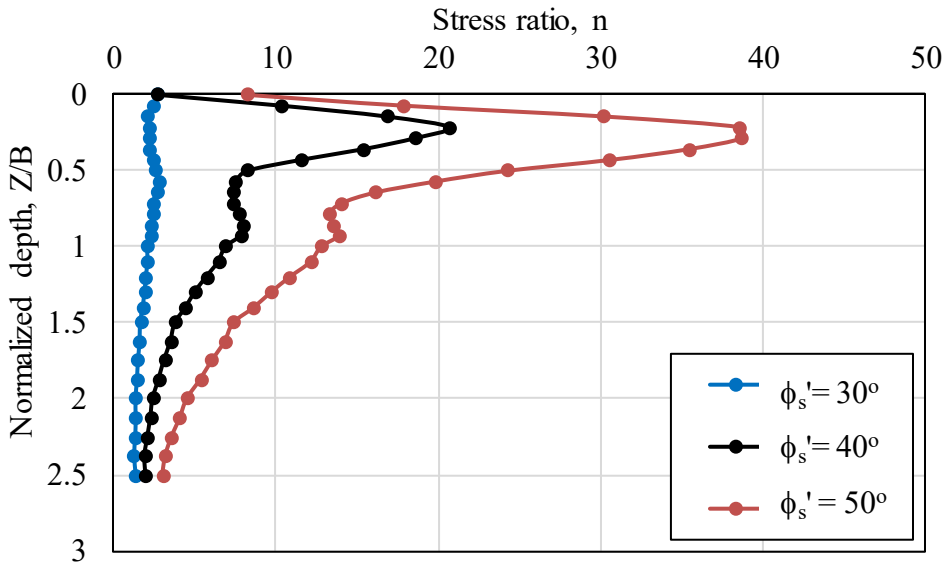

Figure 5.51 Effect of drained friction angle of stone columns materials on the stress ratio (4 stone columns and S/D = 3, A_s = 12.6%, $\phi_{c'}$ = 10°)

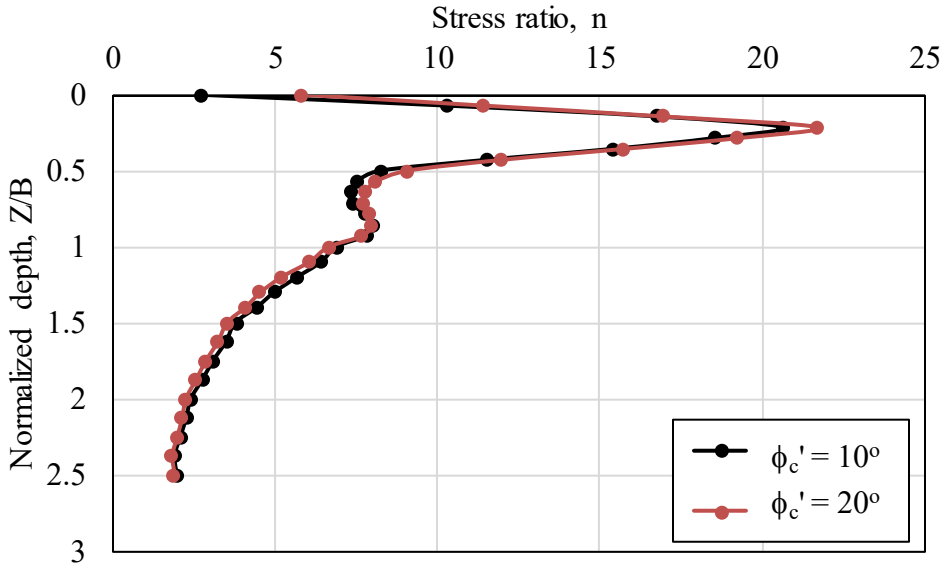

Figure 5.52 Effect of drained angle of shear resistance on clay soil on the stress ratio (4 stone columns, $S/D = 3$, $A_s = 12.6\%$, $\phi_s' = 40^o$)

5.5.5.3 Stress-displacement curve

In this section, the vertical stress-displacement curve for all the numerical models are presented, which is later used to estimate the bearing capacity of rigid footing supported by soft clay soil reinforced by stone columns. Figure 5.53 shows the effect of increasing the replacement ratio on the vertical stress resistance of clay soil ($\phi_c'=10^o$) reinforced by a single stone column ($\phi_s'= 40^o$). It is noticeable that increasing the replacement ratio leads to an increase in the bearing capacity of the reinforced soil. Another noticeable effect is that the replacement ratio is not the only factor that controls the resistance of the reinforced soil. As the footing width increases the resistance on the reinforced soil increases. This phenomenon could be explained by the effect of the stone column diameter described in the previous section. In order to maintain the same replacement ratio in a bigger footing, a bigger stone column diameter is used, which means that the stone columns will carry more stress and the overall resistance of the soil is increased. Therefore, the diameter of the used stone columns, as well as the total replacement ratio under the footing, have a major influence on the resistance of the reinforced soil.

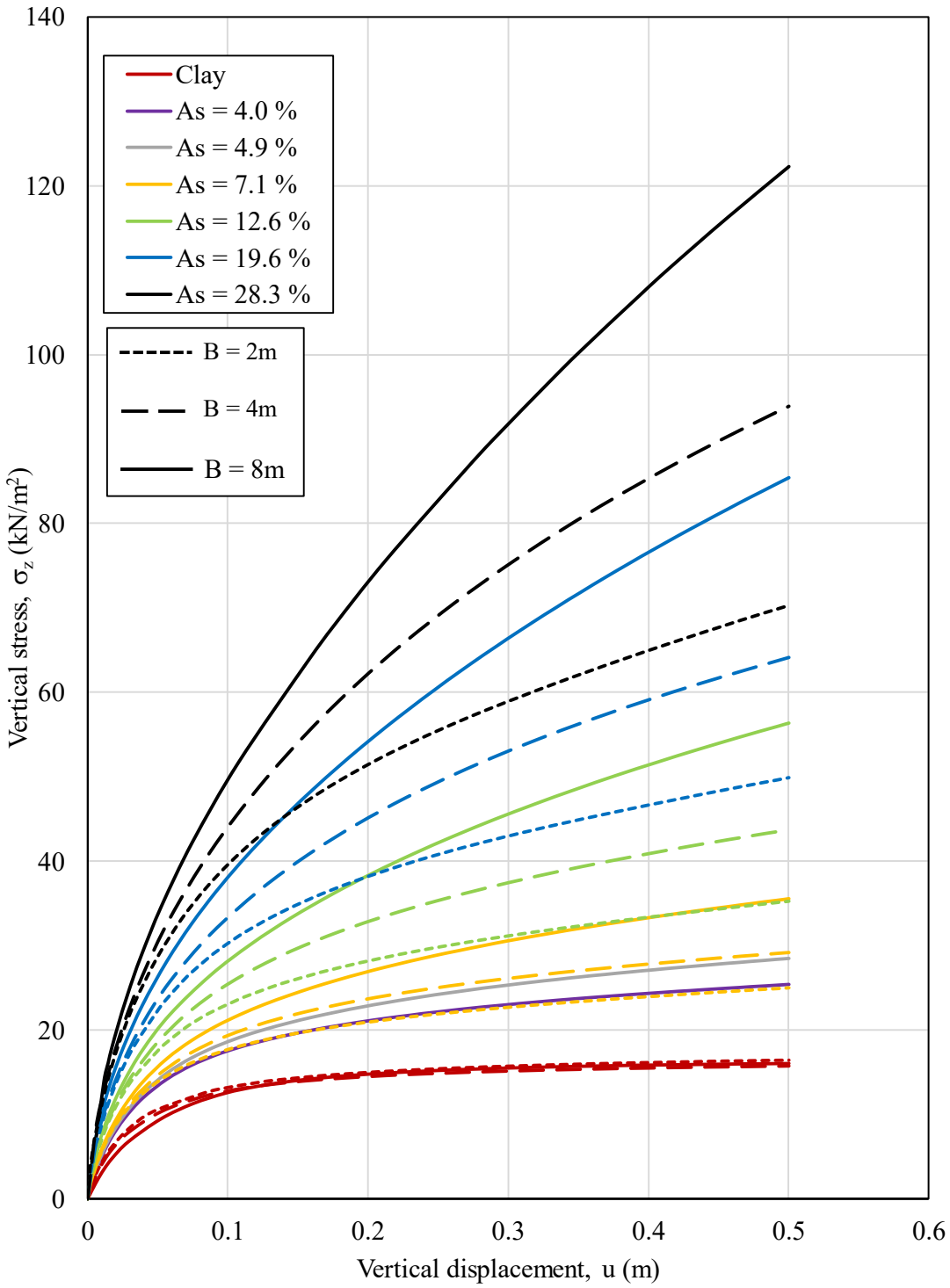

Figure 5.53 Summary of vertical stress-displacement curve for clay soil reinforced by single stone column ($\phi_s' = 40^o$, $\phi_c' = 10^o$)

In order to investigate the effect of increasing the replacement ratio on the performance of clay soil reinforced by a group of stone columns, the width of the footing was changed while keeping all the stone columns geometric parameters constant. Figure 5.54 (a), (b), (c) represent stress-displacement curves for

clay soil (ϕ_c'=10°) stone column group (ϕ_s'= 40°) with diameters of 0.6m, 0.8m and 1.2m, respectively. The resistance of the reinforced soil dramatically increased by increasing the replacement ratio at the same stone column diameter. However, the number of stone columns with the same diameter does not have a significant effect on bearing resistance of the reinforced soil at the same replacement ratio. Furthermore, increasing the diameter of the stone columns enhances the total resistance of the reinforced soil at the same replacement ratio. Stress-displacement curves for different stone column diameters at the same replacement ratio is shown in Figure 5.55. Stone columns diameter is more effective in higher replacement ratio. By increasing the stone column diameter from 0.6m to 1.2m, the bearing resistance increased by 30% and 14.3%, for replacement ratios of 28.3% and 7.1%, respectively. The effect of the spacing between stone columns is investigated in this study. It was noticed that the spacing between stone columns does not have a significant effect on bearing resistance of the reinforced soil, as shown in Figure 5.56.

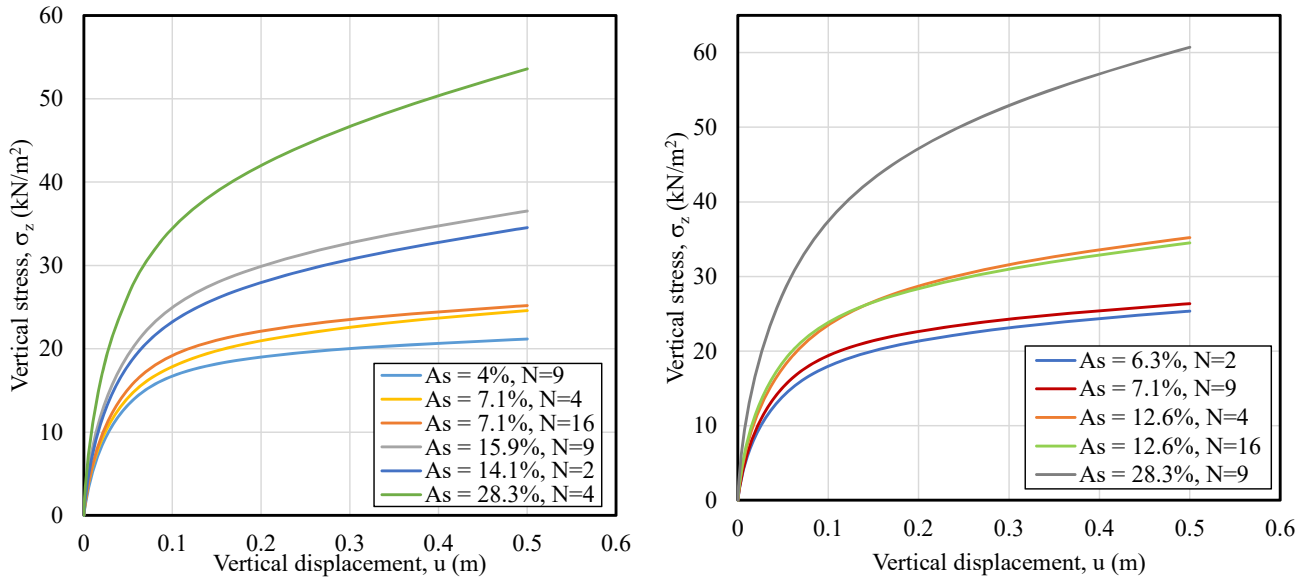

(a) (b)

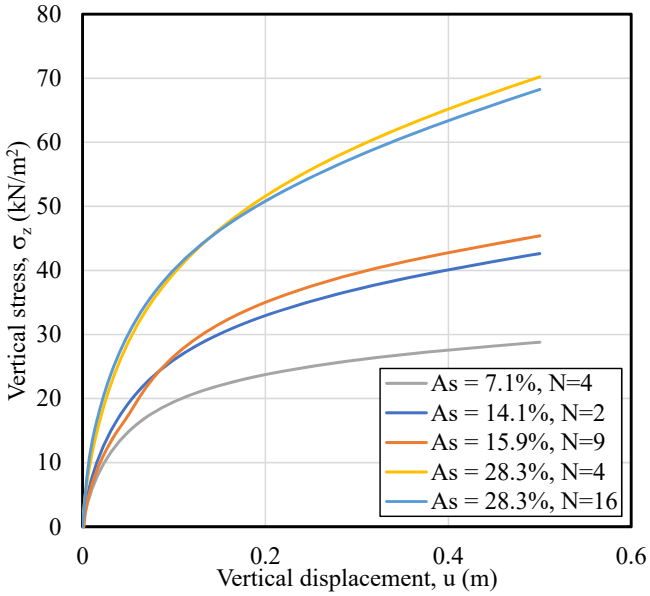

(c)

Figure 5.54 Stress-displacement curve of clay soil reinforced by group of stone columns at different replacement ratios: (a) D = 0.6m, (b) D = 0.8m, (c) D =1.2m

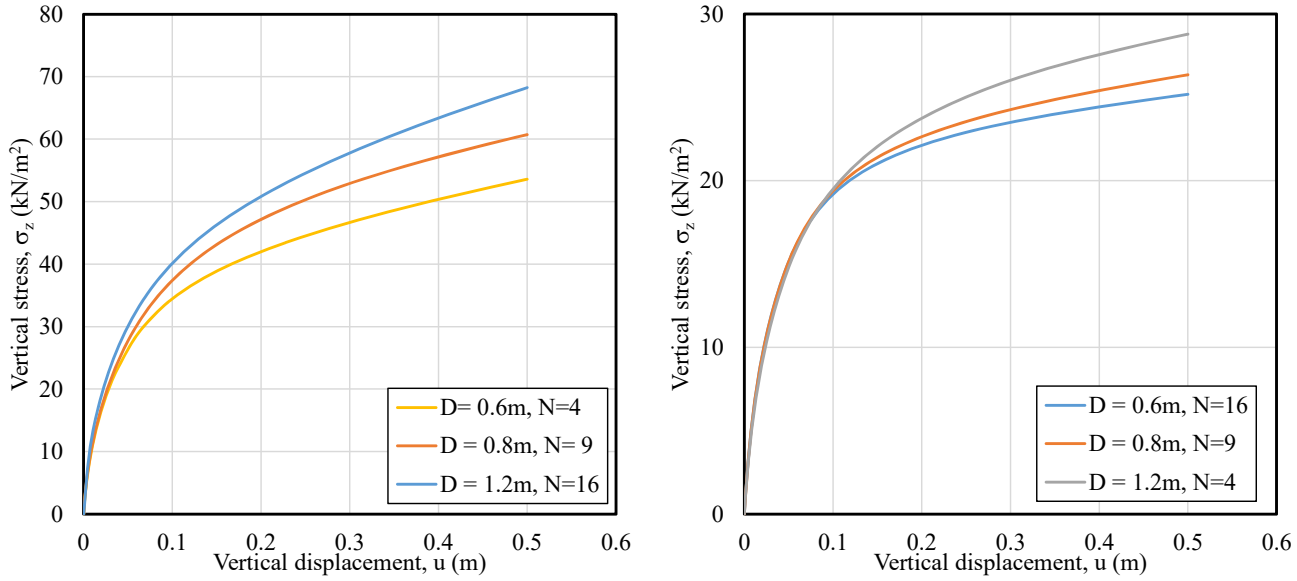

(a) (b)

Figure 5.55 Stress-displacement curve of clay soil reinforced by group of stone columns with different diameters: (a) A_s = 28.3%, (b) A_s = 7.1%

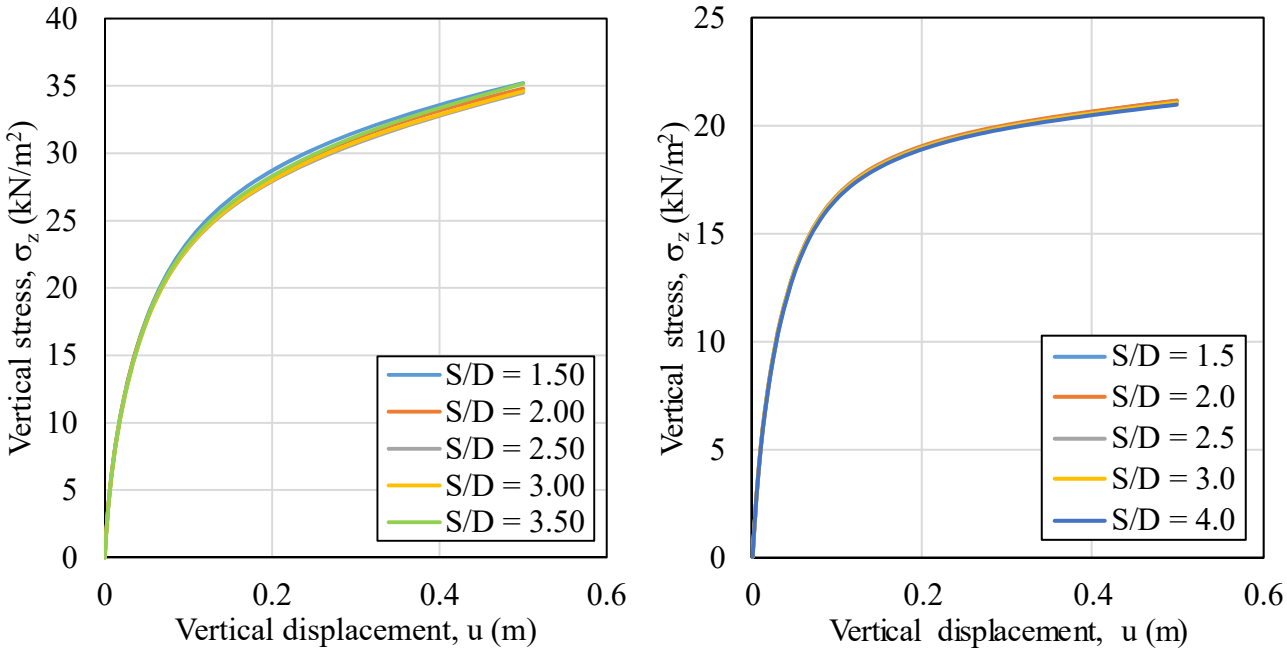

(a) A_s = 12.6%, N = 4, D = 0.8m

(b) A_s = 4.0%, N = 9, D = 0.6m

Figure 5.56 Effect of spacing between stone columns on the bearing resistance of reinforced soil

Changing the drained internal friction angle of the stone column materials, ϕ_s' and clay soil ϕ_c' are expected to have a major influence on the bearing capacity of the reinforced soil. Thus, the effect of the drained friction angle of clay soil and stone columns on the bearing resistance of the system using single and group arrangements are shown in Figure 5.57 and Figure 5.58, respectively. It was noticed that increasing the drained friction angle of the clay soil slightly increases the bearing resistance of the reinforced soil (i.e. for change in ϕ_c' from 10° to 20° the bearing resistance increased by 14% for A_s = 28.3%). However, increasing the drained friction angle of stone columns significantly improved the bearing resistance of the reinforced soil (i.e. by increasing ϕ_s' from 40° to 50° the bearing resistance enhanced by 90% for A_s = 28.3%). The difference between the effect of the drained friction angle of stone columns and clay soil was expected because a higher percentage of the bearing stress was resisted by the stone columns, as described in section 5.5.5.2.

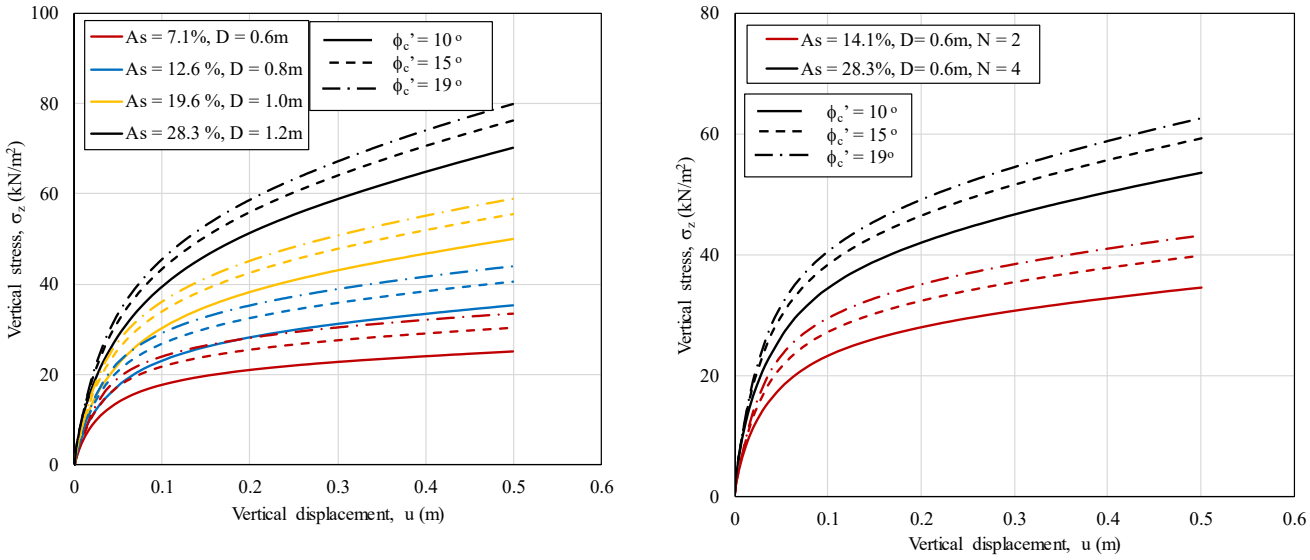

(a) (b)

Figure 5.57 Effect of drained friction angle of clay soil on the bearing resistance of reinforced soil: (a) Single stone column, (b) Group of stone columns

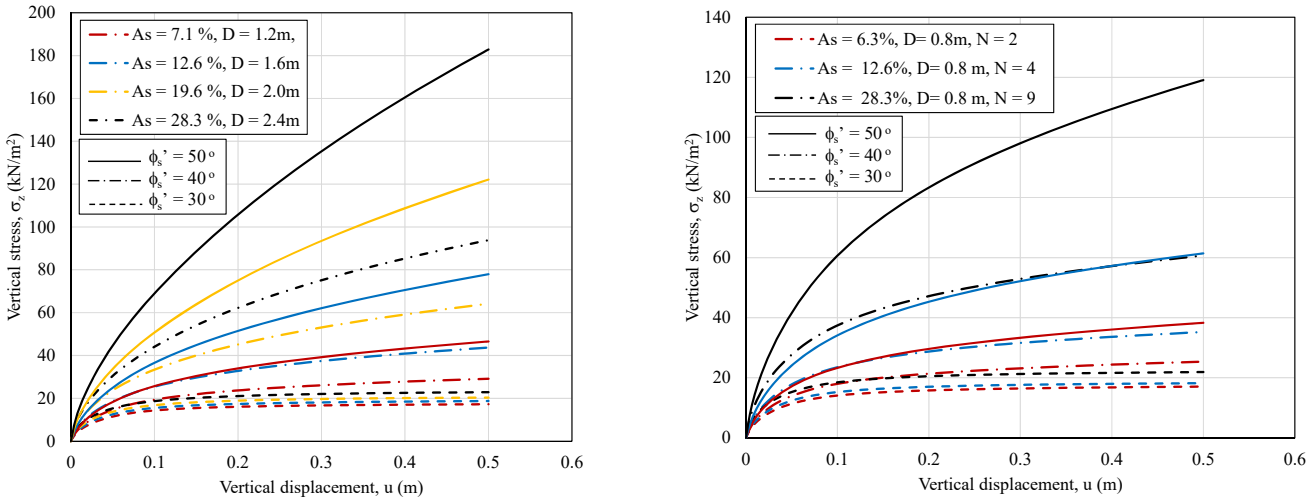

(a) (b)

Figure 5.58 Effect of drained friction angle of stone columns on the bearing resistance of reinforced soil: (a) Single stone column, (b) Group of stone columns

5.5.5.4 Improving factor (I_F) and design charts

In this section, the results are presented as a function of the improvement factor (I_F), which is defined as the ratio between the bearing capacity of reinforced and unreinforced clay soil. The bearing capacity was calculated from the stress-displacement curves obtained from the FEE numerical model based on the tangential method as described in section 5.3.6. Based on the results presented in section 5.5.5.3, the

main factors that control the bearing capacity of the reinforced soil are the replacement ratio and the stone column diameter. Therefore, the relation between the stone column diameter and the improvement factor for a rigid footing reinforced by a single stone column with different replacement ratios is presented in Figure 5.59. For practical use, equation (5-10) could be used to estimate the improvement factor for a single stone column with a given diameter. The factor (a_1, b_1, c_1, d_1) was found to be in a linear relation with the replacement ratio as shown in Figure 5.60, and could be calculated by applying equations (5-11), (5-12), (5-13), and (5-14), respectively

$$I_{F\,\text{single},40} = a_1 e^{b_1 D} + c_1 e^{d_1 D} \tag{5-10}$$

Where

D is stone column diameter (m)

A_s is replacement ratio (%)

$$a_1 = 0.0995 \times A_s + 0.90 \tag{5-11}$$

$$b_1 = 0.00085 \times A_s + 0.032 \tag{5-12}$$

$$c_1 = -0.13 \times A_s + 0.15 \tag{5-13}$$

$$d_1 = 0.005 \times A_s - 1.65 \tag{5-14}$$

The improvement factor ($I_{Fsingle\ 40}$) was estimated for drained friction angle of stone columns and clay soil of 40° and 10°, respectively. In order to involve the effect of drain friction angles of stone columns and clay soil, the improvement factor calculated in equation (5-10) was multiplied by two friction angle coefficients, $K\phi_s$ & $K\phi_c$, for stone columns and clay soil respectively, as shown in equations (5-15). Figure 5.61 shows the relation between the drained friction angle of stone columns and $K\phi_s$ for different replacement ratios. The coefficient $K\phi_s$ could be calculated using equations (5-16), (5-17), and (5-18). Figure 5.63 presents the effect of the replacement ratio on the coefficient $K\phi_c$ at different drained friction angle of the clay soil. It was noticed that increasing the drained friction angle of the clay soil reduces the improvement factor, however the overall resistance of the reinforced soil increased as described in section 5.5.5.3. Equations (5-19), (5-20), and (5-21) could be used to calculate the $K\phi_c$ coefficient.

$$I_{F\,single} = I_{F\,single,40} \times K\phi_s \times K\phi_c \tag{5-15}$$

Where

$$K\phi_s = a_2 \times \tan(\phi_s^{'}) + b_2 \tag{5-16}$$

$$a_2 = -0.0013 \times A_s^2 + 0.0835 \times A_s + 0.5316 \tag{5-17}$$

$$b_2 = 0.0012 \times A_s^2 - 0.0781 \times A_s + 0.6077 \tag{5-18}$$

$$K\phi_c = a_3 A_s + b_3 \tag{5-19}$$

$$a_3 = 0.0897 \tan^2\left(\phi_c^{'}\right) - 0.089 \tan\left(\phi_c^{'}\right) + 0.0129 \tag{5-20}$$

$$b_3 = 1.5039 \tan^2\left(\phi_c^{'}\right) - 1.2193 \tan\left(\phi_c^{'}\right) + 1.1682 \tag{5-21}$$

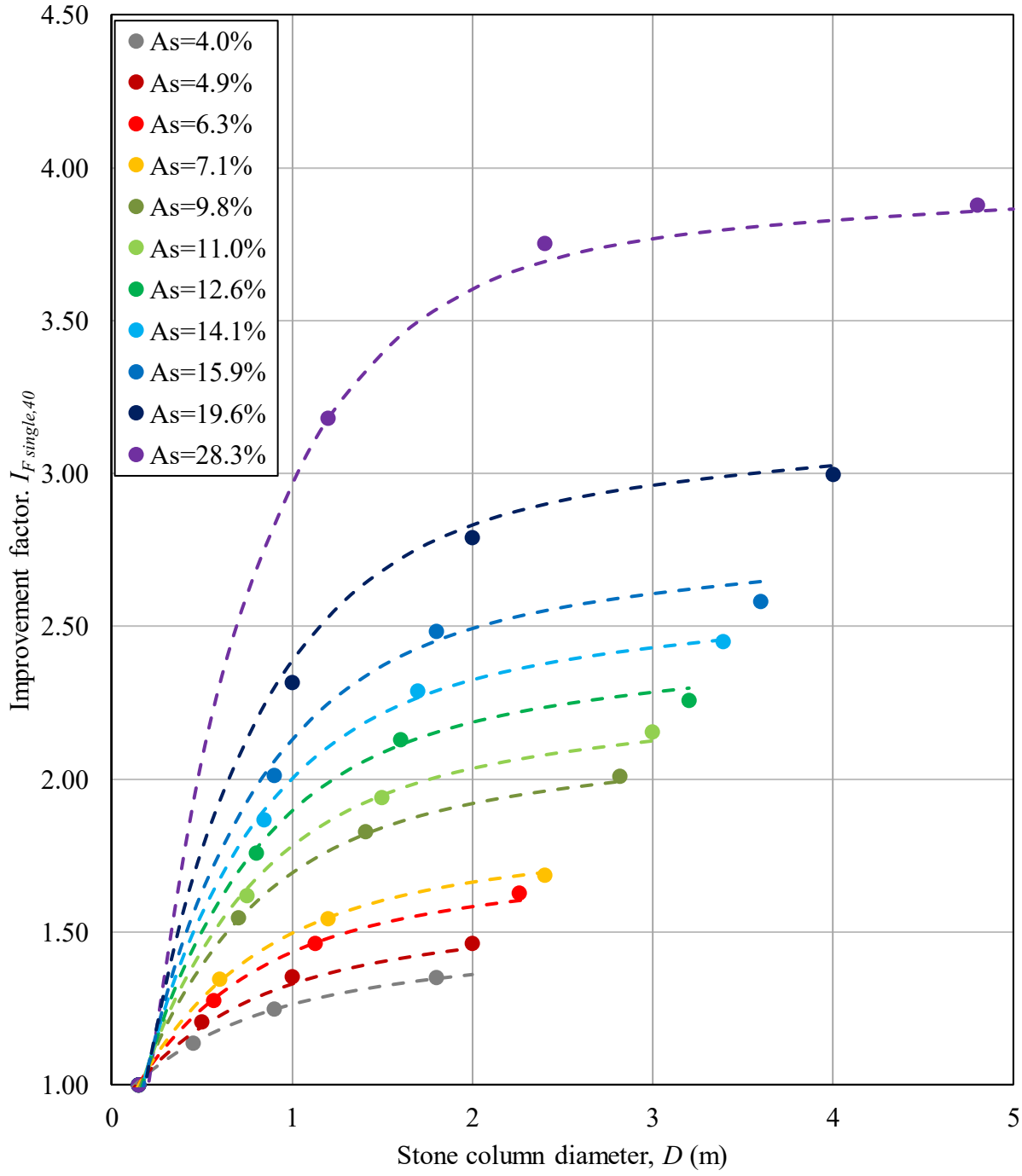

Figure 5.59 Design chart to estimate the bearing capacity improvement factor (Friction angle of stone, $\phi_s' = 40^o$)

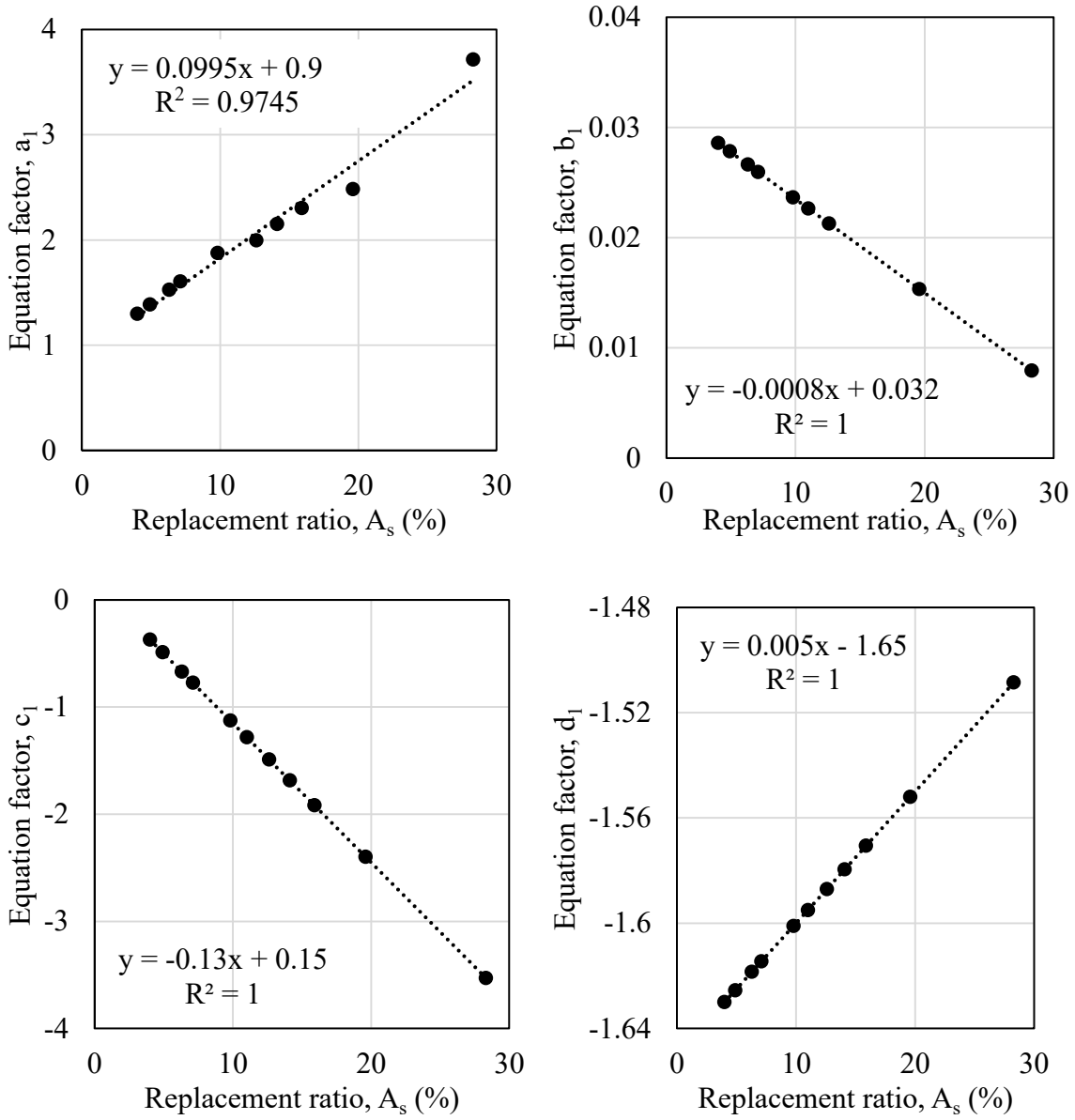

Figure 5.60 Equation's factors to estimate the bearing capacity improvement factor

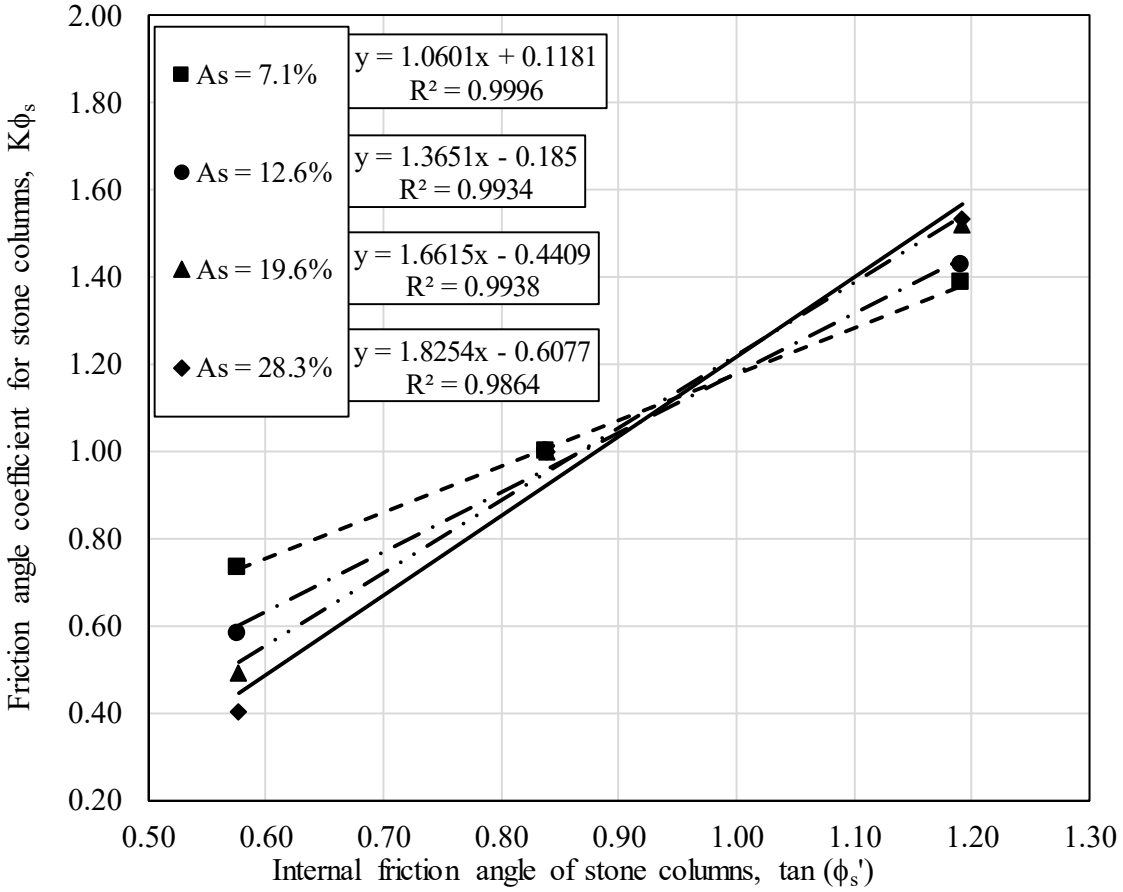

Figure 5.61 Friction angle coefficient for stone columns, $K\phi_s$

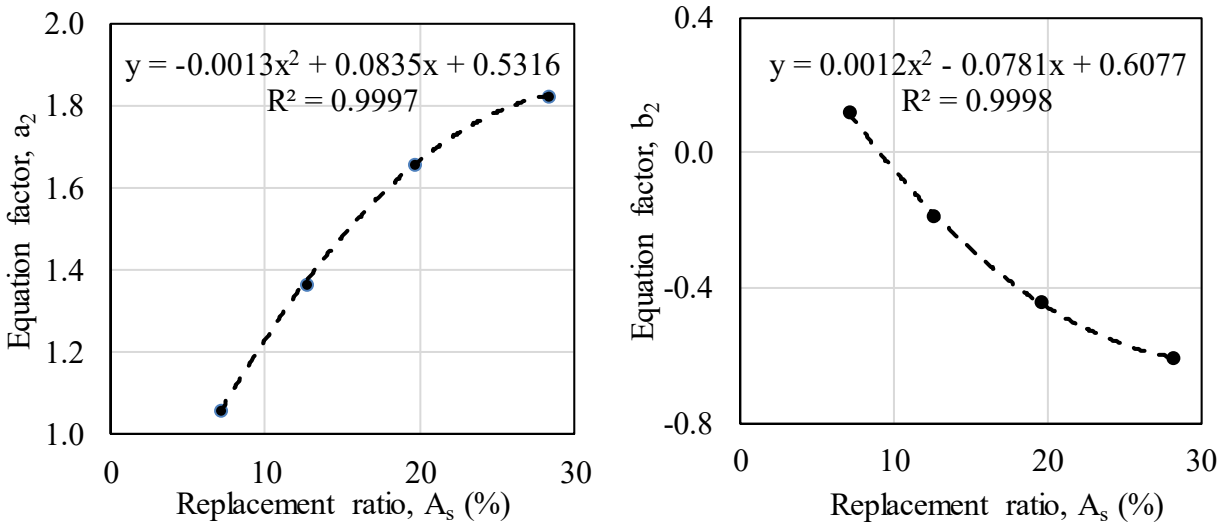

(a) (b)

Figure 5.62 Factors used to calculate stone columns friction angle coefficient for stone columns, $K\phi_s$

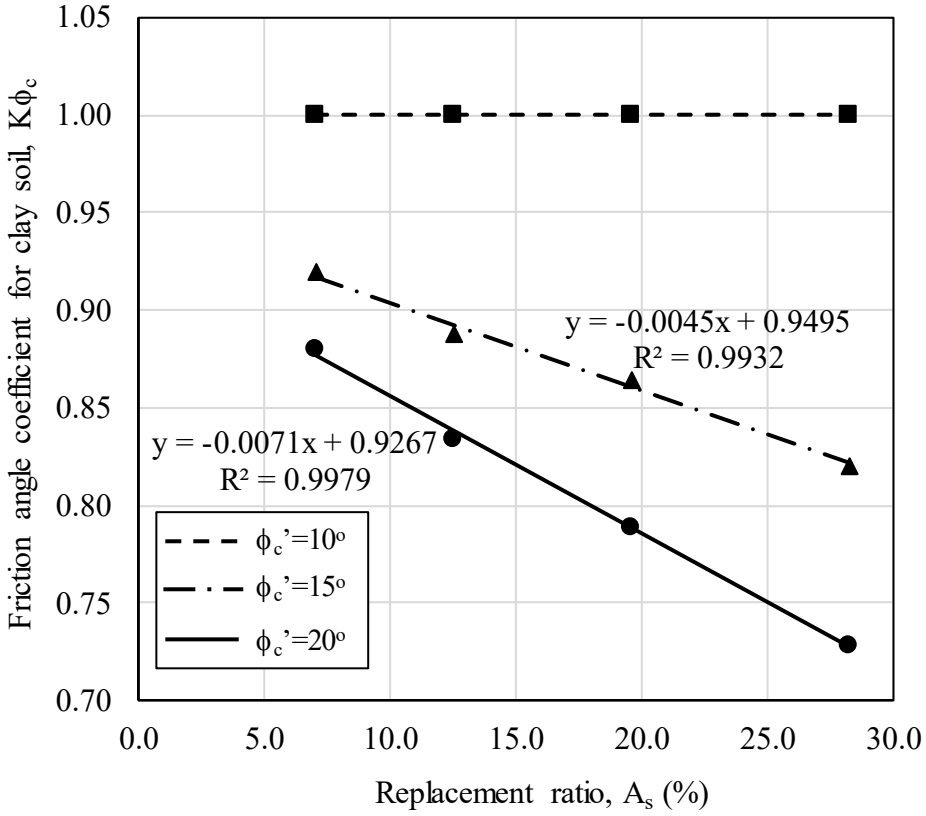

Figure 5.63 Clay soil drained friction angle coefficient, $K\phi_c$

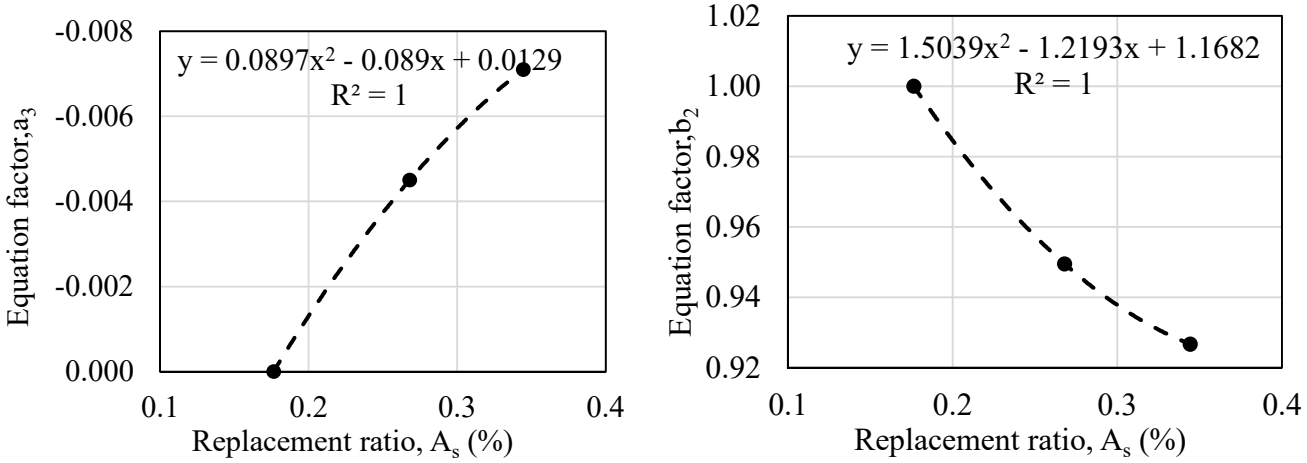

Figure 5.64 Factors used to calculate clay soil friction angle coefficient for clay, $K\phi_c$

Table 5.6 shows a comparison between the bearing resistance of a clay soil reinforced by a single and group of stone columns at the same replacement ratio and diameters. The group action slightly improved the bearing capacity of the reinforced clay soil. This improvement occurs due to the confinement of the clay soil surrounded by stone columns, which results in enhancing the overall capacity of the system. In

order to calculate the improvement factor of a clay soil reinforced by a group of stone columns ($I_{F\,group}$), the improvement factor for a single stone column calculated by equation (5-15) will be multiplied by a group coefficient (K_g) as shown in equation (5-19). Figure 5.65 shows the relation between the replacement ratio and the group coefficient.

Table 5.6 Comparison between IR for single and group of stone columns

Replacement ratio, A_s (%)	Stone column diameter, D (m)	$I_{F\,single}$	$I_{F\,group}$	
			$N = 4$	$N = 16$
7.10	0.60	1.52	1.56	1.57
12.60	0.80	2.15	2.23	2.15
19.60	1.00	3.04	3.17	3.03
28.30	1.20	4.28	4.45	4.26

$$I_{F\,group} = I_{F\,single} \times K_g \tag{5-22}$$

Where

$$K_g = -8\times10^{-5} \times A_s^2 + 0.0035A_s + 1.0058 \tag{5-23}$$

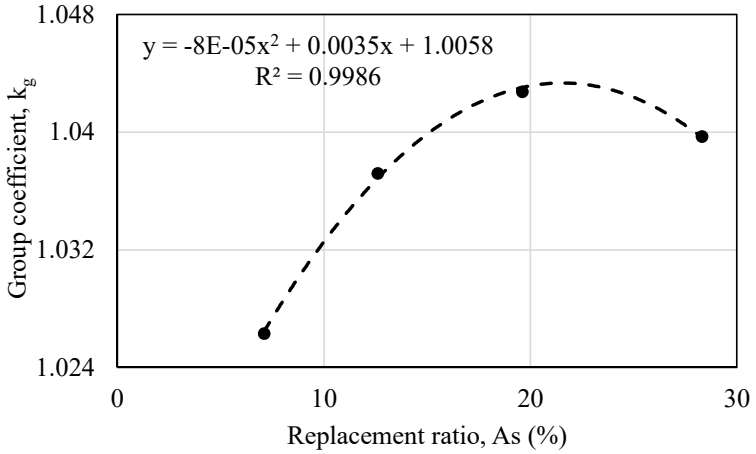

Figure 5.65 Relation between stone column group coefficient and replacement ratio

5.5.5.5 Validation of improvement factor (I_F) calculation

The presented I_F charts are not applicable for stone columns with a diameter less than 0.2m. Thus, the I_F values could not be validated against experimental results available in the literature. Field tests on a clay

soil reinforced by a group of stone columns are uncommon. So, the IR charts were validated against two full-scale tests as shown in Table 5.7.

Table 5.7 Verification of IR design charts

Reference	c_u (kPa)	ϕ_c' (degrees)	ϕ_s' (degrees)	A_s (%)	D (m)	Measured			I_F	Error (%)
						q_u (Reinforced) (kPa)	q_u (Clay) (kPa)	$I_{F\,measured}$		
Terashi et al. (1991)	20	22	40	25	1.7	105	47.60	2.06	2.20	6.63%
Goughnour and Bayuk (1979b)	26	26	38	36	1.1	115	66.30	1.73	1.71	-1.16%

Chapter 6: Analytical Model

6.1 General

Hanna et al. (2013) presented a comprehensive plane-strain numerical study for the case of soft clay reinforced by a group of stone columns. They reported that the mode of failure could be general shear, local shear, or punching shear similar to those reported by Vesic (1972) for homogeneous soil. These three modes of failure were supported by the 3-D numerical models of the present study. In the literature, the reinforced soil mass was treated as a composite material (Barksdale et al., 1983b; Priebe, 1995; Lee et al., 1998; Etezad et al., 2015). Therefore, the plane of failure was assumed to be similar to the case of homogeneous soil, which does not accurately represent reinforced ground conditions (Etezad et al., 2018).

In this chapter, an analytical model is developed to calculate the bearing capacity of a rigid square footing on clay soil reinforced by a single or group of stone columns. In this analysis, a broken plane of failure was deduced from the results of the numerical model. The results are presented in the form of design theory and design charts to estimate the bearing capacity of the reinforced soil for given soil and geometry conditions. In addition, an improvement factor (IR) was introduced, using the limit equilibrium slip circle technique.

6.1.1 Failure plane

Based on the characteristics of clay/column systems used in this investigation, a punching failure plane was often observed. Figure 6.1 presents the plastic strain under a footing under the broken failure plane for the case of a single stone column in soft clay. Figure 6.2 presents the failure plane that occurred for the case of a group of stone columns in soft clay. As reported earlier (section 5.5.5.4), the number and spacing between columns have little effect on the capacity of the system. Accordingly, the analysis was conducted on a rigid footing on clay reinforced with a single stone column, as shown by Figure 6.3. Figure 6.4 presents the effect of column diameter on the failure plane angle at different replacement ratios. It can be noted that the failure plane starts at the edge of the footing and propagates through the clay soil with an angle of (θ_1) and then changes to a horizontal plane through the column material. Furthermore, the angle of the failure plane slightly decreases by increasing the column diameter and increases with the increase of the replacement ratio for the same column diameter. The angle of the

failure plane could be calculated by equations (6-1), (6-2), and (6-3). The factors a_4 and b_4 could be obtained from Figure 6.5.

$$\theta_1(rad.) = a_4 \times D + b_4 \tag{6-1}$$

Where

D is stone column diameter (m)

θ_1 is the angle on failure plane in radians

$$a_4 = -0.0003A_s^2 + 0.015A_s - 0.2267 \tag{6-2}$$

$$b_4 = 0.0143A_s + 0.8338 \tag{6-3}$$

A_s is the replacement ratio in percent (%)

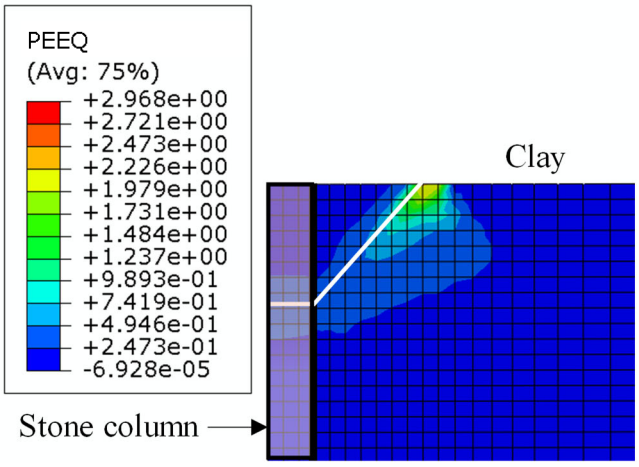

(a) D = 0.6 m, A_s = 7.1%, B = 2m

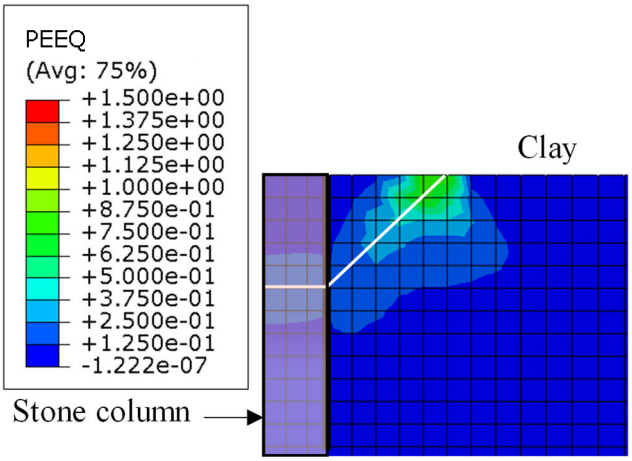

(b) D = 1.6 m, A_s = 12.6%, B = 4m

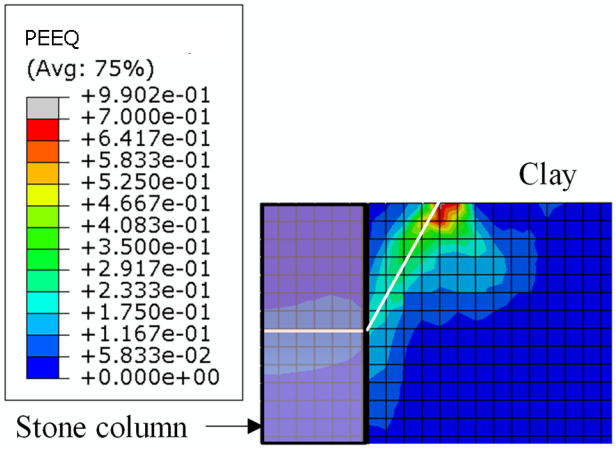

(c) D = 4.8 m, A_s = 28.3%, B = 8m

Figure 6.1 Failure plane under a rigid footing supported by a single stone column

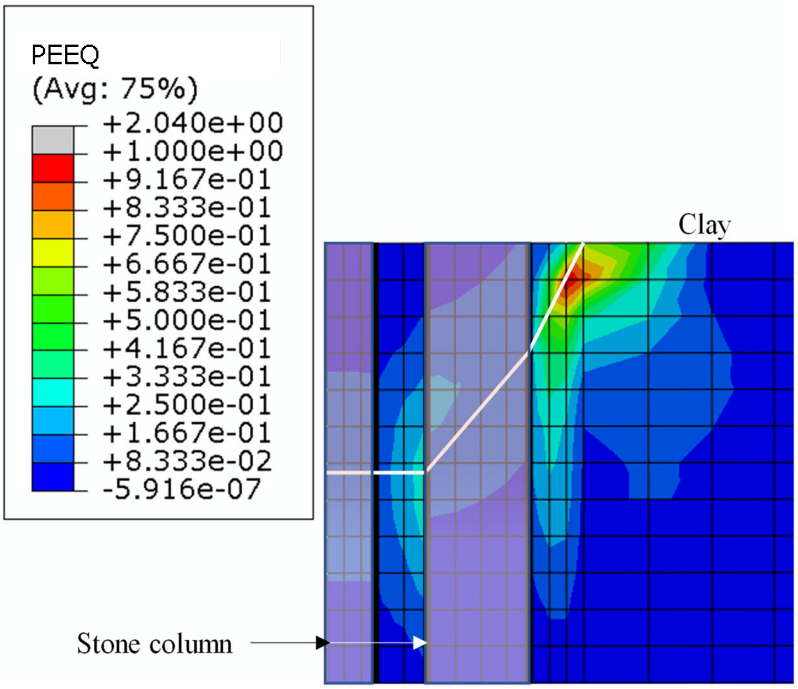

(a) D = 0.8m, A_s = 28.3%, B = 4m, N = 9

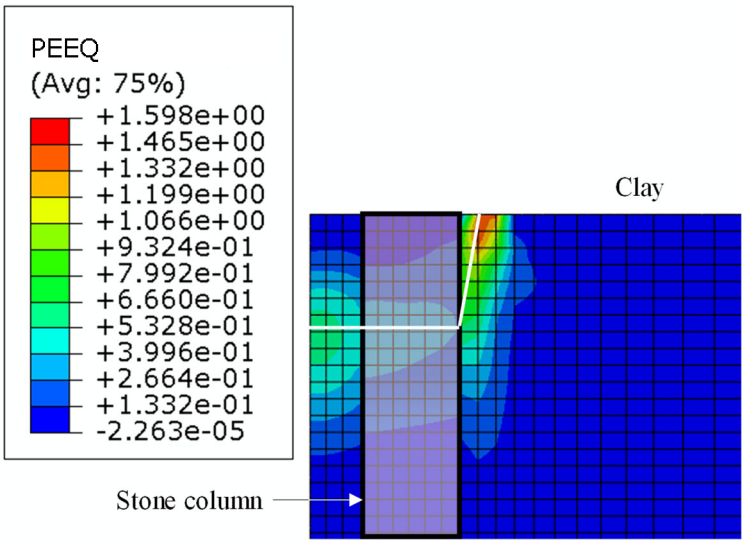

(b) D = 0.6m, A_s = 28.3%, B = 2m, N = 2

Figure 6.2 Failure plane under a rigid footing supported by group stone columns

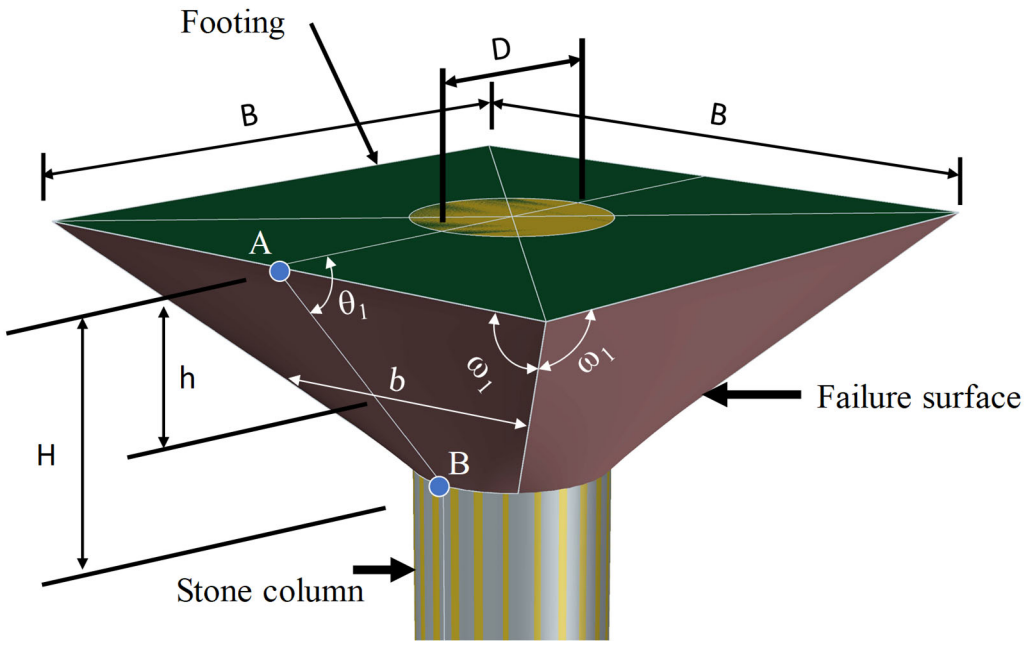

(a) 3-D view of the failure surface

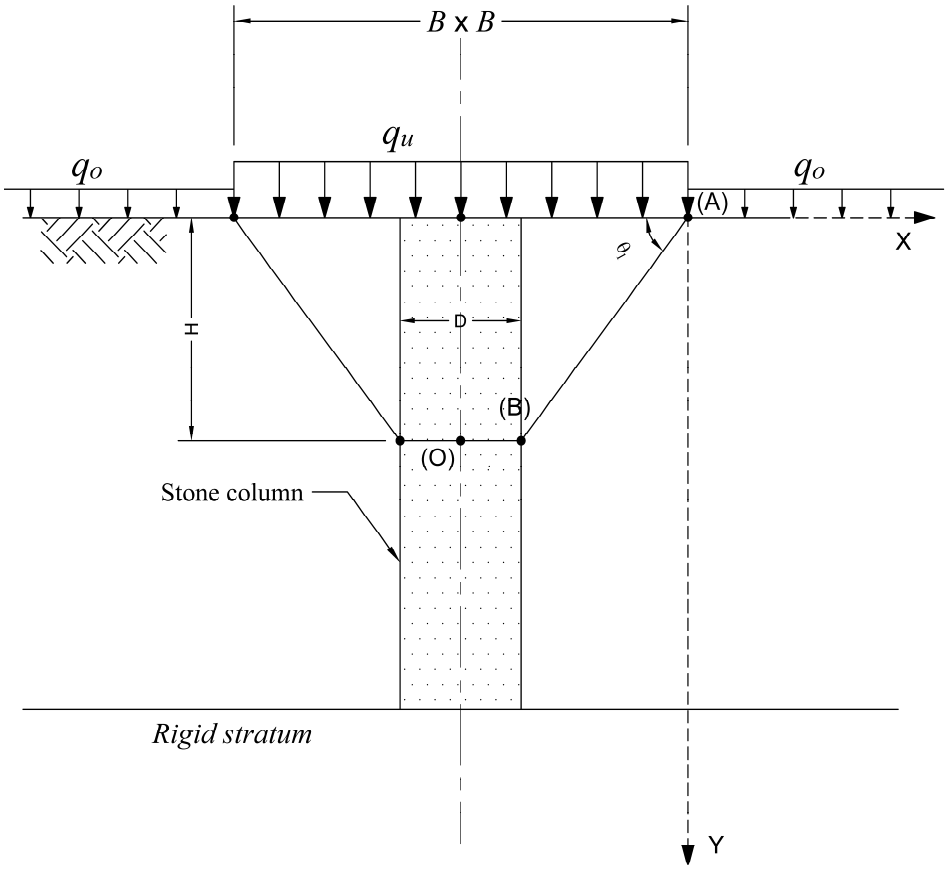

(b) Cross section of the failure plane

Figure 6.3 Proposed punching failure mechanism for clay soil reinforced by a single stone column

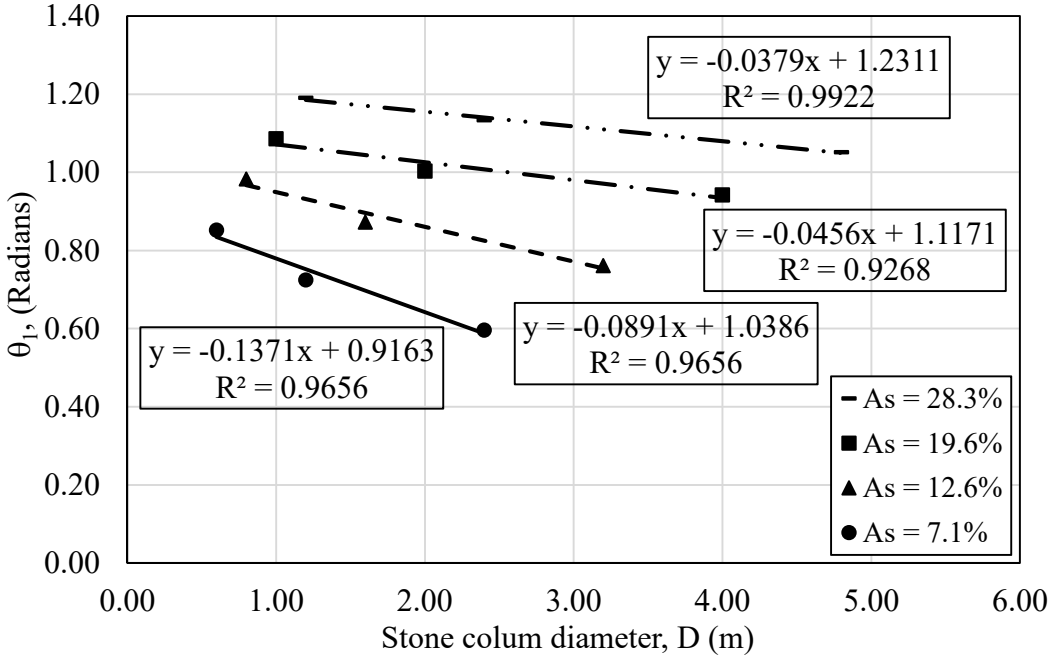

Figure 6.4 Relation between the failure plane angle (θ_1) and the stone column diameter

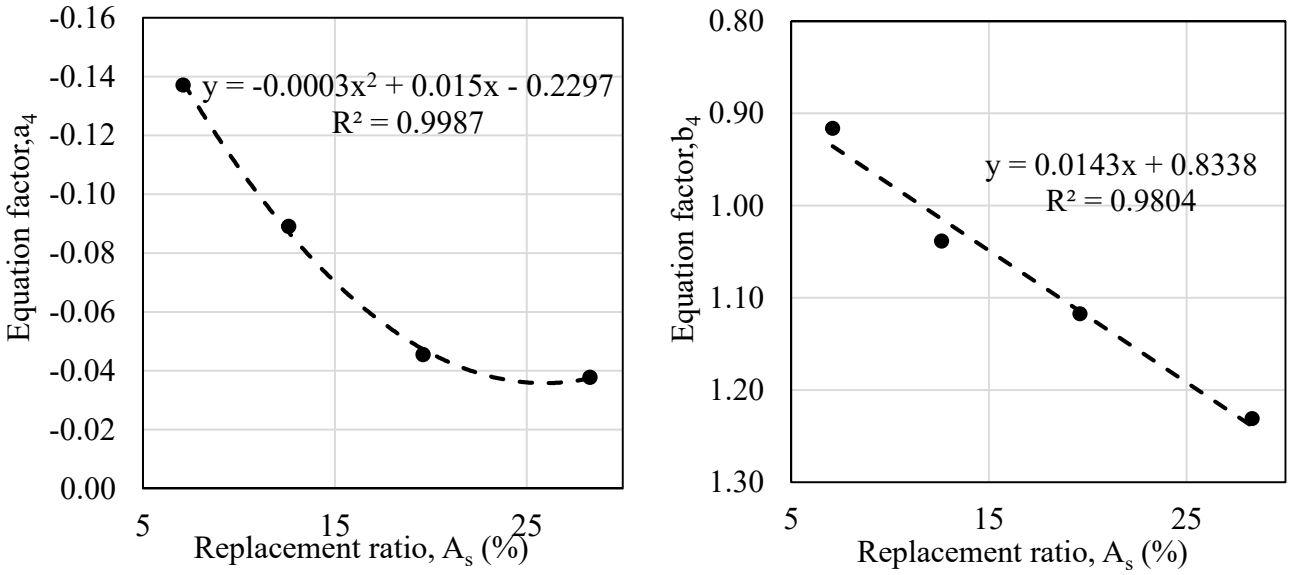

Figure 6.5 Factors used to estimate the failure plane angle

6.1.2 Analytical model.

Based on the proposed failure plane in section 6.1.1, the forces acting on the surface were calculated and then used to estimate the bearing capacity of the reinforced soil. Since the limit equilibrium technique is widely accepted for solving bearing capacity equations, it was used in this analysis. The clay soil was assumed to be frictionless ($\phi_c = 0.0$), while the stone column was assumed to be cohesionless ($c_s = 0.0$).

Figure 6.6 presents the stresses acting on the elastic zone under the footing, from which the passive stresses on the failure plane could be calculated as follows:

$$q_o = D_f \times \gamma_c \quad \text{(kPa)} \tag{6-4}$$

$$q_{po} = q_o \times K_p \quad \text{(kPa)} \tag{6-5}$$

$$q_1 = H \times \gamma_c \quad \text{(kPa)} \tag{6-6}$$

$$q_{p1} = q_1 \times K_p \quad \text{(kPa)} \tag{6-7}$$

Where

D_f = depth of foundation (m),

K_p = coefficient of passive earth pressure

$$H = \text{depth of the failure plane} = \frac{(B-D)}{2} \times \tan\theta \tag{6-8}$$

is the width of the footing, D is diameter of the stone columns, and θ is the angle of failure plane, which was estimated in section 6.1.1.

This passive coefficient was determined using Coulomb's passive earth pressure theory (Coulomb, 1776). The earth pressure distribution was assumed to be linearly distributed on AB surface and uniformly distributed on OB surface.

In this study, the weight $Q_{u\gamma}$, surcharge Q_{uq}, and cohesion Q_{uc} components of the bearing capacity equation were analyzed separately. The surcharge and cohesion components were calculated by solving the equilibrium of the forces in a vertical direction (Figure 6.7). As analysis was conducted on a square footing, the stresses were calculated on one side of the elastic zone. The surcharge (Q_{uq}) and cohesion component (Q_{uc}) of the bearing capacity were determined by equation (6-9).

$$Q_{uq} + Q_{uc} = R_o \cos\theta + P_{po} \cos\phi_s + C \sin\theta \tag{6-9}$$

Where R_o is the earth pressure force of clay soil due to the surcharge load (q_o) on surface AB as shown by equation (6-10), and P_{po} is the passive earth pressure of the stone columns on surface BO, as depicted by equation (6-11). C is the cohesion forces along the surface AB as shown by equation (6-12).

$$R_o = \int_0^H (q_o + 2c_u) \times b \frac{dh}{\sin\theta} \tag{6-10}$$

$$P_{po} = q_o K_p \frac{\pi D^2}{16} \tag{6-11}$$

$$C = c_u \times \frac{\left(B + \frac{D}{\sqrt{2}}\right) H}{2 \sin\theta} \tag{6-12}$$

Where

b = the width of the surface *AB* at depth *h* (Figure 6.3 (a)) = $B - 2 \times \frac{h}{\sin\theta \times \tan\omega}$ (6-13)

c_u is the cohesion of clay soil, B is the footing width, and *D* is the stone column diameter.

Equation (6-14) presents the relation between the failure plane cross-section angle (θ) and the failure surface (ω), thus the width of the failure plane at any depth can be calculated as equation (6-15).

$$\tan\omega = \frac{1}{\cos\theta} \times \frac{B - D}{B - \frac{D}{\sqrt{2}}} \tag{6-14}$$

$$b = B - 2\frac{h\left(B - \frac{D}{\sqrt{2}}\right)}{\tan\theta\left(B - D\right)} \tag{6-15}$$

By applying equations (6-15) in equation (6-10), force R_o was determined as:

$$R_o = \left(q_o + 2c_u\right) \times \frac{\left(B + \frac{D}{\sqrt{2}}\right) H}{2 \sin\theta} \tag{6-16}$$

The values of the ultimate bearing capacity components due to surcharge and cohesion could be calculated as follows:

$$Q_{uq} + Q_{uc} = q_o \left(K_p \frac{\pi D^2}{16} \cos\phi_s + \frac{\left(B + \frac{D}{\sqrt{2}}\right) H}{2 \tan\theta} \right) + c_u \times \left(\frac{\left(B + \frac{D}{\sqrt{2}}\right) H}{2} + \frac{H\left(B + \frac{D}{\sqrt{2}}\right)}{\tan\theta} \right) \tag{6-17}$$

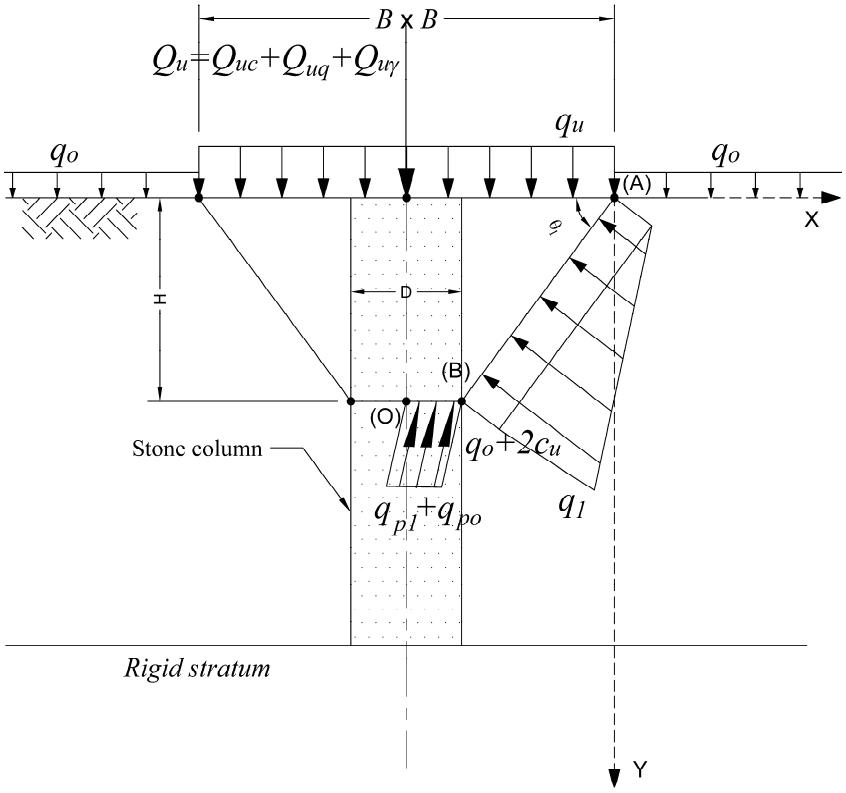

Figure 6.6 Stresses acting on the failure plane due to weight components

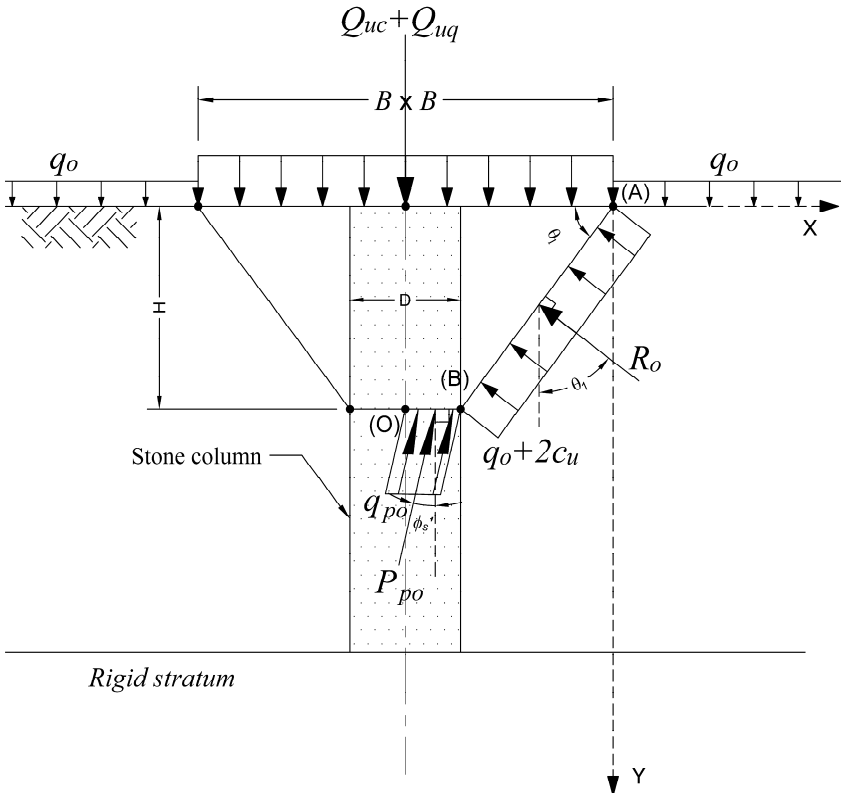

Figure 6.7 Forces acting on the failure plane due to surcharge and cohesion components

The unit weight component ($Q_{u\gamma}$) of the bearing capacity was determined by equation (6-18).

$$Q_{u\gamma} = R_1 \cos\theta + P_{P1} \cos\phi_s - W_1 - W_2 \tag{6-18}$$

Where

$$R_1 = \int_0^H \gamma_c h b \frac{dh}{\sin\theta} \tag{6-19}$$

$$R_1 = \frac{\gamma_c H^2 B}{2\sin\theta} - \frac{2\gamma_c H^3 \left(B - \frac{D}{\sqrt{2}} \right)}{3\tan\theta \sin\theta \left(B - D \right)} \tag{6-20}$$

$$P_{p1} = \gamma_c h K_p \times \frac{\pi D^2}{16} \tag{6-21}$$

$$W_1 = \left(\frac{1}{3} \left(B^2 + \frac{BD}{\sqrt{2}} + \frac{D^2}{2} \right) - \frac{\pi D^2}{4} \right) \frac{H\gamma_c}{4} \tag{6-22}$$

$$W_2 = \left(\frac{\pi D^2}{4} \right) \frac{H\gamma_s}{4} \tag{6-23}$$

By applying equations (6-20), (6-21), (6-22), and (6-23) in equation (6-17), the values of the ultimate bearing capacity components due to weights could be calculated as follows:

$$Q_{u\gamma} = \left(\frac{H^2 B}{2\tan\theta} - \frac{2H^3 \left(B - \frac{D}{\sqrt{2}} \right)}{3\tan^2\theta \left(B - D \right)} + HK_p \times \frac{\pi D^2}{16} \cos\phi_s - \left(\frac{1}{3} \left(B^2 + \frac{BD}{\sqrt{2}} + \frac{D^2}{2} \right) - \frac{\pi D^2}{4} \right) \frac{H}{4} \right) \gamma_c - \left(\frac{\pi D^2 H}{16} \right) \gamma_s \tag{6-24}$$

In order to calculate the bearing capacity, the three bearing capacity components were combined together, as shown in equation (6-25).

$$q_u = \frac{4 \times \left(Q_{uc} + Q_{uq} + Q_{u\gamma} \right)}{B^2} \tag{6-25}$$

By substituting equations (6-17) and (6-24) into equation (6-25), the bearing capacity equation could be rearranged as follows:

$$q_u = c_u N_c + q_o N_q + \frac{1}{2} B\left(\gamma_c N_{\gamma c} - \gamma_s N_{\gamma s}\right) \tag{6-26}$$

Where

$$N_c = \left(\frac{\left(B + \frac{D}{\sqrt{2}}\right)(B-D) \times \tan\theta}{B^2} + \frac{2(B-D) \times \left(B + \frac{D}{\sqrt{2}}\right)}{B^2} \right) \tag{6-27}$$

$$N_q = \left(K_p \frac{\pi D^2}{4B^2} \cos\phi_s + \frac{\left(B + \frac{D}{\sqrt{2}}\right)(B-D)}{B^2} \right) \tag{6-28}$$

$$N_{\gamma s} = \left(\frac{\pi D^2 (B-D)}{4B^3} \tan\theta \right) \tag{6-29}$$

$$N_{\gamma c} = \left(\begin{array}{l} \frac{(B-D)^2 \times \tan\theta}{B^2} - \frac{2(B-D)^2 \left(B - \frac{D}{\sqrt{2}}\right) \times \tan\theta}{3B^3} + \frac{(B-D) K_p \pi D^2}{4B^3} \tan\theta \cos\phi_s \\ -\left(\frac{1}{3}\left(B^2 + \frac{BD}{\sqrt{2}} + \frac{D^2}{2} \right) - \frac{\pi D^2}{4} \right) \frac{(B-D) \times \tan\theta}{B^3} \end{array} \right) \tag{6-30}$$

Based on the column diameter (D) and the replacement ratio (A_s), the angle of failure mechanism (θ) can be calculated as presented in section 6.1.1. For practical use, the bearing capacity coefficients (N_c, N_q, $N\gamma s$, $N\gamma c$) can be obtained from the design charts in Figure 6.9, Figure 6.10, Figure 6.11, and Figure 6.12, respectively.

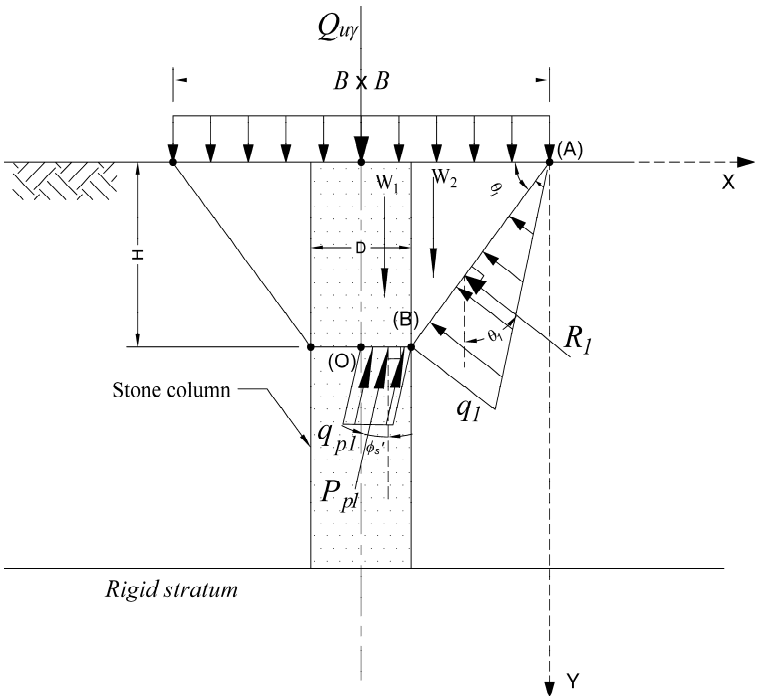

Figure 6.8 Forces acting on the failure plane due to weight components

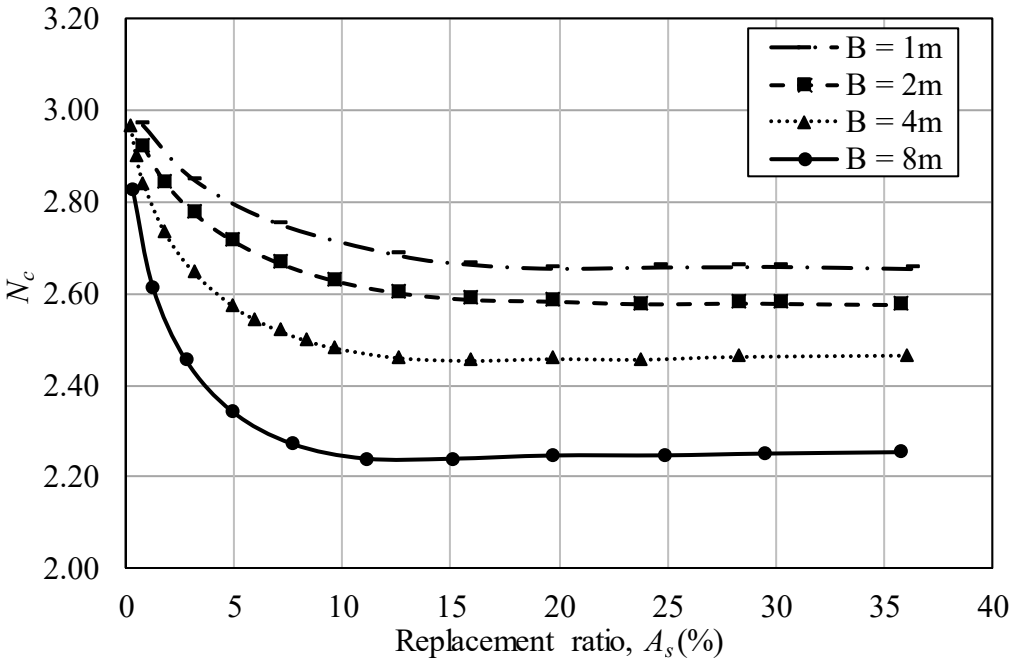

Figure 6.9 N_c for rigid square footing on soft clay soil reinforced by a single stone column

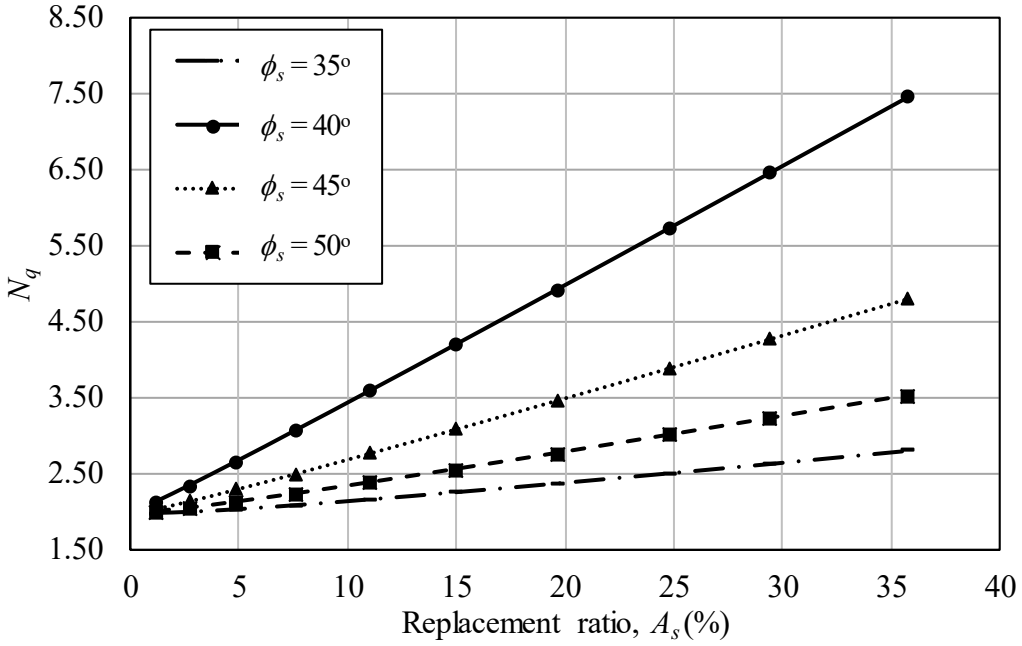

Figure 6.10 N_q for rigid square footing on soft clay soil reinforced by a single stone column

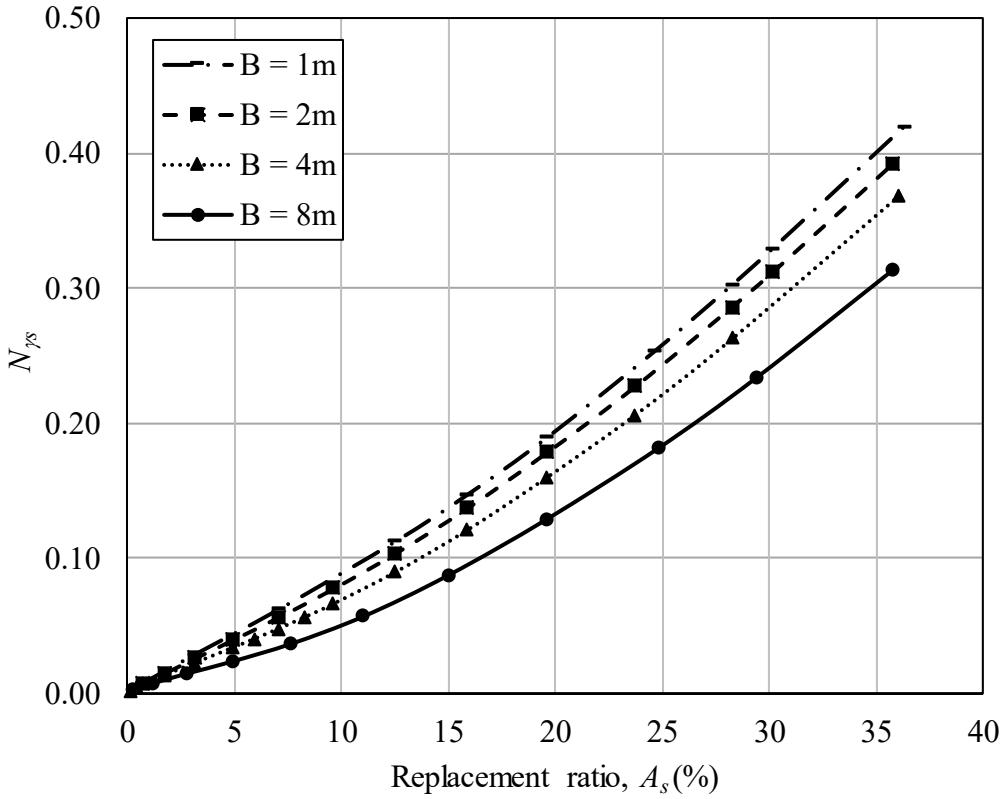

Figure 6.11 $N_{\gamma s}$ for rigid square footing on soft clay soil reinforced by a single stone column

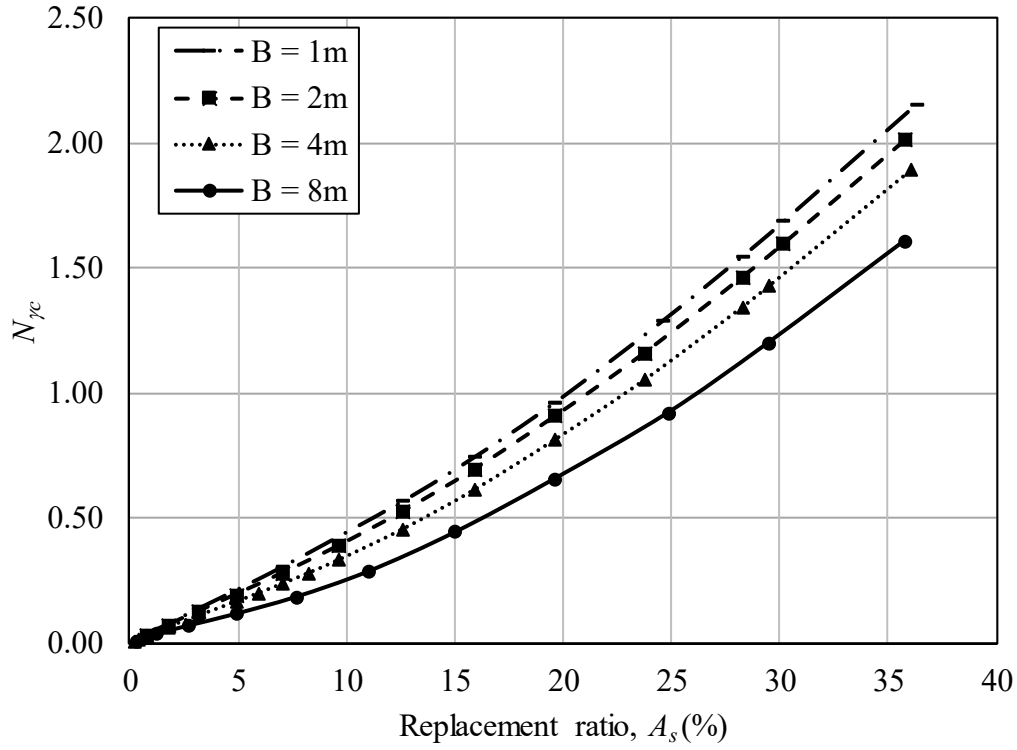

(a) $\phi_s = 35^o$

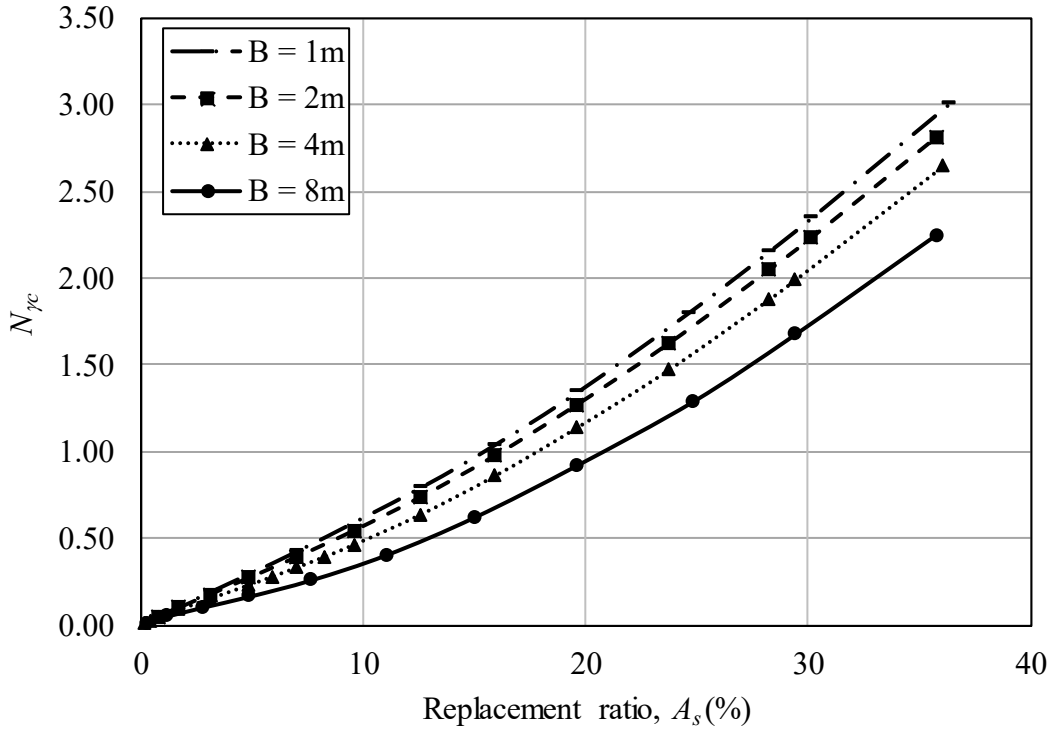

(b) $\phi_s = 40^o$

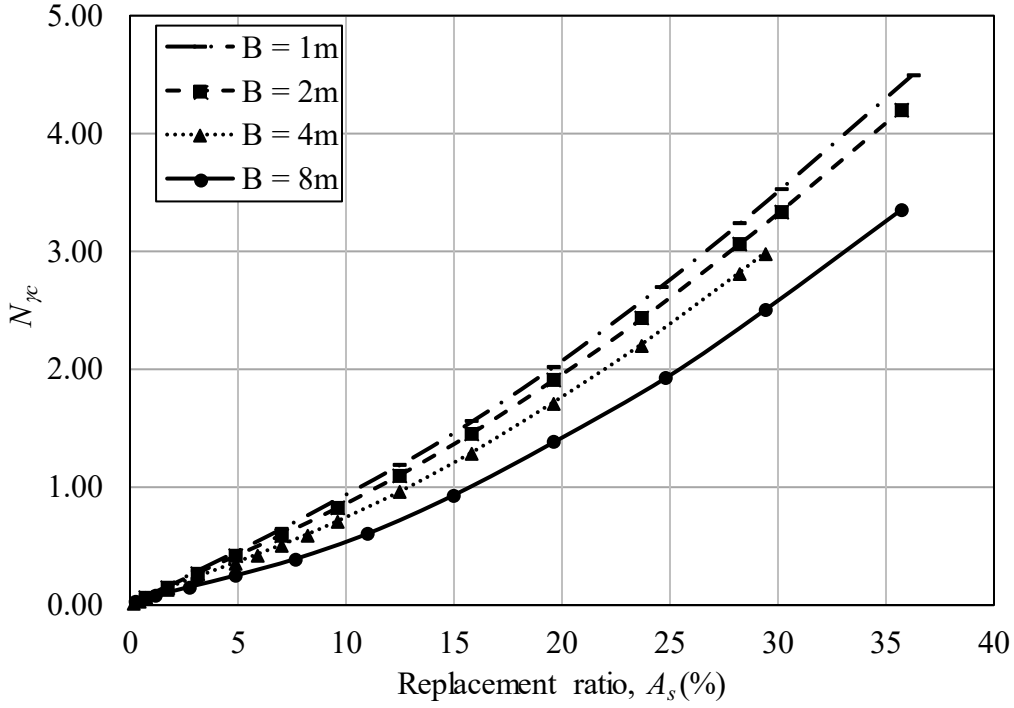

(c) $\phi_s = 45^o$

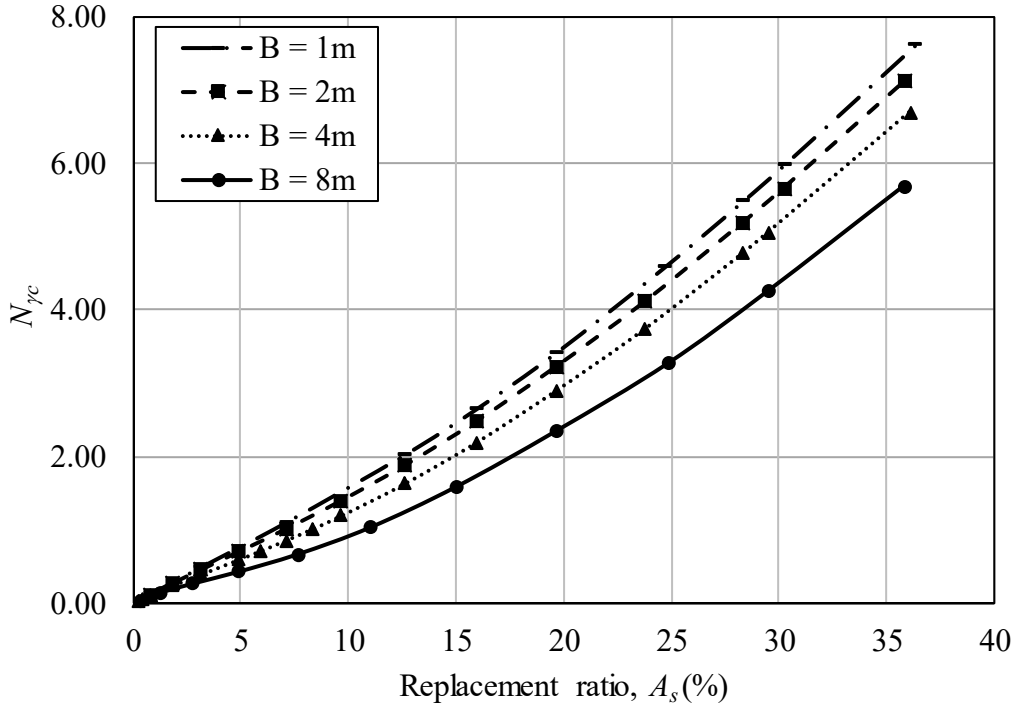

(d) $\phi_s = 50^o$

Figure 6.12 $N_{\gamma c}$ for rigid square footing on soft clay soil reinforced by a single stone column

The proposed analytical model can be used to calculate the bearing capacity of a square rigid footing reinforced by a group of stone columns. An equivalent footing width (B) will be calculated, which represents a footing supported by a single stone column with the same diameter and with the same replacement ratio. For example, when a square footing with a width of 4m is supported by 4 stone columns with a diameter of 0.6m, the replacement ratio will be 7.1%. The equivalent footing width will be considered as 2m, which keeps the replacement ratio at 7.1% when it is supported by a single stone column with the same diameter (0.6m).

6.1.3 Validation of the analytical model

The proposed analytical models were validated using the experimental and field results available in the literature, in addition to the numerical data obtained from the full-scale 3-D numerical model of the present study. Table 6.1 presents a comparison of the 3-D model numerical results and the analytical results developed in the present study, Table 6.2 while presents a comparison of the experimental results from Goughnour et al. (1979b), Terashi et al. (1991), and McKelvey et al. (2004), and results from the presented theory. A good agreement was found both cases. The error reported could be assigned to variability in the experimental data, and the assumptions used to develop the proposed methods; however, the errors were within an acceptable range.

Table 6.1 Comparison of the 3-D model numerical (FFE) results and analytical results from this study

(a) B = 2m, ϕ_s = 40°, γ_s = 20kN/m^3, c_u = 5 kPa, γ_c = 18 kN/m^3

No. of Stone Columns	Stone Columns Diameter, D (m)	Stone Columns Spacing ratio, S/D	Replacement ratio, As (%)	Numerical		Analytical	Error (%)
				Tangential method (kPa)	q_u final (kPa)	q_u, (kPa)	
0	0	0	0.0	15.09	16.42	15.51	1.65
1	0.45	0	4.0	17.17	20.12	17.27	0.59
1	0.5	0	4.9	18.20	21.43	17.95	-1.37
1	0.565	0	6.3	19.28	23.55	19.00	-1.45
1	0.6	0	7.1	20.32	25.02	19.65	-3.31
1	0.705	0	9.8	23.36	29.76	22.03	-5.70
1	0.75	0	11.0	24.46	32.22	23.27	-4.85
1	0.8	0	12.6	26.56	35.26	24.83	-6.51
1	0.846	0	14.1	28.20	38.35	26.45	-6.19
1	0.9	0	15.9	30.37	42.02	28.61	-5.80
1	1	0	19.6	34.97	49.87	33.39	-4.54
1	1.2	0	28.3	48.00	70.31	45.90	-4.37
2	0.6	1.5	14.14	26.53	34.54	22.59	-14.86
4	0.6	1.5	28.27	38.49	53.59	30.01	-22.02

(b) B = 2m, ϕ_s = 40°, γ_s = 20kN/m^3, c_u = 7.5 kPa, γ_c = 18 kN/m^3

No. of Stone Columns	Stone Columns Diameter, D (m)	Stone Columns Spacing ratio, S/D	Replacement ratio, As (%)	Numerical		Analytical	Error (%)
				Tangential method (kPa)	q_u final (kPa)	q_u, (kPa)	
0	0	0	0.00	22.74	25.36	23.26	2.31
1	0.6	0	7.07	26.94	33.51	26.32	-2.31
1	0.8	0	12.57	33.37	43.90	31.34	-6.09
1	1	0	19.63	41.57	58.86	39.84	-4.15
1	1.2	0	28.27	52.63	79.94	52.35	-0.53
2	0.6	1.5	14.14	32.92	43.22	31.96	-2.91
4	0.6	1.5	28.27	45.35	62.56	39.39	-13.13

(c) B = 2m, ϕ_s = 40°, γ_s = 20kN/m^3, c_u = 6.25 kPa, γ_c = 18 kN/m^3

No. of Stone Columns	Stone Columns Diameter, D (m)	Stone Columns Spacing ratio, S/D	Replacement ratio, As (%)	Numerical		Analytical	Error (%)
				Tangential method (kPa)	q_u final (kPa)	q_u, (kPa)	
0	0	0	0.00	19.67	21.93	19.39	-1.43
1	0.6	0	7.07	24.36	30.27	22.98	-5.63
1	0.8	0	12.57	30.74	40.60	28.09	-8.65
1	1	0	19.63	39.37	55.44	36.62	-7.01
1	1.2	0	28.27	51.33	76.27	49.13	-4.30
2	0.6	1.5	14.14	30.76	39.93	25.90	-15.80
4	0.6	1.5	28.27	43.19	59.18	34.68	-19.69

(d) B = 4m, ϕ_s = 40°, γ_s = 20kN/m^3, c_u = 5.0 kPa, γ_c = 18 kN/m^3

No. of Stone Columns	Stone Columns Diameter, D (m)	Stone Columns Spacing ratio, S/D	Replacement ratio, As (%)	Numerical		Analytical	Error (%)
				Tangential method (kPa)	q_u final (kPa)	q_u, (kPa)	
0	0	0	0.00	14.59	15.78	15.51	6.32
1	0.9	0	3.98	18.24	22.03	18.72	2.66
1	1	0	4.91	19.78	23.96	19.83	0.24
1	1.2	0	7.07	22.52	29.16	22.64	0.55
1	1.13	0	6.27	21.35	26.88	21.56	0.96
1	1.41	0	9.76	26.67	36.00	26.67	0.00
1	1.5	0	11.04	28.33	39.16	28.82	1.73
1	1.8	0	15.90	36.23	53.63	38.28	5.64
1	1.695	0	14.10	33.38	48.55	34.52	3.43
1	1.6	0	12.57	31.06	43.71	31.55	1.56
1	2	0	19.63	40.70	64.11	46.85	15.10
1	2.4	0	28.27	54.75	93.85	66.92	22.22
2	0.8	1.5	6.28	20.36	25.35	20.03	-1.64
2	1.2	2	14.14	30.89	42.63	29.74	-3.73
2	1	2	9.82	25.44	32.64	23.95	-5.86
4	0.8	1.5	12.57	27.52	35.21	24.13	-12.31
4	0.6	2	7.07	20.26	24.58	19.27	-4.89
4	1.2	2	28.27	46.89	70.20	43.99	-6.19
4	1	2	19.63	35.86	50.02	32.17	-10.29
9	0.8	1.5	28.27	44.25	60.72	34.89	-21.17
9	0.6	1.5	15.90	28.56	36.53	23.45	-17.89

(e) B = 4m, ϕ_s = 30°, γ_s = 20kN/m^3, c_u = 5.0 kPa, γ_c = 18 kN/m^3

No. of Stone Columns	Stone Columns Diameter, D (m)	Stone Columns Spacing ratio, S/D	Replacement ratio, As (%)	Numerical		Analytical	Error (%)
				Tangential method (kPa)	q_u final (kPa)	q_u, (kPa)	
0	0	0	0.00	14.59	15.78	15.51	6.32
1	1.2	0	7.07	16.54	17.23	15.69	-5.13
1	1.6	0	12.57	18.03	18.72	18.47	2.41
1	2	0	19.63	20.01	20.30	23.61	17.97
2	0.8	1.5	6.28	16.07	17.08	16.07	-0.02
4	0.8	1.5	12.57	17.53	18.16	17.92	2.24
9	0.8	1.5	28.27	20.56	21.91	22.98	11.79

(f) B = 4m, ϕ_s = 50°, γ_s = 20kN/m^3, c_u = 5.0 kPa, γ_c = 18 kN/m^3

No. of Stone Columns	Stone Columns Diameter, D (m)	Stone Columns Spacing ratio, S/D	Replacement ratio, As (%)	Numerical		Analytical	Error (%)
				Tangential method (kPa)	q_u final (kPa)	q_u, (kPa)	
0	0	0	0.00	14.59	15.78	15.51	6.32
1	1.2	0	7.07	31.18	46.54	30.75	-1.39
1	1.6	0	12.57	44.27	77.93	46.81	5.74
1	2	0	19.63	61.84	122.14	73.95	19.58
2	0.8	1.5	6.28	27.84	38.30	33.17	19.13
4	0.8	1.5	12.57	42.75	61.41	44.73	4.64
9	0.8	1.5	28.27	74.58	119.10	74.27	-0.42

(g) B = 8m, ϕ_s = 40°, γ_s = 20kN/m^3, c_u = 5.0 kPa, γ_c = 18 kN/m^3

No. of Stone Columns	Stone Columns Diameter, D (m)	Stone Columns Spacing ratio, S/D	Replacement ratio, As (%)	Numerical		Analytical	Error (%)
				Tangential method (kPa)	q_u final (kPa)	q_u, (kPa)	
0	0	0	0.0%	15.10	16.03	15.51	2.68
1	1.8	0	3.98	20.44	25.35	20.11	-1.62
1	2	0	4.91	22.11	28.45	21.63	-2.17
1	2.4	0	7.07	25.47	35.59	25.71	0.94
1	3.2	0	12.57	34.12	56.33	40.27	18.03
1	3.39	0	14.10	37.04	62.49	45.48	22.81
1	3.2	0	12.57	34.12	56.23	40.27	18.03
1	3	0	11.04	32.57	50.32	35.60	9.29
1	2.26	0	6.27	24.60	33.13	24.10	-2.02
1	2.82	0	9.76	30.35	45.69	32.04	5.56
4	1	1.5	4.91	21.29	25.23	19.82	-6.89
4	1.2	2	7.07	22.96	28.80	22.67	-1.27
9	0.6	1.5	3.98	18.70	21.17	17.71	-5.32
9	0.8	1.5	7.07	22.31	26.36	20.58	-7.77
9	1	1.5	11.04	26.02	34.09	24.93	-4.21
9	1.2	1.5	15.90	33.87	45.80	31.53	-6.89
16	0.6	1.5	7.07	21.72	25.19	19.28	-11.24
16	0.8	1.5	12.57	27.48	34.50	24.15	-12.12
16	1	1.5	19.63	34.87	48.59	32.15	-7.81
16	1.2	1.5	28.27	48.00	68.24	43.99	-8.36

Table 6.2 Comparison of the presented theory with full-scale experimental test results

Reference	c_u (kPa)	ϕ_s (degrees)	γ_c (kN/m^3)	γ_s (kN/m^3)	A_s (%)	D (m)	q_u (measured) (kPa)	q_u (Theory) (kPa)	Error (%)
McKelvey et al. (2004)	27.5	34	18.4	19.6	23	0.021	86	80.07	-6.89
Terashi et al. (1991)	20	40	18	20	25	1.7	105	99.72	-5.03
Goughnour and Bayuk (1979b)	26	38	18	20	36	1.1	115	104.00	-9.57

6.2 Bearing capacity estimation using limit equilibrium and slip circle method

Many of the theories developed to predict bearing capacity utilize the theory for homogeneous soil as a simplified assumption. In this chapter, the method of slices was adopted to estimate the bearing capacity of strip footing on compacted inhomogeneous soil. A series of centrifuge tests and full-scale tests were conducted to estimate the bearing capacity of the improved ground by compacted sand piles. The experimental results agreed well with the bearing capacity calculated using a circular type of slip surface. The Morgenstern-Price method was utilized in this study to calculate the bearing capacity of a footing rests on clay soil reinforced with stone columns.

6.2.1 Bearing capacity calculation based on slip circle method

A 2-D model made of soft clay reinforced with stone columns was developed. The ground was loaded with a uniform pressure to simulate the case of a strip footing. The failure zone was divided into 50 slides and the forces acting on each slide are shown in Figure 6.13 Forces acting on a slide in the slip circleThe limit equilibrium method by (Morgenstern et al., 1965) was used in the computer program SLIDE V6.020, developed by Rocscience (2012), to calculate the minimum factor of safety of the circular slip surface (Figure 6.14). The analysis was also checked with the Bishop's Simplified method for comparison (Bishop, 1955). The footing was loaded to the ultimate capacity in the form of uniform pressure applied to the ground surface.

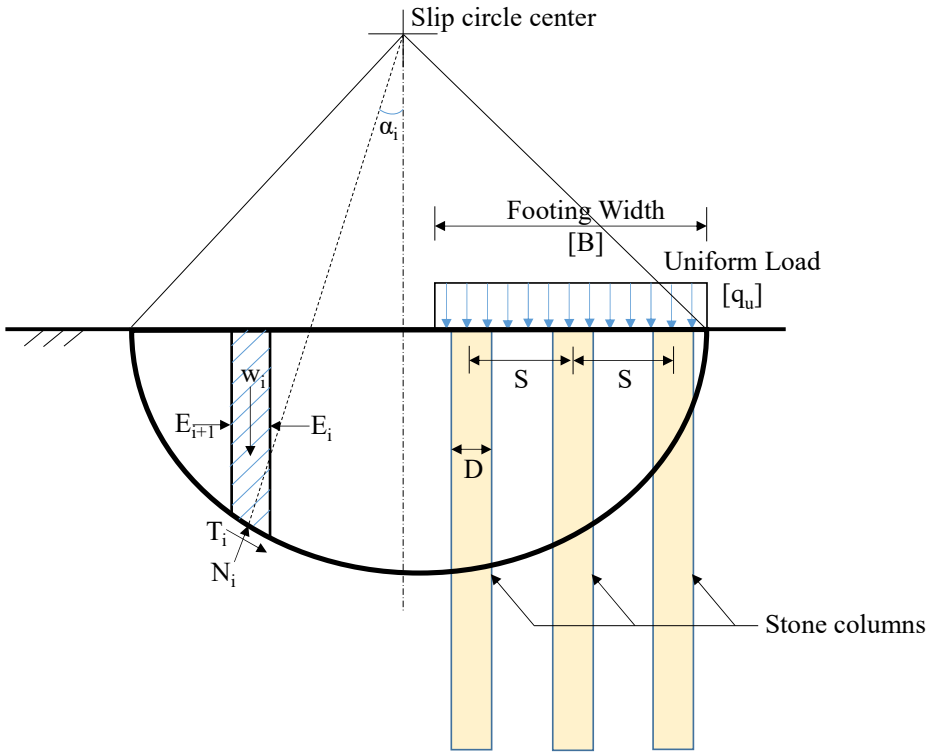

Figure 6.13 Forces acting on a slide in the slip circle

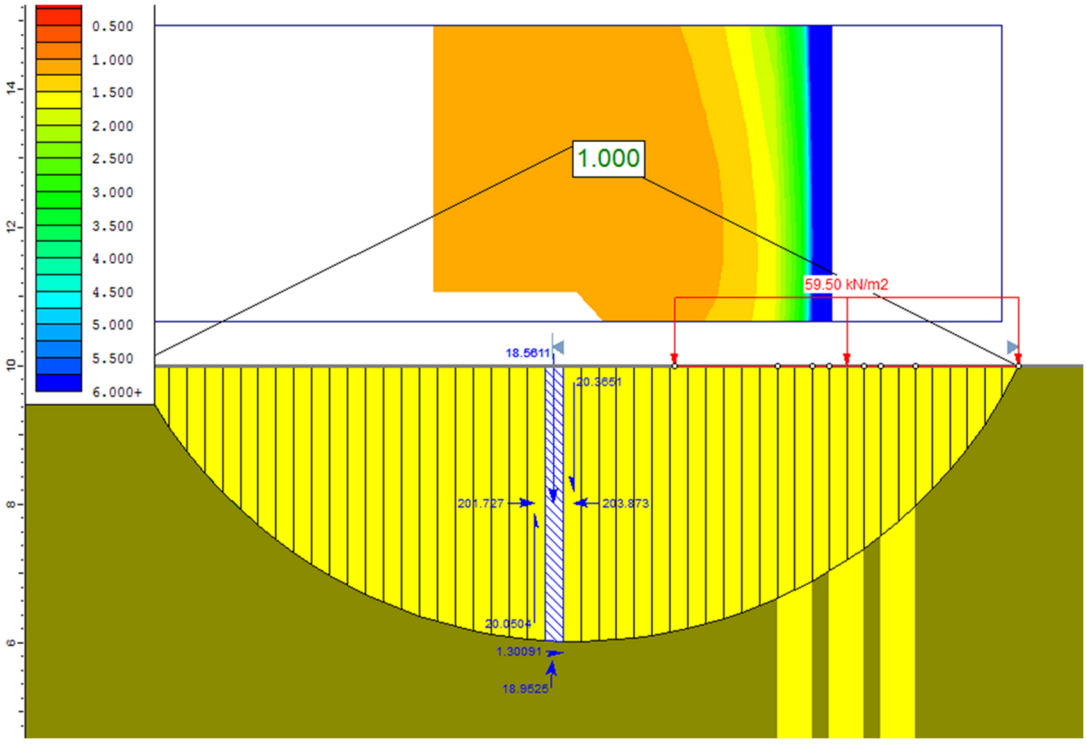

Figure 6.14 Example of the bearing capacity calculation using slip circle method

6.2.3 Validation of limit equilibrium model

The results obtained from the present analysis was compared with the laboratory and numerical results available in the literature (Hu, 1995; McKelvey et al., 2004; Hanna et al., 2013). Table 6.3 presents these comparisons, where a good agreement can be noted. Furthermore, the methods of Morgenstern-Price and the Bishop's Simplified method of slices as viable techniques to estimate the bearing capacity of clay soil reinforced by a group of stone columns were also used. However, Bishop's Simplified method generally overestimates the factor of safety as compared to the Morgenstern-Price method (Turnbull et al. 1967), and both approaches underestimate the bearing capacity of the reinforced soil.

6.2.4 Parametric study

In this study, the results are presented in the form of improvement ratio (*IR*), which is defined as the ratio of the capacity of improved soil to the capacity of the unimproved soil. In this analysis, the effect of the stone columns spacing to diameter ratio (*S/D*), and the number of stone column rows (*N*) on the bearing capacity at a given replacement ratio (A_s *%*) was performed. Each row of the stone columns was assumed as a trench with a width (*b*), and the spacing between trenches was considered the same as the spacing between columns as shown in Figure 6.15. The trench width was calculated using equation (6.31). In this case, the replacement ratio (A_s *%*) was calculated using equation (6-32). The ratio of *S/D* was examined in the range of 1 to 3.0 as given in Table 6.4

$$b = \frac{\pi \times D^2}{4 \times S} \tag{6-31}$$

$$A_s = \frac{N \times b}{B} = \frac{N \times \pi \times D^2}{4 \times S \times B} \tag{6-32}$$

Where

N is the number of stone columns rows, b is the trench width, *B* is footing width, *D* is the stone column diameter, and *S* is the spacing between stone columns.

Table 6.3 Comparison of the bearing capacity of reinforced soil estimated by the slices method and experimental and numerical results

No.	Clay Properties			Stone Properties		Area replacement ratio, As%	Footing width, B [m]	Surcharge load, q [kPa]	$q_{u,}$ Measured [kPa]	$q_{u,}$ B. S.method [kPa]	% Difference from measured	$q_{u,}$ Morgenstern-Price method [kPa]	% Difference from measured
	Cu [kPa]	ϕc [Degree]	γc [kN/m^3]	ϕ_s [Degree]	γs [kN/m3]								
1a	32	0	14	34	17.3	24	0.09	0	272	222	19.56	218.8	18.38
2a	20.5	0	9.9	34	20.3	40	0.05	0	160	165	0.63	161	3.13
3b	10.5	0	13.1	30	15.47	30	0.1	0	75	73	4.40	71.7	2.67
4b	11.5	0	13.1	30	15.47	30	0.1	0	79	80	0.63	78.5	1.27
5c	5	13	13	40	19	35	2.5	2.6	280	250	11.96	246.5	10.71
6c	5	15	14	45	21	35	2.5	2.8	420	380	9.48	380.2	9.52
7c	15	15	14	45	21	35	2.5	2.8	660	644	2.12	646	2.00

a experimantal work of McKelvey et al. (2004)
b experimental work of Hu (1995)
c numerical work of Hanna et al. (2013)

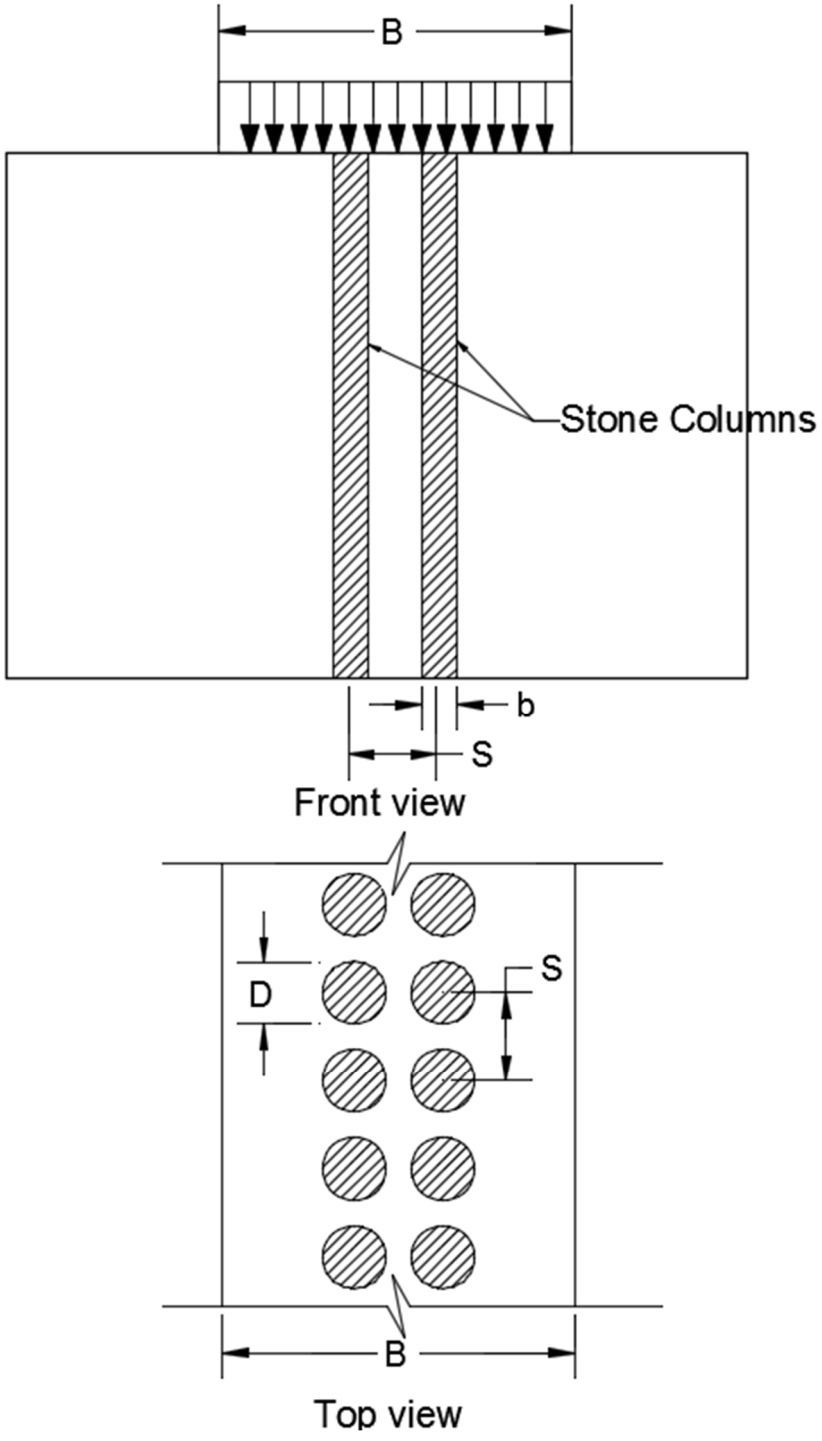

Figure 6.15 Stone columns arrangement

Table 6.4 Range of stone columns dimensions used in the parametric study

Area replacement ratio, As%	No. of columns, N	Column diameter,D [m]	Column spacing, S [m]	Spacing/Diameter ratio, S/D	trench width, b [m]
10%	1	0.70	0.70	1.00	0.50
	2	0.35	0.38	1.09	0.25
	2	0.40	0.50	1.25	0.25
	2	0.45	0.63	1.40	0.25
	2	0.49	0.75	1.53	0.25
	2	0.63	1.25	1.98	0.25
	2	0.89	2.50	2.80	0.25
20%	1	1.30	1.30	1.00	1.00
	2	0.69	0.75	1.09	0.50
	2	0.80	1.00	1.25	0.50
	2	0.89	1.25	1.40	0.50
	2	0.98	1.50	1.53	0.50
	2	1.26	2.50	1.98	0.50
	2	1.69	4.50	2.66	0.50
	3	0.46	0.50	1.09	0.33
	3	0.53	0.67	1.25	0.33
	3	0.59	0.83	1.40	0.33
	3	0.65	1.00	1.53	0.33
	3	0.84	1.67	1.98	0.33
	3	1.00	2.33	2.34	0.33
30%	1	2.10	2.10	1.00	1.50
	2	1.04	1.13	1.09	0.75
	2	1.20	1.50	1.25	0.75
	2	1.34	1.88	1.40	0.75
	2	1.47	2.25	1.53	0.75
	2	1.89	3.75	1.98	0.75
	3	0.69	0.75	1.09	0.50
	3	0.80	1.00	1.25	0.50
	3	0.89	1.25	1.40	0.50
	3	0.98	1.50	1.53	0.50
	3	1.13	2.00	1.77	0.50
	4	0.52	0.56	1.09	0.38
	4	0.60	0.75	1.25	0.38
	4	0.67	0.94	1.40	0.38
	4	0.73	1.13	1.53	0.38
	4	0.85	1.50	1.77	0.38

This method was also used to determine the effect of the undrained strength of the clay soil (C_u), and the replacement ratio (A_s%). In this analysis, the replacement ratio ranged from 10% to 30%, which is widely

used in practice (Hu, 1995; Hanna et al., 2013). The range of the other parameters believed to govern the bearing capacity are presented in Table 6.5.

Table 6.5 Range of parameter used in the parametric study

Parameter	Range of value
Cohesion of clay soil, C_u [kPa]	5, 10, and 15
Unit weight of clay soil, γ_c [kN/m^3]	18
Angle of shear resistance of stone, ϕ_s [Degree]	35, 38, and 40
Unit weight of stone, γ_s [kN/m^3]	20
Stone column diameter, D [m]	0.3 - 1.60
Stone column diameter to spacing ratio	1.00 - 2.50
Replacement ratio, A_s [%]	10, 20, and 30
Footing width, B [m]	5

The effect of the column arrangement on the bearing capacity was also investigated. Figure 6.16 presents the spacing/diameter ratio of stone columns versus replacement ratios, assuming all other parameters are constant. It can be noted that the bearing capacity increases with the increase of the replacement ratio. It can also be noted that the spacing between stone columns slightly influences the improvement ratio. For low replacement ratios (<10%), the improvement ratio is almost constant, which agrees well with the observations of Castro (2014). However, the improvement ratio reduces with the increase of the column spacing ratio. For higher replacement ratios (20%, and 30%), which confirm small spacing between columns, the lateral support from the surrounding soil increases and shows significant improvement.

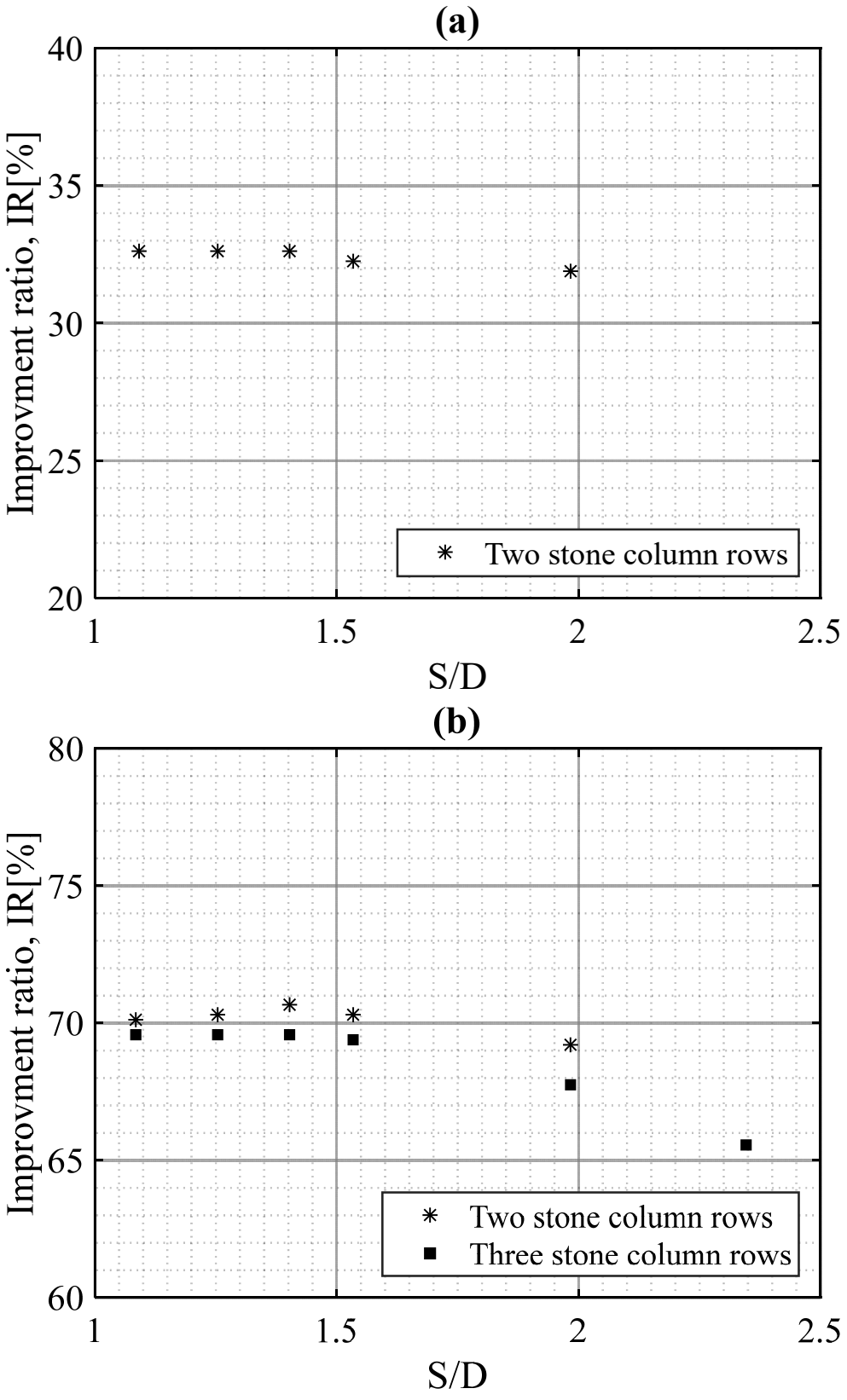
(a)
Improvment ratio, IR[%]
40
35
30
25
20
1
1.5
2
2.5
S/D
Two stone column rows
(b)
Improvment ratio, IR[%]
80
75
70
65
60
1
1.5
2
2.5
S/D
Two stone column rows
Three stone column rows

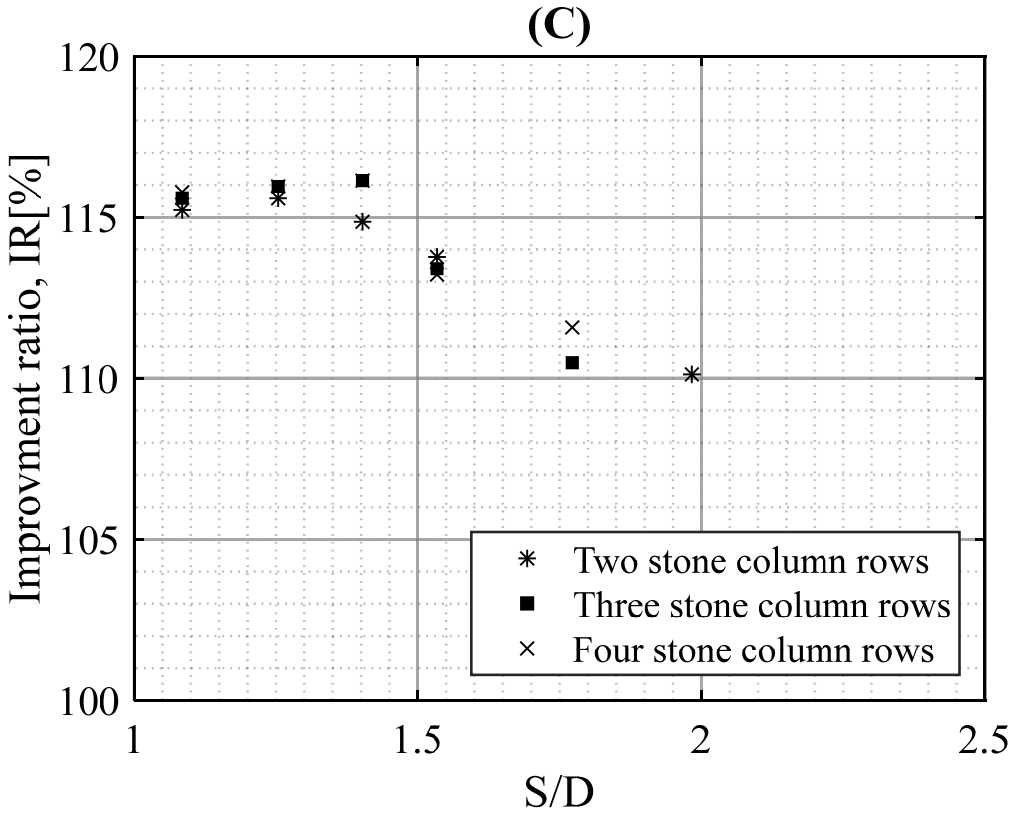

Figure 6.16 Improvement ratio (IR) versus *S/D* for different replacement ratios, C_{uo} = 5kPa, Φ_s = 35°: (a) A_s = 10%; (b) A_s = 20%; (c) A_s = 30%

Regarding the effect of the clay shearing resistance, it is noticeable that the improvement ratio reduces with the increase of shear strength of clay soil (C_u) for the same spacing/diameter ratio as shown in Figure 6.17. By contrast, the improvement ratio is raised by the increase of the stone columns shearing resistance angle, as shown in Figure 6.18.

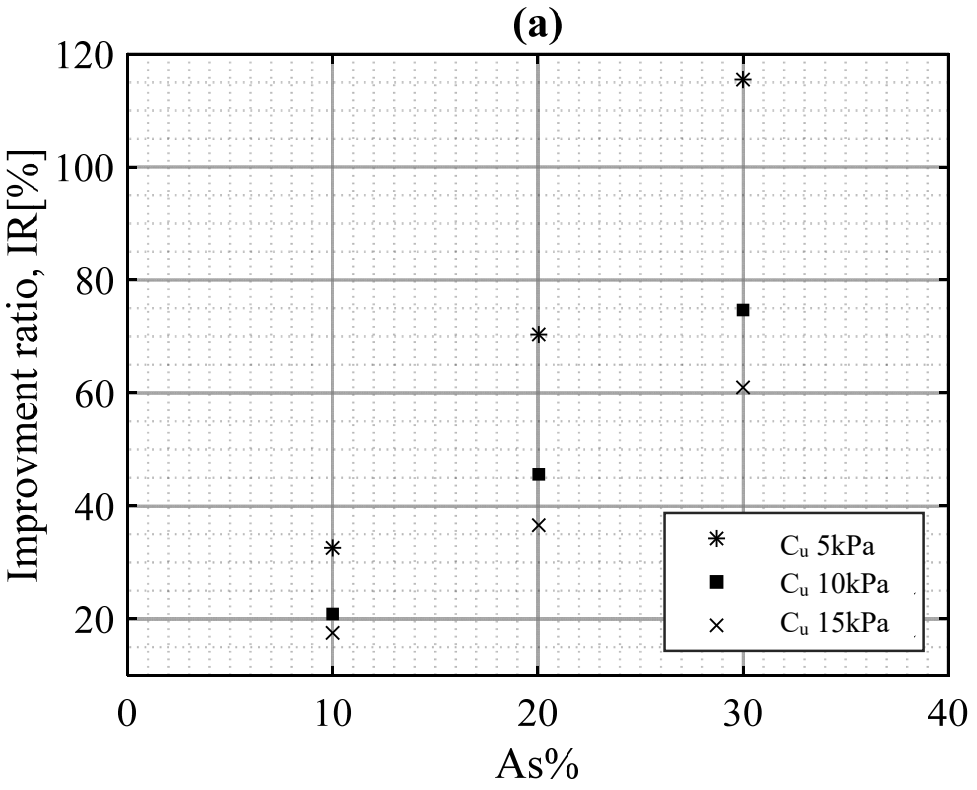
(a)
Improvment ratio, IR[%]
120
100
80
60
40
20
0
10
20
30
40
As%
Cu 5kPa
Cu 10kPa
Cu 15kPa

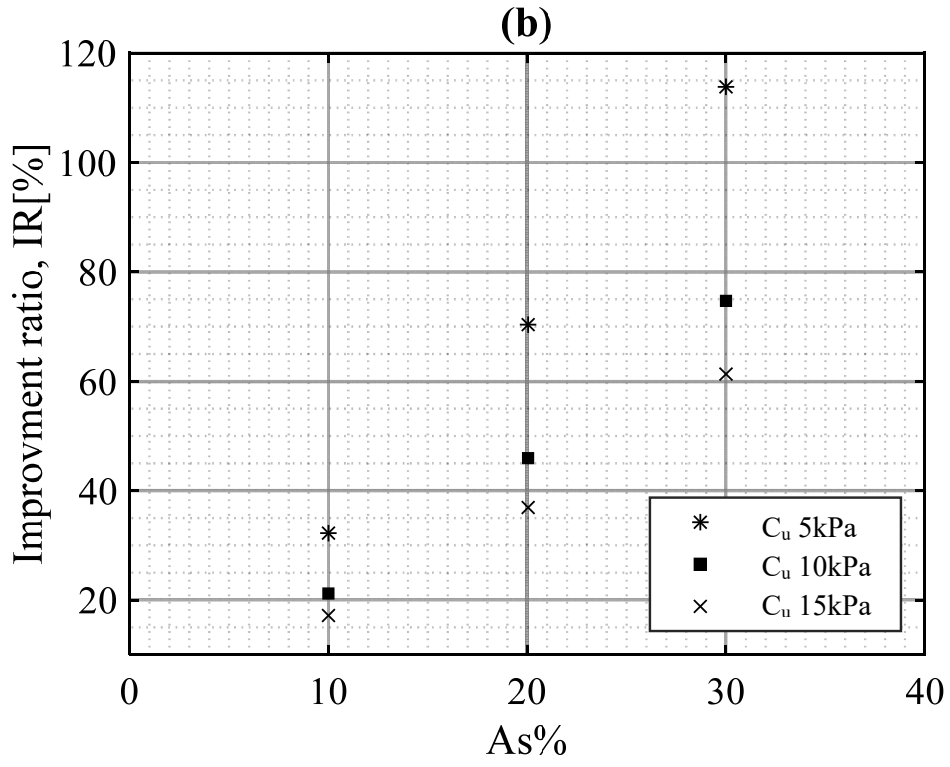
(b)
Improvment ratio, IR[%]
120
100
80
60
40
20
0
10
20
30
40
As%
Cu 5kPa
Cu 10kPa
Cu 15kPa

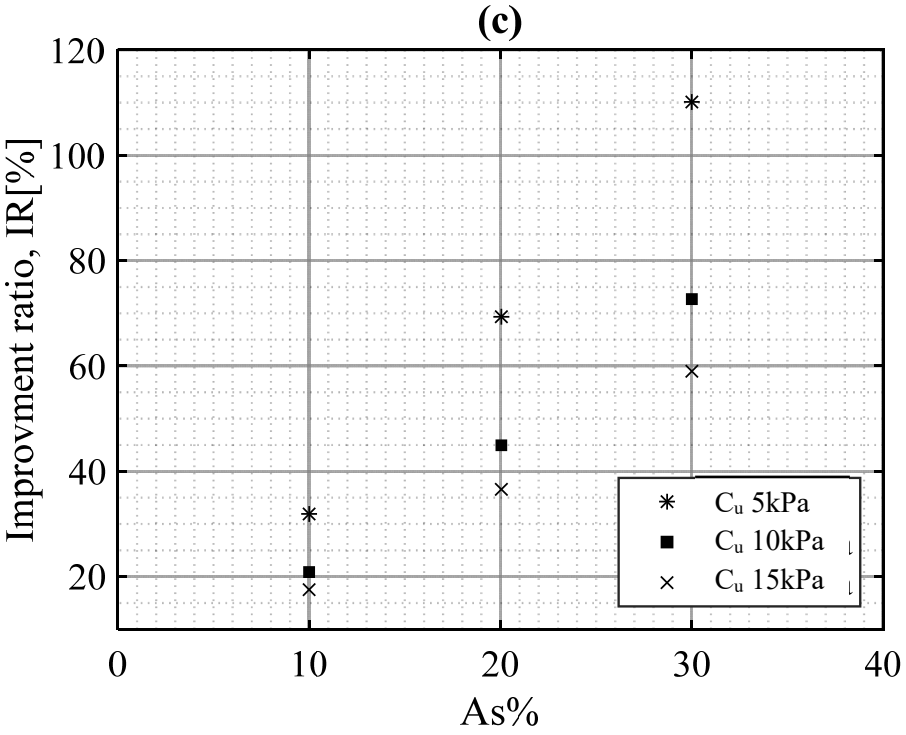

Figure 6.17 Effect of shear resistance of clay on the improvement ratio for different replacement ratios, $\Phi_s = 35^o$: (a) $S/D = 1.25$; (b) $S/D = 1.50$; (c) $S/D = 2.00$

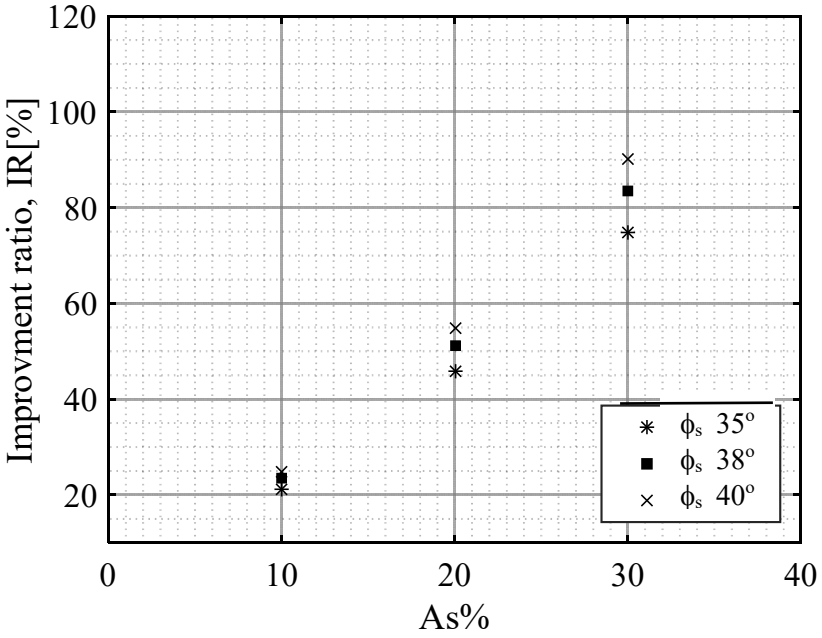

Figure 6.18 Effect of shear resistance of stone on the improvement ratio for different replacement ratios, $C_{uo} = 10$kPa; $S/D = 1.50$

The influence of the number of stone columns under the footing has been also investigated. In this analysis, the number of stone columns varied from N=1 to N=4. The diameter of the columns ranged from 0.3m to 1.6m, which covers the maximum and minimum ranges that may be used in practice. Figure

6.19 presents the effect of the number of stone columns on the bearing capacity. It can be seen that there is no remarkable change in the improvement ratio particularly for low replacement ratios (<10%). However, there is a slight reduction in the improvement ratio for higher values of replacement ratios (30%). For a large number of stone columns, a small diameter was used to keep the replacement ratio constant. By reducing the column diameter, more load will be transferred to the clay soil (less strength material), which leads to a reduction in the improvement ratio (Black et al., 2007; Hanna et al., 2013).

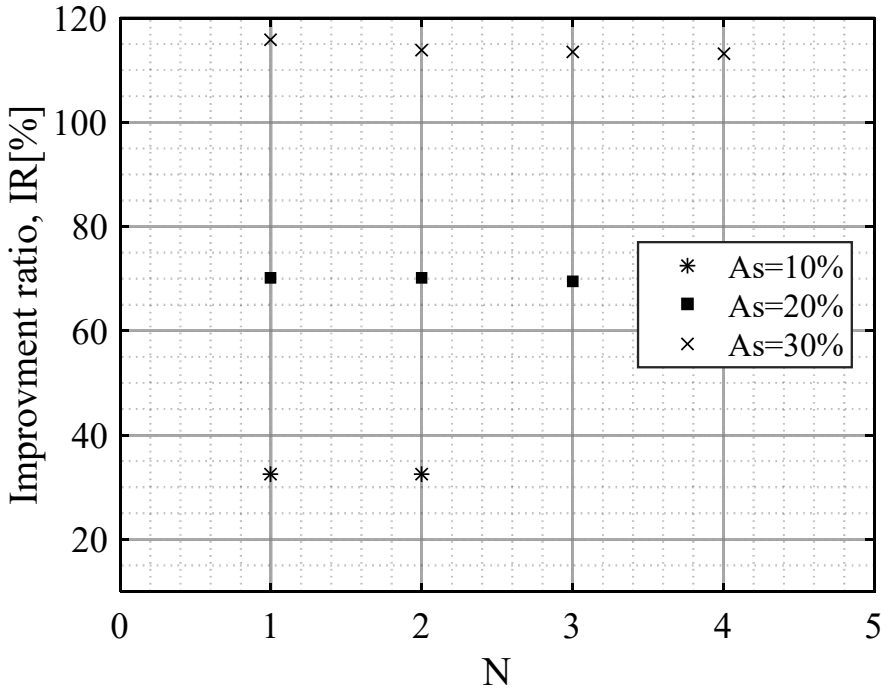

Figure 6.19 Relation between the number of stone columns rows versus the improvement ratio at S/D = 1.5, C_{uo} = 5kPa, Φ_s = 35°

6.3 Design procedures

Knowing the angle of the shearing resistance of the soft soil, angle of shearing resistance of the granular column material, unit weight of the soft soil, cohesion of soft soil, column diameter, and width and depth of the foundation, the charts presented by Hanna et al. (2013) can be used to determine the mode of failure.

For any mode of failure, the improvement factor (I_F) can be determine as follows:

1- Knowing the diameter of the stone columns (D) and the replacement ratio (A_s) the improvement factor for single stone column ($I_{F\ single,40}$) was determined.

2- Based on the drained angle of shear resistance of stone columns (ϕ_s') and clay soil (ϕ_c'), The friction angle coefficients $K\phi_s$ –for stone columns- and $K\phi_c$ -for clay soil- were determined from figures 5.61 and 5.63, respectively.

3- For a single stone column, the improvement factor could be determined using the following equation:

$$I_{F\,single} = I_{F\,singl,40} \times K_{\phi s} \times K_{\phi c} \qquad (6\text{-}33)$$

4- For a group of stone columns, the group coefficient K_g was determined from figure 5.65, and the improvement factor could be determined using the following equation:

$$I_{F\,group} = I_{F\,singl,40} \times K_{\phi s} \times K_{\phi c} \times K_g \qquad 6\text{-}34)$$

In case of punching shear failure, the current analytical model could be used to calculate the bearing capacity of the reinforced clay soil as follows:

A- For a rigid square footing reinforced by a single stone column

1- Based on the replacement ratio (A_s), footing width (B), and angle of shear resistance of stone column (ϕ_s), the bearing capacity factor (N_c, N_q, $N\gamma_s$, $N\gamma_c$) were determined from figures 6.9 ~ 6.12

2- The ultimate bearing capacity then could be calculated using equation (6-26)

B- For a rigid square footing reinforced by a group of stone columns

1- Calculate an equivalent footing width a shown equation (6-35)

$$B_{eq} = \sqrt{\frac{N \times \frac{\pi D^2}{4}}{A_s} \times 100} \qquad (6\text{-}35)$$

Where,

N = number of stone columns under the footing

D = diameter of stone columns

A_s = replacement ratio (%)

2- Determine the bearing capacity factors (N_c, N_q, $N\gamma_s$, $N\gamma_c$) using replacement ratio (A_s), equivalent footing width (B_{eq}), and angle of shear resistance of stone column (ϕ_s).

3- The ultimate bearing capacity then could be calculated using equation (6-26).

6.4 Limitation of the presented study

A wide range of the stone columns properties was covered numerically in the current study. Therefore, the equations and design charts presented in this research are limited:

1- The improvement factor and the bearing capacity calculation are valid for replacement ratio ranges from (5% to 36%).
2- The presented design charts for calculating the improvement factor are also valid for stone column diameters that vary between 0.2m and 2.00m.

Chapter 7: Conclusions

7.1 General

This chapter summarizes the major findings from this study and provides recommendations for future related research.

Experimental program

Consolidated undrained triaxial experiments were conducted on stone columns surrounded with soft clay to investigate the performance of clay soil reinforced by single and groups of stone columns. Conclusions from the tests are as follows:

1. For a single stone column, the deviator stress linearly increases with the increase of the replacement ratio.
2. The performance of a single and a group of stone columns is similar for replacement ratios less than 15%.
3. For a replacement ratio more than 15%, there is a significant reduction in the shearing resistance for the group of stone columns as compared to a single stone column at the same replacement ratio.
4. Increasing the spacing/diameter (*S/D*) ratio leads to a slight reduction in the shear resistance of clay soil reinforced by a group of stone columns at the same replacement ratio.

Numerical analysis

Numerically, high-fidelity full-scale 3-D finite element models were developed to simulate the case of soft clay reinforced with a single or a group of displacement stone columns. The aim was to simulate the installation stage and loading stage in order to examine the columns/soil interaction, determine the improvement factor when using stone columns as reinforcement, assess the effect of the column installation, conduct parametric studies on the parameters governing the column performance, and to establish the footing capacity. Conclusions from the validated numerical model:

1. The effect of stone columns installation extends to a distance of 2.0D from the center of the stone columns
2. The drained shear resistance of the clay soil does not have influence on the effect of installation

3. Failure mechanism starts as bulging in the stone columns then extends to general, local, or punching under the footing based on soil/stone columns properties.
4. Number and spacing between stone columns with the same diameter do not have a significant effect on bearing resistance of the reinforced soil at the same replacement ratio.
5. Diameter of the stone column, as well as the total replacement ratio under the footing, have a major influence on the resistance of the reinforced soil.
6. Design charts were provided to determine the improvement factor for a given soil/stone columns properties.
7. The numerical model can define the actual failure plane that occurred under a rigid footing supported by reinforced clay soil.

Analytical analysis

An analytical model was developed using the limit equilibrium technique and the deduced failure mechanism from the results of the numerical model to develop a theory to predict the capacity of footings on clay reinforced by a single and a group of stone columns. The following was achieved:

1. Design theories were developed to predict the ultimate bearing capacity of a rigid square footing on soft clay reinforced by a single and a group of stone columns.
2. Design charts were developed to assist practicing engineers find the bearing capacity for reinforced clay soil.
3. The Morgenstern-Price method of slices was successfully used to estimate the bearing capacity of reinforced clay soil.
4. The Morgenstern-Price method of slices was utilized to introduce an improvement ratio (*IR*) to determine the benefits of using stone columns as reinforcement as a function of the replacement ratio.
5. For the same stone column arrangement, the improvement ratio (*IR*) increases with a decrease of the shear strength of the surrounding clay, as the ultimate bearing capacity of the system is significantly increased due to the increase of the shear strength of the clay soil as well as the stone.

Design procedures

Based on the results obtained from the current study, design procedures were developed to determine the improvement factor (I_F) and the bearing capacity (q_u) of a clay soil reinforced by a single or a group of stone columns at a given soil/stone columns properties.

7.2 Future research

Based on the results obtained and presented in this thesis, the following future research is recommended:

1. There is a need for full-scale field testing to validate theories developed from small-scale experimental modelling.
2. The research in this study is limited to rigid foundations. However, flexible foundations may be considered to simulate the case of embankments, roads, and earth dams.
3. Extend the current study to simulate the dynamic behavior of groups of stone columns.
4. Study the liquefaction effect on stone columns installed in sand.
5. Extend the current study to estimate the bearing capacity of encased stone columns.

References

ABAQUS Ver. 6.11 (2011). Dassault System Simulia Corp., Providence, RI, USA. © Dassault Systems, 2010.

Al-Khafaji, Z., & Craig, W. (2000). Drainage and reinforcement of soft clay tank foundation by sand columns. *Geotechnique, 50*(6), 709-713.

Al Ammari, K., & Clarke, B. G. (2018). Effect of Vibro Stone-Column Installation on the Performance of Reinforced Soil. *Journal of Geotechnical and Geoenvironmental Engineering, 144*(9), 04018056.

Alamgir, M., & Zaher, S. (2001). *Field investigation on a soft ground of Bangladesh reinforced by granular piles.* Proceedings, International Symposium on Earth Reinforcement. Land marks in earth reinforcement. Kyushu, Japan

Almeida, M., Santa Maria, P., Martins, I., Spotti, A., & Coelho, L. (2000). Consolidation of a very soft clay with vertical drains. *Geotechnique, 50*(6), 633-643.

Ambily, A., & Gandhi, S. R. (2007). Behavior of stone columns based on experimental and FEM analysis. *Journal of Geotechnical and Geoenvironmental Engineering, 133*(4), 405-415.

ASTM. (2004). D 4767-04: Standard test method for consolidated undrained triaxial compression test for cohesive soils *ASTM Int., West Conshohocken, Pa*.

ASTM. (2011). D2435 / D2435M-11 *Standard Test Methods for One-Dimensional Consolidation Properties of Soils Using Incremental Loading*. West Conshohocken, PA: ASTM International.

Babu, M. D., Nayak, S., & Shivashankar, R. (2013). A critical review of construction, analysis and behaviour of stone columns. *Geotechnical and Geological Engineering, 31*(1), 1-22.

Bae, W.-S., Shin, B.-W., An, B.-C., & Kim, J.-S. (2002). *Behaviors of Foundation System Improved with Stone Columns.* Paper presented at the The Twelfth International Offshore and Polar Engineering Conference. Kitakyushu, Japan.

Balaam, N. P. (1978). *Load settlement behaviour of granular piles.* (Ph.D.), University of Sydney.

Balaam, N., & Booker, J. (1985). Effect of stone column yield on settlement of rigid foundations in stabilized clay. *International Journal for Numerical and Analytical Methods in Geomechanics, 9*(4), 331-351.

Balaam, N., & Booker, J. R. (1981). Analysis of rigid rafts supported by granular piles. *International Journal for Numerical and Analytical Methods in Geomechanics, 5*(4), 379-403.

Balaam, N., & Poulos, H. G. (1983). *The behaviour of foundations supported by clay stabilised by stone columns.* Paper presented at the European Conference on Soil Mechanics and Foundation Engineering, 8th, 1983, Helsinki, Finland.

Barksdale, R., & Bachus, R. (1983a). *Design and Construction of Stone Columns Volume I*. Retrieved from Wishington, DC, USA.

Barksdale, R., & Bachus, R. (1983b). *Design and Construction of Stone Columns Volume II, Appendixes*. Retrieved from Wishington, DC, USA.

Baumann, V., & Bauer, G. (1974). The performance of foundations on various soils stabilized by the vibro-compaction method. *Canadian Geotechnical Journal, 11*(4), 509-530.

Bergado, D. T., & Lam, F. L. (1987). Full scale load test of granular piles with different densities and different proportions of gravel and sand on soft Bangkok clay. *Soils andcFoundations, 27*(1), 86-93.

Bishop, A. W. (1955). The use of the slip circle in the stability analysis of slopes. *Geotechnique, 5*(1), 7-17.

Black, J., Sivakumar, V., & Bell, A. (2011). The settlement performance of stone column foundations. *Geotechnique, 61*(11), 909-922.

Black, J., Sivakumar, V., & McKinley, J. (2007). Performance of clay samples reinforced with vertical granular columns. *Canadian Geotechnical Journal, 44*(1), 89-95.

Bolton, M. (1986). Strength and dilatancy of sands. *Geotechnique, 36*(1), 65-78.

Bouassida, M., & Jellali, B. (2002). Capacité portante ultime d'un sol renforcé par une tranchée. *Revue Française de Génie Civil, 6*(7-8), 1381-1395.

Bouassida, M., Jellali, B., & Porbaha, A. (2009). Limit analysis of rigid foundations on floating columns. *International Journal of Geomechanics, 9*(3), 89-101.

Bowles, L. (1996). *Foundation analysis and design*. McGraw-hill Book Company, New York.

Brauns, J. (1978). *Initial bearing capacity of stone column and sand piles.* Proceedings of Soil Reinforcing and Stabilizing Techniques in Engineering Practise, Sydney.

BSI. (1990). Methods of test for soils for civil engineering purposes. British Srandard Institutuin *BS1377-2*. London.

Cairncross, A. M. (1973). *Deformations around model tunnels in stiff clay.* (Ph.D. Thesis), University of Cambridge.

Castro, J. (2014). Numerical modelling of stone columns beneath a rigid footing. *Computers and Geotechnics, 60*, 77-87.

Castro, J., & Karstunen, M. (2010). Numerical simulations of stone column installation. *Canadian Geotechnical Journal, 47*(10), 1127-1138.

Castro, J., Karstunen, M., & Sivasithamparam, N. (2014). Influence of stone column installation on settlement reduction. *Computers and Geotechnics, 59*, 87-97.

Chen, W.-F., & Liu, X. (2012). Limit analysis in soil mechanics (Vol. 52): Elsevier.

Christoulas, S., Bouckovalas, G., & Giannaros, C. (2000). An experimental study on model stone columns. *Soils and Foundations, 40*(6), 11-22.

Coulomb, C. A. (1776). *Essai sur une application des règles de maximis & minimis à quelques problèmes de statique, relatifs à l'architecture*. Paris: De l'Imprimerie Royale.

Domingues, T., Borges, J., & Cardoso, A. (2007). *Parametric study of stone columns in embankments on soft soils by finite element method.* Paper presented at the Proceedings of the 5th International Workshop on Applications of Computational Mechanics in Geotechnical Engineering, Guimaraes, Portugal.

Drucker, D. C., & Prager, W. (1952). *Soil mechanics and plastic analysis or limit design*. Quarterly of Applied Mathematics*, 10*(2), 157-165.

Egan, D., Scott, W., & McCabe, B. (2008). *Installation effects of vibro replacement stone columns in soft clay.* Proceedings of the 2nd International Workshop on the Geotechnics of Soft Soils, Glasgow.

Elshazly, H., Elkasabgy, M., & Elleboudy, A. (2008). *Effect of inter-column spacing on soil stresses due to vibro-installed stone columns: interesting findings*. Geotechnical and Geological Engineering Journal*, 26*(2), 225-236.

Etezad, M., Hanna, A., & Ayadat, T. (2015). Bearing capacity of a group of stone columns in soft soil. *International Journal of Geomechanics, 15*(2), 04014043, 1-15.

Etezad, M., Hanna, A., & Khalifa, M. (2018). Bearing Capacity of a Group of Stone Columns in Soft Soil Subjected to Local or Punching Shear Failures. *International Journal of Geomechanics, 18*(12), 04018169, 1-14.

Genna, F., & Pandolfi, A. (1994). Accurate numerical integration of Drucker-Prager's constitutive equations. *Meccanica, 29*(3), 239-260.

Gerrard, C. M., Pande, G. N., & Schweiger, H. F. (1984). *Modeling behavior of soft clay reinforced with stone columns.* Proceedings of In-situ Soil and Rock Reinforcement Conference, Paris.

Gibson, R., & Anderson, W. (1961). In situ measurement of soil properties with the pressuremeter. *Civil engineering and public works review, 56*(658), 615-618.

Goughnour, R. (1983). *Settlement of vertically loaded stone columns in soft ground.* Proceedings of 8th European Conference. on Soil Mechanics, and Foundations Engineering., Helsinki, Finland.

Goughnour, R., & Barksdale, R. (1984). *Performance of a stone column supported embankment.* proceedings, The Case Histories in Geotechnical Engineering Conference, University of Missouri-rolla.

Goughnour, R., & Bayuk, A. (1979). *Analysis of stone column-soil matrix interaction under vertical load*. Proceedings of International Conference on Soil Reinforcement, Paris. 279-285.

Goughnour, R. R., & Bayuk, A. A. (1979b). *A field study of long-term settlements of loads supported by stone column in soft ground*. Proceedings of International Conference on Soil Reinforcement, 279-285.

Griffiths, D. (1982). Computation of bearing capacity factors using finite elements. *Geotechnique, 32*(3), 195-202.

Guetif, Z., Bouassida, M., & Debats, J. (2007). Improved soft clay characteristics due to stone column installation. *Computers and Geotechnics, 34*(2), 104-111.

Hanna, A., Etezad, M., & Ayadat, T. (2013). Mode of failure of a group of stone columns in soft soil. *International Journal of Geomechanics, 13*(1), 87-96.

Hansen, J. B. (1970). A revised and extended formula for bearing capacity. Danish Geotechnical Institute Bulletin, *28*, 5-11

Helwany, S. (2007). *Applied soil mechanics with ABAQUS applications*: John Wiley & Sons.

Henke, S., & Grabe, J. (2006). *Simulation of pile driving by 3-dimensional finite-element analysis.* Paper presented at the Proceedings of 17th European Young Geotechnical Engineers' Conference, Zagreb, Crotia, ed. by V. Szavits-Nossan, Croatian Geotechnical Society.

Hu, W. (1995). *Physical modelling of group behaviour of stone column foundation.* (Ph.D. Thesis), University of Glasgow, UK.

Hughes, J., & Withers, N. (1974). Reinforcing of soft cohesive soils with stone columns. *Ground Engineering, 7*(3), 42-49.

Hughes, J., Withers, N., & Greenwood, D. (1975). A field trial of the reinforcing effect of a stone column in soil. *Geotechnique, 25*(1), 31-44.

Indraratna, B., Basack, S., & Rujikiatkamjorn, C. (2012). Numerical solution of stone column–improved soft soil considering arching, clogging, and smear effects. *Journal of Geotechnical and Geoenvironmental Engineering, 139*(3), 377-394.

Indraratna, B., & Redana, I. (1998). Laboratory determination of smear zone due to vertical drain installation. *Journal of Geotechnical and Geoenvironmental Engineering, 124*(2), 180-184.

Kelly, P. (2014). *Soil Structure Interaction and Group Mechanics of Vibrated Stone Column Foundations.* University of Sheffield.

Khalifa, M., Etezad, M., Hanna, A., & Sabry, M. (2017). *Bearing Capacity of Strip Foundation on Soft Soil Reinforced with Stone Columns Using Method of Slices.* Proceedings, International Congress and Exhibition" Sustainable Civil Infrastructures: Innovative Infrastructure Geotechnology", Egypt.

Kirsch, F. (2006). *Vibro stone column installation and its effect on ground improvement.* Paper presented at the Proceedings of the International Conference on Numerical Modelling of Construction Processes in Geotechnical Engineering for Urban Environment, London.

Kirsch, F. (2008). *Evaluation of ground improvement by groups of vibro stone columns using field measurements and numerical analysis.* Proceedings of the 2nd International Workshop on the Geotechnics of Soft Soils, Glasgow.

Kulhawy, F. H., & Mayne, P. W. (1990). *Manual on estimating soil properties for foundation design*. Technical report, Final Report EL 6800, Research Project 1493-6, Electric Power Research Institute, Palo Alto, California, US

Lee, J. S., & Pande, G. N. (1998). Analysis of stone-column reinforced foundations. *International Journal for Numerical and Analytical Methods in Geomechanics, 22*(12), 1001-1020.

Mabsout, M. E., & Tassoulas, J. L. (1994). A finite element model for the simulation of pile driving. *International Journal for numerical methods in Engineering, 37*(2), 257-278.

Madhav, M., & Vitkar, P. (1978). Strip footing on weak clay stabilized with a granular trench or pile. *Canadian Geotechnical Journal, 15*(4), 605-609.

McCabe, B. (2009). A review of field performance of stone columns on soft soils. *Geotechnical Engineering*. 162(6): 323-334.

McCabe, B., & Killeen, M. (2016). Small Stone-Column Groups: Mechanisms of Deformation at Serviceability Limit State. *International Journal of Geomechanics*, 04016114.

McKelvey, D. (2002). *The performance of vibro stone column reinforced foundations in deep soft ground.* Queen's University of Belfast.

McKelvey, D., Sivakumar, V., Bell, A., & Graham, J. (2004). A Laboratory Model Study of the Performance of Vibro Stone Columns in Soft Clay. *Journal of Geotechnical Engineering, 152*, 1-13.

Meyerhof, G. (1951). The ultimate bearing capacity of foundations. *Geotechnique, 2*(4), 301-332.

Miranda, M., Da Costa, A., Castro, J., & Sagaseta, C. (2015). Influence of gravel density in the behaviour of soft soils improved with stone columns. *Canadian Geotechnical Journal, 52*(12), 1968-1980.

Mitchell, J. K. (1981). *Soil improvement: state-of-the-art*: Department of Civil Engineering, University of California.

Mitchell, J. K., & Huber, T. R. (1985). Performance of a stone column foundation. *Journal of Geotechnical Engineering, 111*(2), 205-223.

Mohanty, P., & Samanta, M. (2015). Experimental and numerical studies on response of the stone column in layered soil. *International Journal of Geosynthetics and Ground Engineering, 1*(3), 27.

Morgenstern, N., & Price, V. E. (1965). The analysis of the stability of general slip surfaces. *Geotechnique, 15*(1), 79-93.

Muir Wood, D., Hu, W., & Nash, D. (2000). Group effects in stone column foundations: model tests. *Geotechnique, 50*(6), 689-698.

Pitt, J. M., White, D. J., Gaul, A., & Hoevelkamp, K. (2003). *Highway applications for rammed aggregate piers in Iowa soils*. LOWA Dot project TR- 443, OTRE Project 00-06

Poorooshasb, H., & Meyerhof, G. (1997). Analysis of behavior of stone columns and lime columns. *Computers and Geotechnics, 20*(1), 47-70.

Priebe, H. J. (1991). Vibro Replacement-Design Criteria and Quality Control. *Deep Foundation Improvements: Design, Construction, and Testing*. ed. M. Esring and R. Bachus (West Conshohocken, PA: ASTM International, 1991), 62-72.

Priebe, H. J. (1995). The design of vibro replacement. *Ground Engineering, 28*(10), 31-37.

Qiu, G., Henke, S., & Grabe, J. (2011). Application of a Coupled Eulerian–Lagrangian approach on geomechanical problems involving large deformations. *Computers and Geotechnics, 38*(1), 30-39.

Rao, S., Reddy, K., & Kumar, P. (1997). Studies on groups of stone columns in soft clays. *Geotechnical Engineering, 28*(2).

Rocscience. (2012). SLIDE 6.0—2D slope stability analysis for soil and rock slopes. *Rocscience Inc*.

Schweiger, H., & Pande, G. (1986). Numerical analysis of stone column supported foundations. *Computers and Geotechnics, 2*(6), 347-372.

Shahu, J., & Reddy, Y. (2011). Clayey soil reinforced with stone column group: model tests and analyses. *Journal of Geotechnical and Geoenvironmental Engineering, 137*(12), 1265-1274.

Sinha, A., & Hanna, A. (2016). 3D numerical model for piled raft foundation. *International Journal of Geomechanics, 17*(2), 04016055.

Sivakumar, V., Glynn, D., Black, J., & McNeill, J. (2007). *A laboratory model study of the performance of vibrated stone columns in soft clay.* Proceedings of the 14th European Conference on Soil Mechanics and Geotechnical Engineering, Madrid, Spain.

Sivakumar, V., McKelvey, D., Graham, J., & Hughes, D. (2004). Triaxial tests on model sand columns in clay. *Canadian Geotechnical Journal, 41*(2), 299-312.

Sorensen, K., & Okkels, N. (2013). *Correlation between drained shear strength and plasticity index of undisturbed overconsolidated clays.* Proceedings of the 18th International Conference on Soil Mechanics and Geotechnical Engineering, Paris.

Soubra, A.-H. (1999). Upper-bound solutions for bearing capacity of foundations. *Journal of Geotechnical and Geoenvironmental Engineering, 125*(1), 59-68.

Steuerman, S. (1939). A new soil compaction device. *Engineering News Record, 1*, 56-58.

Terashi, M., Kitazume, M., & Minagawa, S. (1991). Bearing capacity of improved ground by sand compaction piles. *Deep Foundation Improvements: Design, Construction, and Testing*. ed. M. Esring and R. Bachus (West Conshohocken, PA: ASTM International, 1991), 47-61

Terzaghi, K. (1925). Principles of soil mechanics. *Engineering News-Record, 95*(19-27), 19-32.

Terzaghi, K. (1943). *Theory of consolidation*: Wiley Online Library.

Terzaghi, K. (1947). *Theoretical soil mechanics*: New York: John Wiley & Sons.

Terzaghi, K., & Peck, R. B. (1967). Soil Mechanics in Engineering Practice, John Wiley & Sons. *Inc., New York*.

Vautrain, J. (1978). Reinfirced earth wall on stone columns in soil. *BULL LIAISON LAB PONTS CHAUSS*(SPEC VI-E), 94-188.

Vautrain, J. (1980). Comportement et dimensionnement des colonnes ballastées. *Revue française de géotechnique, 11*, 59-73.

Vesic, A. S. (1972). Expansion of cavities in infinite soil mass. *Journal of Soil Mechanics & Foundations Div, 98*(sm3), 265-290.

Watts, K., Johnson, D., Wood, L., & Saadi, A. (2000). An instrumented trial of vibro ground treatment supporting strip foundations in a variable fill. *Geotechnique 50(6),* 699-708

Weber, T. M., Plötze, M., Laue, J., Peschke, G., & Springman, S. M. (2010). Smear zone identification and soil properties around stone columns constructed in-flight in centrifuge model tests. *Geotechnique, 60*(3), 197-206.

Wehr, J. (2004). *Stone columns–single columns and group behavior.* Proceedings of 5th International Conference on Ground Improvement Technologies, Kuala Lumpur.

Wood, D., Hu, W., & Nash, D. (2000). Group effects in stone column foundations: model tests. *Geotechnique, 50*(6), 689-698.